Reconstructing depositional architecture and stratigraphy of coastal- to shallow-marine strata in a low-accommodation system: McMurray Formation, Alberta, Canada

by

Chloé Château

MSc, University of Bordeaux, 2014

BSc, University of Angers, 2011

Thesis Submitted in Partial Fulfillment of the

Requirements for the Degree of

Doctor of Philosophy

in the

Department of Earth Sciences

Faculty of Science

© Chloé Château 2020

SIMON FRASER UNIVERSITY

Fall 2020

Copyright in this work rests with the author. Please ensure that any reproduction or re-use is done in accordance with the relevant national copyright legislation.

Declaration of Committee

Name:	**Chloé Château**
Degree:	**Doctor of Philosophy**
Thesis title:	**Sedimentology and stratigraphy of delta deposits in limited accommodation space settings: Southwest McMurray Sub-Basin, Alberta, Canada**
Committee:	**Chair: Gwenn Flowers** Professor, Earth Sciences
	Shahin Dashtgard Supervisor Professor, Earth Sciences
	James MacEachern Committee Member Professor, Earth Sciences
	Stephen Hubbard Committee Member Associate Professor, Geoscience University of Calgary
	Dale Leckie Committee Member Adjunct Professor, Geoscience University of Calgary
	Jessica Pilarczyk Examiner Assistant Professor, Earth Sciences
	Gary Hampson External Examiner Professor, Earth Science and Engineering Imperial College London

Abstract

A new and novel sedimentological-statistical approach is applied to Lower Cretaceous McMurray Formation strata in the southwest quadrant of the McMurray depocenter to further comprehend the impact of accommodation space creation on the preserved record of coastal- to shallow-marine deposits in a low-accommodation setting. Across the study area, the McMurray Formation consists of discrete depositional units bounded by flooding surfaces and/or transgressive surfaces of erosion. The facies characteristics, depositional architecture and sequence stratigraphy of these depositional units are investigated, focused in the three main areas: quantitatively defining the controls on localized accommodation creation, recognizing new depositional units within the McMurray Formation, and quantifying and characterizing the speed of the Boreal Sea transgression. First, depositional architecture work tied to statistical analysis in the Sparrow Paleovalley (≈1/3 of the study area) reveals the local overthickening of +21% to +45% of the depositional units. The local accommodation space creation is demonstrated to have resulted from syndepositional epikarst subsidence within the underlying Devonian carbonates. Second, the detailed facies analysis and depositional architecture analysis of the Regional C depositional unit reveals a regionally extensive allogenic flooding surface (Top C2) dividing the Regional C depositional unit. Recognition of this new stratigraphic surface further reinforces the persistent and slow drowning of the McMurray depocenter during accumulation of the McMurray Fm, and that deposition occurred in a low-accommodation setting. Finally, detailed facies analysis, depositional architecture analysis, sequence stratigraphic work and statistical methods applied to the entire McMurray Formation across the study area reveals that the thicknesses of depositional units decrease markedly upward, and that this thickness decrease correlates to a change in the facies character of the transgressive mudstones underlying each depositional unit. Together, these data record the acceleration in the rate of the transgression of the Boreal Sea across the McMurray depocenter.

Keywords: Low-accommodation space settings; coastal- to shallow-marine deposits; sedimentological-statistical approach; depositional units architecture; mechanisms of accommodation space creation; rate of transgression

Dedication

À ma famille et à mes ami.e.s de toujours pour votre soutient tout au long de mon parcours universitaire. Je vous dédie cette thèse.

To my loved ones, your support made all of this possible. I dedicate you this thesis.

Acknowledgements

First and foremost, I would like to express my gratitude to my supervisor Prof. Shahin Dashtgard for believing in my abilities and providing me with the opportunity to learn and grow as a researcher. Thank you for your patience, encouragement and insight over the five and a half years that I spent at SFU – I could not have asked for a better supervisor! I would also like to express my sincere thanks to Prof. James MacEachern for his time and guidance. Our numerous discussions on sedimentology and stratigraphy pushed the limits of my knowledge and inspired the numerous ideas presented in this thesis.

I would also like to thank my thesis committee, Dr. Stephen Hubbard and Dr. Dale Leckie, for their insights and feedback. I would especially like to thank Dr. Dale Leckie for his time and mentorship over the years. You have supported me in my academic pursuits since we met during my M.Sc. in France, and I will always be grateful for opportunities to share my thoughts on the sciences with you – geology or otherwise.

I would like to extend my thanks to my internal examiner Jessica Pilarczyk and my external examiner Gary Hampson for taking the time to read my thesis and for sitting on my examining committee.

I would like to thank all the past and present members of the ARISE group for their support and feedback over the years. I also want to express my gratitude to my fellow graduate student friends for providing endless moral support and an unforgettable journey at SFU: Aspen Anderson, Dr. Flavien Beaud, Andy Clark, Dr. Davide Donati, Susanne Fietz, Dr. Anja Frank, Anna Gribon, Snowy Haiblen, Chuqiao Huang, Sarah Makin, Lucian Rinke-Hardekopf, Dr. Gioachino Roberti, Teresa Rosales, Surhabi Simha, Sarah Schultz, Dr. Thomas Vigié and Erik Young.

Finally, I would like to thank the members of the McMurray Geological consortium for all of the help provided and ideas shared during our meetings and conferences, and during my time at the core research center of Calgary. I also extend my appreciation to the sponsors of the McMurray Geology Consortium: BP plc, Cenovus Energy Inc., Husky Energy, Nexen CNOOC Ltd. and Woodside Energy Ltd., for funding this research.

Table of Contents

List of Tables

List of Figures

List of Acronyms

^{2}	Square
−	To
%	Per cent
+	Plus
<	Less than
>	Greater than
±	Plus or minus
≈	Almost equal to
°	Degree
3D	Three dimensions
AB	Alberta
AER	Alberta Energy Regulator
AEUB	Alberta Energy and utilities board
API	American Petroleum Institute
Ar	*Arenicolites*
As	*Asterosoma*
AWR	Aggradational wave ripples
B	Breccia
BI	Bioturbation Index
cf.	Confer
CFR	Combined flow ripples
Ch	*Chondrites*
cm	Centimetre
CO-SPV	Composite of central and outer zones of the Sparrow Paleovalley
CPL	Curvilinear parallel laminae
CR	Current ripples
CS	Dune scale cross-stratification
Cy	*Cylindrichnus*
D	Standardised difference between two means (Cohen's D)
dam	Decametre
dc	Decimetre

DC	Distributary channel
Di	*Diplocraterion*
DLS	Dominion Land Survey
Dr.	Doctor
DU	Depositional unit
e	Ten to the power of
e.g.	*Exempli gratia*
et al.	*Et alia*
F	Facies; Fracture
FA	Facies association
Fig	Figure
fL	Lower fine
Fm	Formation
FS	Flooding surface
FTC	Fluvio tidal channel
fu	Fugichnia
fU	Fine upper
GR	Gamma-ray
Gy	*Gyrolithes*
HCS	Hummocky cross-stratification
i.e.	*Id est*
IHS	Inclined heterolithic stratification
Inc.	Incorporated
km	Kilometre
K-S	Kolmogorov-Smirnov
LAS	LIDAR DATA Exchange
LD	Load structure
LM	Lower member of the McMurray Formation
Ltd	Limited company
m	Metre
M.Sc.	Master of Science
Ma	Million years (absolute dating method)
max	Maximum
MC	Mudstone clasts

MDC	McMurray Depocenter
MFS	Maximum flooding surface
MGC	McMurray Geology Consortium
m-HCS	Micro hummocky cross-stratification
mi	Mile
mL	Medium lower
mm	Millimetre
MSB	McMurray Sub-Basin
mU	Medium upper
Myr	Million years
n	Sample size
N	North
na	Navichnia
NE	Northeast
NW	Northwest
OR	Oscillatory ripple
p.	Page
Pa	*Palaeophycus*
Ph	*Phycosiphon*
Pl	*Planolites*
Plc	Public limited company
PPL	Planar-parallel lamination
Prof.	Professor
PS	Parasequence
PV	Paleovalley
p-value	Probability value
R	Range
RDC	Regulatory DataCorp
rt	Roots
SC	Syneresis crack
SCS	Swaly cross-stratification
SCU	Sub-Cretaceous Unconformity
SD	Standard deviation
SE	Southeast

Seq.	Sequence
SFU	Simon Fraser University
SHL	Sand heterolithic lenses
Si	Siderite nodule
Si	*Siphonichnus*
Sk	*Skolithos*
SK	Saskatchewan
SL	Silt lamina
SPV	Sparrow Paleovalley
SSD	Soft-sediment deformation
STATS	Statistic
SU	Sub-aerial unconformity
SW	Southwest
T	Township; Tide-dominated delta
t	Time
Ta	*Taenidium*
Te	*Teichichnus*
Tfw	Tide-dominated, fluvial-influenced, storm wave-affected delta
Th	*Thalassinoides*
Tks	Thickness
TSE	Transgressive surface of erosion
TSE/FS	Amalgamated transgressive surface of erosion and flooding surface
TSE/SE	Composite transgressive surface of erosion and subaerial exposure surface
Tw	Tide-dominated, storm wave-affected delta
Twf	Tide-dominated, storm wave-influenced, fluvial-affected delta
TWP	Township
UWI	Unique well identifier
v.	Volume
vfL	Very fine lower
vfU	Very fine upper
vs	*Versus*
W	West

WCSB	Western Canada Sedimentary Basin
WPL	Wavy parallel laminae
WR	Wave ripples
Wtf	Wave-dominated, tide-influenced, fluvial-affected delta

Opening Poem

Ce qu'il m'aura fallu de temps pour tout comprendre
Je vois souvent mon ignorance en d'autres yeux
Je reconnais ma nuit je reconnais ma cendre
Ce qu'à la fin j'ai su comment le faire entendre
Comment ce que je sais le dire de mon mieux

Aragon, 1956

Le roman inachevé_ La beauté du diable : Ce qu'il m'aura fallu de temps pour tout comprendre.

(Long time it took me to understand
Often, have I seen my ignorance through the eyes of others
I recognize my night I recognize my cinders
This at the end I knew how to make heard
How to my best I know to express it)

Chapter 1.

Introduction

Shallow-marine deposits in low-accommodation space settings are typically expressed by complex architectures dominated by thin parasequences and composite stratigraphic bounding surfaces. A sedimentological approach is generally used to recognize stratigraphic surfaces and reconstruct the architecture and stratigraphic framework of those paleo-depositional environments. This thesis resolves the sedimentology, depositional architecture and sequence stratigraphy of coastal- to shallow-marine deposits in a low-accommodation space setting, by using statistical analysis where possible. As such, detailed facies analysis is linked to statistical work in a new and novel approach to sedimentary research.

This work focuses on strata in the low-accommodation McMurray Depocenter (MDC), Alberta, Canada. Despite several decades of research on the Lower Cretaceous McMurray Formation (Fm) (Carrigy, 1963, 1967; Christopher, 1984; Alberta Energy and Utilities Board, 2003), reconstructing the stratigraphy of these shallow-marine units remains challenging. Research is focused on the Lower Cretaceous McMurray Fm in the southwestern quadrant of the MDC (townships (T) 69–83, ranges (R) 9–20W4; Fig. 1.1).

The results of this study are used to advance our understanding of three aspects of the McMurray Fm's depositional framework, and to low-accommodation space settings in general. First, the depositional architecture of McMurray Fm depositional units in the Sparrow Paleovalley is assessed, and statistical methods are used to identify controls on the timing and amount of accommodation created before, during, and after deposition. Second, detailed facies analysis and depositional architecture analysis of the lowermost units of the Middle-Upper McMurray Fm (informally referred to as the 'Regional C' depositional unit) is completed. These data are used to comment on the amount of accommodation space created during the early stages of the transgression of the Boreal Sea, and to present a refined stratigraphic framework of this relatively poorly understood stratigraphic interval. Third, high-resolution facies analysis, depositional architecture analysis, sequence stratigraphic work and statistical methods are applied to the entire Middle-Upper McMurray Fm through the southwest quadrant of the MDC in

order to constrain and quantify changes in the rate of transgression in a low-accommodation space setting. The methodologies and results of these approaches employed herein are applicable to low- and limited-accommodation (i.e. slightly greater accommodation than low) depositional settings.

Figure 1.1. Study Area

A) Position of Alberta (AB) and Saskatchewan (SK) in North America. B) The 3 main oil sands regions – Peace River, Athabasca, and Cold Lake are demarcated by the black polygons. The blue-shaded area in the Athabasca oil sands region marks the approximate limit of the McMurray Fm and time-equivalent strata, which is taken to represent the limits of the MDC. The study area is outlined by the red rectangle (modified from Château et al., in press).

1.1. McMurray depocenter stratigraphic framework

The McMurray depocenter (MDC) is situated in the northeast corner of Alberta, Canada, and is part of the foreland basin succession of the Western Canada Sedimentary Basin (Mossop and Shetsen, 1994). From the Late Jurassic to Early Eocene, the oblique collision of allochthonous terranes against the western margin of the westward-moving

North American craton led to tectonic loading and the formation of a foreland basin in the craton interior (Porter et al., 1982; Mossop and Shetsen, 1994; Price, 1994). Prior to, and during the onset of foreland basin development, uplift and eastward migration of the forebulge generated forced sea-level fall (Poulton, 1994). This led to the erosion of previously deposited carbonate-dominated, passive-margin strata and the formation of the Sub-Cretaceous Unconformity (SCU; Jardine, 1974; Plint et al., 1993). Relief on the SCU defines the paleotopography of the basal surface of the MDC, and significantly influenced much of the architecture of McMurray Fm strata. Elongated paleotopographic lows on the SCU are in this thesis regarded as paleovalleys. McMurray Formation deposition primarily take place within the paleovalleys. Removal of up to 200 m of salt from the Devonian-aged Prairie Evaporite Formation led to the concomitant collapse and subsidence of overlying carbonate and shale of the Beaverhill Lake Group; this modified the paleotopography of the SCU and impacted sediment distribution during McMurray Formation deposition in the Assiniboia Valley (McPhee and Wightman, 1991; Crerar and Arnott, 2007; Schneider and Grobe, 2013; Broughton, 2013, 2015a; Schneider et al., 2014; Barton et al., 2017; Hauck et al., 2017).

The stratigraphic subdivision of the McMurray Fm is complex and has been revised several times over the past 60 years (Fig. 1.2). The McMurray Fm consists of fluvial strata at the base, informally referred to as the “lower McMurray”. These strata are progressively overlain by estuarine and then shallow-marine strata, informally named the “middle” and “upper” McMurray, respectively (Carrigy, 1963, 1967; Flach and Mossop, 1985). This initial stratigraphic model did not address the complexity of the McMurray Fm stratigraphic subdivision, and hence, a coupled lithostratigraphic and sequence stratigraphic model was proposed later by the Alberta Energy and Utilities Board (2003; now Alberta Energy Regulator, AEUB). The AER model subdivides the McMurray Fm based on the occurrence of mudstone intervals at the bases of regionally extensive stratigraphic units, and this framework remains largely accepted. Regionally extensive stratigraphic units (e.g., stacked parasequences or parasequence sets) are interpreted as prograding coastal- and shallow-marine successions deposited during short-lived periods of relative stillstand during an overall transgression.

These regionally extensive stratigraphic units are incised into by channels of variable thickness, which have been interpreted to subtend from the tops of the units (Alberta Energy and Utilities Board, 2003). Hence, channels are commonly interpreted

as the products of valley incision that occurred during major relative sea-level falls and during subsequent relative sea-level rise (Hein et al., 2013). The implications of this model are that valley fills are genetically unrelated to the deposition of the regionally extensive stratigraphic units they cross-cut. Other workers (e.g., Ranger et al., 2008; Musial et al., 2012) do not consider all of the channels to be of incised valley fill origin, and instead regard them as channel belt complexes. Regardless of the origin of the channels themselves, some workers interpret them as mainly fluvial, based on scaling relationships with modern fluvial systems (e.g., Hubbard et al., 2011; Durkin et al., 2017a, b; Horner et al., 2019)

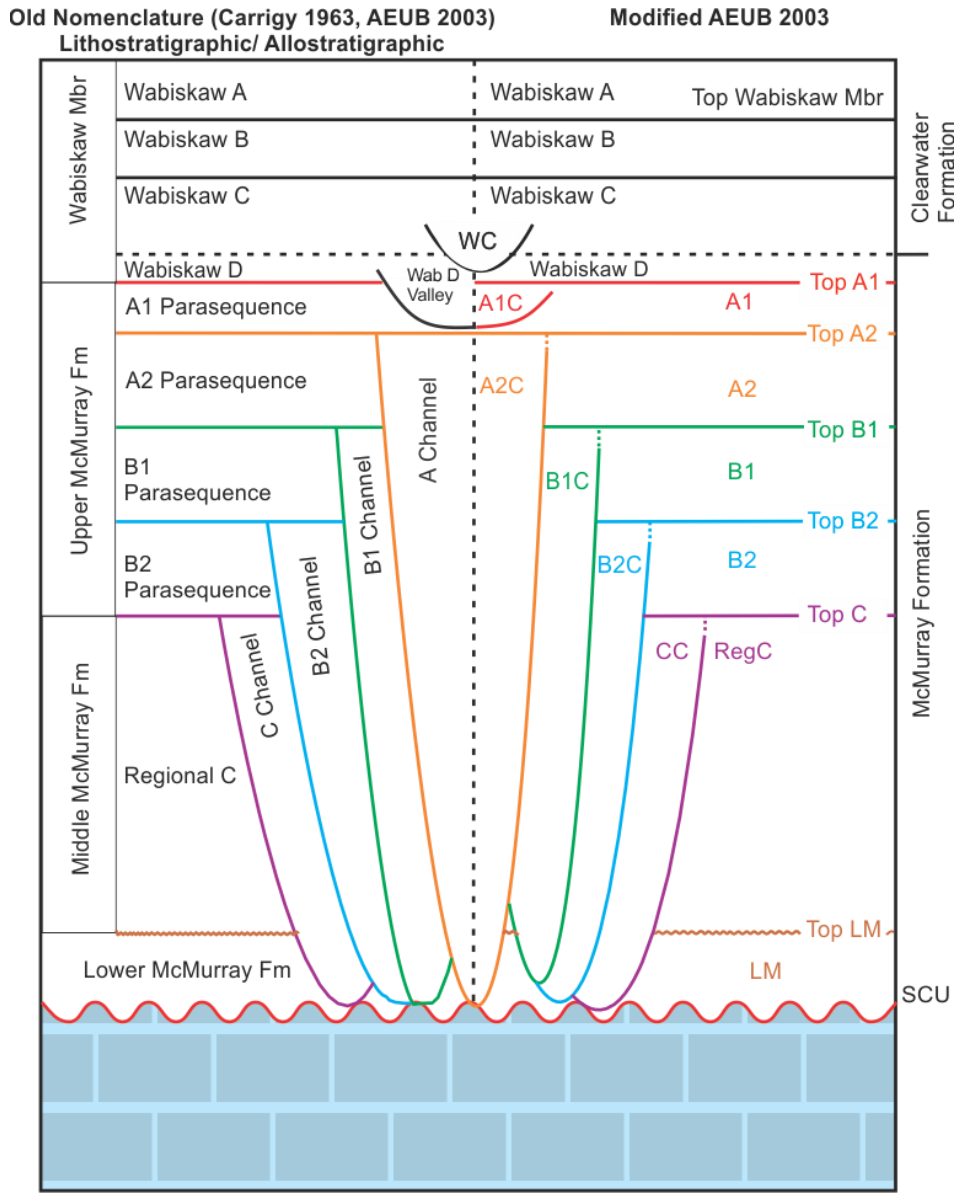

Figure 1.2 Comparison of stratigraphic frameworks proposed for the MDC
The McMurray Fm overlies the Sub-Cretaceous Unconformity (SCU; red wavy line) and is, in turn, overlain by the Wabiskaw Member of the Clearwater Fm. Three stratigraphic models are proposed for the McMurray Fm. On the far left (vertical text) is the lithostratigraphic nomenclature proposed by Carrigy (1963). In the middle (left of the black vertical dashed line) is the lithostratigraphic/allostratigraphic model developed by the Alberta Energy and Utilities Board (2003; now Alberta Energy Regulator). To the right of the black, vertical dashed line is a modified version of the Alberta Energy and Utilities Board (2003) model used by the McMurray Geology Consortium. Key here is that the cross-cutting channel belts are not regarded to universally subtend from the parasequence set (depositional unit) boundaries, and therefore are may be genetically linked to those cycles (modified from Château et al., 2019).

Herein, a revised version of the Alberta Energy and Utilities Board (2003) stratigraphic model is employed, where the subdivision of McMurray Fm is based on the presence of mudstone intervals overlying regionally significant allogenic flooding

surfaces. Stratigraphic units are referred to as depositional units (DU) and represent regressive cycles deposited during minor sea-level fluctuations (i.e. the equivalent of sequences in the AEUB (2003) stratigraphic model). Channel belts are interpreted to be genetically related with each DU (Fig. 1.2; Ranger and Pemberton, 1997; Musial et al., 2012; Weleschuk and Dashtgard, 2019). The low-accommodation space created was rapidly infilled by sediment supplied by the paleo-distributive channel system, and during periods of stable or only slowly rising base level, this led to progradation of the shoreline and concomitant basinward shift of the channel belts (e.g., Ranger and Pemberton, 1997; Ranger et al., 2008; Weleschuk and Dashtgard, 2019).

1.2. Low-accommodation space settings

Accommodation, originally defined by Jervey (1988), refers to the amount of space available for sediment accumulation, and changes in accommodation play an important role in the distribution and geometry of sequences and parasequences, as well as in the nature of their bounding surfaces (Jervey, 1988; Zaitlin et al., 2002). Accommodation is controlled by the interplay of sediment supply, eustasy and tectonics (Jervey 1988; Posamentier and Allen, 1999; Catuneanu, 2002). Changes in the sedimentation rate relative to changes in relative sea-level lead to accommodation space creation, and this controls shoreline trajectories. During transgression, an increase in accommodation is responsible for the landward shift of the shoreline (Mitchum, 1977). During normal regression, sediment supply outpaces relative sea-level rise and this results in the seaward shift of the shoreline (Posamentier and Allen, 1999; Catuneanu, 2002). Based on the thickness of (compacted) sediment deposited over a specific time period, paleo-depositional environments are characterised as low- accommodation (meters−decameters per million years (Myr-1)) through to high-accommodation (kilometers Myr-1; Zaitlin et al., 2002; Davies and Gibling, 2003; Ratcliffe et al., 2004; Rygel and Gibling, 2006; Allen and Fielding, 2007). This definition only accounts for the thickness of sedimentary units. The lateral extent of the paleoshoreline within paleovalleys probably influenced the thickness of sedimentary units but this was not assessed.

As an example of a low-accommodation system, the middle-upper McMurray Fm includes DUs that range in thickness from 6–10 m deposited during the Early Cretaceous over a period of 8.4 Myr (121.4−113 Ma; Hein and Dolby, 2017; Rinke-

Hardekopf et al., 2019). Accommodation space creation during deposition of the McMurray was primarily controlled by the onset of transgression of the Boreal Sea, although evaporite karst and carbonate epikarst are recognized to have created additional accommodation space locally as well (e.g., McPhee and Wightman, 1991; Crerar and Arnott, 2007; Fustic et al., 2012; Broughton, 2013, 2014, 2015a, b; Barton et al., 2017; Hauck et al., 2017).

1.3. Study area

The MDC extends over 44 000 km^2 within the Alberta Foreland Basin, from 55–58° N and 110–114° W (Fig. 1.1). Paleotopography of the basal surface of the MDC is defined by the relief on the Sub-Cretaceous Unconformity (SCU) with the main north-south topographic low commonly referred to as the "Assiniboia Valley" (e.g., Christopher, 1984; Blum and Pecha, 2014). Along the axis of the Assiniboia Valley, DUs were completely removed by subsequent channel-belt incision and migration. The southwestern quadrant of the MDC (townships (T) 69–83, ranges (R) 9–20W4; Figs. 1.1 and 1.3) is located west of the Assiniboia Valley and along the margins of the Grosmont Highlands. It extends over 15 850 km^2 and includes the Grouse, Sparrow, and Pelican paleovalleys. These paleovalleys preserve minimal strata from the lower member of the McMurray Fm (LM, Fig. 1.2), and a nearly continuous succession of DUs from the middle and upper McMurray Fm with only limited removal by channel belts (Ranger and Pemberton, 1997; Weleschuk and Dashtgard, 2019).

Grouse Paleovalley extends over 150 km from SW to NE and covers an area of 4 570 km^2. Sparrow Paleovalley extends over 139 km from SW to NE and covers an area of 3 260 km^2. Pelican Paleovalley extends over 96 km from SW to NE and covers an area of 2 420 km^2. All three paleovalleys coalesce towards the NE (Fig. 1.3).

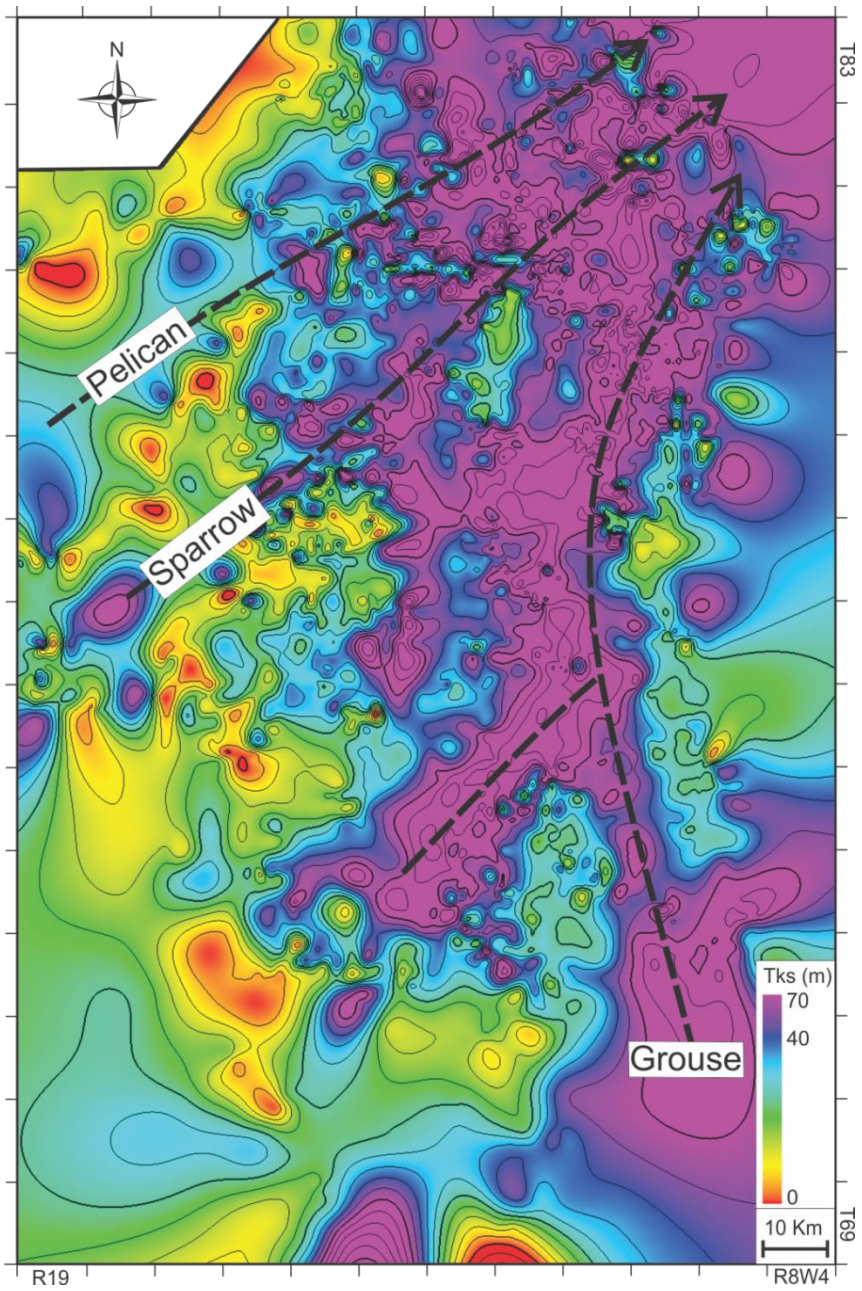

Figure 1.3. Isopach map of the McMurray Fm in the study area.
Maximum thicknesses are observed along the axes of the Pelican, Sparrow and Grouse paleovalleys and minimum thicknesses over the carbonate highlands (tks = thickness; modified from Château et al., in press).

1.4. Objectives

The main research objective of this thesis is to further refine our understanding of the impact of accommodation space creation on the facies characteristics, depositional architectures and stratigraphic framework of coastal- to shallow-marine deposits in a

low-accommodation space setting. This is done using detailed facies analyses linked to statistical analyses, depositional architecture and sequence stratigraphic work of the Lower Cretaceous McMurray Fm in the southwest quadrant of the MDC. The primary objectives are to: 1) recognize mechanisms that created accommodation space in the study area; 2) determine the amount of accommodation space created during deposition of the formation; and 3) analyse changes in accommodation space creation and outline changes in the rate of transgression in a low-accommodation space setting.

1.5. Thesis organization

This thesis is divided into five chapters, comprising this introduction (Chapter 1), three manuscripts (one published, one in press and one in preparation; Chapters 2-4) and the conclusions (Chapter 5)).

Chapter 2 focuses on a statistical approach to sedimentary research to recognise mechanisms creating accommodation space in a low-accommodation space setting. Stratigraphic cross-sections are generated to resolve the geometry and the architecture of DUs comprising the middle and upper McMurray Fm in the Sparrow Paleovalley (SPV). In the SPV, isopach mapping delineates the extent of accommodation space creation and identifies areas of anomalous thickness. Statistics are used to quantitatively assess the anomalies in DUs thickness and determine the amount of accommodation created before, during, and after deposition of the McMurray Fm in the area. Finally, mechanisms responsible for accommodation space creation and the impacts of these processes on deposition in a low-accommodation setting are discussed. A version of this chapter has been published as Chateau et al. (2019) in the Journal of Marine and Petroleum Geology.

Chapter 3 focuses on the amount of accommodation space created during the deposition of the Regional C (equivalent to middle McMurray), the most understudied depositional unit of the McMurray Fm. In the southwest quadrant of the MDC, the Regional C is well preserved and areally extensive; hence, a detailed facies analysis, depositional architecture and stratigraphic work were undertaken in the Grouse, Sparrow and Pelican paleovalleys. The stratigraphy of Regional C is revised and then used to complete the reconstruction of the depositional history of the McMurray Fm, and determine the amount of accommodation space created, which is then used to comment

on the early evolution and transgression of the Alberta Foreland Basin. A version of this chapter is currently in press, and will be published in the Journal of Sedimentary Research.

Chapter 4 focuses on the application of facies analysis and depositional architecture, tied to statistical methods to constrain and quantify changes in the rate of transgression in a low-accommodation space setting. In the Grouse, Sparrow and Pelican paleovalleys, detailed facies analysis, depositional architecture, sequence stratigraphic and statistical work were undertaken to quantitatively assess thickness variations between DUs of the Middle-Upper McMurray Fm. In a novel statistical approach, the variation in DU thicknesses is tied to transgressive mudstone facies, in order to analyse mechanisms responsible for changes in accommodation space creation and discuss these changes in the context of the rate of transgression of the Lower Cretaceous Boreal Sea. A version of this chapter is currently in preparation.

1.6. References

Alberta Energy and Utilities Board, 2003, Athabasca Wabiskaw-McMurray regional geological study: Alberta Energy and Utilities Board, Report 2003-A, 187p.

Allen, J.P., and Fielding, C.R., 2007, Sequence architecture within a low-accommodation setting: an example from the Permian of the Galilee and Bowen basins, Queensland, Australia: AAPG Bulletin, v. 91, p. 1503–1539.

Barton, M.D., Porter, I., O'Byrne, C., and Mahood, R., 2017, Impact of the Prairie Evaporite dissolution collapse on McMurray stratigraphy and depositional patterns, Shell Albian Sands Lease 13, northeast Alberta: Bulletin of Canadian Petroleum Geology, v. 65, p. 175–199.

Blum, M., and Pecha, M., 2014, Mid-Cretaceous to Paleocene North American drainage reorganization from detrital zircons: Geology, v. 42, p. 607−610.

Broughton, P.L., 2013, Devonian salt dissolution-collapse breccias flooring the Cretaceous Athabasca oil sands deposit and development of lower McMurray Formation sinkholes, northern Alberta Basin, Western Canada: Sedimentary Geology, v. 283, p. 57–82.

Broughton, P.L., 2014, Syndepositional architecture of the northern Athabasca Oil Sands Deposit, northeastern Alberta: Canadian Journal of Earth Sciences, v. 52, p. 21–50.

Broughton, P.L., 2015a, Collapse-induced fluidization structures in the Lower Cretaceous Athabasca Oil Sands Deposit, Western Canada: Basin Research, v. 28, p. 507–535.

Broughton, P.L., 2015b, Incipient vertical traction carpets within collapsed sinkhole fills: Sedimentology, v. 62, p. 845–866.

Carrigy, M.A., 1963, Paleocurrent directions from the McMurray Formation: Bulletin of Canadian Petroleum Geology, v. 11, p. 389–395.

Carrigy, M.A., 1967, Some sedimentary features of the Athabasca oil sands: Sedimentary Geology, v. 1, p. 327–352.

Catuneanu, O., 2002, Sequence stratigraphy of clastic systems: concepts, merits, and pitfalls: Journal of African Earth Sciences, v. 35, p. 1−43.

Château, C.C., Dashtgard, S.E., MacEachern, J.A., and Hauck, T.E., 2019, Parasequence architecture in a low-accommodation setting, impact of syndepositional carbonate epikarstification, McMurray Formation, Alberta, Canada: Journal of Marine and Petroleum Geology, v. 104, p. 168−179.

Château, C.C., Dashtgard, S.E., and MacEachern, J.A., in press, Refinement of the stratigraphic framework for the Regional C depositional unit of the McMurray Formation and implications for the early transgression of the Alberta Foreland Basin, Canada: Journal of Sedimentary Research.

Château, C.C., Dashtgard, S.E., and MacEachern, J.A., in preparation, Changes in the rate of transgression in the Lower Cretaceous McMurray Depocenter, Canada and implications for the advance of the Boreal Sea.

Christopher, J.E., 1984, The Lower Cretaceous Mannville group, northern Williston basin region, Canada: *in* Stott, D. F., and D. J. Glass, eds., The Mesozoic of middle North America: Calgary, Alberta, Canada, Canadian Society of Petroleum Geologists Memoir 9, Calgary, p. 109−126.

Crerar, E.E., and Arnott, R.W.C., 2007, Facies distribution and stratigraphic architecture of the Lower Cretaceous McMurray Formation, Lewis property, northeastern Alberta: Bulletin of Canadian Petroleum Geology, v. 55, p. 99–124.

Davies, S.J., and Gibling, M.R., 2003, Architecture of coastal and alluvial deposits in an extensional basin: the Carboniferous Joggins Formation of eastern Canada: Sedimentology, v. 50, p. 415– 439.

Durkin, P.R., Boyd, R.L., Hubbard, S.M., Shultz, A.W., and Blum, M.D., 2017a, Three-dimensional reconstruction of meander-belt evolution, Cretaceous McMurray formation, Alberta Foreland Basin, Canada: Journal of Sedimentary Research, v. 87, p. 1075−1099.

Durkin, P.R., Hubbard, S.M., Holbrook, J.M., and Boyd, R., 2017b, Evolution of fluvial meander-belt deposits and implications for the completeness of the stratigraphic record: Geological Society of America Bulletin, v. 130, p. 721−739.

Flach, P.D., and Mossop, G.D., 1985, Depositional environments of Lower Cretaceous McMurray Formation, Athabasca Oil Sands, Alberta: American Association of Petroleum Geologists Bulletin, v. 69, p. 1195–1207.

Fustic, M., Bennett, B., Huang, H., and Larter, S., 2012, Differential entrapment of charged oil – new insights on McMurray Formation oil trapping mechanisms: Journal of Marine and Petroleum Geology, v. 36, p. 50−69.

Hauck, T.E., Peterson, J.T., Hathway, B., Grobe, M., and MacCormack, K., 2017, New insights from regional-scale mapping and modelling of the Paleozoic succession in northeast Alberta: paleogeography, evaporite dissolution, and controls on Cretaceous depositional patterns on the Sub-Cretaceous Unconformity: Bulletin of Canadian Petroleum Geology, v. 65, p. 87–114.

Hein, F.J., Dolby, G., and Fairgrieve, B., 2013, A regional geologic framework for the Athabasca oil sands, northeastern Alberta, Canada: *in* Hein F.J., Leckie D., Larter S., and Suter J.R., eds., Heavy-oil and Oil-sand Petroleum Systems in Alberta and Beyond: American Association of Petroleum Geologists Studies in Geology 64, p. 207–250.

Hein, F., and Dolby, G., 2017, Lithostratigraphy, palynology, and biostratigraphy of the Athabasca Oil Sands deposit, northeastern Alberta: Alberta Geological Survey, Open File Report 8, 105 p.

Horner, S.C., Hubbard, S.M., Martin, H.K., and Hagstrom, C.A., 2019, Reconstructing basin-scale drainage dynamics with regional subsurface mapping and channel-bar scaling, Aptian, Western Canada Foreland Basin: Sedimentary Geology, v. 385, p. 26-44.

Hubbard, S.M., Smith, D.G., Nielsen, H., Leckie, D.A., Fustic, M., Spencer, R.J., and Bloom, L., 2011, Seismic geomorphology and sedimentology of a tidally influenced river deposit, Lower Cretaceous Athabasca Oil Sands, Alberta, Canada: American Association of Petroleum Geologists Bulletin, v. 95, p. 1123−1145.

Jardine, D., 1974, Cretaceous oil sands of Western Canada: *in* Hills, L.V., ed., Oil Sands, Fuel of the Future: Canadian Society of Petroleum Geologists, Memoir 3, p. 50−67.

Jervey, M.T., 1988, Quantitative geological modeling of siliciclastic rock sequences and their seismic expression: *in* Wilgus, C.K., Hasting, B.S., Kendall, C.G.St.C, Posamentier, HW, Ross, CA, and Van Wagoner, JC, eds., Sea-level changes: an integrated approach: Society of Economic Paleontologists and Mineralogists, Special Publication 42, p. 47−69.

McPhee, D.A., and Wightman, D.M., 1991, Timing of the dissolution of Middle Devonian Elk Point Group Evaporites - Twps. 47 to 103 and Rges. 15 W3M to 20 W4M (abs.): Bulletin of Canadian Petroleum Geology, v. 39, p. 218.

Mitchum Jr., R.M., 1977, Seismic stratigraphy and Global Changes of Sea Level: Part 11. Glossary of Terms used in Seismic stratigraphy: Section 2: Application of Seismic Reflection Configuration to Stratigraphic Interpretation, Memoir 26, p. 205−212.

Mossop, G.D., and Shetsen, I., 1994, Introduction to the Geological Atlas of the Western Canada Sedimentary Basin: *in* Mossop G.D., and Shetsen, I., eds, Geological Atlas of the Western Canadian Sedimentary Basin: Canadian Society of Petroleum Geologists and Alberta Research Council, Calgary, Alberta, p. 1–12.

Musial, G., Reynaud, J.Y., Gingras, M.K., Féniès, H., Labourdette, R., and Parize, O., 2012, Subsurface and outcrop characterization of large tidally influenced point bars of the Cretaceous McMurray Formation (Alberta, Canada): Sedimentary Geology, v. 279, p. 156–172.

Plint, A.G., Hart, B.S. and Donaldson, W.S., 1993, Lithospheric flexure as a control on stratal geometry and fades distribution in Upper Cretaceous rocks of the Alberta foreland basin: Basin Research, v. *5*, p.69−77.

Porter, J.W., Price, R.A., and McCrossan, R.G., 1982, The Western Canada Sedimentary Basin: Philosophical Transactions of the Royal Society A: Mathematical, Physical and Engineering Sciences, v. 305, p. 169–192.

Posamentier, H.W., and Allen, G.P., 1999, Siliciclastic sequence stratigraphy: concepts and applications: SEPM, Concepts in Sedimentology and Paleontology, 210 p.

Poulton, T.P., Christopher, J.E., Hayes, B.J.R., Losert, J., Tittemore, J. and Gilchrist, R.D., 1994, Jurassic and Lowermost Cretaceous strata of the Western Canada Sedimentary Basin: *in* Mossop, G.D., Shetsen, and I., eds., Geological Atlas of the Western Canada Sedimentary Basin: Canadian Society of Petroleum Geologists and Alberta Research Council, Chapter 18, 20 p.

Ranger, M.J., and Pemberton, S.G., 1997, Elements of a stratigraphic framework for the McMurray Formation in south Athabasca area, Alberta: *in* Pemberton S.G. and James D.P., eds., Petroleum Geology of the Cretaceous Mannville Group, Western Canada,Canadian Society of Petroleum Geologists, Memoir 18, p. 263–291.

Ranger, M.J., Gingras, M.K., and Pemberton, S.G., 2008, The role of ichnology in the stratigraphic interpretation of the Athabasca oil sands: Search and Discovery Article, v.30, p. 1–8.

Ratcliffe, K.T., Wright, A.M., Hallsworth, C., Morton, A., Zaitlin, B.A., Potocki, D., and Wray, D.S., 2004, An example of alternative correlation techniques in a low-accommodation setting, nonmarine hydrocarbon system: the (Lower Cretaceous) Mannville Basal Quartz succession of southern Alberta: AAPG Bulletin, v. 88, p. 1419–1432.

Rinke-Hardekopf, L., Dashtgard, S.E., and MacEachern, J.A., 2019, Earliest Cretaceous transgression of North America recorded in thick coals: McMurray Sub-Basin, Canada: International Journal of Coal Geology, v. 204, p. 18–33.

Rygel, M.C., and Gibling, M.R., 2006, Natural geomorphic variability recorded in a high-accommodation setting: Fluvial architecture of the Pennsylvanian Joggins Formation of Atlantic Canada: Journal of Sedimentary Research, v. 76, p. 1230–1251.

Schneider, C.L., and Grobe, M., 2013, Regional Cross-sections of Devonian stratigraphy in northeastern Alberta (NTS 74D, E): Alberta Energy Regulator, AER/AGS Open File Report, v. 5, 25 p.

Schneider, C., Mei, S., Haug, K., and Grobe, M., 2014, The Sub-Cretaceous Unconformity and the Devonian subcrop in the Athabasca Oil Sands area, townships 87–99, ranges 1–13, west of the Fourth Meridian: Alberta Geological Survey, Open File Report 2014-07, 39 p.

Weleschuk, Z.P., and Dashtgard, S.E., 2019, Evolution of an ancient (Lower Cretaceous) marginal-marine system from tide-dominated to wave-dominated deposition, McMurray Formation: Sedimentology, v. 66, p. 2354−2391.

Zaitlin, B.A., Warren, M.J., Potocki, D., Rosenthal, L., and Boyd, R., 2002, Depositional styles in a low accommodation foreland basin setting: An example from the Basal Quartz (Lower Cretaceous), southern Alberta: Bulletin of Canadian Petroleum Geology, v. 50, p. 31–72.

Chapter 2.

Parasequence architecture in a low-accommodation setting: Impact of syndepositional carbonate epikarstification, McMurray Formation, Alberta, Canada

Abstract

The Sparrow Paleovalley (SPV) is situated in the southwest corner of the McMurray Sub-Basin, Alberta, Canada, and drained a portion of the Grosmont Highlands on a sub-Cretaceous paleotopographic surface. The regional stratigraphic architecture of the Lower Cretaceous McMurray Formation in SPV comprises a series of regressive parasequences (PS) organized into depositional units (DU), the latter of which are separated by regionally mappable flooding surfaces. Isopach maps of individual DUs show that in general they have a consistent thickness, although stratal thickening of DUs occurs in the landward part of the SPV and extends over an area of 400 km^2. This stratal thickening ranges from +21% to +45% and is accompanied by increases in both the abundance of soft-sediment deformation structures (SSD) and normal micro-faults in PSs, and an increase in the number and thickness of PSs. The thickness disparity between the overthickened zone compared to the rest of the SPV is statistically significant and points to an external control on the accumulation of DUs.

The McMurray Formation unconformably overlies a complex distribution of Devonian strata that subcrop at the Sub-Cretaceous Unconformity below the SPV. Devonian strata include, from east to west (oldest to youngest), the Beaverhill Lake, Woodbend, and Winterburn groups. In the western reaches of the SPV, McMurray Fm deposits overlie and are flanked by strata of the Woodbend and Winterburn groups, the latter of which experienced erosion and carbonate epikarstification when subaerially exposed. Subsidence through epikarstification of Devonian carbonates generated localized deepening in the McMurray Sub-Basin, which was infilled during deposition of

Chapter 2 was previously published in the Journal of Marine and Petroleum Geology as
Château, C.C., Dashtgard, S.E., MacEachern, J.A., and Hauck, T.E., 2019, Parasequence architecture in a low-accommodation setting, impact of syndepositional carbonate epikarstification, McMurray Formation, Alberta, Canada: Marine and Petroleum Geology, v.104, p.168−179.

DUs and resulted in overthickening of McMurray strata. The correspondence of topographic lows on the Sub-Cretaceous Unconformity and overthickening of DUs overlying these topographic lows indicates that active carbonate epikarstification of Devonian strata was contemporaneous with deposition of the McMurray Formation.

2.1. Introduction

The regional stratigraphic architecture of the Lower Cretaceous McMurray Formation in the McMurray Sub-Basin (MSB), Alberta, Canada comprises a series of regressive parasequences (PS) organized into discrete depositional units (DU) that are cut into by nested and deeply incised fluvio-estuarine channel belts (Ranger and Pemberton, 1997; Hein et al., 2000; Alberta Energy and Utilities Board, 2003). Depositional units encompass multiple progradational cycles (PSs) each bound by autogenic flooding surfaces (cf. Van Wagoner et al., 1990; Allen and Posamentier, 1993; Kamola and Van Wagoner, 1995), and DUs are bounded by regionally extensive transgressive flooding surfaces. Fluvio-estuarine channel belts, which are prevalent throughout the MSB and form the primary hydrocarbon reservoirs, consist of both channel bars and channel fills of tidally influenced rivers that experienced brackish-water conditions (e.g., Pemberton et al., 1982; Gingras et al., 2016; Baniak et al., 2018; Weleschuk and Dashtgard, 2019). While the DUs themselves are not the primary reservoir target in the McMurray Formation, determining their stratal architecture is vital for resolving the stratigraphic framework of the MSB (Ranger et al., 1994, 2008; Ranger and Pemberton, 1997; Alberta Energy and Utilities Board, 2003; Hein and Cotterill, 2006; Hein et al., 2013). Five DUs are distinguished in the MSB (from oldest to youngest): Regional C, B2, B1, A2 and A1 (Fig. 2.1). The thickness of most DUs (B2 to A1) ranges from 6–10 m, and this has led to the interpretation that the MSB was a low-accommodation setting during deposition of the McMurray Fm (Ranger and Pemberton, 1997; Hein and Cotterill, 2006; Ranger et al., 2008; Hein et al., 2013). Accommodation refers to the amount of space available for sediment accumulation, and changes in accommodation play an important role in the distribution and geometry of sequences and parasequences, as well as the character of their bounding surfaces (Jervey, 1988; Zaitlin et al., 2002). Syndepositional accommodation tied to evaporite karst has been recognized in the Assiniboia Paleovalley in the lower McMurray Fm based on sedimentological and stratigraphic evidence of accommodation space creation

(Broughton, 2013; LM1 and LM2 of Barton et al., 2017; equivalent to LM1 in Fig. 2.1). Accommodation space creation in overlying units (Regional C–A1, Fig. 2.1) was primarily controlled by the onset of transgression of the Boreal Sea (Ranger and Pemberton, 1997; Hein and Cotterill, 2006; Ranger et al., 2008; Hein et al., 2013) and regionally extensive flooding surfaces that bound DUs record rapid transgression. By contrast, shoreline progradation responsible for deposition of DUs occurred during periods of stable or slowly rising base level (Weleschuk and Dashtgard, 2019). The succession from depositional unit Regional C to A1 records stacking of DUs and reflects Boreal Sea transgression. However, the impact of localized accommodation space creation (syndepositional collapse) on the depositional architecture of Regional C (middle McMurray), and B2 to A1 (upper McMurray) has not been described. Herein, we evaluate the geometry and stratigraphy of DUs comprising the middle and upper McMurray Formation in Sparrow Paleovalley (SPV; Fig. 2.1), and use statistics to quantitatively assess variations in isopach thicknesses. Isopach mapping is employed to determine the extent and amount of accommodation space creation that occurred in the SPV during deposition of Regional C to A1. We then discuss the mechanisms that created accommodation space and the impacts of these processes on deposition in a low-accommodation setting.

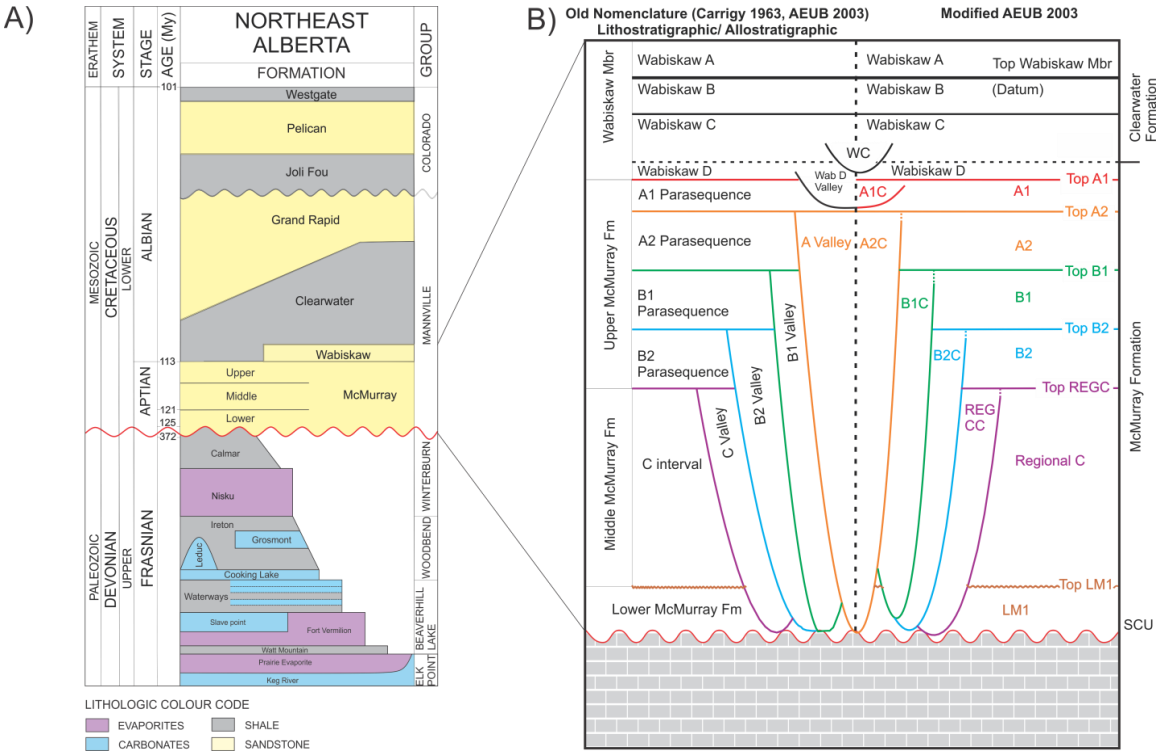

Figure 2.1. Comparison of stratigraphic frameworks proposed for the McMurray Sub-Basin.

(A) Chronostratigraphic framework for the McMurray Sub-Basin. The age of the top of the lower McMurray Fm is derived from Rinke-Hardekopf et al. (2019). (B) High-resolution stratigraphic model for the McMurray Formation. On the far left (vertical text) is the lithostratigraphic nomenclature proposed by Carrigy (1963). In the middle left is the lithostratigraphic/allostratigraphic model developed by the Alberta Energy and Utilities Board (2003; now Alberta Energy Regulator), and on the right is a modified version of the Alberta Energy and Utilities Board (2003) model used by the McMurray Geology Consortium. In the modified AEUB (2003) stratigraphy, fluvio-tidal channels are labelled as McMurray channel belts rather than valleys (e.g., A2C), as the latter term implies valley incision during relative base-level fall. Instead we consider depositional units to represent regressive cycles cut into by channel belts that are both contemporaneous and post-depositional. The channel belts are bounded at their bases by autogenic erosion surfaces, and by either a regional flooding surface (i.e., transgressive surface of erosion (TSE)) or local flooding surface (i.e., parasequences overlying channel belts deposits) at their tops.

2.1.1. Geological setting: regional context

The Late Jurassic to Early Eocene development of the foreland basin portion of the WCSB occurred during successive collisional tectonic phases. Oblique collision of allochthonous terranes against the western margin of the westward-moving North American craton led to tectonic loading and the formation of a foreland basin in the craton interior (Porter et al., 1982; Mossop and Shetsen, 1994; Price, 1994). The uplift of the WCSB associated with relative sea-level fall led to erosion of previously deposited

carbonate strata and the formation of the Sub-Cretaceous Unconformity (SCU; Jardine, 1974). The paleotopography of the SCU significantly influenced the architecture of deposits within the MSB.

Along the axis and eastern extent of the MSB, variations in the creation of accommodation space have been attributed to the removal of up to 200 m of halite and anhydrite/gypsum from the underlying Devonian-aged Prairie Evaporite Formation. This intrastratal evaporite karst occurred through the influx of undersaturated waters and led to concomitant collapse and subsidence of overlying carbonates and shales of the Beaverhill Lake Group (McPhee and Wightman, 1991; Crerar and Arnott, 2007; Schneider and Grobe, 2013; Broughton, 2013, 2015a; Schneider et al., 2014; Barton et al., 2017; Hauck et al., 2017). Collapse of Devonian-aged strata modified the paleotopography of the SCU and impacted sediment distribution during McMurray Fm deposition in the Assiniboia Paleovalley (Fig. 2.2; Broughton, 2013, 2014, 2015a). The regional subsidence trough (thousands of square kilometres) that underlies the Assiniboia Paleovalley forms over and east of the Prairie Evaporite halite dissolution scarp (Meijer Drees, 1994; Broughton, 2015b; Hauck et al., 2017). Outside of the main Assiniboia Paleovalley, evaporite karst within the Prairie Evaporite Formation has not been documented (Hauck et al., 2017).

West of the salt dissolution scarp, deposits of the McMurray Formation unconformably overlie the subcrop of multiple Devonian formations. The lithologies of these Devonian strata vary between carbonates (variably dolomitized) and intervening calcareous shales and argillaceous carbonates. The study area is located above subcropping Waterways, Cooking Lake, lower Ireton, Grosmont, upper Ireton, and Nisku formations (listed from northeast to southwest (oldest to youngest); Fig. 2.1). The Nisku and Grosmont are both mostly clean carbonates, with a thin intervening argillaceous carbonate (marl) known as the upper part of the Ireton Formation. The Nisku and Grosmont experienced erosion and carbonate epikarstification during subaerial exposure when in close proximity to the water table (Anderson and Knapp, 1993; Dembicki and Machel, 1996).

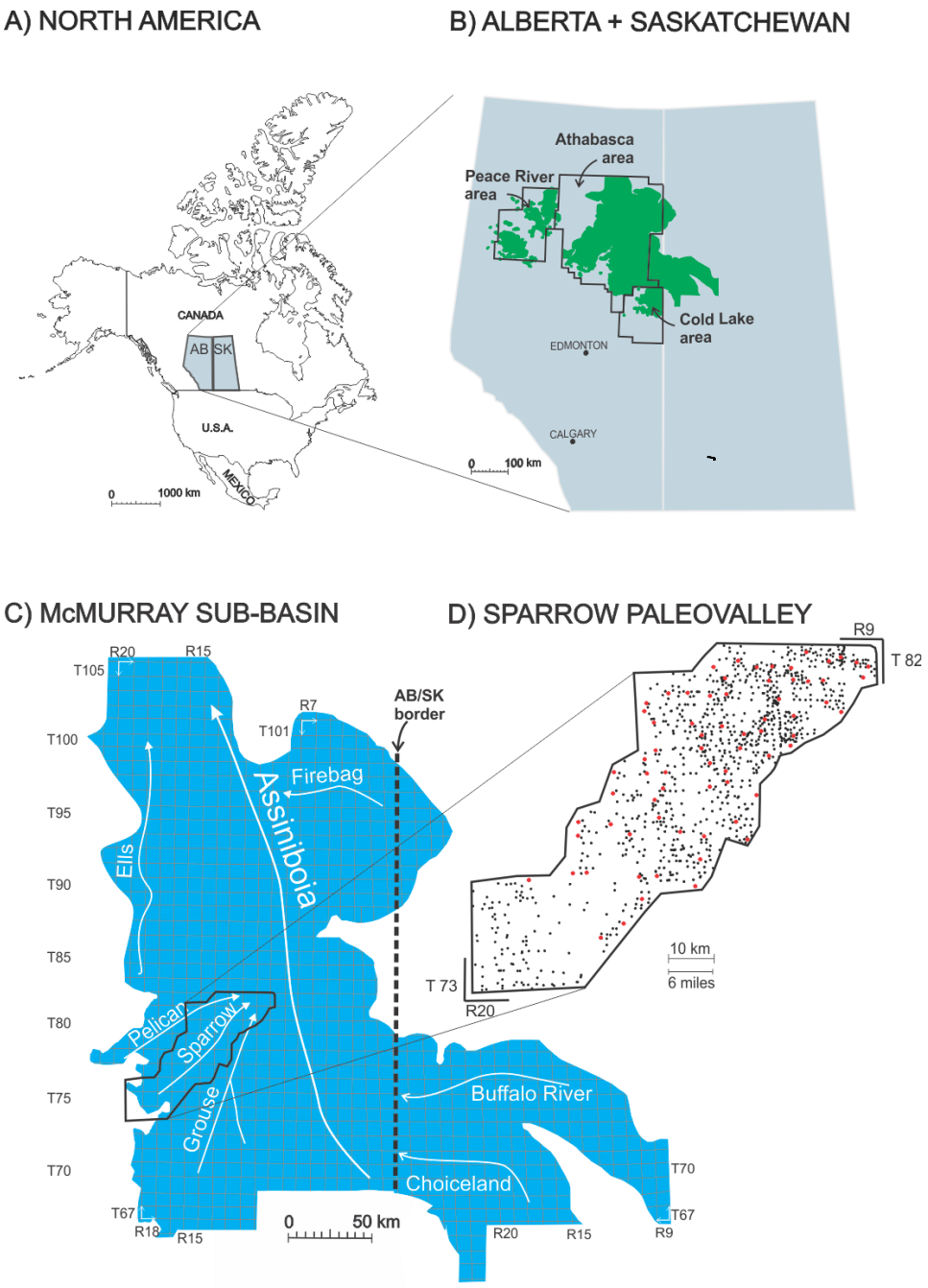

Figure 2.2. Sparrow Paleovalley location map.

A) Position of Alberta (AB) and Saskatchewan (SK) in Canada, and B) the 3 main oil sands deposits (green). C) McMurray Fm strata define the limit of the MSB, and the extent of the McMurray Fm and time-equivalent deposits in AB and SK are shown in blue. The arrows in C demarcate the main paleovalley axes as defined by depositional lows on the Sub-Cretaceous Unconformity. Pelican, Sparrow, Grouse, and Firebag refer to secondary paleovalleys that drained into the main Assiniboia Valley (Christopher, 1997). Ells Paleovalley is a distinct valley disconnected from the Assiniboia Valley. Sparrow Paleovalley outlined with a black polygon is the study area described herein. The margins of the MSB in the south, west and north are derived from the Alberta Energy and Utility Board (AEUB, 2003), whereas the eastern extent is theoretical, and based on surface projections and basin reconstruction presented in Jean (2018).

D) Distribution of the 1 000 wells (black dots) and 70 cores (red dots) that form the dataset used in this project.

2.1.2. Study Area: Sparrow Paleovalley (SPV)

The McMurray Sub-Basin extends over 26 000 km^2 from latitude 55–58° N and longitude 110–114° W (Fig. 2.2; Ranger and Pemberton, 1997; Hein et al., 2013). Paleotopography in the MSB is largely dictated by relief on the Sub-Cretaceous Unconformity. The MSB includes multiple paleovalleys filled with regionally extensive DUs that are cut into by nested and deeply incised fluvio-tidal channel belts (cf. Pattison, 2018). Along the main axis of the Assiniboia Valley, DUs have been completely removed by channel belt incision and migration. The southwestern quadrant of the MSB (townships (T) 69–83, ranges (R) 9–20W4; Fig. 2.2) also comprises paleovalleys; however, these paleovalleys record a continuous succession of DUs from Regional C to A1 with only limited removal of DUs by channel belts.

Sparrow Paleovalley extends over 139 km from SW to NE and covers an area of 3 260 km^2 (Fig. 2.2D). Within the paleovalley, DUs are well preserved in the SW reaches, but are increasingly removed by channel-belt erosion to the NE. The limited removal of DUs in SPV makes this an ideal setting for characterizing these deposits and for evaluating their thickness variations. Sparrow Paleovalley is located between T73–83 and R9–20W4, and traverses the Winterburn and Woodbend Group subcrop belts on the SCU, including the Nisku Formation and the Grosmont Highlands in the western reaches (Fig. 2.2D). Eastward, the McMurray Fm in SPV overlies older strata of the Woodbend and Beaverhill Lake groups (Fig. 2.1). Transgressive lags of the Wabiskaw Member of the Clearwater Formation cap the McMurray Formation (Fig. 2.1).

Isopach thickness of the McMurray Fm in SPV reaches 71 m (Fig. 2.3), and thickness variations reflect paleotopography on the SCU. The McMurray Fm thickness varies spatially and can be grouped into three zones (Fig. 2.3). The first or inner zone (T73–75, R16–20W4) is characterized by a SW–NE-oriented paleotopographic low on the SCU. In the inner zone, isopach values thin to the NW and SE corresponding to paleotopographic highs referred to as the Grosmont Highlands. The central zone (T77–80, R13–15W4) is a continuation of the SW–NE-oriented SCU depression, but also contains multiple confluences with adjacent, smaller-scale depressions interpreted as SPV tributaries. Finally, the outer zone (T80–83, R8–12W4) is typified by a paucity of

paleotopographic highs and includes the confluence of the SPV with two major paleotopographic lows on the SCU, referred to as Grouse and Pelican paleovalleys.

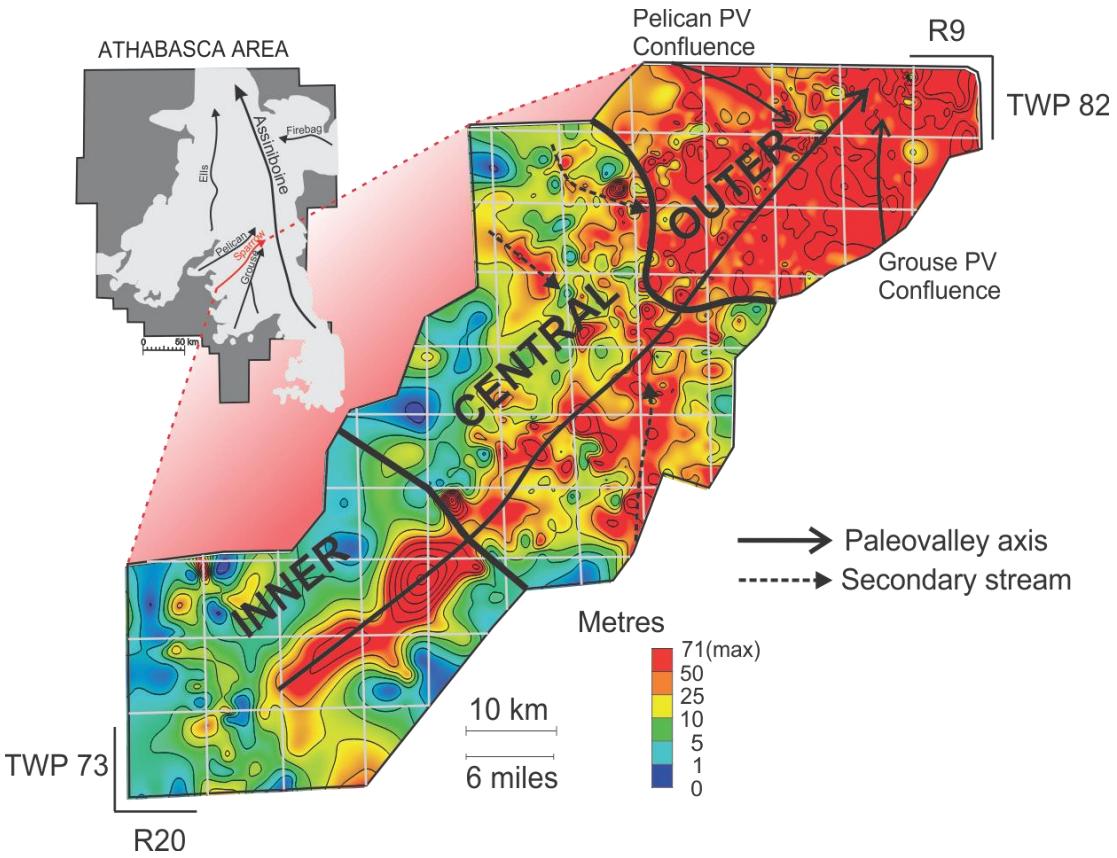

Figure 2.3 McMurray Fm isopach map along the axis of the Sparrow Paleovalley.

The thick black arrow demarcates the Sparrow Paleovalley axis. Secondary tributary valleys that drain into SPV are denoted by the thin dashed black arrows. The axes of the Pelican and Grouse paleovalleys are shown by thin solid black arrows. Blues and greens reflect paleotopographic highs (thin intervals), and reds and oranges demarcate paleotopographic lows. Sparrow Paleovalley can be divided into three zones: inner, central, and outer. See the text for details.

2.2. Methods and Database

In this study, 70 cores were logged and correlated with geophysical well logs from 1 000 wells along the SPV (Fig. 2.2D). In each core, sedimentological and ichnological characteristics were recorded using AppleCORE logging software (donated by Mike Ranger). In the area, 4000 geophysical well logs with wireline logging through the McMurray Formation are listed from the database of geoSCOUT software; however only 1000 well logs include LAS files with geophysical data attached to it (gamma-ray, spontaneous potential, caliper, resistivity, neutron porosity, sandstone density porosity)

and were exported into Petrel software for correlation and mapping purposes. Geophysical characteristics tied to sedimentology were used to define PSs, DUs and channels using existing parameters previously defined for the MSB (Ranger and Pemberton, 1997; Hein and Cotterill, 2006; Ranger et al., 2008; Hein et al., 2013, Weleschuk and Dashtgard, 2019).

Well positions are given as unique well identifiers (UWI) that define a position based on the Dominion Land Survey (DLS) coordinate system. The DLS system is a grid system used in western Canada. The grid, based on 6-mile increments, divides western Canada into south−north columns of ranges and east-west rows of townships. Each township and range block is referred to as a township and covers an area of 36 mi^2 (approximately 93 km^2). The position of each well can be determined by comparison of the UWI to the DLS system. All cross-sections and maps presented in the results and discussion sections are made accordingly to the DSL coordinate system.

Cross-sections on-axis and across-axis of the SPV were generated to resolve the architecture of PSs and DUs in SPV. The Top Wabiskaw Member surface is a horizontal surface easy to correlate across the MSB and is used as a datum. Cross-sections are used to extend flooding surfaces westward to their termination against the Grosmont Highlands and aid in distinguishing between PSs and DUs. Finally, isopach maps are constructed using an interpolation method into Petrel for each DU to delineate their distribution and identify areas of anomalous thickness (i.e., overthickening).

2.2.1. Statistical analyses

Statistical analyses are done to quantitatively assess thickness trends using 1 000 geophysical well logs (Fig. 2.2D) from the SPV. Isopach thicknesses of Regional C to A1 DUs, UWI, longitude, latitude, zone (i.e., inner, central, outer), kelly bushing, and true vertical depth for all wells were exported from Petrel into a spreadsheet. Exported data were statistically analyzed using RStudio environment of the open-source R Project software (Marx, 2013; Gandomi and Haider, 2015; Rs. Team, 2015). Statistical analysis of the mean, median, variance, standard deviation and mean growth rate (i.e. the variation in percent of means between a standard zone (SPV) and the other zones (inner, central, outer and CO-SPV)) were calculated to quantitatively estimate DU thickness variations in the SPV. In order to limit the impact of DUs distribution on the

DUs thickness values (i.e. zone with high DU distribution is paired with high DU mean thickness value while zone with low DU distribution is associated with low DU mean thickness value) only positive thickness values were included in the calculus.

A two-sample Kolmogorov–Smirnov test (K-S) compared the distributions of thickening for each DU using the STATS package in R Project software (RDC Team, 2013). The aim of the K-S test is to determine whether two samples (overthickened vs background) are similarly distributed. The K-S test calculates the distance between two empirical cumulative distribution functions and tests the null hypothesis that two cumulative distribution functions from two samples randomly drawn from the same population should be close (*P* value > 0.05; one-sided population). If the two samples are drawn from populations with different distributions (*P* value < 0.05; two-sided population), then it indicates a statistically significant DU thickness variation. For a valid test, each sample needs n > 30.

Analytical work was conducted on strata from each zone of the SPV (Fig. 2.3). The purpose of the statistical tests is to determine whether visually recognizable overthickening falls within the normal range of thickness variations (<10% from the mean) or whether it is anomalous (>10% from the mean) compared to the background thickness variation of DUs in the SPV. The thickness distributions of DUs are plotted using the ggplot functionality of the tydiverse package in R (Wickham, 2016; Wickham and Grolemund, 2016).

2.3. Results

2.3.1. Characterization of parasequences and depositional units

Parasequences in Sparrow Paleovalley are similar to those defined by Ranger and Pemberton (1997) and Hein et al., (2013). Complete parasequences form coarsening-upward successions marked by a basal dark-grey wavy parallel laminated mudstone that passes upwards into a bioturbated silty and fine-grained sandy heterolithics and is capped by fine-grained sand that exhibits wave ripples, micro-hummocky cross stratification and low-angle parallel lamination. While most parasequences are complete, there are numerous occurrences of incomplete PSs that terminate at a flooding surface prior to deposition of the upper fine-grained sand unit.

Depositional units differ from PSs in that DUs can encompass multiple PSs and are separated by regionally mappable allogenic surfaces that extend across the SPV (Hein and Cotterill, 2006). Mudstones at the base of DUs are darker grey and show more intense bioturbation than do their basal counterparts in PSs (Fig. 2.4B–D). On well logs, basal mudstones of DUs show higher gamma-ray responses (>100 API gamma-ray) and lower density-porosity values (< 18%) compared to mudstones separating PSs (<100 API gamma-ray; > 24% density porosity; Fig. 2.4A), and the most reliable way to distinguish PSs from DUs is through the mapping of bounding discontinuities.

Parasequences and DUs are incised by channel belts, which show a blocky to fining-upward succession both in core and on gamma ray logs. The basal surface of channels is erosive and is overlain by a cross-bedded coarser grained sand that pass upward into bioturbated, inclined heterolithic stratification and capped by a rooted organic-rich mudstone. These channel belts are referred to as fluvio-tidal channels based on the work of Weleschuk and Dashtgard (in press) done in the outer reach of the SPV. On well logs, channel belts show a basal erosive surface overlain by a sandstone with low gamma-ray responses (≈ 75API gamma-ray) and high density-porosity values (>30%; Hein and Cotterill, 2006) .

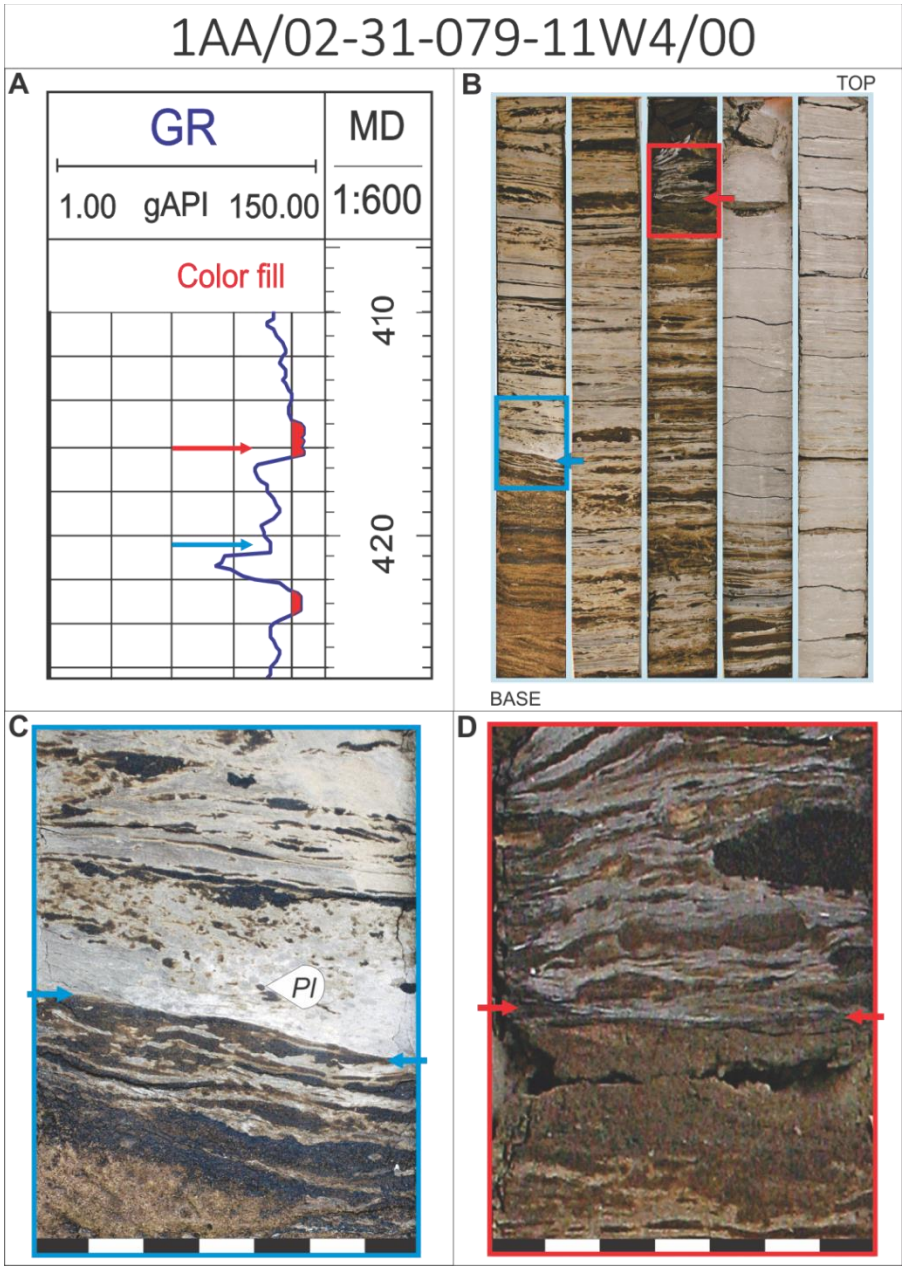

Figure 2.4 (A) Gamma-ray log of 1AA/02-31-079-11W4/00 from 410–426 m showing the characteristics of a minor flooding surface (blue arrow) and a major flooding surface (red arrow).

The red arrow marks the Top_B1 contact (416.3 m). The red shading indicates the position of the basal mudstone of A2 (416.3−415 m) and the basal mudstone of B1 (423.7−422.3 m). The blue arrow marks the top of a PS internal to B1 (420.3 m). (B) Core interval for 1AA/02-31-079-11W4/00 and from 416–420.5 m showing the two types of flooding surfaces. Beige to light gray and dark gray coloured beds are mudstones. Dark brown beds are bitumen-saturated sands. The position of Fig. 4C is shown in blue and Fig. 4D is shown in red. (C) Close-up photo of the minor flooding surface at the base of a PS internal to DU B1 (blue arrows; depth: 420.3 m). (D) Close-up photo of a major flooding surface at the base of DU A2 (Top_B1 surface) (red arrows; depth: 416.3 m).

2.3.2. Distribution of parasequences and depositional units

Parasequences bounded by flooding surfaces of local extent (<100 km^2) shingle laterally (northeastward) to form DUs constrained by allogenic flooding surfaces of regional extent (>1 000 km^2; Fig. 2.5). Each PS exhibits an asymmetrical geometry; the base pinches out to the SW (landward) and the top pinches out at their depositional limits towards the northeast (seaward). Flooding surfaces bounding individual PSs cannot be correlated regionally, while flooding surfaces bounding DUs can be correlated over the entire SPV (Figs. 2.5–2.9). All five DUs overlying the Lower McMurray are present in SPV and include multiple PSs showing substantial thickness variations between zones (Table 2.1). Depositional unit Regional C is the oldest and thickest DU, with an average thickness of 25 m. Regional C is composed of up to 10 PSs, each ranging from 3–12 m thick.

Depositional unit B2 has an average thickness of 9 m and comprises 1–5 PSs that range from 1–9 m thick (Table 2.1; Fig. 2.5). The inner zone includes thick parasequences (up to 9 m) with the thicknesses of PSs decreasing toward the top of the DU. By contrast, the central and outer zones contain numerous (up to 5) relatively thin PSs (up to 4 m).

Depositional unit B1 has an average thickness of 8 m and contains 1–6 PSs ranging from 2–7 m thick. These PSs, however, show significant thicknesses variations between zones (Table 2.1; Fig. 2.5). The inner zone includes up to 6 PSs, ranging from 1–4.5 m thick, and displays an upward decrease in parasequence thickness toward the top of B1. The central zone and outer zones contain fewer PSs (1–3), each ranging from 1.5–4.5 m in thickness.

Depositional unit A2 has an average thickness of 4 m and includes 1–3 PSs ranging from 0.5–4 m thick. Parasequence thickness variations in DU A2 are significant between zones (Table 2.1; Fig. 2.5). The inner zone includes up to 3 relatively thick PSs (up to 4 m), with the thicknesses of PSs decreasing toward the top of A2. The central zone contains 1 PS ranging from 2–3 m thick, and the outer zone encompasses up to 3 PSs ranging from 1 to 3.5 m thick.

Depositional unit A1, the youngest DU of the succession, is also the thinnest with an average thickness of 2 m. Depositional unit A1 is not regionally extensive throughout

SPV (Table 2.1; Fig. 2.5). The inner zone includes 1–2 PSs ranging from 1–3 m thick, whereas the central and outer zones contain only 1 PS up to 2 m thick.

Cross-sections (Figs. 2.6–2.9) and isopach maps (Fig. 2.10) also show trends in DU distributions. Regional C is present mainly in the central and outer zones of SPV, with rare deposits in the inner zone (Fig. 2.10). The sporadic distribution of Regional C reflects the paleotopography of the SCU, with Regional C preserved only in pronounced depositional lows. Depositional unit B2 is sparsely distributed in the inner zone of the SPV and is discontinuous in the central and outer zones (Fig. 2.10). Depositional unit B2 distribution is also impacted by SCU paleotopography and in the inner zone is only preserved in paleotopographic lows on the SCU. B1 is laterally continuous in the outer zone, and onlaps the valley margins in the NW and SE parts of the central and inner zones (Fig. 2.10). A2 deposits are regionally extensive throughout the SPV (Fig. 2.10). A1 shows a heterogeneous distribution, with deposition occurring in two areas only: T77–82, R13–15W4 and T73–75, R16–20W4 (Fig. 2.10).

Table 2.1. Data of isopach thicknesses (excluding null values) of depositional units (DU) within the SPV (all 3 zones), outer zone, central zone and inner zone (see Fig. 3 through zones). Data columns include DU, zone, mean isopach thickness (m); number of parasequences (PSs) within each DU and PSs thickness range (in metres).

Depositional Unit	Zone	Mean	PS number	PS thickness
A1	SPV	2.37	1–2 (rare)	0.5–3
	OUTER	2.18	1	0.5–2
	CENTRAL	2.18	1	0.5–2
	INNER	3.43	1–2	1–3
A2	SPV	3.87	1–3	0.5–4
	OUTER	3.76	2–3	1–3.5
	CENTRAL	3.44	1	2–3
	INNER	5.11	1–3	0.5–4
B1	SPV	8.15	1–6	2–7
	OUTER	8.01	1–3	2.5–4.5
	CENTRAL	7.96	2–3	1.5–3.5
	INNER	9.84	3–6	1–4.5
B2	SPV	8.97	1–5	1–9
	OUTER	8.84	2–5	2–4
	CENTRAL	8.77	2–3	1–3
	INNER	11.6	3–5	2–9
Regional C	SPV	24.7	1–10	0.5–12
	OUTER	24.98	4–10	0.5–7
	CENTRAL	22.34	2–7	3–12
	INNER	9.8	1–4	1–4

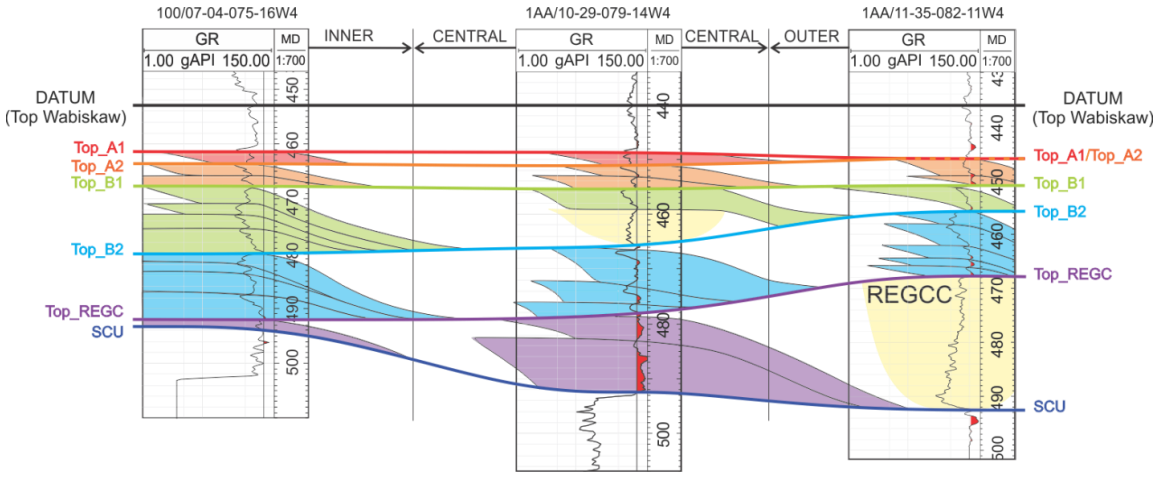

Figure 2.5 Along-axis SPV cross-section including wells 100/07-04-075-16W4 (inner zone), 1AA/10-29-079-14W4 (central zone) and 1AA/11-35-082-11W4 (outer zone) and showing depositional units (DUs) Regional C to A1.

In each DU, the internal distribution of parasequences (PSs) is shown. Parasequences are bounded by flooding surfaces of local extent and shingle laterally (northeastward) to form DUs bounded by flooding surfaces (Top_REG C, Top_B2, Top_B1, Top_A2 and Top_A1) of regional extent. Coloured PSs corresponding to individual DUs show substantial thicknesses variation in the SPV. Parasequences in the inner zone display a decrease in thickness from the base to the top of the McMurray Fm (B2−A2). Depositional units in the central zone include few, relatively thick PSs, while DUs in the outer zone include numerous, thin PSs. Fining-upward channel belt deposition occurs locally in the central and outer zones.

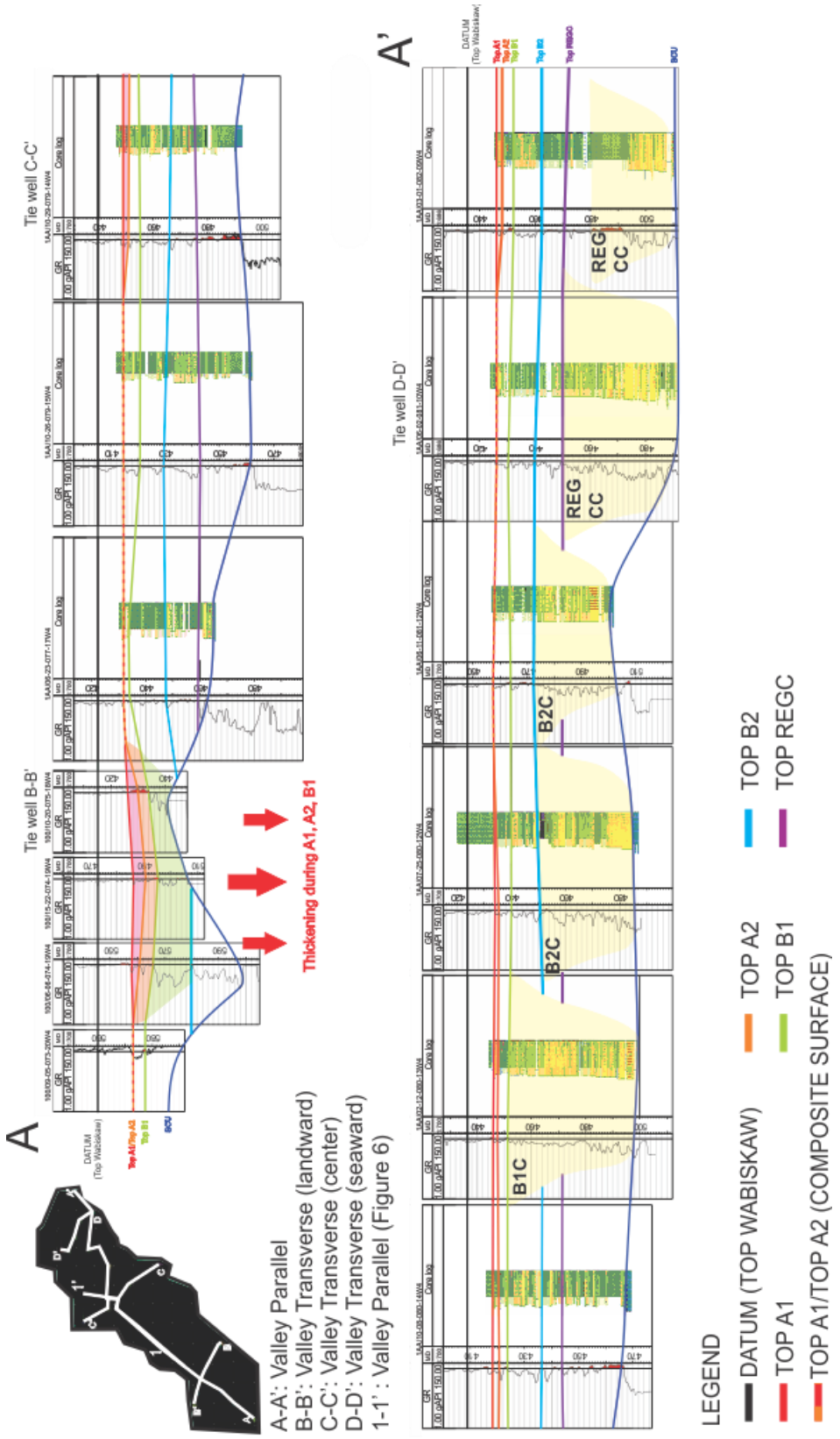

Figure 2.6 **Longitudinal cross-section A–A' extending along the entire length of the SPV.**

The map at the top left shows the lines of section for A-A' as well as those in Figures 2.7 (B–B'), 2.8 (C–C'), and 2.9 (D–D'). The datum is the top of the Wabiskaw Member of the Clearwater Formation. The top of the McMurray succession is equivalent to the TOP A1 surface or to the combined Top A1 / TOP A2 surface.

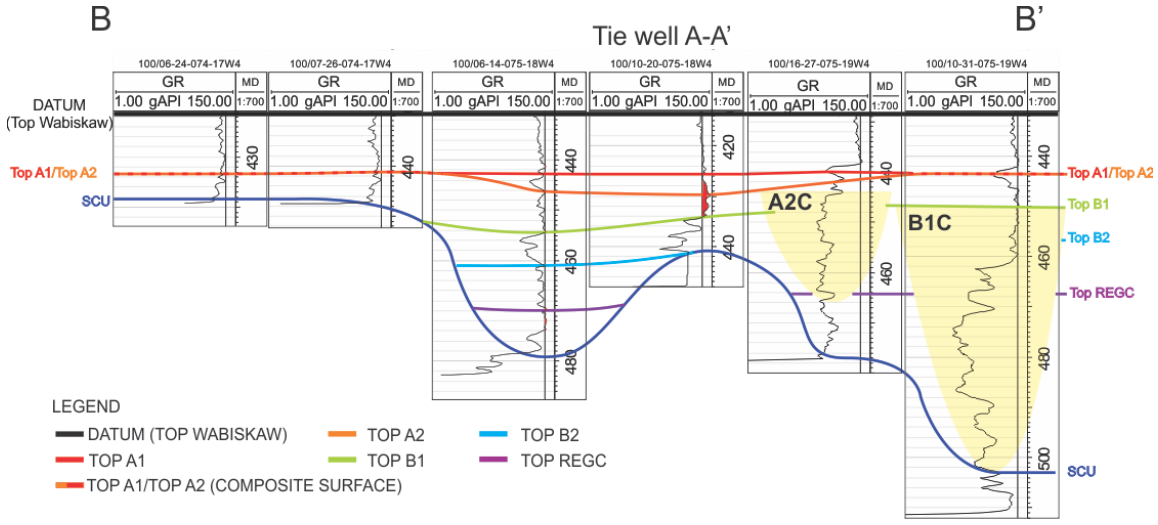

Figure 2.7 Cross-section B–B' (valley transverse) in the inner zone of the SPV.
The cross-section extends from southeast (100/06-24-074-17W4 (B)) to northwest (100/10-31-075-19W4 (B')) and the location of the line of section is shown on Figure 2.6. The datum is the top of the Wabiskaw Member of the Clearwater Formation. The top of the McMurray succession is equivalent to the combined Top A1 / TOP A2 surface.

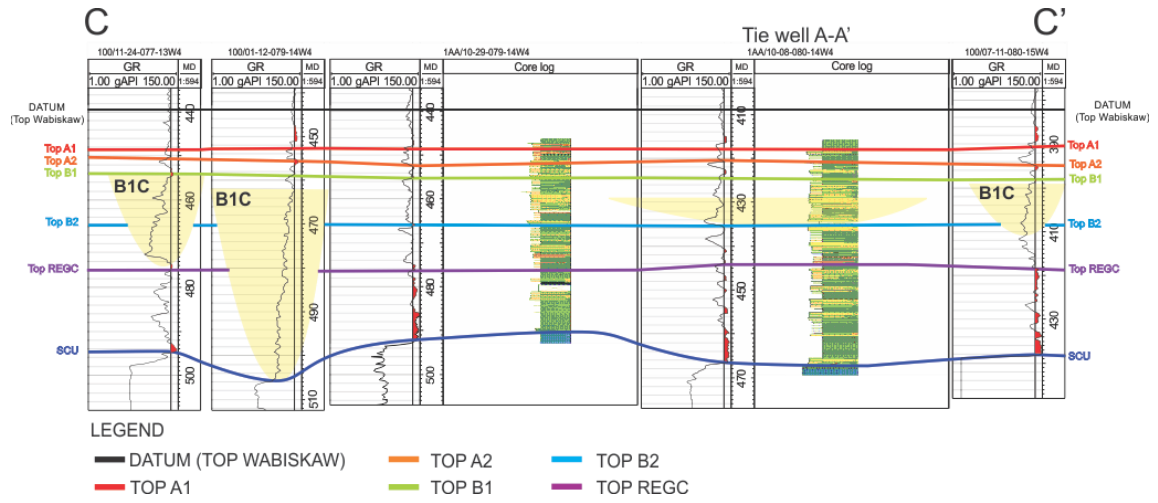

Figure 2.8 Cross-section C–C' (valley transverse) in the central zone of the SPV.
The cross-section extends from southeast (100/11-24-077-13W4 (C)) to northwest (100/07-11-080-15W4 (C')), and the line of section is shown in Figure 2.6. The datum is the top of the Wabiskaw Member of the Clearwater Formation and the top of the McMurray succession is equivalent to the TOP A1 surface.

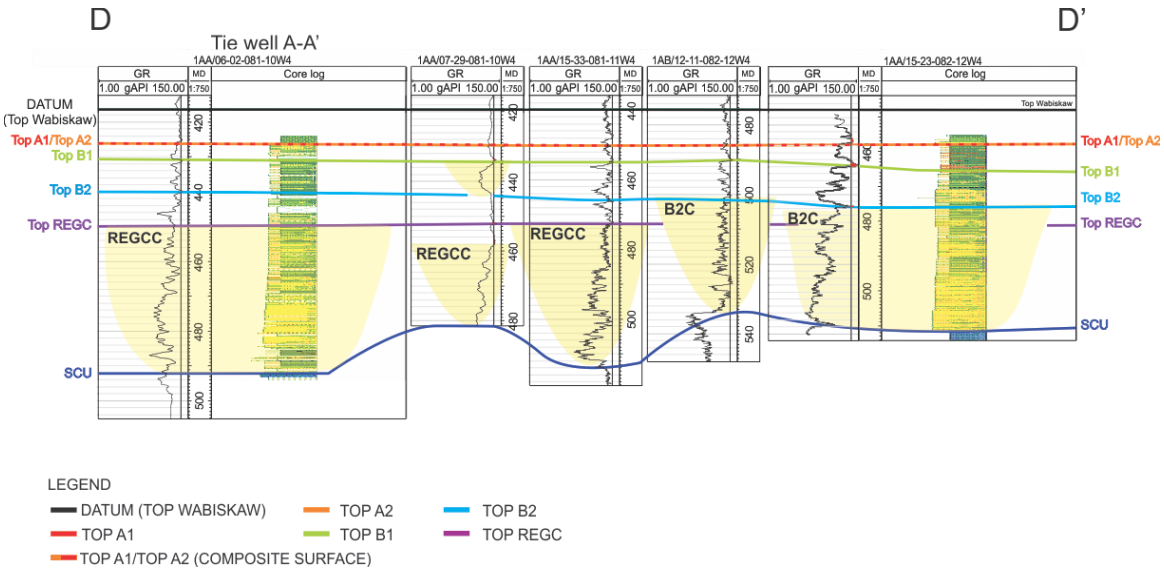

Figure 2.9 Cross-section D–D' (valley transverse) in the outer zone of the SPV. The cross-section extends from southeast (1AA/06-02-081-10W4) to northwest (1AA/15-23-082-12W4), and the line of section is shown in Figure 2.6. The datum is the top of the Wabiskaw Member of the Clearwater Formation and the top of the McMurray succession is equivalent to the combined Top A1 / TOP A2 surface.

2.3.3. Isopach trends in depositional units

In the Sparrow Paleovalley, cross-sections (Figs. 2.6–2.9) and isopach maps (Fig. 2.10) highlight zones of DU overthickening, manifest by greater numbers and thicknesses of parasequences within the DUs (Fig. 2.5). At the base of the succession, Regional C thins landward (westward) from a mean thickness of 25 m in the outer zone, to 22 m in the central zone, and 10m in the inner zone (Fig. 2.10). Depositional unit B2 has a mean thickness of 9 m across the outer and central zones (Fig. 2.10) and shows an increase in mean thickness to 11.6 m in the inner zone (Fig. 2.10). Depositional unit B1 is also thicker in the inner zone (mean: 9.8 m) than in the outer and central zones (mean: 8 m; Fig. 2.10). Depositional unit A2 thins slightly landward from a mean thickness of 3.8 m in the outer zone to 3.4 m in the central zone (Fig. 2.10). A2 also contains localized areas of anomalously thick strata in the inner zone (mean: 5.1 m). Finally, A1 exhibits a net thickness increase from the outer and central zones (mean of 2.2 m) to the inner zone (mean of 3.4 m; Figs. 2.6, 2.10).

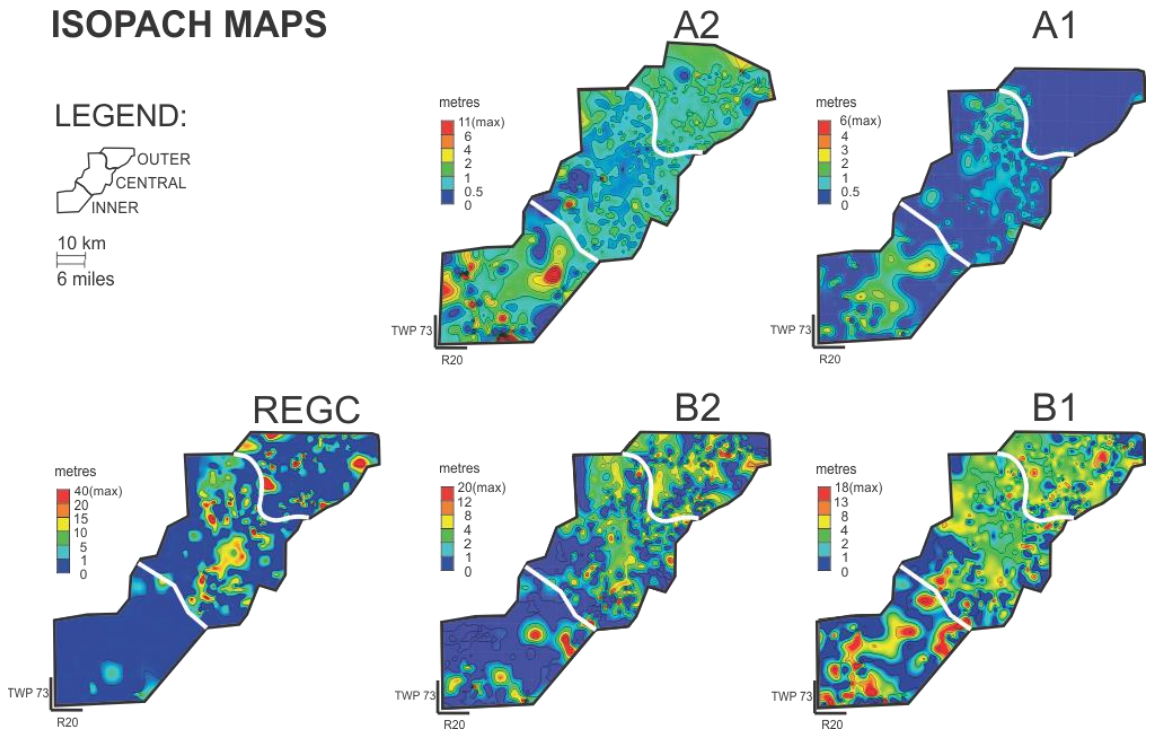

Figure 2.10 Isopach maps for each depositional unit (and excluding channel deposits) in the SPV.

Refer to text for explanation of sediment distributions within each DU. White lines divide the outer, central and inner zones of the SPV.

2.3.4. Statistical analysis of thickness trends

Initial recognition of anomalous thicknesses in DUs throughout the SPV is based on visual examination of isopach maps (Fig. 2.10). From these maps, we define one region of anomalously thick strata (i.e., the inner zone) relative to the SPV in general (Fig 2.10). Isopach data are then used to define populations within each DU for statistical comparison. Populations tested include the inner zone, central zone, outer zone, all zones (SPV), and combined central and outer zones (CO-SPV) of the Sparrow Paleovalley. Population in each DU are analyzed for the mean, median, variance, standard deviation, and mean growth rate (given in percent) of isopach thickness of the DU in each well (excluding null values) in the population. The two-sample K–S statistical test compares isopach thicknesses (excluding null values) of DUs between the inner zone and CO-SPV (combined central and outer zones), where the test shows whether the isopach thicknesses reflect the same population (i.e., there are no statistically significant anomalous thicknesses in the DU within the SPV), or indicates two distinct

populations (i.e., the thickness of the DU in the inner zone is statistically distinct from those of the CO-SPV; Table 2.2).

Table 2.2 **Statistical data of isopach thicknesses of depositional units (DU) in SPV (all 3 zones), outer zone, central zone, inner zone and CO-SPV (composite of the outer and central zones). Data columns include DU, area, mean and median isopach thickness (m); variance and standard deviation (SD) in DU thickness; mean growth rate (in percent) between SPV and the other zones, and the two-sample Kolmogorov-Smirnov test calculated between the inner zone and the CO-SPV. The two-sample Kolmogorov-Smirnov test shows whether the isopach thicknesses reflect the same population (P value > 0.05) or indicates two populations (P value < 0.05).**

Depositional Unit	Area	Mean/Median	Variance/SD	Growth rate	Kolmogorov-Smirnov
A1	SPV	2.37/2.25	0.68/0.83	0%	
	OUTER	2.18/2.11	0.44/0.66	-8%	
	CENTRAL	2.18/2.12	0.42/0.64	-8%	
	INNER	3.43/3.44	0.78/081	+45%	D=0.57, *P* value=1.99e-09 (distinct populations)
	CO-SPV	2.18/2.12	0.43/0.65	-8%	
A2	SPV	3.87/3.79	1.92/1.39	0%	
	OUTER	3.76/3.71	1.58/1.26	-3%	
	CENTRAL	3.44/3.31	1.37/1.17	-11%	
	INNER	5.11/4.77	3.51/1.87	+32%	D=0.43, *P* value=1.11e-11 (distinct populations)
	CO-SPV	3.65/3.57	1.53/1.24	-6%	
B1	SPV	8.15/7.62	6.98/2.64	0%	
	OUTER	8.01/7.42	6.44/2.54	-2%	
	CENTRAL	7.96/7.21	7.04/2.65	-2%	
	INNER	9.84/9.51	10.34/3.22	+21%	D=0.36, *P* value=1.2e-06 (distinct populations)
	CO-SPV	7.99/7.37	6.63/2.57	-2%	
B2	SPV	8.97/8.6	9.11/2.85	0%	
	OUTER	8.84/8.59	7.03/2.65	-1%	
	CENTRAL	8.77/8.21	7.93/2.81	-2%	
	INNER	11.6/10.31	23.9/4.89	+29%	D=0.39, *P* value=0.004 (distinct populations)
	CO-SPV	8.81/8.42	7.33/2.71	-2%	
REGC	SPV	24.7/26.3	82.43/9.08	0%	
	OUTER	24.98/26.47	80.05/8.95	+1%	
	CENTRAL	22.34/22.01	77.41/8.8	-9%	
	INNER	9.8/9.63	10.55/3.25	-60%	Insufficient data
	CO-SPV	24.1/24.7	80.5/8.97	-2%	

At the base of the succession, Regional C exhibits -60% thinning in the inner zone population compared to Regional C across the entire SPV. For Regional C, insufficient data (n=8) means that the two-sample Kolmogorov-Smirnov statistical test cannot be used to determine whether the Regional C isopach thickness variations lie within a single population (all SPV population), or whether there are two distinct populations (inner zone vs. CO-SPV populations). Depositional unit B2 displays +29% thickening in the inner zone and a slight thinning in the central (-2%) and outer zones (-1%), compared to the mean thickness of B2 throughout the SPV (Table 2.2; Fig. 2.11). The data suggest that the thickness of the inner zone vs. CO-SPV are from two distinct populations (*P* value = 0.004). Depositional unit B1 shows +21% thickening in the inner zone and -2% thinning in the central and outer zones, compared to the mean thickness through all of the SPV (Table 2.2; Fig. 2.11). The thickness distribution of B1 in the inner zone is statistically distinct (*P* value=1.2e-06) from that in CO-SPV. Depositional unit A2 is +32% thicker in the inner zone, -11% thinner in the central zone, and -3% thinner in the outer zone, relative to the mean A2 thickness across all the SPV (Table 2.2; Fig. 2.11). Furthermore, the thicknesses of A2 in the inner zone vs. CO-SPV are also significantly different (*P* value=1.11e-11). Compared to the SPV, A1 shows thickening of +45% in the inner zone and thinning of -8% in the outer and central zones (Table 2.2; Fig. 2.11). The A1 thickness distribution between the inner zone vs. CO-SPV demonstrates preservation of two distinct populations (*P* value = 1.99e-09).

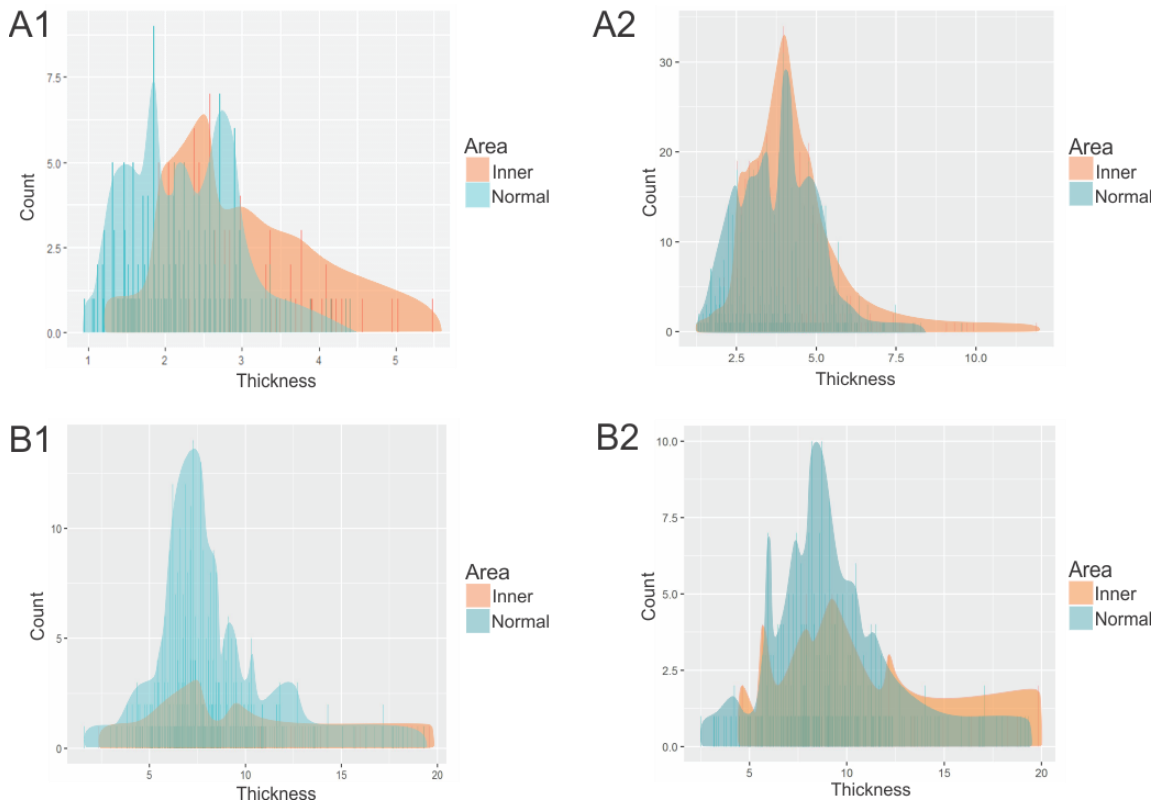

Figure 2.11 Graphical comparison of DU thickness for DUs A1 to B2, comparing the inner zone and the rest of the SPV (CO-SPV) using isopach thickness data derived from 1 000 wells.

The mean increase in thickness of depositional units in the inner zone is 29% for B2, 21% for B1, 32% for A2, and 45% for A1. REGIONAL C is not shown, as it displays substantial thinning into the inner zone, which is attributed to paleotopographically high positions that restricted deposition of its PSs.

2.3.5. Deformation within overthickened strata of the inner zone of the Sparrow Paleovalley

Deformation structures are observed across the entire SPV; however, deformation structures are significantly more common in the inner zone. In the SPV, these include soft-sediment deformation and partially indurated sediment deformation structures (Fig. 2.12). The thicknesses of soft-sediment structures range from 0.5–10 cm and include deformed laminae and beds to convolute bedding. Partially indurated deformation structures are only rarely observed and constitute mainly of synsedimentary micro-faults showing normal vertical displacement (Fig. 2.12B–C). Offsets along micro-faults range from 0.2–14.0 cm.

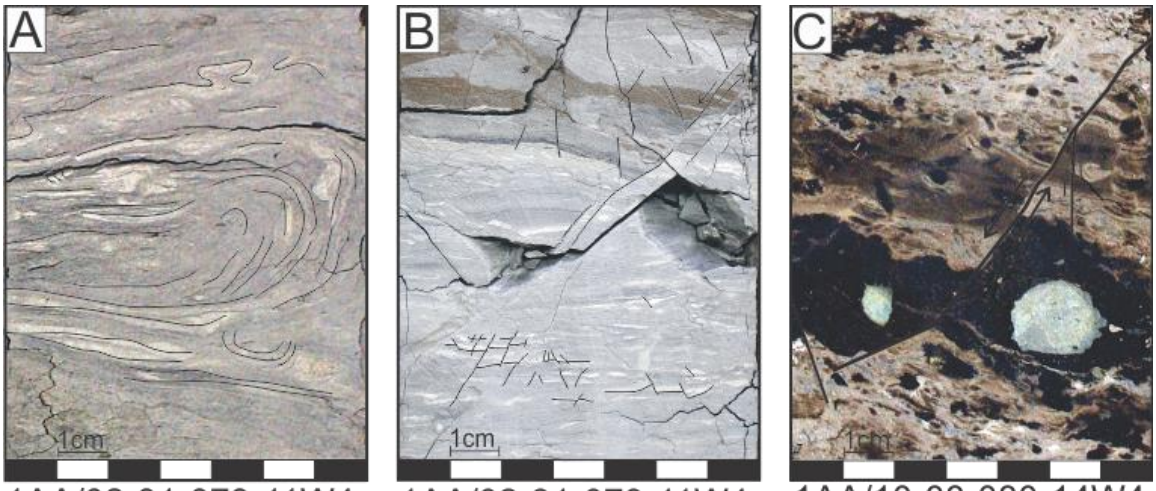

Figure 2.12 Examples of soft-sediment deformation features found in cores throughout regions of statistically significant overthickened areas in the Sparrow Paleovalley.

A) Irregular convolute bedding in silty mudstone. B) Synsedimentary micro-faults in silty mudstone. C) Synsedimentary micro-faults that show normal displacement in interbedded silty mudstone and sandstone beds.

2.4. Discussion

Sparrow Paleovalley deepens and widens to the NE, and as relative sea-level rose, the SPV was flooded progressively, shifting shoreline positions further landward to the southwest. Accommodation space creation was primarily controlled by the onset of transgression of the Boreal Sea in the SPV, with each depositional unit from Regional C to A1 backstepping landward. Parasequences are shallowing-upward successions recording progradation in the northeast direction during normal regression. The reduced area and more landward depositional position up-valley, therefore, would be expected to be manifested in a net thinning of DUs from CO-SPV (combined central and outer zones) to the inner zone, as they thinned onto the Nisku and Grosmont carbonate highlands (Fig. 2.13). This is the case for Regional C; however, from B2 to A1, anomalous thickening of strata occurs preferentially in the inner zone, which cannot be explained by flooding and infill of the SPV solely due to relative sea-level rise. In the inner zone of the SPV, where B2 to A1 are anomalously thick, each DU records a higher number of PSs in relation to CO-SPV (Fig. 2.5). The higher number of PSs in the upstream portion of SPV, combined with the statistical results, suggests an external control (other than sea-level rise) on accommodation space creation. Parasequence

thicknesses indicate local creation of accommodation space prior to and penecontemporaneously with accumulation of DUs B2 to A1. Parasequence thicknesses decrease upwards within each DU from B2 to A1 in the inner zone, and this corresponds to paleotopographic lows generated by localized creation of accommodation space. The lowermost PS in each DU (B2−A1) are overthickened and reflect epikarst subsidence or collapse prior to the onset of deposition. The increase in numbers of relatively small PSs on top of the lowermost thick PS is interpreted to reflect syndepositional collapse that prevented the seaward progradation of the shoreline. Once the creation of accommodation space was surpassed by sediment supply in the inner zone, the depocenter was able to migrate seaward and only a limited number (commonly 2) of medium-sized PSs were deposited in the central zone. The seaward migration of the depocenter finally reached the outer zone where PSs rapidly shifted laterally, and multiple thinner PSs accumulated. While the shoreline occupied the middle and outer zones, epikarst continued in the inner zone, creating new and largely unfilled accommodation space. With resumption of base-level rise and transgression of the valley, signaling the onset of the next DU, initial deposition had greater accommodation space to fill, leading to thicker parasequences at the base of the cycle.

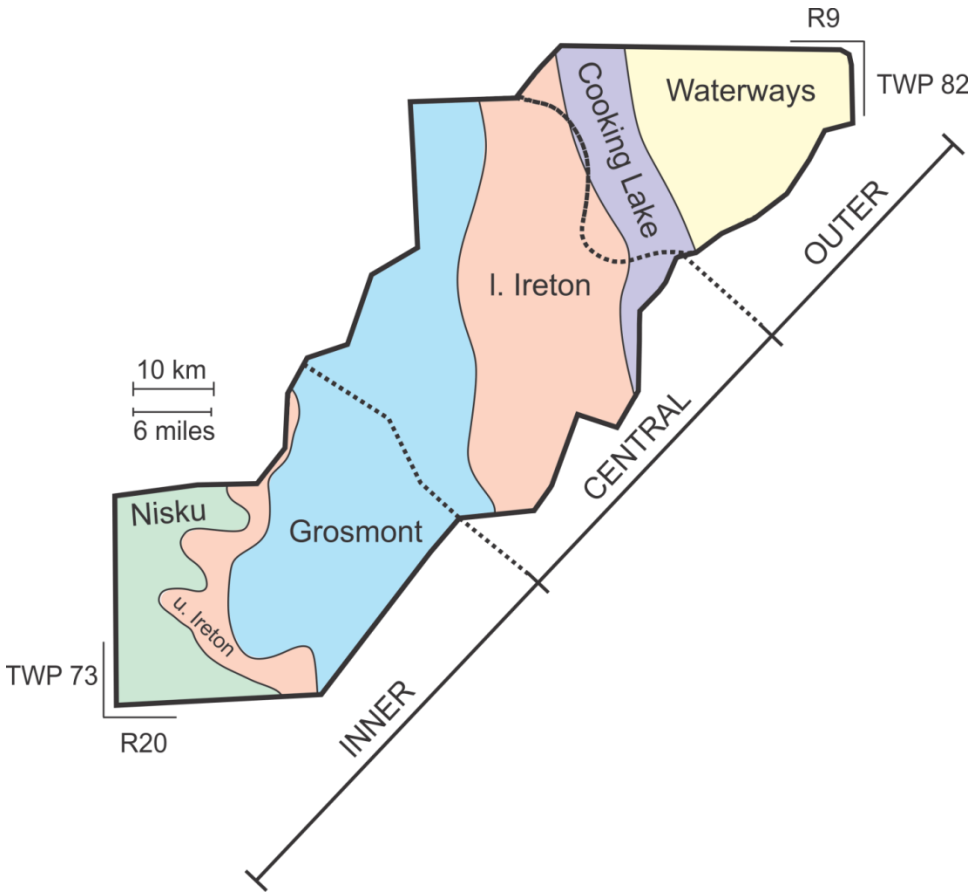

Figure 2.13 Map of Devonian carbonates that subcrop at the Sub-Cretaceous Unconformity below the McMurray Sub-Basin in the Sparrow Paleovalley.

From west to east, these include the Nisku, upper Ireton, Grosmont, lower Ireton, Cooking Lake, and Waterways formations (Hauck et al., 2017). The inner, central and outer zone boundaries are demarcated by black dashed lines.

The collapse of Devonian carbonates through the dissolution of evaporites that underlie the McMurray Sub-Basin in the Assiniboia Paleovalley is a well-known phenomenon associated with the creation of accommodation space. Within the main Assiniboia Paleovalley, the generation of both medium- and large-scale deformation within McMurray Fm strata is associated with the contemporaneous removal of halite and sulphates of the Prairie Evaporite Formation (e.g., McPhee and Wightman, 1991; Wightman and Pemberton, 1997; Broughton, 2014, 2015a,b; Barton et al., 2017). This process likely amplified local-scale manifestations of carbonate karst (e.g., breccia pipes) in the carbonate strata that overlies the Prairie Evaporite Formation within and proximal to the Assiniboia Paleovalley (Broughton, 2014, 2015a,b; Walker et al., 2017).

West of the salt dissolution scarp, the Sparrow Paleovalley is located above (from northeast to southwest = oldest to youngest; Fig. 2.13) subcropping Waterways, Cooking Lake, lower Ireton, Grosmont, upper Ireton, and Nisku formations. The inner zone of the SPV overlies and is flanked by strata of the Nisku, upper Ireton and Grosmont formations (Fig. 2.13). The Nisku and Grosmont are both mostly clean carbonates, with a thin intervening argillaceous carbonate (marl) corresponding to the upper part of the Ireton Formation. The Nisku and Grosmont experienced erosion and epikarstification during subaerial exposure and while they were in close proximity to the water table (Anderson and Knapp, 1993; Dembicki and Machel, 1996). Erosion and epikarstification of carbonates within the SPV are hypothesized to have generated localized accommodation space, forming areas of preferential infill during deposition of DUs B2–A1. The areas corresponding to the most statistically significant overthickening (local generation of accommodation space) occur in the inner zone of the SPV, which overlies carbonates of the Grosmont and Nisku (Fig. 2.13). Here, the SCU structure contour map shows topographic lows (Fig. 2.14) directly below overthickening in DUs B2 to A1 (Table 2.1). The SCU structure contour map represents the present-day elevation of SCU relative to the current sea-level. Variation in its elevation represents both the MSB paleotopography Regional dip, and local stratal collapse in the inner zone of the SPV. The overthickening on the isopach maps suggests that carbonate epikarstification and dissolution of Devonian strata were initiated at the start of McMurray deposition, and likely before as well. The increase of deepening of the anomalies from the McMurray isopach map (10−20 m) and the SCU contour map (60−100 m) are interpreted to indicate that the stratal collapse continued during post-McMurray deposition.

Carbonate epikarst within the Nisku and Grosmont formations have been documented in wireline logs and from core to the north of the SPV study area (Dembicki and Machel, 1996). These authors describe the development of paleokarst within the Grosmont Formation during exposure at the SCU, where exposure to meteoric waters produced paleosols, fractures, collapse breccias, and dissolution cavities. Paleokarst zones within the Grosmont are common near the SCU, but also occur to depths of up to 35 m below the SCU and, importantly, multiple paleokarst zones can be found at depth within a single well (Dembicki and Machel, 1996). It is likely that such epikarstification of carbonate also occurred at the Grosmont-Nisku subcrop within the SPV, and is responsible for the localized structural lows in the inner zone (Fig. 2.14). Furthermore,

creation of additional accommodation space by carbonate epikarstification during deposition of DUs B2 to A1 is suggested by thickness trends and is substantiated by statistical analysis and parasequence architecture throughout the SPV.

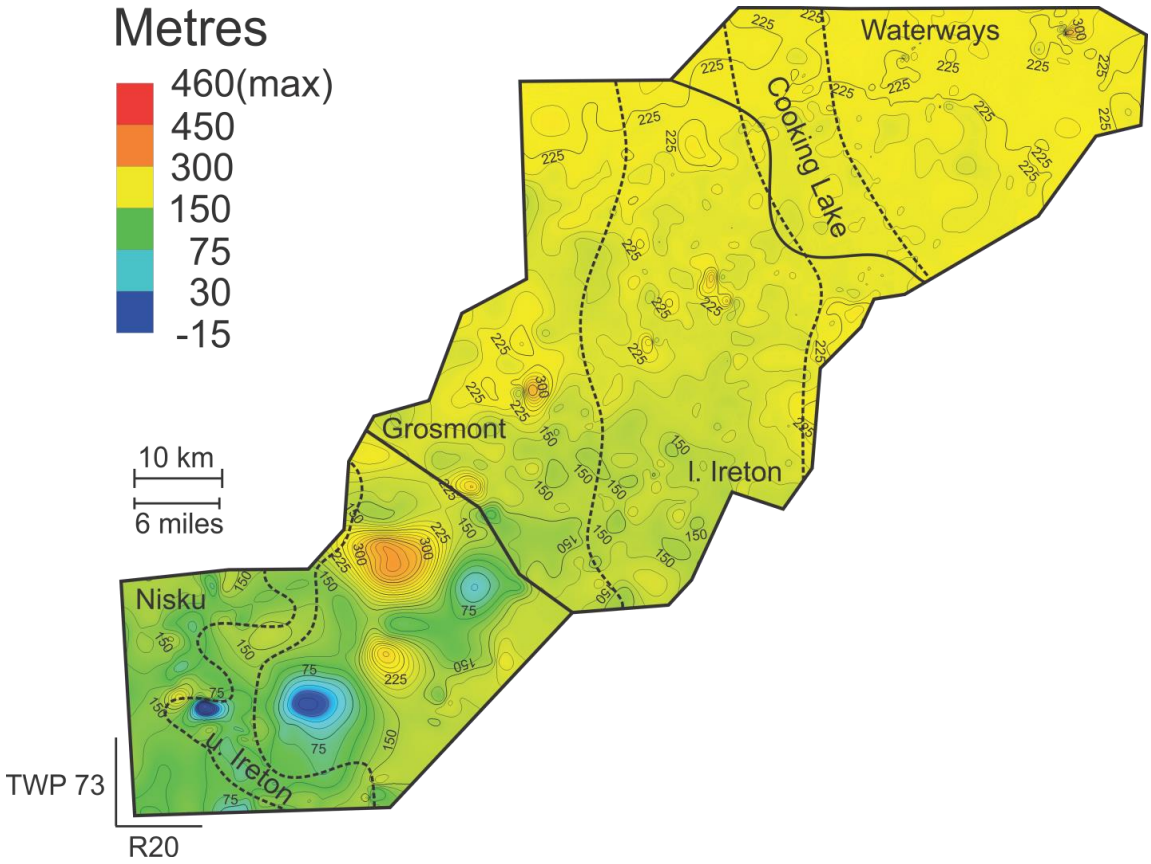

Figure 2.14 Sub-Cretaceous Unconformity (SCU) structure contour map along the Sparrow Paleovalley.

The SCU structure contour map represents the present-day elevation of SCU relative to sea-level. Blue and green reflect paleotopographic lows (small values), close to current mean sea-level, and orange and yellow demarcate paleotopographic highs (high values). The inner, central and outer zones are delineated by black line. In addition, from west to east, the Nisku, upper Ireton, Grosmont, lower Ireton, Cooking Lake, and Waterways formations are delineated by dashed black lines.

Soft-sediment deformation (SSD) features are common in all DUs within the SPV, and form as a result of both autogenic and allogenic processes. Autogenic processes responsible for SSD formation in the McMurray Sub-Basin include sediment loading (Edwards, 1976; Bhattacharya and Davies, 2001; Huang and Bhattacharya, 2017) and small-scale slope failures (Brekke et al., 2017). Both convolute bedding and micro-faulting in the SPV occur at the bed scale, and are attributed to either sediment loading or slope failures along small tidal creeks and drainages. However, such SSD

should be homogeneously distributed through all strata in the SPV if autogenic processes alone are responsible for their formation. By contrast, higher concentrations of SSD features occur in beds and bedsets within the inner zone, which cannot be explained as a function of autogenic mechanisms alone. In the inner zone of the SPV, SSD occur in higher abundances over a 400 km^2 area, and coincide with the region of statistically significant anomalously thick isopach values. This supports the contention that an allogenic control was operating in the preferential development of SSD structures in the inner zone. We hypothesize that sediment failure in the inner zone was also impacted by slumping due to syndepositional epikarst processes occurring within the carbonates of the Grosmont and Nisku formations.

2.5. Conclusions

Syndepositional carbonate epikarstification in limited accommodation settings is investigated in the Sparrow Paleovalley (SPV), southeast McMurray Sub-Basin. The location of the SPV west of the main Assiniboia Paleovalley, was responsible for the preservation of stacked depositional units (DU) in the McMurray Formation from erosional incision by younger channel belts. From core observations, stratigraphic correlations, isopach maps, and statistical treatments of thickness variations, an overthickening of DUs is identified and quantified in the inner (most landward) zone of the SPV. We calculate a DU thickness mean growth rate of +21% (B1) to +45 % (A1) over a 400 km^2 zone, extending from T73–75, R16–20W4 (Figs. 6−10). The thickness distribution of B2−A1 in the inner zone is statistically distinct from that expressed in CO-SPV (i.e., from two distinct populations) and hence, suggests an external control on DU thicknesses. The higher proportion of soft-sediment deformation (SSD) features in beds and bedsets in the inner zone of the SPV also supports an external (allogenic) control, which we hypothesize to be the result of sediment failure and slumping due to syndepositional epikarst subsidence within underlying Devonian carbonates. This carbonate epikarst subsidence is also interpreted to have been responsible for generating accommodation space, which correspondingly impacted the distribution and thickness trends of parasequences within DUs B2−A1. Finally, the SCU structure contour map demonstrates that post-depositional collapse impacted the McMurray Formation in the MSB.

Regressive stratigraphic units (i.e., depositional units) in limited accommodation space are generally poorly preserved; however, these units are essential for reconstructing the stratigraphic framework. Here, we demonstrate that DUs can be used to accurately outline local and restricted anomalies in thickness trends generated by allogenic control on accommodation space, and refine the stratigraphic architecture of deposits in marginal-marine environments.

Acknowledgements

The authors thank the sponsors of the McMurray Geology Consortium: BP plc, Cenovus Energy Inc., Husky Energy, Nexen CNOOC Ltd, and Woodside Energy Ltd, for funding this research. Susanne Fietz, Chuqiao Huang, Bryan Kent, Lucian Rinke-Hardekopf, Sarah Schultz and Miranda Walters are thanked for providing input on this manuscript. The manuscript was substantially improved through the external reviews of Dr. Paul L. Broughton and Paul Durkin.

References

Alberta Energy and Utilities Board, 2003, Athabasca Wabiskaw-McMurray regional geological study: Alberta Energy and Utilities Board, Report 2003-A, p. 1–195.

Allen, G.P., and Posamentier, H.W., 1993, Sequence stratigraphy and facies model of an incised valley fill: the Gironde estuary, France: Journal of Sedimentary Research, v. 63,no. 3, p. 378−391.

Anderson, N.L., and Knapp, R., 1993, An overview of some of the large scale mechanisms of salt dissolution in western Canada: Geophysics, v. 58, no. 9, p. 1375–1387, doi:10.1190/1.1443520.

Baniak, G.M. and Kingsmith, K.G., 2018, Sedimentological and stratigraphic characterization of Cretaceous upper McMurray deposits in the southern Athabasca oil sands, Alberta, Canada: AAPG Bulletin, 102, no. 2, p. 309-332.

Barton, M.D., Porter, I., O'Byrne, C., and Mahood, R., 2017, Impact of the Prairie Evaporite dissolution collapse on McMurray stratigraphy and depositional patterns, Shell Albian Sands Lease 13, northeast Alberta: Bulletin of Canadian Petroleum Geology, v. 65, no. 1, p. 175–199.

Bhattacharya, J.P., and Davies, R.K., 2001, Growth faults at the prodelta to delta-front transition, Cretaceous Ferron sandstone, Utah: Marine and Petroleum Geology, v. 18, no. 5, p. 525–534, doi:https://doi.org/10.1016/S0264-8172(01)00015-0.

Brekke, H., MacEachern, J.A., Roenitz, T., and Dashtgard, S.E., 2017, The use of micro-resistivity image logs for facies interpretations: An example in point-bar deposits of the McMurray Formation, Alberta, Canada. AAPG Bulletin, 101, no. 5, p. 655–682.

Broughton, P.L., 2013, Devonian salt dissolution-collapse breccias flooring the Cretaceous Athabasca oil sands deposit and development of lower McMurray Formation sinkholes, northern Alberta Basin, Western Canada: Sedimentary Geology, v. 283, p. 57–82.

Broughton, P.L., 2014, Syndepositional architecture of the northern Athabasca Oil Sands Deposit, northeastern Alberta: Canadian Journal of Earth Sciences, v. 52, no. 1, p. 21–50.

Broughton, P.L., 2015a, Collapse-induced fluidization structures in the Lower Cretaceous Athabasca Oil Sands Deposit, Western Canada: Basin Research, v. 28, p. 507–535.

Broughton, P.L., 2015b, Incipient vertical traction carpets within collapsed sinkhole fills: Sedimentology, v. 62, no. 3, p. 845–866, doi:10.1111/sed.12163.

Carrigy, M.A., 1963, Paleocurrent directions from the McMurray Formation: Bulletin of Canadian Petroleum Geology, v. 11, no. 4, p. 389–395.

Christopher, J., 1997, Evolution of the Lower Cretaceous Mannville sedimentary basin in Saskatchewan: Canadian Society of Petroleum Geologists, v. 18, p. 191−210.

Crerar, E.E., and Arnott, R.W.C., 2007, Facies distribution and stratigraphic architecture of the lower Cretaceous McMurray Formation, Lewis property, northeastern Alberta: Bulletin of Canadian Petroleum Geology, v. 55, no. 2, p. 99–124.

Dembicki, E.A., and Machel, H.G., 1996, Recognition and Delineation of Paleokarst zones by the use of wireline logs in the bitumen-saturated Upper Devonian Grosmont Formation of northeastern Alberta, Canada: American Association of Petroleum Geologists Bulletin, v. 80, no. 5, p. 695–712.

Edwards, M.B., 1976, Growth faults in Upper Triassic deltaic sediments, Svalbard: AAPG Bulletin, v. 60, no. 3, p. 341–355.

Gandomi, A., and Haider, M., 2015, Beyond the hype: Big data concepts, methods, and analytics: International Journal of Information Management, v. 35, no. 2, p. 137–144.

Gingras, M.K., MacEachern, J.A., Dashtgard, S.E., Ranger, M.J., and Pemberton, S.G., 2016, The significance of trace fossils in the McMurray Formation, Alberta, Canada: Bulletin of Canadian Petroleum Geology, 64, 233-250.

Hauck, T.E., Peterson, J.T., Hathway, B., Grobe, M., and MacCormack, K., 2017, New insights from regional-scale mapping and modelling of the Paleozoic succession in northeast Alberta: Paleogeography, evaporite dissolution, and controls on Cretaceous depositional patterns on the Sub-Cretaceous Unconformity: Bulletin of Canadian Petroleum Geology, v. 65, no. 1, p. 87–114, doi:10.2113/gscpgbull.65.1.87.

Hein, F.J., and Cotterill, D.K., 2006, The Athabasca oil sands—a regional geological perspective, Fort McMurray area, Alberta, Canada: Natural Resources Research, v. 15, no. 2, p. 85–102.

Hein, F.J., Berhane, H., and Cotterill, D.K., 2000, An atlas of lithofacies of the McMurray formation, Athabasca oil sands deposit, Northeastern Alberta: surface and subsurface: Earth Sciences Report, v. 7.

Hein, F.J., Dolby, G., and Fairgrieve, B., 2013, A regional geologic framework for the Athabasca oil sands, northeastern Alberta, Canada: AAPG Studies in Geology, v. 64, p. 207–250.

Huang, C., and Bhattacharya, J.P., 2017, Facies analysis and its relation to point-sourced growth faults in river-dominated prodeltaic delta front deposits of the Cretaceous Ferron Notom Delta, Utah, USA: Marine and Petroleum Geology, v. 81, p. 237–251, doi:https://doi.org/10.1016/j.marpetgeo.2017.01.016.

Jardine, D. 1974, Cretaceous Oil Sands of Western Canada: *DOB* 3, 2009.

Jean, T.R., 2018, The Eastern Flank: Predicting the Architecture of the McMurray Formation beyond its Subcrop Edge (master's thesis): Simon Fraser University, 99 p.

Jervey, M.T., 1988, Quantitative geological modeling of siliciclastic rock sequences and their seismic expression, in Sea-Level Changes: An Integrated Approach, edited by C. K. Wilgus et al., Spec. Publ. Soc. Econ. Paleontol. Mineral., v. 42, p. 47–69.

Kamola, D.L., and Van Wagoner, J.C., 1995, Stratigraphy and facies architecture of parasequences with examples from the Spring Canyon Member, Blackhawk Formation, Utah: *in* Van Wagoner J.C., and Bertram, G.T., Sequence Stratigraphy of Foreland Basin Deposits: Outcrop and Subsurface Examples from the Cretaceous of North America: AAPG Memoir, v. 64, p. 27–54.

Marx, V., 2013, The big challenges of big data: Nature, v. 498, p. 255–260, doi: 10.1038/498255a.

McPhee, D.A., and Wightman, D.M., 1991, Timing of the dissolution of Middle Devonian Elk Point Group Evaporites - Twps. 47 to 103 and Rges. 15 W3M to 20 W4M (abs.): Bulletin of Canadian Petroleum Geology, v. 39, p. 218.

Meijer Drees, N.C., 1994, Devonian Elk Point Group of the Western Canada Sedimentary Basin: *in* G. D. Mossop, and I. Shetsen, eds., Geological Atlas of the Western Canada Sedimentary Basin: Canadian Society of Petroleum Geologists and Alberta Research Council Edmonton, AB, Canada, p. 129–138.

Mossop, G., and Shetsen, I., 1994, Introduction to the geological atlas of the Western Canada Sedimentary Basin: Geological Atlas of the Western Canadian Sedimentary Basin.Compiled by GD Mossop and I.Shetson.Canadian Society of Petroleum Geologists and Alberta Research Council, Calgary, Alberta, p. 1–12.

Pattison, S.A.J., 2018, Using classic outcrops to revise sequence stratigraphic models : Reevaluating the Campanian Desert Member (Blackhawk Formation) to lower Castlegate Sandstone interval, Book Cliffs, Utah and Colorado, USA: Geology, v. 47, n. 1, p. 11–14, doi:10.1130/G45592.1

Pemberton, S.G., Flach, P.D., and Mossop, G.D., 1982, Trace fossils from the Athabasca oil sands, Alberta, Canada: Science, v. 217, n. 4562, p. 825-827.

Porter, J.W., Price, R.A., and McCrossan, R.G., 1982, The Western Canada Sedimentary Basin: Philosophical Transactions of the Royal Society A: Mathematical, Physical and Engineering Sciences, v. 305, no. 1489, p. 169–192, doi:10.1098/rsta.1982.0032.

Price, R.A., 1994, Cordilleran Tectonics and the Evolution of the Western Canada Sedimentary Basin: *in* Mossop, G.D., and Shetsen, I., eds., Geological Atlas of the Western Canada Sedimentary Basin: Canadian Society of Petroleum Geologists and Alberta Research Council Edmonton, AB, Canada, p. 13–24.

Ranger, M.J., McPhee, D., and Pemberton, S.G., 1994, Elements of a stratigraphic framework for the McMurray Formation in south Athabasca: Petroleum Geology of the Cretaceous Mannville Group, Western Canada., v. Memoir, 18, p. 263–291.

Ranger, M.J., and Pemberton, S.G., 1997, Elements of a stratigraphic framework for the McMurray Formation in south Athabasca area, Alberta: Petroleum Geology of the Cretaceous Mannville Group, Western Canada., v. Memoir, 18, p. 263–291.

Ranger, M.J., Gingras, M.K., and Pemberton, S.G., 2008, The role of ichnology in the stratigraphic interpretation of the Athabasca oil sands: Search and Discovery Article, v. 50065, p. 1–8.

Rinke-Hardekopf, L., Dashtgard, S.E., and Maceachern, J.A., 2019, Earliest Cretaceous Transgression of North America Recorded in Thick Coals: McMurray Sub-Basin, Canada: International Journal of Coal Geology, v. 204, p. 18–33, doi: 10.1016/j.coal.2019.01.011.

Schneider, C.L., and Grobe, M., 2013, Regional Cross-sections of Devonian stratigraphy in northeastern Alberta (NTS 74D, E): Alberta Energy Regulator, AER/AGS Open File Report, v. 5, p. 25.

Schneider, C., Mei, S., Haug, K., and Grobe, M., 2014, The Sub-Cretaceous Unconformity and the Devonian subcrop in the Athabasca Oil Sands area, townships 87–99, ranges 1–13, west of the Fourth Meridian: Alberta Geological Survey, Open File Report 2014-07, p.39.

RDC Team (R Development Core Team), , 2013, R: A language and environment for statistical computing: R Foundation for Statistical Computing, Vienna: 2009, Retrieved from https://www.r-project.org/.

Rs. Team (Rstudio Team), , 2015, RStudio: integrated development for R: RStudio, Inc., Boston, MA URL http://www. rstudio. com.

Van Wagoner, J.C., Mitchum, R., Campion, K.M., and Rahmanian, V.D., 1990, Siliciclastic sequence stratigraphy in well logs, cores, and outcrops: concepts for high-resolution correlation of time and facies: Methods in Exploration Series 7, p. 55, doi: 0-89181-657-7.

Walker, J., Almási, I., Stoakes, F., Potma, K., and Jennifer, O.K., 2017, Hypogenic karst beneath the Athabasca Oil Sands: Implications for oil sands mining operations. Bulletin of Canadian Petroleum Geology, v. 65, no. 1, p. 115–146.

Weleschuk, Z.P., and Dashtgard, S.E., 2019, Evolution of an ancient (Lower Cretaceous) marginal-marine system from tide-dominated to wave-dominated deposition, McMurray Formation: Sedimentology, v. 66, p. 2354−2391.

Wickham, H., 2016, ggplot2: elegant graphics for data analysis: Springer.

Wickham, H., and Grolemund, G., 2016, R for data science: import, tidy, transform, visualize, and model data: " O'Reilly Media, Inc."

Wightman, D.M., and Pemberton, S.G., 1997, The Lower Cretaceous (Aptian) McMurray Formation; an overview of the Fort McMurray area, northeastern Alberta: Petroleum Geology of the Cretaceous Mannville Group, Western Canada: Memoir - Canadian Society of Petroleum Geologists, Memoir 18, p. 312–344.

Zaitlin, B.A., Warren, M.J., Potocki, D., Rosenthal, L., and Boyd, R., 2002, Depositional styles in a low accommodation foreland basin setting: an example from the Basal Quartz (Lower Cretaceous), southern Alberta: Bulletin of Canadian Petroleum Geology, v. 50, no. 1, p. 31–72.

Chapter 3.

Refinement of the stratigraphic framework for the Regional C depositional unit of the McMurray Formation and implications for the early transgression of the Alberta Foreland Basin, Canada

Abstract

The Lower Cretaceous McMurray Formation in Alberta and Saskatchewan, Canada, comprises a series of depositional units (DUs) consisting of stacked parasequences bounded by flooding surfaces and incised by fluvio-estuarine channel belts. The fluvio-estuarine channel belts of the McMurray Fm have been the focus of numerous studies whereas the regional DUs have received substantially less attention. Of the regional DUs, Regional C (equivalent to the middle McMurray) is the most understudied; yet this interval records the history of the McMurray Formation between deposition of fluvial strata in the Lower McMurray and marine facies in the upper McMurray and overlying Clearwater Formation. Determining the history of the Regional C DU is fundamental for accurately reconstructing the stratigraphic evolution of the McMurray Fm and, by extension, the early evolution of the Alberta Foreland Basin.

The Regional C is divided into two DUs separated by a regionally mappable flooding surface. This surface occurs 11 to 15 m below the top of the Regional C and is traceable over a 2,550 km^2 area. This flooding surface divides the thick interval of undifferentiated Regional C into a lower C2 DU and an upper C1 DU, each with a maximum thickness of < 15 m. The thickness of the C2 and C1 DUs indicates that deposition at this time also occurred in a setting of low to moderate accommodation creation, which is consistent with the rest of the McMurray Formation. The limited available accommodation space was easily surpassed by sediment supplied by the paleo-distributive channel system, leading to a basinward progradation of the shoreline.

Chapter 3 is currently in press in the Journal of Sedimentary Research as
Château, C.C., Dashtgard, S.E., and MacEachern, J.A., in press, Refinement of the stratigraphic framework for the Regional C depositional unit of the McMurray Formation and implications for the early transgression of the Alberta Foreland Basin, Canada: Journal of Sedimentary Research.

The C2 and C1 DUs are retrogradationally stacked, with the maximum regressive paleo-shoreline of C1 lying landward of that of C2. This stacking arrangement indicates that the shoreline backstepped during the early stages of transgression of the Boreal Sea. The backstepping of the paleo-shoreline from C2 to C1 time is consistent with previous studies that show continued and stepwise retrogradation and/or transgression of the paleo-shoreline from the onset of deposition in the lower McMurray Formation through to maximum transgression in the Clearwater Formation. Together, these studies demonstrate that the early drowning of the Alberta Foreland Basin was persistent and slow.

3.1. Introduction

The Lower Cretaceous McMurray Formation is situated in the northeast quadrant of the Alberta Foreland Basin, Alberta and Saskatchewan, Canada, and was deposited during overall transgression of the Boreal Sea (Flach and Mossop, 1985). The region in which the McMurray Fm is distributed is referred to herein as the McMurray Fm depocenter (MDC; Fig. 3.1). Fluvial strata are preserved at the base of the McMurray Fm and are informally referred to as the lower McMurray. The lower McMurray is separated from overlying strata by a thick paleosol and/or coal interval (Flach and Mossop, 1985; Hein and Cotterill, 2006; Rinke-Hardekopf et al., 2019), which is, in turn, progressively overlain by strata informally named the middle and the upper McMurray. The middle and upper McMurray are more widely distributed throughout the MDC. These comprise a series of regressive stratigraphic units consisting of stacked parasequences or parasequence sets bounded by flooding surfaces (referred to herein as depositional units or DU). Depositional units are incised by nested and deeply excavated fluvio-estuarine channel belts (Ranger and Pemberton, 1997; Alberta Energy and Utilities Board, 2003) (Fig. 3.2). Fluvio-estuarine channel belts consist of both channel bars and channel fills of tidally influenced rivers that experienced brackish-water conditions (e.g., Pemberton et al., 1982; Gingras et al., 2016; Baniak and Kingsmith 2018; Weleschuk and Dashtgard, 2019). While the overall preservation of DUs in the MDC is poor compared to that of the fluvio-estuarine channel belts, determining DU architecture is vital for interpreting both the stratigraphic framework and the depositional evolution of the McMurray Fm and, by extension, the early evolution of the Alberta Foreland Basin

(see Ranger and Pemberton, 1997; Alberta Energy and Utilities Board, 2003; Hein and Cotterill, 2006; Ranger et al, 2008; Hein et al., 2013).

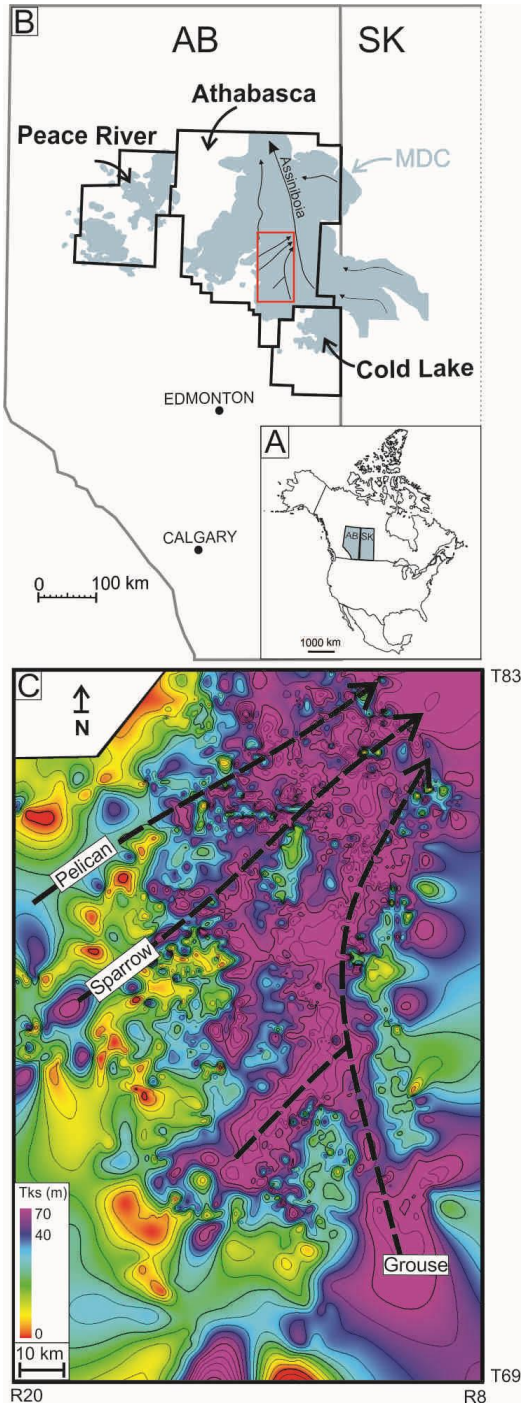

Figure 3.1 Southwest quadrant of the McMurray Depocenter location map
A) Position of Alberta (AB) and Saskatchewan (SK) in North America. B) The three main oil sands regions, Peace River, Athabasca, and Cold Lake are demarcated by the black polygons. The blue shaded area in the Athabasca oil sands region marks the approximate limit of the McMurray Fm and time-equivalent strata, herein referred as the McMurray Formation depocenter (MDC). The

margins of the MDC in the south, west, and north are derived from the AEUB (2003), while the eastern extent is theoretical and is based on surface projections and basin reconstruction presented in Jean (2018). The arrows in part B demarcate the main paleovalley axes as defined by depositional lows on the Sub-Cretaceous Unconformity. The study area is outlined by the red rectangle. C) Isopach map of the McMurray Fm in the study area with maximum thicknesses observed along the axes of the Pelican, Sparrow, and Grouse paleovalleys and minimum thicknesses over the carbonate highlands. Pelican, Sparrow, and Grouse are secondary paleovalleys that drained into the Assiniboia Valley (Christopher, 1997; Horner et al., 2018).

Five DUs are defined in the middle and upper members of the McMurray Fm, including (from oldest to youngest): Regional C, B2, B1, A2, and A1 (Fig. 3.2). The thicknesses of most DUs (B2 to A1) range from 6 to10 m, and this led to the interpretation that the MDC was a low-accommodation setting during deposition of the McMurray Fm (e.g., Ranger and Pemberton, 1997; Hein and Cotterill, 2006; Ranger et al., 2008; Hein et al., 2013; Château et al., 2019). Creation of accommodation space during deposition of Regional C to A1 DUs was mainly controlled by transgression of the Boreal Sea, marked by regionally extensive flooding surfaces that bound them (Ranger and Pemberton, 1997; Hein and Cotterill, 2006; Ranger et al., 2008; Hein et al., 2013). By contrast, shoreline progradation is responsible for subsequent deposition of the DUs during periods of stable or only slowly rising base level (Ranger and Pemberton, 1997; Hein and Cotterill, 2006; Ranger et al., 2008; Hein et al., 2013; Château et al., 2019; Weleschuk and Dashtgard, 2019).

The Regional C DU overlies the coal and/or paleosol interval at the top of the lower McMurray and is the oldest and most understudied DU in the McMurray Fm. Across the MDC, the Regional C DU is thick (20 to 45 m) compared to younger DUs (Flach and Mossop, 1985; Ranger and Pemberton, 1997; Hein and Cotterill, 2006). Herein, we investigate the southwest quadrant of the MDC, where the Regional C DU is well preserved and areally extensive. We interpret the sedimentology, architecture, and stratigraphy of the Regional C in the Grouse, Sparrow, and Pelican paleovalleys (Fig. 3.1). Sedimentological descriptions are derived from cores taken from wellbores, and these observations are used to define facies and facies associations (FAs). Facies and facies associations are integrated into the Ainsworth et al. (2011) semi-quantitative classification based on processes impacting coastal depositional systems. Core descriptions, facies, and FAs are then compared to well-log signatures of the cored intervals. Both core and well-log signatures are used to identify local and regional flooding surfaces in the Regional C DU. The extent of internal discontinuities (local flooding surfaces) and regionally extensive bounding surfaces are mapped to

reconstruct Regional C architecture and propose a revised stratigraphic framework for these strata. Resolving the stratigraphic architecture of Regional C completes reconstruction of the depositional history of the McMurray Formation, which is then used to comment on the early evolution and transgression of the Alberta Foreland Basin.

3.1.1. Geological Setting

The stratigraphic subdivision of the McMurray Fm is complex, and multiple models have been proposed (Fig. 3.2). Subdivision of the McMurray Fm was initially lithostratigraphic with informal lower, middle, and upper members defined on the basis of the degree of marine influence interpreted from the sedimentological, ichnological, and paleontological characteristics of the strata (Carrigy, 1963, 1967). The main controls on deposition of the McMurray Fm are regarded to be relative sea-level rises and falls during a period of overall sea-level rise (Ranger and Pemberton, 1997; Hein et al., 2013). Evaporite karst and carbonate epikarst have been recognized to have created additional accommodation space, which locally impacted deposition of the McMurray Fm in the basin (e.g., McPhee and Wightman, 1991; Crerar and Arnott, 2007; Fustic et al., 2012; Broughton, 2013, 2014, 2015a, 2015b; Barton et al., 2017; Hauck et al., 2017; Chateau et al., 2019). However, syndepositional accommodation tied to evaporite karst principally impacted the deposition of the lower member of the McMurray Fm (lower McMurray) along the axis of the Assiniboia Paleovalley (Fig. 3.1; Broughton, 2013, 2014, 2015a).

The lower McMurray comprises dominantly fluvial strata that are preserved in topographic lows on the Sub-Cretaceous Unconformity. Lower McMurray deposits are most prevalent in the north and northeastern extents of the MDC (Carrigy, 1971; Hein et al., 2000; Rinke-Hardekopf et al., 2019). A coupled lithostratigraphic and sequence stratigraphic model developed by the Alberta Energy and Utilities Board (2003; now Alberta Energy Regulator, AEUB) equates the Regional C to A1 DUs to the middle and upper members of the McMurray Fm (Fig. 3.2). The AEUB (2003) model subdivides the McMurray Fm on the basis of the occurrence of mudstone intervals at the bases of regional stratigraphic units, which are interpreted to overlie regionally significant (allogenic) flooding surfaces. Depositional units (i.e., stacked parasequences or parasequence sets 8 to 12 m thick) are interpreted as prograding shorelines deposited during short periods of relative stillstand during overall transgression (e.g., south extents

of the MSB). In some areas, DUs were eroded during incision and accretion of channels that are tens of meters thick and commonly referred to as “valleys” (e.g., Smith et al., 2009; Hubbard et al., 2011; La Croix et al., 2019). Valleys are labelled, based on their stratigraphic position in relation to the mudstone markers, and all channel incision is interpreted to have occurred during major relative sea-level fall while channel fill took place during sea-level rise (Hein et al., 2000, 2013; Hein and Cotterill, 2006; Horner et al., 2018). The top of the Lower McMurray Fm was geochronologically dated at 121.4 Ma (Rinke-Hardekopf et al., 2019) while the top of the McMurray Fm is approximately defined biostratigraphically at the Aptian to Albian boundary (113 Ma; Hein and Dolby, 2017). Correspondingly, the intervening strata records approximatively 8.4 Myr.

Herein, we employ a modified version of the Alberta Energy and Utilities Board (2003) stratigraphic model (Fig. 3.2). In this revised stratigraphic model, the basis of subdividing the McMurray Fm remains the presence of mudstone intervals overlying regionally mappable allogenic flooding surfaces. Channel belts are bounded at their bases by autogenic erosion surfaces and at their tops by either regional flooding surfaces (i.e., transgressive surfaces of erosion or TSE) or local flooding surfaces (i.e., parasequences overlying channel-belt deposits).

By consequence, fluvio-tidal channels are labelled as McMurray “channel belts” rather than as valleys (e.g., A2C), because the latter term implies valley incision induced by sea-level fall. Instead, we demonstrate that DUs represent regressive cycles deposited under minor sea-level fluctuations (i.e., equivalent of sequences in AEUB (2003) stratigraphic model), and that channel belts were both contemporaneous with the DUs and progradational (Ranger and Pemberton, 1997; Musial et al., 2012; Weleschuk and Dashtgard, 2019).

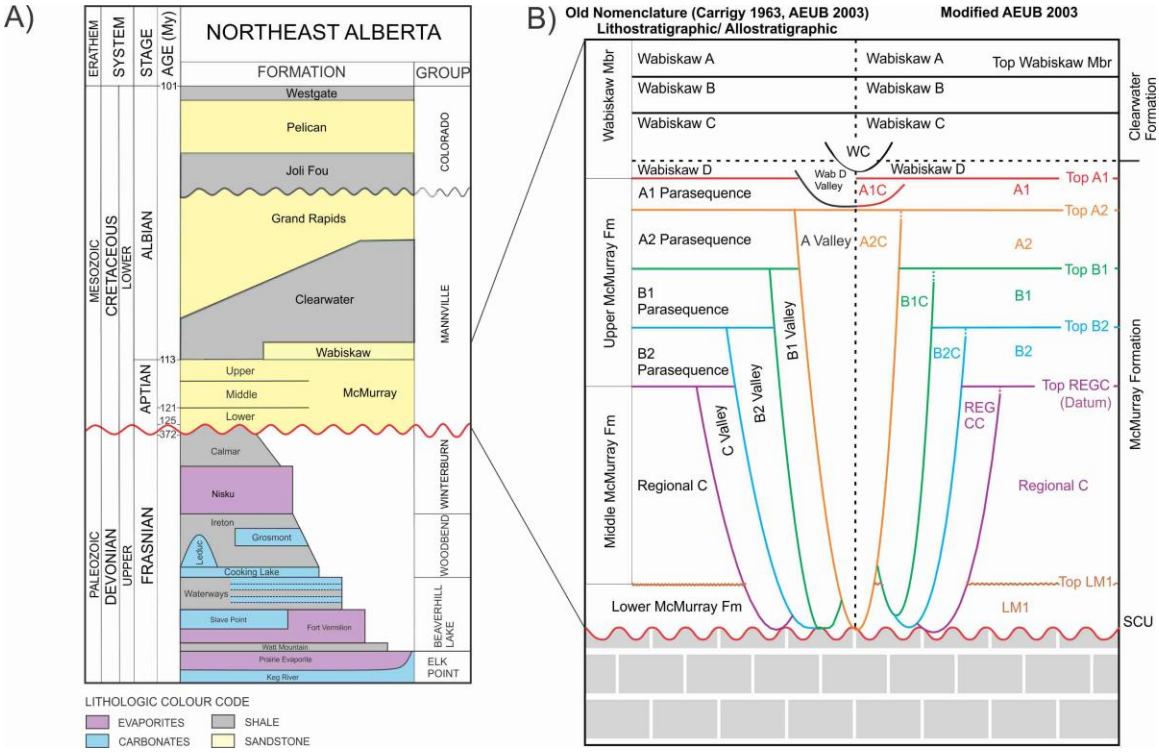

Figure 3.2 Comparison of stratigraphic frameworks proposed for the McMurray Formation depocenter (MDC)

A) Chronostratigraphic framework for Northeast Alberta (Alberta Geological Survey, 2015). The McMurray Formation overlies the Sub-Cretaceous Unconformity (SCU, red wavy line) and is, in turn, overlain by the Wabiskaw Member of the Clearwater Formation. The age date at the top of the lower McMurray Fm is derived from Rinke-Hardekopf et al. (2019). B) Three stratigraphic models proposed for the McMurray Formation. On the far left (vertical text) is the lithostratigraphic nomenclature proposed by Carrigy (1963). In the middle left is the lithostratigraphic and allostratigraphic model developed by the Alberta Energy and Utilities Board (2003; now Alberta Energy Regulator). On the right is a modified version of the Alberta Energy and Utilities Board (2003) model used by the McMurray Geology Consortium. In the modified AEUB (2003) stratigraphy, fluvio-tidal channels are labelled as McMurray channel belts rather than as paleovalleys (e.g., A2C), as the latter term implies valley incision during relative base-level fall. Instead, we consider depositional units to represent regressive cycles that were cut into by channel belts that were both contemporaneous and post depositional. These channel belts are bounded at their bases by autogenic erosion surfaces, and by either a regional flooding surface (i.e., transgressive surface of erosion, TSE) or a local flooding surface (e.g., parasequences overlying channel-belt deposits) at the top.

3.1.2. Study Area

The McMurray Fm depocenter extends over 44,000 km^2 in the Alberta Foreland Basin, from 55 to 58° N and 110 to 114° W (Fig. 3.1). Paleotopography of the basal surface of the MDC is defined by relief on the Sub-Cretaceous Unconformity (SCU), with the main north to south topographic low commonly referred to as the “Assiniboia Valley”. Along the axis of the Assiniboia Valley, DUs have been completely removed by channel-

belt erosion and migration. The study area (Townships (T) 69 to 83, Ranges (R) 9 to 20W4; Fig. 3.1) is located west of the Assiniboia Valley and along the margins of the Grosmont Highlands. It extends over 15,850 km^2 and includes three paleovalleys, herein named Grouse, Sparrow, and Pelican. These paleovalleys preserve minimal strata from the lower member of the McMurray Fm (LM1 of Fig. 3.2), but do contain a continuous succession of DUs from Regional C to A1 with only limited removal of DUs by channel belts (Ranger and Pemberton, 1997; Château et al. 2019; Weleschuk and Dashtgard, 2019). The Grouse Paleovalley extends over 150 km from SW to NE and covers an area of 4,570 km^2, the Sparrow Paleovalley extends over 139 km from SW to NE and covers an area of 3,260 km^2, and the Pelican Paleovalley extends over 96 km from SW to NE and covers an area of 2,420 km^2 (Fig. 3.1C). All three paleovalleys coalesce towards the NE and the uppermost part of the McMurray Fm. In the three paleovalleys, DUs are well preserved in the southwest reaches (T69 to 75, R14 to 20W4), but are increasingly removed by channel belts towards the northeast (T80 to 83, R08 to 12W4). The thicknesses of DUs are somewhat constant throughout the study area.

3.2. Methods and Database

Data used in this study include 100 cores and 2,750 well logs with LAS files (Fig. 3.3). Cores were logged at the Core Research Centre in Calgary, Alberta, Canada, during the summer of 2015 and 2016. Well logs and core locations are given as unique well identifiers (UWI) that define a position based on the Dominion Land Survey (Fig. 3.3). The position of each well can be determined by comparison of the UWI to the DLS system. All cross sections and maps presented herein are based on the DLS coordinate system. In each core, sedimentological and ichnological characteristics were recorded using AppleCORE logging software (donated by Mike Ranger). Strata were then grouped into facies and facies associations.

Geophysical wells logs were exported from geoSCOUT® (donated to SFU by geoLOGIC Systems ltd.) and manipulated in the 3D modeling software, Petrel® 2016 (donated to SFU by Schlumberger). In the study area, over 11,000 wells have been drilled through the McMurray Formation and have publicly available well logs. Of these, 6,500 wells include digital (LAS) well-log files with gamma-ray, spontaneous potential, caliper, resistivity, neutron porosity, and sandstone density porosity curves, thus

enabling correlation and mapping in Petrel® 2016. Of the 6,500 wells with LAS files, only 2,750 completely penetrate the Regional C interval, and constitute this study's dataset.

Cross sections are generated to resolve the architecture of the Regional C interval. The Top_Regional C surface corresponds to a regionally extensive and readily correlated marine flooding surface that caps a healed paleotopography largely filled by strata; it is interpreted to have been more are less horizontal at the time of formation. On that basis, the Top_Regional C surface is used as the stratigraphic datum. Reconstructing the architecture of Regional C requires the correlation of flooding surfaces (FS) in the interval. Depositional units bounded by regionally mappable flooding surfaces of sequence stratigraphic importance differ from parasequences, in that DUs can encompass multiple parasequences that are separated by local flooding surfaces deemed to reflect autogenic processes (Château et al., 2019). Local flooding-surface correlations were undertaken in Township 82, Range 12W4, where the well density is the highest in the study area (15 wells in 93 km^2).

Isopach maps were constructed to delineate the distribution of Regional C in the study area and were created using a convergent interpolation method in Petrel® 2016. The convergent interpolation algorithm reduces extrapolation by tuning values (i.e., decreasing or increasing values) using neighboring data points (Sibson, 1981) and is the most suitable algorithm to map the somewhat flat depositional units of the McMurray Formation. Outlier values remaining in the dataset are interpreted to represent complex geologic features (e.g., faulting, karsting). Regional C is not laterally continuous across the study area; a zero thickness is assigned to wells without Regional C to limit extrapolation and improve the accuracy of Petrel's interpolation algorithm (e.g., Rinke-Hardekopf et al., 2019). In addition, to better visualize thickness trends on maps, all fluvio-tidal channels over 15 m thick are colored purple (main sediment fairways), making the "thalwegs of paleovalleys" apparent.

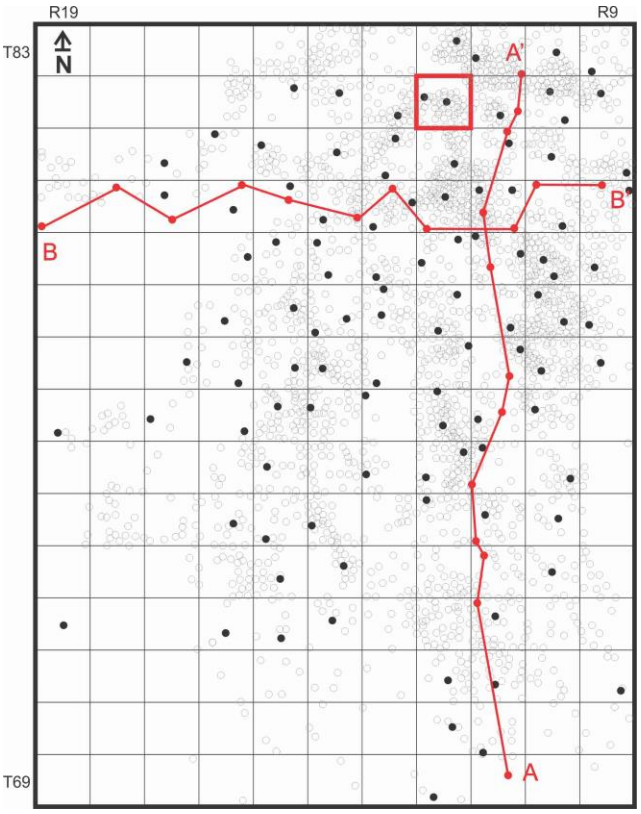

Figure 3.3 Map of the well-logs (grey dots) and core (black dots) used in this study

The grid (Dominion Land Survey (DLS) coordinate system), based on six-mile increments, divides western Canada into south to north columns of ranges (R) and east to west rows of townships (T). Each township and range block is referred to as a "township" and covers an area of 36 mi^2 (approximately 93 km^2). Well logs and core locations are given as unique well identifiers (UWI) that define a position based on the Dominion Land Survey. The position of each well can be determined by comparison of the UWI to the DLS system. The position of cross-sections A−A' and B−B' are delineated by red lines (Figs. 3.11, 3.12). A red square outlines Township 82, Range 12W4, in which autogenic parasequences are defined and mapped in cross-section C-C' (Fig. 3.14).

3.3. Facies and Facies Associations

3.3.1. Sedimentology of the Regional C Depositional Unit

For each of the 100 logged cores, lithology (grain size, sorting, roundness, color, and accessories), primary sedimentary structures, post-depositional features (diagenesis, fractures), bioturbation index (BI), and trace-fossil diversities were recorded. Based on the sedimentological and ichnological characteristics, strata are grouped into 10 discrete facies (Table 3.1; Figs. 3.4 to 3.6, 3.9). Facies successions are defined from

the distribution of those 10 facies in cores, and facies successions are grouped into three facies associations (FAs) that reflect depositional environments (Table 3.2).

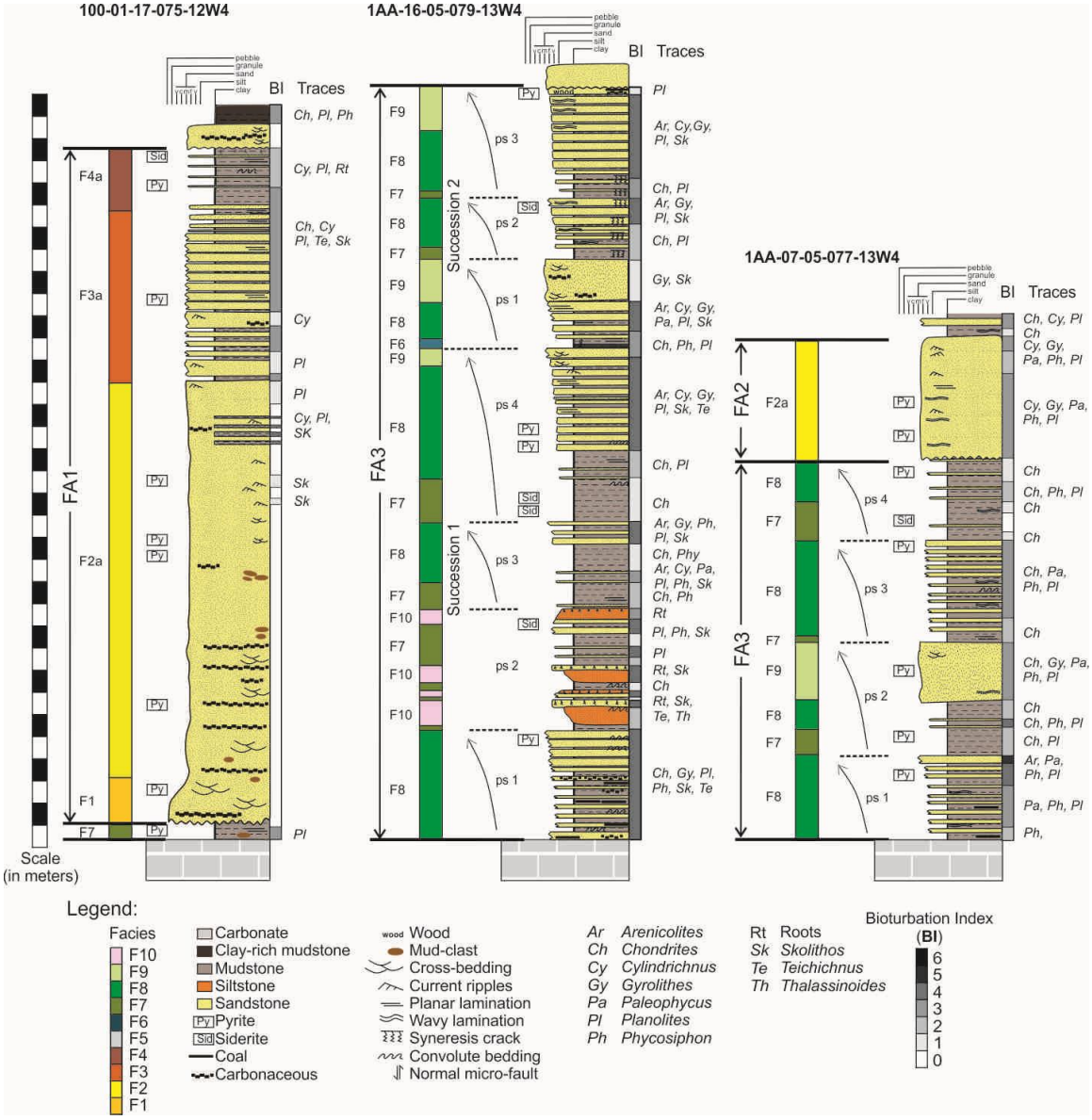

Figure 3.4 Core logs for 100-01-17-075-12W4, 1AA-16-05-079-13W4, and 1AA-07-05-077-13W4 showing lithology, sedimentary structures, bioturbation index (BI) and trace fossils

The 100-01-17-075-12W4 core interval depicts a fluvio-tidal channel (FA1) succession; the 1AA-16-05-079-13W4 interval records a series of stacked tide-dominated, storm-affected delta cycles (FA3), and the 1AA-07-05-077-13W4 interval depicts stacked tide-dominated, storm-affected delta cycles (FA3) capped by a distributary channel (FA2). Facies associations are subdivided into facies (F1 to F10). In successions 1 and 2 of FA3, parasequences are bounded by flooding surfaces (black dashed lines).

Table 3.1 **Sedimentological and ichnological characteristics, geophysical character, and contacts of facies in the McMurray Fm, southwest quadrant of the MDC. Figures showcasing the characteristics of each facies are listed (Figs. 4 to 10). Acronyms in the Facies Name, Grain Size, and Facies Description/Sedimentology columns include: inclined heterolithic stratification (IHS) very-fine lower (vfL), very-fine upper (vfU), fine lower (fL), fine upper (fU), medium lower (mL), medium upper (mU), millimeter (mm), centimeter (cm), decimeter (dc), meter (m), and decameter (dam). Ichnology is recorded in two ways: bioturbation index (BI; Taylor and Goldring, 1993) and trace-fossil diversity. Traces includes *Arenicolites* (*Ar*), *Chondrites* (*Ch*), *Cylindrichnus* (*Cy*), *Diplocraterion* (*Di*), fugichnia (fu), *Gyrolithes* (*Gy*), navichnia (na), *Palaeophycus* (*Pa*), *Phycosiphon* (*Ph*), *Planolites* (*Pl*), roots (rt), *Siphonichnus* (*Si*), *Skolithos* (*Sk*), *Taenidium* (*Ta*), *Teichichnus* (*Te*), and *Thalassinoides* (*Th*). All trace fossils in the facies are diminutive (i.e., smaller than traces deposited under optimal fully marine conditions). Gamma-ray log signature reports values in American Petroleum Institute (API) units.**

Facies			Fig. #	Facies Name	Grain-Size	Facies Description/Sedimentology	Ichnology		Depositional Process(es)	Contacts	Depositional Setting	Gamma-Ray Log Signature
							BI	Traces				
	F1		3.4a	Unbioturbated sand and/or conglomerate with mud clasts	Gravel: granule−pebble Sand: vfU to mU Mud clasts: pebble−cobble	cm−dm-scale lag overlain by dune-scale cross-stratified sands, with uncommon pebble and granule stringers. Abundant mud clasts and mud-clast breccias; abundant carbonaceous debris and pyrite concretions.	0	None	Traction transport of sand as dunes by unidirectional currents.	Erosional basal contact. Gradational upper contact with F2a.	Channel thalweg or base of channel lag.	Blocky signature with values < 45 API.
	F2	a	3.4b, c	Weakly bioturbated cross-stratified to current-rippled sand	Sand: vfU to mU Mud clasts: pebble−cobble	dm−dam-scale intervals of cm-dm-thick, dune-scale cross-stratified and/or current-rippled sand with reactivation surfaces. Mud drapes, mud clasts, mud-clast breccia, thin mud flasers (mm-cm scale), and carbonaceous debris.	0−2	*Cy*, fu, *Pl, Sk* (diminutive)	Mainly traction transport of sand as dunes and ripples by unidirectional and/or bidirectional currents.	Gradational lower contact with F1. Gradational upper contact with F3a. Sharp or gradational upper contact F4a.	Base of channel or lower (subtidal) point bar.	Blocky to upward increasing API values that range from > 45 to < 75 (*i.e.*, fining upward).
		b	3.5a		Sand: vfU to mU Mud clasts: pebble	m-scale interval of cm-dm-thick, dune-scale cross-stratified sand beds, current ripples, and rare oscillation ripples. Mud drapes, mud clasts, thin (mm-cm-thick) mud flasers, and carbonaceous debris.	0−4	*Ar, Ch, Cy, Di, Pa, Pl, Si, Sk* (diminutive)	Mainly traction transport of sand as dunes and ripples by unidirectional, bidirectional and/or oscillatory currents.	Erosional basal contact. Gradational upper contact with F3b.	Distributary channels (bay head delta or bay margin).	
	F3	a	3.4d, e	Weakly to thoroughly bioturbated sand-dominated IHS	Sand: vfU to mL Mud: undifferentiated	dm−dam-scale interval of cm−dm-thick beds of sand and mudstone with current ripples (locally aggradational), planar parallel lamination, reactivation surfaces, mud drapes, thin (mm-cm-scale) mud flasers, and abundant carbonaceous debris.	Sand: 0−5 Mud: 1−5	Sand: *Cy*, na, *Pa, Pl, Sk, Th* Mud: *Ch,* na, *Pa, Pl, Te* (diminutive)	Lateral and downstream accretion of sand and mud on bars by unidirectional and/or bidirectional currents.	Gradational lower contact with F2a. Gradational upper contact with F4a. Sharp internal contacts.	Subtidal point bar IHS (lateral accretion).	Serrated profile, generally upward increasing API values that range from < 75 to < 90 (*i.e.*, fining upward).
		b	3.5b			dm−m-scale interval of cm−dm-thick beds of sand and mudstone with current ripples, planar parallel lamination, rare oscillation ripples, uncommon syneresis cracks, mud drapes, thin (mm-cm-scale) mud flasers, and abundant carbonaceous debris.	Sand: 1−4 Mud: 2−5	Sand: *Cy,* na, *Pa, Pl, Si, Sk, Th* Mud: *Ch,* na, *Pa, Pl, Te, Th* (diminutive)	Accretion of sand and mud along channel margins by unidirectional, bidirectional and/or oscillatory currents.	Gradational lower contact with F2b. Gradational upper contact with F4b. Sharp internal contacts.	Channel margin IHS.	
	F4	a	3.4f	Thoroughly bioturbated mudstone-dominated IHS	Sand: vfU to mL Mud: undifferentiated	dm−dam-scale interval of mm−cm-thick sand units in a mudstone matrix with planar parallel lamination, normal grading, soft-sediment deformation structures, and abundant carbonaceous debris.	Sand: 1−5 Mud: 1−5	Sand: *Cy,* fu, *Pl,* roots, *Sk, Te* Mud: *Ch,* na, *Pl,* rt, *Te, Th* (diminutive)	Bar-top deposition during high tide by ebb-oriented currents and possibly upstream *via* flow separation.	Gradational lower contact with F3a. Sharp or erosional upper contact with F1/F2a,b/F5/F6. Sharp internal contacts commonly overprinted by bioturbation.	Upper (intertidal) point bar IHS, counter point bar.	Oblong signature, with API values > 90.
		b	3.5c			dm−m-scale interval of mm−cm-thick sand layers in a mudstone matrix with planar parallel lamination (normal grading), rare syneresis cracks, soft-sediment deformation structures, and abundant carbonaceous debris.	Sand: 1−5 Mud: 1−5	Sand: *Cy,* fu, *Pl, Sk, Te* Mud: *Ch,* na, *Pl, Ta, Te*		Gradational lower contact with F3b. Sharp or erosional upper contact with F1/F2a,b/F5/F6. Sharp internal contacts commonly overprinted by bioturbation.	Channel-margin IHS.	

Facies	Fig. #	Facies Name	Grain-Size	Facies Description/Sedimentology	Ichnology		Depositional Process(es)	Contacts	Depositional Setting	Gamma-Ray Log Signature
					BI	Traces				
F5	3.4g, h	Weakly bioturbated preserved to pedogenetically altered silty mudstone	Sand: vfL to fU Mud: undifferentiated	dm−dam-scale interval of mm−cm-thick silty sand layers in a mudstone matrix, with planar parallel lamination, rare syneresis cracks, soft-sediment deformation structures, normal micro-faults, carbonaceous debris, abundant fractures, siderite concretion, and rare pyrite concretion.	Sand: 0−2 Mud: 0−1	Sand: *Ar,* na*, Pl, Sk, Te* Mud: *Ch, Pl,* rt	Vertical aggradation of sediment during channel abandonment (unidirectional currents) by settling and/or accretion of sediment *via* bidirectional currents; subaerial exposure.	Sharp lower contact with F2a/F3a. Erosional upper contact, locally with omission suite of the *Glossifungites* Ichnofacies.	Abandoned channel.	Oblong signature, with API values > 100.
F6	3.8a	Weakly to moderately bioturbated, dark gray mudstone	Sand: vfL to fL Mud: undifferentiated	cm−dm-scale interval of mm−cm-thick silty sand lenses/beds in a dark gray mudstone matrix, with planar to wavy parallel lamination, normal micro-faults, and syneresis cracks.	1−3	*Ch*, *Pl*, *Ph*, *Sk* (diminutive)	Vertical aggradation of sediment by unidirectional and/or oscillatory currents.	Sharp or erosional basal contact. Gradational upper contact with F6.	Distal prodelta	Oblong signature with values >100 API.
F7	3.8b, c	Weakly to moderately bioturbated, convolute-bedded silty mudstone	Sand: vfL to fL Mud: undifferentiated	cm−dm-scale interval of rare mm−cm-thick silty sand beds in a mudstone matrix, with carbonaceous debris and convolute bedding.	1−4	*Ch*, *Cy*, fu, *Ph*, *Pl*, *Sk, Th* (diminutive)	Vertical aggradation of sediment by unidirectional currents.	Sharp or gradational (F6) basal contact. Gradational upper contact with F8a. Sharp internal contacts.	Proximal prodelta. Protected embayment or lagoon	Oblong signature with API values ranging from 80−100.
F8	3.8d, e	Weakly to thoroughly bioturbated, heterolithic sand and mudstone bedset	Sand: vfL to mL Mud: undifferentiated	dm−m scale interval of interbedded cm−dm thick interbedded sand and mudstone beds, with planar to undulatory-parallel lamination, current ripples, combined flow ripples, convolute bedding, normal micro-faults, syneresis cracks, carbonaceous debris, and pyrite and siderite concretions.	1−5	*Ar*, *Ch*, *Cy*, fu, *Gy*, na, *Pa*, *Ph*, *Pl*, *Sk*, *Te*, *Th* (diminutive)	Vertical aggradation of sediment by unidirectional and/or oscillatory currents.	Gradational lower contact with F7. Gradational upper contact with F9. Sharp internal contacts typically overprinted by bioturbation.	Distal tidal sand bar	Upward decreasing signature with API values that range from >75 to >100 (*i.e.,* coarsening upward).
F9	3.8f, g	Unburrowed to thoroughly bioturbated, current-rippled to low-angle cross-stratified sand	Sand: vfL to mL	m-scale interval of cm−dm-thick dune-scale cross-stratified sand, with micro-hummocky cross-stratificion, hummocky cross-stratification, current ripples with reactivation surfaces, rare oscillation ripples, combined-flow ripples, normal micro-faults, mud drapes, and carbonaceous debris.	0−5	*Ar*, *As*, *Ch*, *Cy*, *Di*, *Gy*, fu, na, *Pa*, *Ph*, *Pl*, *Sk*, *Te* (diminutive)	Vertical aggradation of sediment by unidirectional, bidirectional, and/or oscillatory currents.	Gradational lower contact with F8. Sharp or erosional upper contact.	Tidal sand bar	Upward decreasing to blocky signature with API values <75 (*i.e.,* coarsening upward).
F10	3.8h, i	Moderately bioturbated, siltstone to root-bearing sand	Sand: vfL to fL Mud: silt	dm−m-scale coarsening-upward interval of siltstone to sand, with rare convolute bedding. Most structures are overprinted by bioturbation and locally by rooting.	2−4	*Ch*, rt, *Sk*, *Te*, *Th* (diminutive)	Vertical aggradation of sediment, subaerial exposure at the top (rooting).	Gradational (F6/F7/F8) or sharp lower contact. Sharp upper contact.	Supratidal bar	API values ranging from 60−90.

Table 3.2 Table summarizing the three facies associations, fluvio-tidal channels (FA1), distributary channels (FA2), and tide-dominated storm-affected deltas (FA3), and the 2 to 3 recurring facies successions that define each FA. The interpretation column includes the acronym Tfw for tide-dominated, fluvial -influenced, storm-affected delta and Twf for tide-dominated, storm-influenced, fluvial-affected delta.

Facies Association	Facies Succession	Facies (Base to Top)	Succession Interpretation
Fluvio-Tidal Channels (FA1)	1	F1, F2a, F3a, F4a	Point-bar
	2	F1, F3a, F4a	Muddy point-bar or counter point-bar
	3	F1, F2a, F3a or F4a, thick F5	Abandoned channel
Distributary Channels (FA2)	1	F2b, F3b, F4b	Channel margin
	2	Thin F2b, F3b, F4b	Channel bar
Tide-dominated storm-affected deltas (FA3)	1	F6, F7, F8, F9, F10	Tfw delta
	2	F6, F7, F8, F9	Twf delta

Facies Association 1 (FA1): Fluvio-Tidal Channels

Description: Five facies define FA1 (Table 3.1; Figs. 3.4 to 3.5, 3.7). In those facies, physical sedimentary structures are exclusively of current origin and dominated by dune-scale cross-stratified sand beds, subordinate planar parallel lamination, flaser bedsets, and stacked current-ripple cross-lamination. Facies 1 to 5 also contain mudstone interbeds with parallel laminae and normal grading, carbonaceous detritus, soft-sediment deformation, and local occurrences of syneresis cracks, particularly in bedsets of F3 and F4. Facies 3 and 4 consist of decimeter to meter thick intervals of alternating and inclined (< 20°) beds of sand and mudstone, stratification commonly referred to as inclined heterolithic stratification (IHS; Thomas et al., 1987). Ichnologically, the facies of FA1 exhibit a number of predictable trends. First, the bioturbation index (BI; Taylor and Goldring, 1993) increases upwards from BI 0 in cross-bedded sands of F1 to BI 5 in some intervals of muddy IHS (F4a; Table 3.1; Figs. 3.4, 3.7). The trace-fossil suites encompass eight ichnogenera: *Arenicolites, Chondrites, Cylindrichnus, Palaeophycus, Planolites, Skolithos, Teichichnus,* and *Thalassinoides*, as well as fugichnia and navichnia. Root structures also occur in mudstone-dominated intervals of F4a and F5 towards the tops of some successions. The trace fossils in FA1 are generally diminutive (i.e., smaller than traces deposited under optimal fully marine conditions; see Pemberton and Wightman, 1992)(Table 3.1). Trace fossils mainly record mobile deposit-feeding and dwellings of deposit feeders and carnivores; in all cases, the suites are dominated by facies-crossing structures. On gamma-ray well logs, FA1 shows a blocky to upward-increasing API (fining-upward) signature. The gamma-ray response in FA1 increases from F1 into F5 with values < 45 API (Table 3.1).

In FA1, three facies successions are defined based on the distribution of these five facies (Table 3.2). Facies Succession 1 exhibits a general fining-upward trend directly overlying an erosion surface. This surface is overlain by unbioturbated sand with mud clasts of Facies 1 (F1), which passes upward into weakly bioturbated, cross-stratified to current-rippled sand (F2a) and then into weakly to thoroughly bioturbated, sand-dominated IHS (inclined heterolithic stratification; F3a). The complete succession is capped by thoroughly bioturbated, mudstone-dominated IHS (F4a; Tables 3.1, 3.2; Figs. 3.4 to 3.5, 3.7). Facies Succession 2 is less common, and likewise exhibits a fining-upward profile resting on an erosional basal surface overlain by F1. Unlike Facies Succession 1, however, the interval lacks the cross-stratified sand of Facies 2a, and

passes directly upward into thick intervals of sand-dominated IHS (F3a) and/or mudstone-dominated IHS (F4a). Facies Succession 3 is also a fining-upward succession (Table 3.2), which rests on an erosional surface overlain by F1 and passes upward into F2a. In contrast with facies successions 1 and 2, the current-rippled sands of F2a are both overlain by a thin IHS unit of F3a and/or F4a and abruptly capped by a thick interval of weakly bioturbated silty mudstone (F5).

Interpretation: The three fining-upward facies successions record spatial variations in facies that record deposition in a fluvio-tidal channel complex. Facies Succession 1 (F1, F2a, F3a, F4a; Table 3.2; Figs. 3.4, 3.7) is interpreted as a tidally influenced point bar. Facies Succession 2 (F1, F3a, F4a) is interpreted as a muddy point bar and/or counter point bar deposit. As such, both facies successions result from the lateral and downstream accretion of channels. Facies succession 3 (F1, F2a, F3a or F4a, F5), by contrast, corresponds to channel abandonment and shows remnant channel-floor deposits abruptly overlain by the abandonment mud plug.

Channel belts observed in the Regional C DU has facies similar to those previously defined in the MDC (e.g., Mossop and Flach, 1983; Smith, 1988; Ranger and Pemberton, 1997; Hein and Cotterill, 2006; Hubbard et al., 2011; Smith et al., 2011; Musial et al., 2012; Martinius et al., 2017; Hagstrom et al., 2019; Horner et al., 2019; Martin et al., 2019). Physical sedimentary structures observed in FA1 arise either in purely fluvial or tidally influenced fluvial settings (Dalrymple and Choi, 2007; Davis and Dalrymple, 2011; Ashworth et al., 2015; Dashtgard and La Croix, 2015; La Croix and Dashtgard, 2015). The ichnological dataset comprises diminutive trace fossils in a suite that includes ichnogenera not known to be made by freshwater organisms and not known in fluvial deposits. Consequently, the trace-fossil suite is interpreted to indicate brackish-water conditions (Pemberton et al., 1982; Pemberton and Wightman, 1992; Gingras et al., 1999; Gingras et al., 2012; Gingras et al., 2016; La Croix et al., 2015). The combined sedimentological and ichnological observations suggest that these channel belts are fluvio-tidal channels (Weleschuk and Dashtgard, 2019).

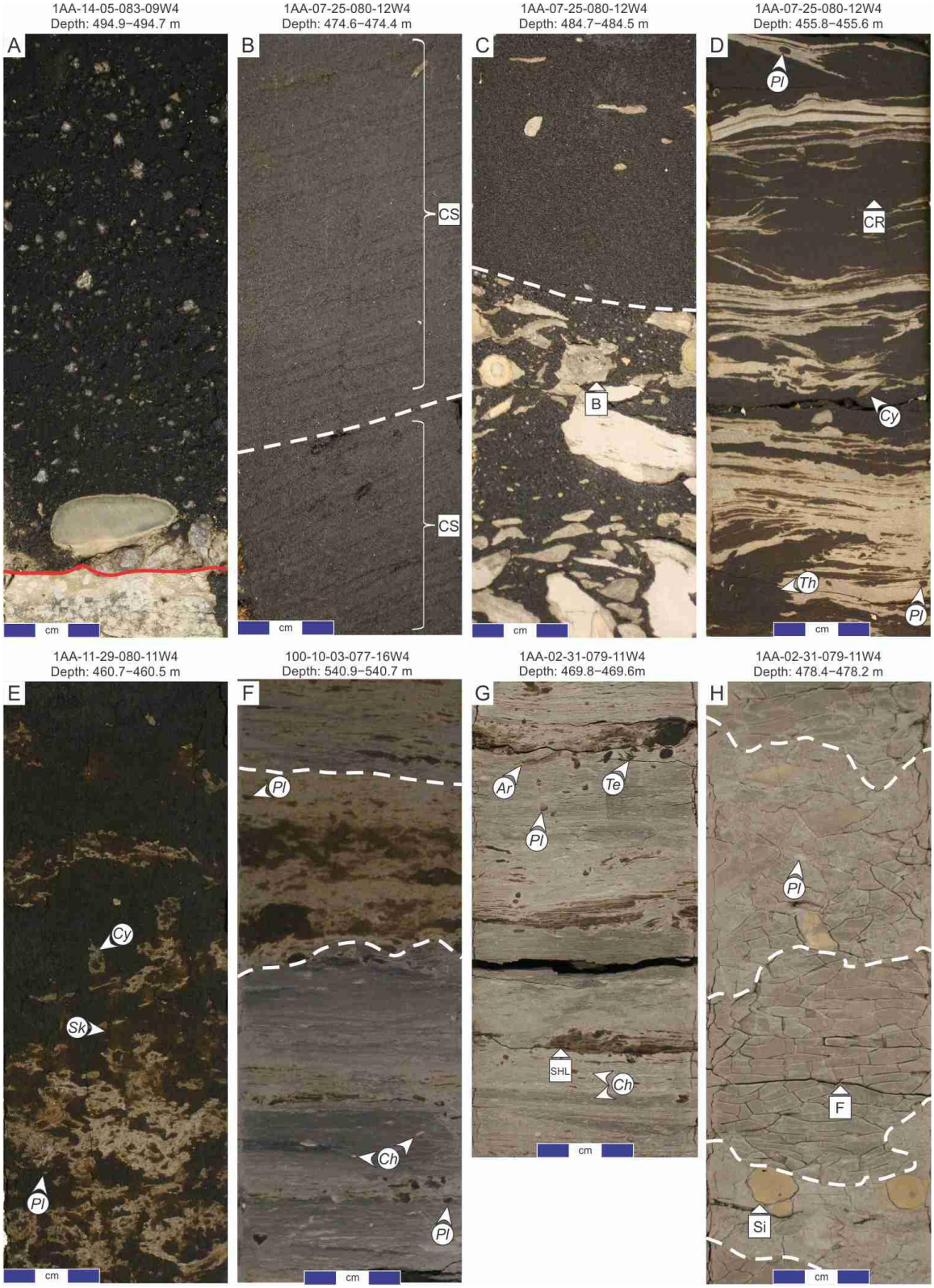

Figure 3.5 **Core photos for Facies Association 1 (F1, F2a, F3a, F4a, F5): fluvio-tidal channels**

Note that the sand is brown to dark brown in color, reflecting bitumen saturation. Mudstone beds are either beige or light to dark gray. A) Facies 1 (F1) consists of unbioturbated (BI 0) sand with granules and mud clasts. These deposits overlie the Sub-Cretaceous Unconformity (red line) excavated into Paleozoic carbonates. B, C) Facies 2a showing dune-scale cross-stratification (CS) with a scour surface between cross-bed sets (dashed white line). Photo C displays mud-clast breccia with quartz and chert granules below the dashed white line. D, E) Facies 3a (F3a) corresponding to weakly to thoroughly bioturbated (BI 0 to 5) sand-dominated IHS. Photo D shows weakly bioturbated (BI 0 to 2), wavy-bedded, sand-dominated IHS with mud drapes on current-ripple (CR) foresets and a trace-fossil suite that includes *Cylindrichnus* (Cy), *Planolites* (Pl), and *Thalassinoides* (Th). Photo E shows thoroughly bioturbated (BI 3 to 5), sand-dominated IHS with a trace-fossil suite composed of *Cylindrichnus*, *Planolites,* and *Skolithos* (Sk). F) Facies 4a (F4a) consisting of thoroughly bioturbated (BI 1 to 5), mudstone-dominated IHS with a sand-bed demarcated by the dashed white lines, and a trace-fossil suite composed of *Chondrites* and *Planolites*. G) and H) Facies 5 (F5), corresponding to weakly bioturbated (BI 0 to 2) to pedogenetically altered silty mudstone. Photo G displays weakly bioturbated (BI 0 to 2) silty mudstone, with sand heterolithic lenses (SHL) and a suite composed of *Arenicolites* (Ar), *Chondrites*, *Planolites*, and *Teichichnus* (Te). Photo H shows pedogenetically altered, weakly bioturbated (BI 0 to 2) silty mudstone, with silty beds marked out by dashed white lines. Facies also contains siderite nodules (Si), fractures (F), and a monogeneric suite of *Planolites.*

Facies Association 2 (FA2): Distributary Channels

Description: FA2 encompasses fining-upward successions similar to FA1. FA2 differs from FA1, however, in the scale of the packages (i.e., FA2 channels are one order of magnitude smaller than those in FA1). Additionally, facies in FA2 record a stronger degree of marine influence than facies in FA1.

FA2 successions encompass three facies (F2b, F3b, and F4b) (see Table 3.2) and include both current- and oscillation-generated primary sedimentary structures. Primary structures include dune-scale cross-stratification, subordinate planar parallel lamination, current ripples, rare oscillation ripples, mud drapes, and flaser bedding. The three facies also include abundant carbonaceous detritus as well as local occurrences of soft-sediment deformation and syneresis cracks, particularly in IHS bedsets of F3b and F4b. Ichnologically, bioturbation intensities of FA2 deposits range from BI 0 to 5, and the trace-fossil suite comprises 11 ichnogenera: *Arenicolites, Chondrites, Cylindrichnus, Diplocraterion, Palaeophycus, Planolites, Siphonichnus*, *Skolithos, Taenidium, Teichichnus,* and *Thalassinoides*, as well as fugichnia and navichnia (Fig. 3.6). The trace fossils in FA2 are diminutive (Table 3.1). Like FA1, these biogenic structures mainly record mobile deposit-feeding behaviors and the dwellings of inferred deposit-feeders and carnivores. The suites are dominated by facies-crossing elements in all three facies. On gamma-ray well logs, FA2 shows a blocky to upward-increasing API (fining-upward) signature. The gamma-ray response increases from F2b through to F4b, with values ranging from 45 to 90 API (Table 3.1).

In FA2, two distinct facies successions are defined, based on the proportion of these three facies (Table 3.2). Facies Succession 1 typically exhibits a fining-upward trend that comprises an erosional basal surface overlain by a thick interval of weakly bioturbated, cross-stratified to current-rippled sand of Facies 2b (F2b). This passes into a thin interval of weakly to thoroughly bioturbated sand-dominated IHS of F3b. The succession is typically top truncated, but where fully preserved is capped by a thin interval of thoroughly bioturbated, mudstone-dominated IHS of F4b. There are numerous occurrences of facies succession 1 that end before the deposition of F3b or F4b (Table 3.2; Fig. 3.8). Facies Succession 2 is also a fining-upward succession and only differs from Facies Succession 1 with respect to facies thicknesses; Facies Succession 2 comprising only a thin interval F2b overlain by well-developed intervals of F3b and F4b.

Interpretation: The two fining-upward facies successions record lateral facies changes reflecting deposition in a complex of distributary channel. Facies Succession 1 (thick F2b, absent or thin F3b and absent or thin F4b) is interpreted as a channel margin, while Facies Succession 2 (thin F2b, thick F3b, and thick F4b) is interpreted as an internal channel bar. These channel deposits are of limited thickness, ranging from 2 to 15 m and typically 3 to 8 m in the Regional C DU (Fig. 3.4). Channels of similar scale were previously defined in the McMurray Fm for the B2, B1, and A2 DUs (Baniak and Kingsmith, 2018). Physical sedimentary structures observed in the successions are characteristic of fluvial settings subjected to tidal and wave influence (e.g., Olariu and Bhattacharya, 2006; Dashtgard and La Croix, 2015; La Croix and Dashtgard, 2015). The ichnological suites are of low diversity, but consist of diminutive facies-crossing ichnogenera not known to be made by freshwater organisms and not known from fluvial and freshwater deposits; correspondingly, the facies are interpreted to indicate brackish-water conditions (e.g., Pemberton et al., 1982; Pemberton and Wightman, 1992; Gingras et al., 1999; Gingras et al., 2012; Gingras et al., 2016; La Croix et al., 2015). The combined sedimentological and ichnological observations indicate that these channel-belt deposits represent distributary channels.

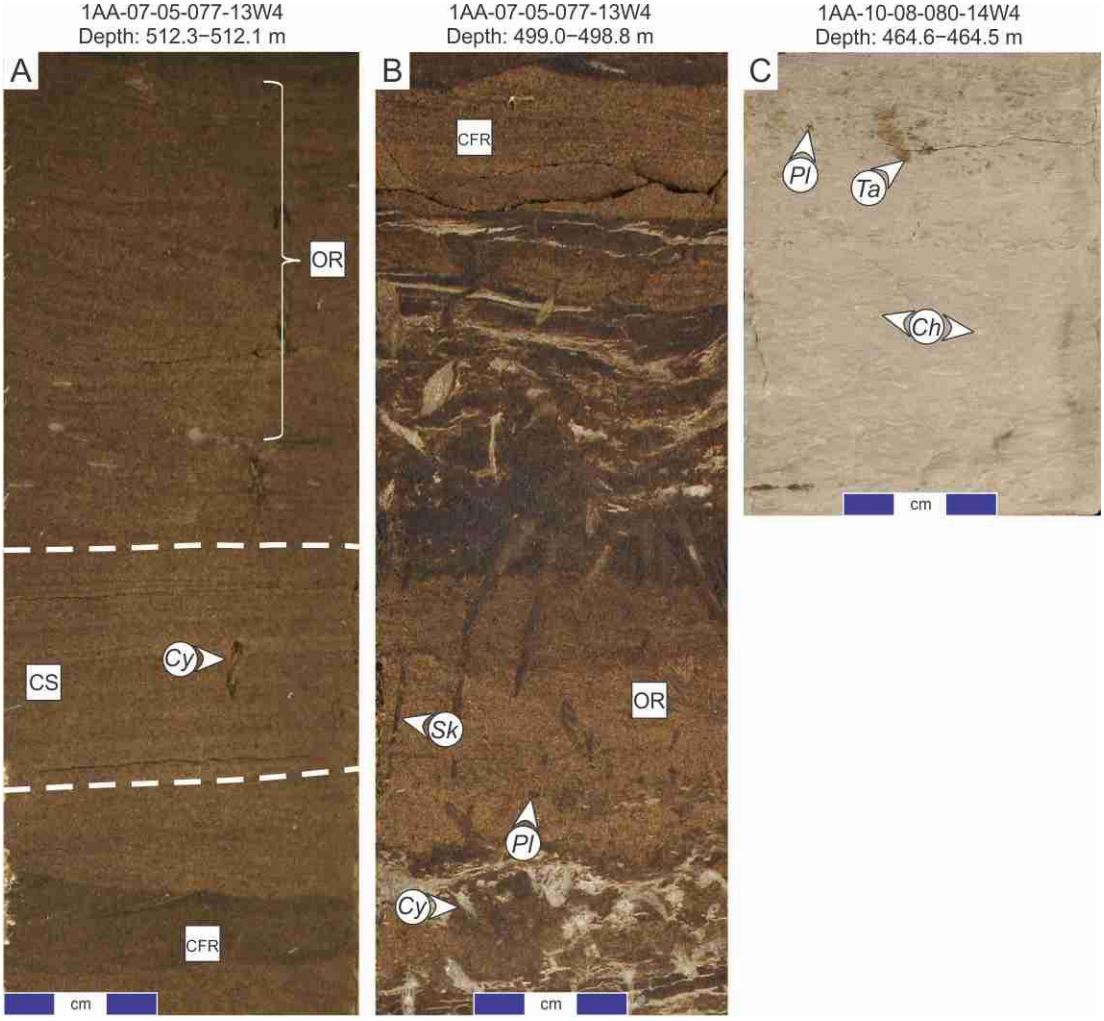

Figure 3.6 Core photos for Facies Association 2 (F2b, F3b, F4b): Distributary channels

Note that the sand is either light brown (bitumen stained or water saturated) or dark in color (bitumen saturated). Mudstone beds are either beige or light gray. A) Facies 2b (F2b) consists of weakly bioturbated (BI 0 to 4), cross-stratified to current-rippled sand. Photo A shows combined-flow ripples (CFR), low-angle, dune-scale cross-stratification (CS), oscillation ripples (OR), and a monogeneric trace fossil-suite of *Cylindrichnus* (Cy). Beds dominated by distinct physical sedimentary structures are marked by white dashed lines. B) Facies 3b (F3b) consists of weakly to thoroughly bioturbated (BI 1 to 5), sand-dominated IHS with oscillation ripples, combined-flow ripples, and a trace-fossil suite composed of *Cylindrichnus, Planolites* (Pl), and *Skolithos* (Sk). C) Interval shows thoroughly bioturbated (BI 1−5) mudstone beds of Facies 4b (F4b). Trace fossil suite is composed of *Chondrites, Planolites*, and *Taenidium* (Ta).

Figure 3.7 Facies Association 1 (FA1): fluvio-tidal channel extending from 532−501 m in the 100-01-17-075-12W4 well

Note that the sand is either light brown (bitumen stained but water saturated) or dark in color (bitumen saturated). Mudstone beds are either beige or light to dark gray. Core columns are 7.6 cm wide and 75 cm long, and facies and facies-association distributions are labelled on either the left or right and at bottom of the core box photos. From the base to the top: Devonian carbonates are separated from the overlying Lower Cretaceous McMurray Fm by the Sub-Cretaceous Unconformity (SCU; red line near base of cored interval, first column, bottom row). The initial McMurray Fm deposits consist of F6 (weakly to moderately bioturbated, dark gray mudstone) and are sharply overlain by FA1. FA1 fines upwards from weakly bioturbated cross-stratified to current-rippled sand (F2a) through weakly to thoroughly bioturbated, sand-dominated IHS (F3a), and into thoroughly bioturbated, mudstone-dominated IHS (F4a). Contacts between F2a, F3a, and F4a are gradational (yellow dashed line). A sharp contact (red line near top of cored interval, last column, top row) separates FA1 from the overlying F2b facies of FA2.

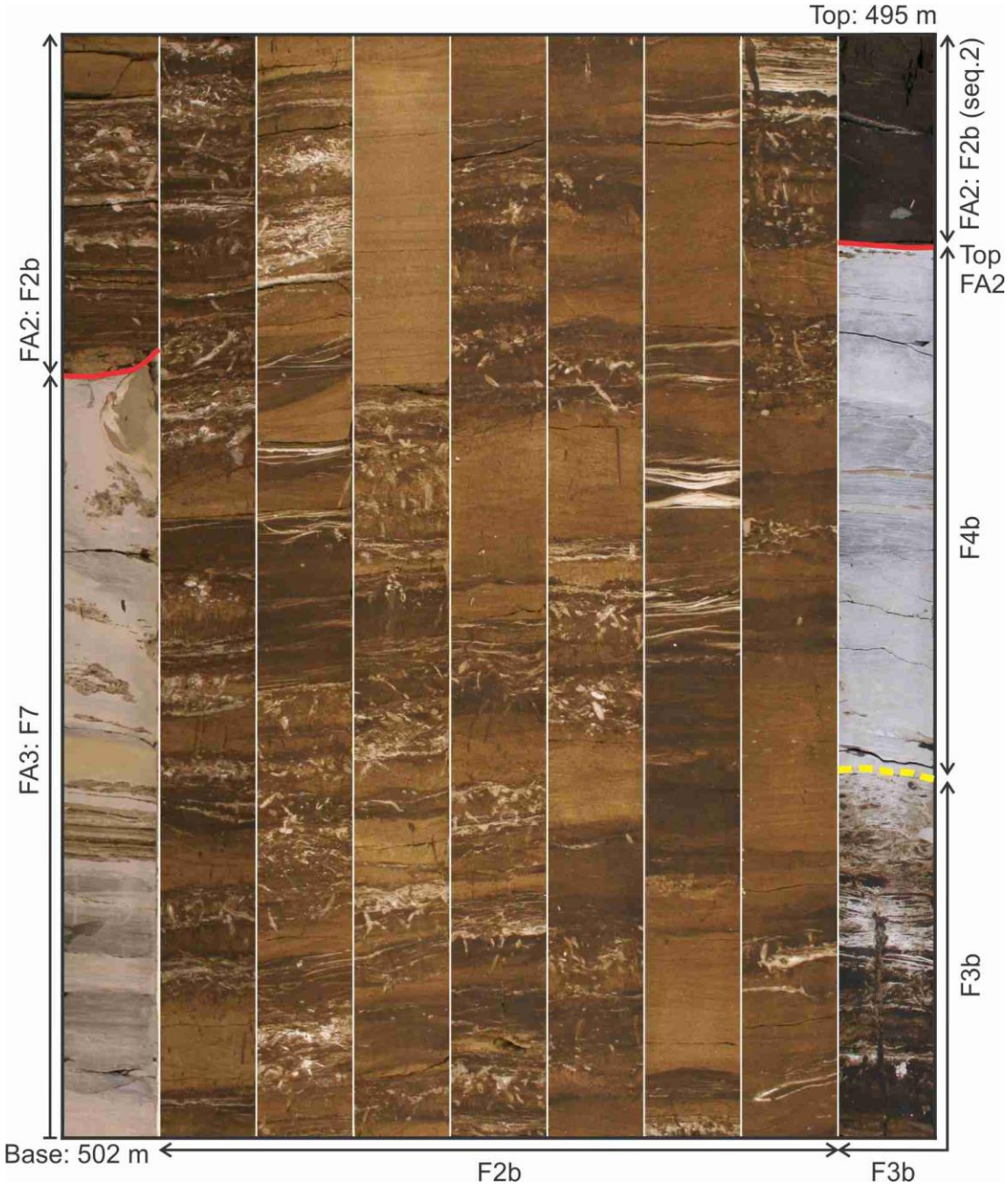

Figure 3.8 Facies Association 2 (FA2): distributary channel extending from 502−495 m in the 1AA-07-05-077-13W4 well

Note that the sand is either light brown (bitumen stained but water saturated) or dark in color (bitumen saturated). Mudstone beds are either beige or light to dark gray. Core columns are 7.6 cm wide and 75 cm long, and facies and facies-association distributions are labelled on the left, right, and at bottom of the core box photos. From base to top: tide-dominated, storm-affected delta deposits (FA3) are separated from overlying FA2 deposits by a scour surface (red line near bottom of cored interval). FA2 fines upwards from weakly bioturbated, cross-stratified to current-rippled sand (F2b) into weakly to thoroughly bioturbated, sand-dominated IHS (F3b), and is capped by thoroughly bioturbated, mudstone-dominated IHS (F4b). Contacts between F2b, F3b, and F4b are gradational (yellow dashed line). A sharp contact (red line near top of cored interval) separates a lower FA2 succession from the overlying F2b facies of a second FA2 succession.

Facies Association 3 (FA3): Tide-Dominated, Storm-Affected Deltas

Description: Facies Association 3 includes five facies (F6 to F10; Table 3.1; Figs. 3.4, 3.9, 3.10). In these facies, both current- and oscillation- generated physical sedimentary structures are observed. Primary structures include current, oscillation and combined-flow ripples, dune-scale cross-stratification, micro-hummocky and hummocky cross-stratification, and soft-sediment deformation. Facies (F6 to F10) also contain mudstone interbeds with planar to wavy parallel laminae and/or sand lenses, carbonaceous debris, and syneresis cracks. Ichnologically, bioturbation intensities are typically variable (BI 0 to 5, but mainly BI 1 to 4). The trace-fossil suite encompasses 12 ichnogenera: *Arenicolites, Asterosoma, Chondrites, Cylindrichnus, Diplocraterion, Gyrolithes, Palaeophycus, Phycosiphon, Planolites, Skolithos*, *Teichichnus,* and *Thalassinoides*, with fugichnia and navichnia. Root structures are common in F10. Trace fossils are diminutive (Table 3.1) and mainly record mobile deposit-feeding behaviors and the dwellings of deposit-feeders and carnivores. On gamma-ray well logs, FA3 deposits are typically expressed as a decreasing-upward API (i.e., increase in sand content upward) profile. In FA3, the gamma-ray response is higher than 60 API gamma-ray (Table 3.1).

In FA3, two facies successions are defined on the basis of the distribution of facies (F6 to F10; Table 3.2). Facies Succession 1 forms an interval consisting of vertically stacked, coarsening-upward cycles. The succession typically overlies a sharp but generally non-erosional basal surface overlain by weakly to moderately bioturbated, dark gray mudstone (F6) and/or weakly to moderately bioturbated, convolute bedded silty mudstone (F7; Tables 3.1, 3.2, Figs. 3.4, 3.9, 3.10). Facies 6 and 7 pass upward into weakly to thoroughly bioturbated, heterolithic sand and mudstone (F8) and unburrowed to thoroughly bioturbated, current rippled to low-angle cross-stratified sand (F9) and into moderately bioturbated, siltstone to root-bearing sand (F10; Figs. 3.4, 3.9, 3.10). There are numerous occurrences of Facies Succession 1 in FA3 that end without deposition of F9 and/or F10. Facies Succession 2 also comprises vertically stacked, coarsening-upward stratal packages, but unlike Facies Succession 1, lacks F10.

Interpretation: The stacked coarsening-upward facies successions of FA3 are interpreted as shoaling-upward cycles (Wilson 1975) bounded by flooding surfaces, and are referred to as parasequences (PS; Van Wagoner et al., 1988, 1990). Physical

sedimentary structures observed in the PS were formed by unidirectional currents, bidirectional currents, and/or oscillatory flow. Facies Succession 1 is dominated by unidirectional and/or bidirectional current-generated structures (> 80%) and subordinate oscillation-generated structures (< 15%). By contrast, Facies Succession 2 shows that the proportion of oscillation-generated structures reaches 40%. The ichnological suite in FA3 comprises diminutive traces indicative of persistent brackish-water conditions (e.g., Pemberton et al., 1982; Pemberton and Wightman, 1992; Gingras et al., 1999; Gingras et al., 2012; Gingras et al., 2016; La Croix et al., 2015). Root-bearing intervals at the top of F10 are attributed to subaerial exposure. Based on the combination of sedimentological and ichnological characteristics, and following process classification of paralic settings by Ainsworth et al. (2011), FA3 is interpreted as a tide-dominated, storm-affected delta (Tw). Facies Succession 1 is interpreted as stacked tide-dominated, fluvial-influenced, storm-affected (Tfw) parasequences, whereas Facies Succession 2 represents tide-dominated, storm-influenced, fluvial-affected (Twf) parasequences. These parasequences shallow upward from the prodelta (F7 and F8), through tidal sand bars (F8 and F9), and into subaerially exposed (supratidal) bar tops (F10).

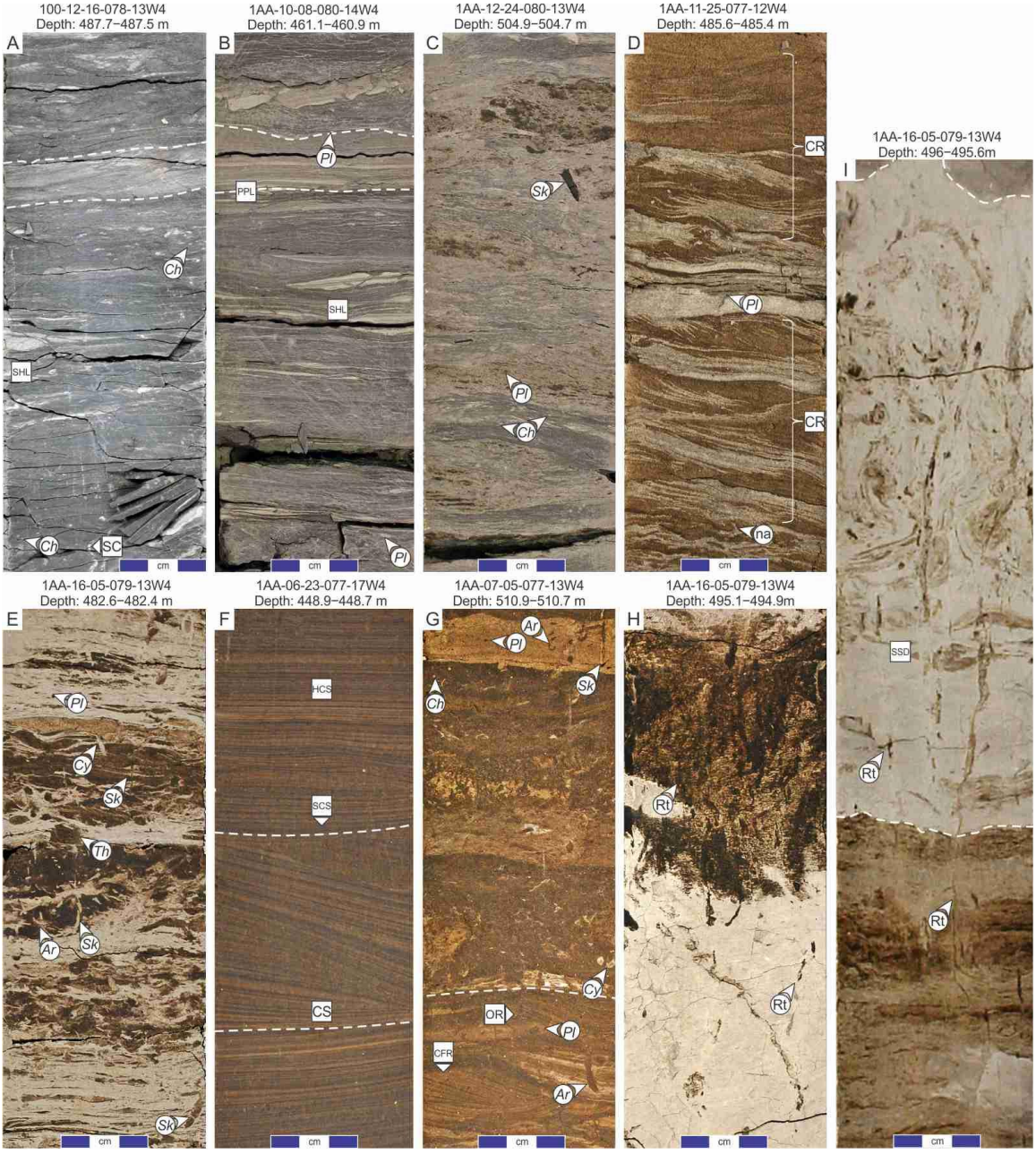

Figure 3.9 Core photos for Facies Association 3 (F6, F7, F8, F9 and F10): tide-dominated storm-affected deltas

Note that the sand is either light brown (bitumen stained but water or gas saturated) or dark brown (bitumen saturated). Mudstone beds are either beige or light to dark gray. A) Facies 6 (F6) consists of weakly to moderately bioturbated (BI 1 to 3), dark gray mudstone. Photo A displays silty sand beds delineated by the white dashed lines. The facies also contains sandy heterolithic lenses (SHL), syneresis cracks (SC), and a monogeneric trace-fossil suite of *Chondrites* (Ch). B, C) Facies 7 (F7) showing silty mudstone. Photo B displays weakly bioturbated (BI 1) F7 with planar parallel laminae (PPL; dashed white lines), sandy heterolithic lenses (SHL), and a monogeneric trace-fossil suite of *Planolites* (Pl). Photo C shows thoroughly bioturbated (BI 3 to 5) F7 with a trace-fossil suite composed of *Chondrites*, *Planolites*, and *Skolithos* (Sk). D, E) Facies 8 (F8) corresponds to weakly to thoroughly bioturbated (BI 1 to 5), heterolithic sand and mudstone bedsets. Photo D shows weakly bioturbated (BI 0 to 1), wavy bedded heterolithics with mud-

draped current-ripple foresets (CR) and a trace-fossil suite composed of *Planolites* and navichnia (na). Photo E shows thoroughly bioturbated (BI 3 to 5), heterolithic sand and mudstone bedsets with a trace-fossil suite composed of *Arenicolites* (Ar), *Cylindrichnus* (Cy), *Planolites, Skolithos*, and *Thalassinoides* (Th). F, G) Facies 9 (F9) corresponds to unburrowed to thoroughly bioturbated (BI 0 to 5), current-rippled to low-angle cross-stratified sand. Photo F displays dune-scale cross-stratification (CS) overlain by swaly cross-stratification (SCS) to hummocky cross-stratification (HCS). Structures are delineated by the white dashed lines. In Photo G, F9 includes weakly bioturbated beds (below white dashed line), with oscillation ripples and combined-flow ripples as well as thoroughly bioturbated beds (above white dashed line). Photo G shows a trace fossil-suite composed of *Arenicolites, Chondrites, Cylindrichnus, Planolites*, and *Skolithos.* H, I) Facies 10 (F10) corresponds to moderately bioturbated (BI 2 to 4), siltstone to root-bearing (rt) sand. In photo H, the mudstone at the base is pedogenetically altered. In photo I, F10 (delineated by white dashed lines), overlies thoroughly bioturbated heterolithic sand and mudstone bedsets (F8) and is, in turn, overlain by weakly to moderately bioturbated (BI 1 to 4) convolute-bedded silty mudstone (F7). In this photo, F10 also shows soft-sediment deformation structures (SSD) and roots (rt).

Figure 3.10 Facies Association 3 (FA3): tide-dominated, storm-affected delta, extending from 498−473 m in the 1AA-16-05-079-13W4 well

Note that the sand is either light brown (bitumen stained but water saturated) or dark in color (bitumen saturated). Mudstone beds are either beige or light to dark gray. Core columns are 7.6 cm wide and 75 cm long, and facies and facies-association distributions are labelled on the left, right, and at bottom of the core box photos. From the base to the top, FA3 exhibits vertically stacked, coarsening-upward facies successions. The FA3 succession is expressed by a basal surface overlain by weakly to moderately bioturbated (BI 1 to 4), convolute-bedded silty mudstone of F7. This passes upward into moderately bioturbated (BI 2 to 4), siltstone to rooted (rt) sand (F10; base core interval) or a weakly to thoroughly bioturbated (BI 1 to 5), heterolithic sand and mudstone bedset (F8; top core interval). Where parasequences are complete, F8 passes upwards into unburrowed to thoroughly bioturbated (BI 0 to 5), current-rippled to low-angle cross-

stratified sand (F9). Contacts between F6, F7, F8, F9, and F10 vary from sharp, scoured, or gradational (yellow dashed line).

3.4. Stratigraphy and Paleogeographic Reconstructions

3.4.1. Recognition of Stratigraphic Surfaces in the Regional C Depositional Unit

Multiple stratigraphic surfaces are present in the Regional C DU of the MDC, and encompass those of autogenic and allogenic origin. Additionally, autogenic and allogenic surfaces may vary from erosional to non-erosional (depositional). Autogenic erosion surfaces correspond to lateral and downstream accretion of channels or channel avulsion during regression, and are observed primarily at the bases of fluvio-tidal channels (FA1) and distributary channels (FA2; Table 3.3; Fig. 3.11). It is relatively easy to identify channel-associated erosion surfaces in core (e.g., scoured contacts overlain by unbioturbated coarse-grained lags) as well as on well logs (> 45 API gamma-ray; > 30% density porosity). Non-erosional autogenic surfaces correspond to localized marine flooding surfaces, marking delta lobe switching associated with channel avulsion during regression. Allogenic surfaces in the Regional C are exclusively associated with transgression and vary from erosional to non-erosional flooding surfaces. Discerning whether any single flooding surface is of autogenic or allogenic origin, however, is challenging, even in core. Flooding surfaces are numerous in the Regional C succession, and are grouped in two sub-categories: 1) spatially limited non-erosional flooding surfaces; and 2) regionally extensive erosional and non-erosional flooding surfaces (Table 3.3, Fig. 3.11).

Table 3.3 **Recognition and distinction of three surface types defined in this study: locally extensive flooding surfaces (FS), regionally extensive FSs, and erosional surfaces. The table includes the core signature, well-log signature, lateral extent, and stratigraphic significance of mud beds directly overlying surfaces. Acronyms: Bioturbation Index (BI), *Chondrites* (*Ch*); *Phycosiphon* (*Ph*), and *Planolites* (*Pl*). The gamma-ray log signature reports values in American Petroleum Institute (API) units.**

	Locally extensive FS	**Regionally extensive FS**	**Erosive surface**
Core signature	Mud marker: light to medium gray color; BI: 0−2; Traces: *Pl* Contact: Sharp	Mud marker: medium to dark gray color; BI: low to moderate (1−3); Traces: *Ch, He, Ph, Pl* Contact: Scour	Coarse-grained lag with pebbles grain-size; BI: 0 Contact: Scour
Well-log signature	>90 API gamma-ray >24% density porosity	>100 API gamma-ray <18% density porosity	>45 API gamma-ray > 30% density porosity
Lateral extent	<100 km^2	>1000 km^2	variable
Stratigraphic significance	Autogenic: Delta avulsion, shift in depocenter	Allogenic: Base-level rise	Allogenic: Base-level drop Autogenic: channel-belt migration and confluences

Mapping and Correlation of Flooding Surface

Local and regional flooding surfaces are distinguished initially on the basis of their core and geophysical expressions (see Table 3.3; Fig. 3.11). Mudstones directly overlying regional flooding surfaces are darker gray and show higher gamma-ray responses (> 100 API gamma-ray) and lower density-porosity values (< 18%), compared to mudstones associated with local flooding surfaces (< 90 API gamma-ray; > 24% density porosity), similar to previously defined responses in the area (e.g., Hein et al., 2013) and in the Sparrow Paleovalley (Château et al., 2019). That said, the most reliable way to distinguish between the two surface types is through the mapping of their spatial extents. Localized flooding surfaces rarely cover more than 100 km^2, whereas regional flooding surfaces can be traced over at least 1,000 km^2 (Figs. 3.12 to 3.14). Localized flooding surfaces are internal to individual DUs and are interpreted to record an autogenic origin. Regional flooding surfaces are bounded DUs and are interpreted to record allogenic controls.

South to north and west to east cross-sections reveal two regionally extensive flooding surfaces in Regional C DU that are recognizable both in core and on well logs using the criteria described above (Figs. 3.12, 3.13). The lower flooding surface is identified in 796 well logs and extends from T 69 to 83 and R 8 to 16W4 (Figs. 3.12, 3.13). This surface is located 11 to 15 m below the top of the Regional C and is traceable over 2,550 km^2 in the Grouse, Pelican, and Sparrow paleovalleys. In core, this lower flooding surface separates stacked successions of FA3. Below this surface, tide-dominated, fluvial-influenced, and storm-affected parasequences (Tfw; Ainsworth et al., 2011) are present, whereas above the surface, tide-dominated, storm and wave-influenced, fluvial-affected parasequences (Twf; Ainsworth et al., 2011) dominate (Figs. 3.4, 3.10). Following the Alberta Energy and Utilities Board (2003) nomenclature, this surface is herein named “Top C2”, and the Regional C deposits located below Top C2 are herein named “C2” (Figs. 3.12 to 3.15).

The upper regional flooding surface was correlated in 1,505 wells and extends from T 69 to 83 and R 8 to 16W4 (Figs. 3.12, 3.13). This surface is located at the top of Regional C and is traceable over 4,000 km^2 in the Grouse, Pelican, and Sparrow paleovalleys. In core, the flooding surface overlies tide-dominated, storm-influenced, fluvial-affected parasequences (Twf; Ainsworth et al., 2011) of FA3. The upper surface

separates the Regional C from overlying B2 deposits and is equivalent to the lower contact of the mudstone interval at the base of the B2 sequence (i.e., B2 mudstone; Alberta Energy and Utilities Board, 2003). This surface is herein named “Top C1”, and the Regional C deposits between Top C2 and Top C1 are herein named “C1” (Fig. 3.15).

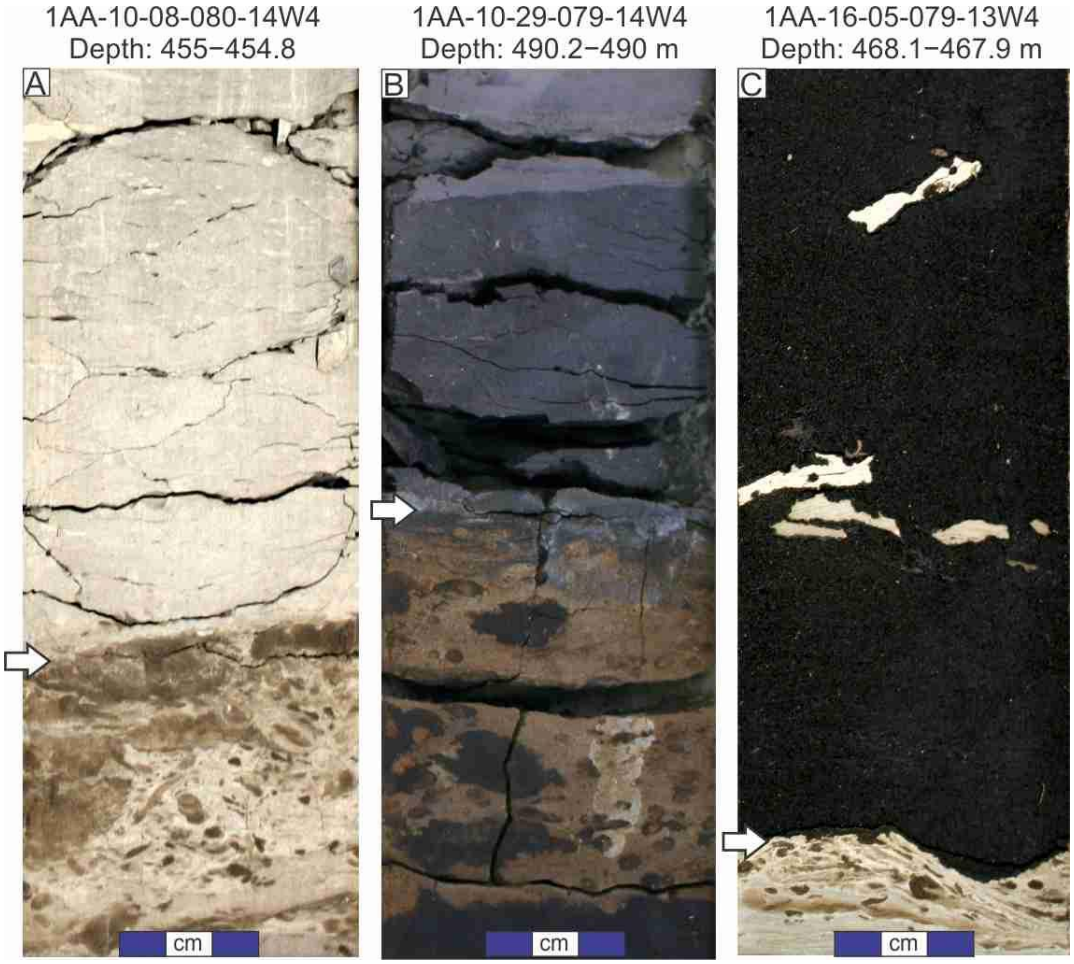

Figure 3.11 Core photos for bounding surfaces

Note that the sand is either light brown (bitumen stained but water or gas saturated) or dark brown (bitumen saturated). Mudstone beds are either beige or light to dark gray. In each photo, the arrow points to the surface. A) A locally extensive flooding surface at 455.0 m in the 1AA-10-08-080-14W4 well. In the photo, the sharp surface separates thoroughly bioturbated (BI 3 to 5) heterolithic sand and mudstone bedsets (F8; below the surface) from weakly bioturbated, convolute-bedded silty mudstone (F7; above the surface). B) A regionally extensive erosional flooding surface at 490.0 m in the 1AA-10-29-079-14W4 well. The scour surface separates underlying Devonian carbonate rocks from weakly to moderately bioturbated (BI 1 to 3) dark gray mudstone (F6; above the surface). Toward the top of photo B, a locally extensive flooding surface separates F6 from F7. C) An autogenic erosion surface at 468.1 m in the 1AA-16-05-079-13W4 well. The scour surface separates thoroughly bioturbated mudstone-dominated IHS (F4a; below the surface) from weakly bioturbated cross-stratified to current rippled sand (F2a; above the surface).

3.4.2. C1 and C2 Architecture

In the study area, the Lower McMurray is encountered in less than 5% of all wells, and hence, the Regional C typically directly overlies Devonian carbonates. The maximum thickness of Regional C (C2 and C1 combined) is 35 m. Regional C includes multiple channel belts, ranging from 1 to 35 m in thickness. Thin channel belts correspond to distributary channels (FA2), whereas thick channel belts equate to the fluvio-tidal channels (FA1). Both distributary channels and fluvio-tidal channels hang from various elevations in C2 and C1 units, or cut through them. Based on their positions relative to the Top C2 and Top C1 flooding surfaces, channel belts are labeled C2C or C1C (Figs. 3.12 to 3.15).

The thickness of the C2 depositional unit between the SCU and Top C2 surfaces averages 12.6 m (Figs. 3.12, 3.13). C2 encompasses 1 to 4 PSs of FA3 that range in thickness from 0.8 to 12.0 m each. These deposits are cross cut by distributary channels (FA2) that average 3.8 m thick and fluvio-tidal channels (FA1) that average 7.2 m and reach up to 26 m thick (Figs. 3.12, 3.13).

The architecture of C2 parasequences, based on the recognition of local flooding surfaces and their spatial correlation, cannot be investigated regionally but can be tracked locally in some cases. For example, in Township 82, Range 12W4, multiple parasequences are identified in C2 from west to east; however, C2 is incised by multiple fluvio-tidal channels, and so their regional correlation is challenging (Fig. 3.14).

Depositional unit C1 has an average thickness of 14.4 m and encompasses 1 to 7 PSs ranging in thickness from 0.8 to 11.0 m each. C1 deposits are cross cut by both distributary channels (FA2) with an average thickness of 3.7 m and fluvio-tidal channels that average 10.9 m and reach up to 35 m thick (Figs. 3.12, 3.13). In T82, R12W4, seven internal (autogenically bound) parasequences can be correlated over a down dip linear distance of 9.6 km (6 miles). Each PS exhibits an asymmetrical geometry, the base pinching out to the west (paleolandward) and the top pinching out at the PS's depositional limit towards the east (paleoseaward; Fig. 3.14).

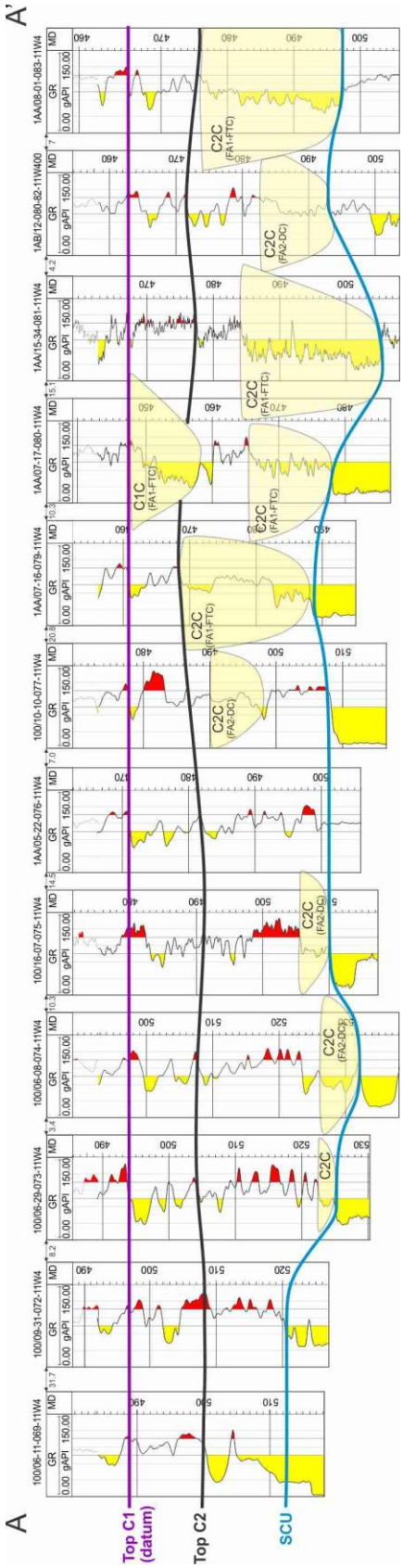
A
A'
Top C1 (datum)
Top C2
SCU
C1C (FA1-FTC)
C2C (FA1-FTC)
C2C (FA2-DC)
C2C
1AA/08-01-083-11W4
1AB/12-080-82-11W400
1AA/15-34-081-11W4
1AA/07-17-080-11W4
1AA/07-16-079-11W4
100/10-10-077-11W4
1AA/05-22-076-11W4
100/16-07-075-11W4
100/06-08-074-11W4
100/06-29-073-11W4
100/09-31-072-11W4
100/06-11-069-11W4

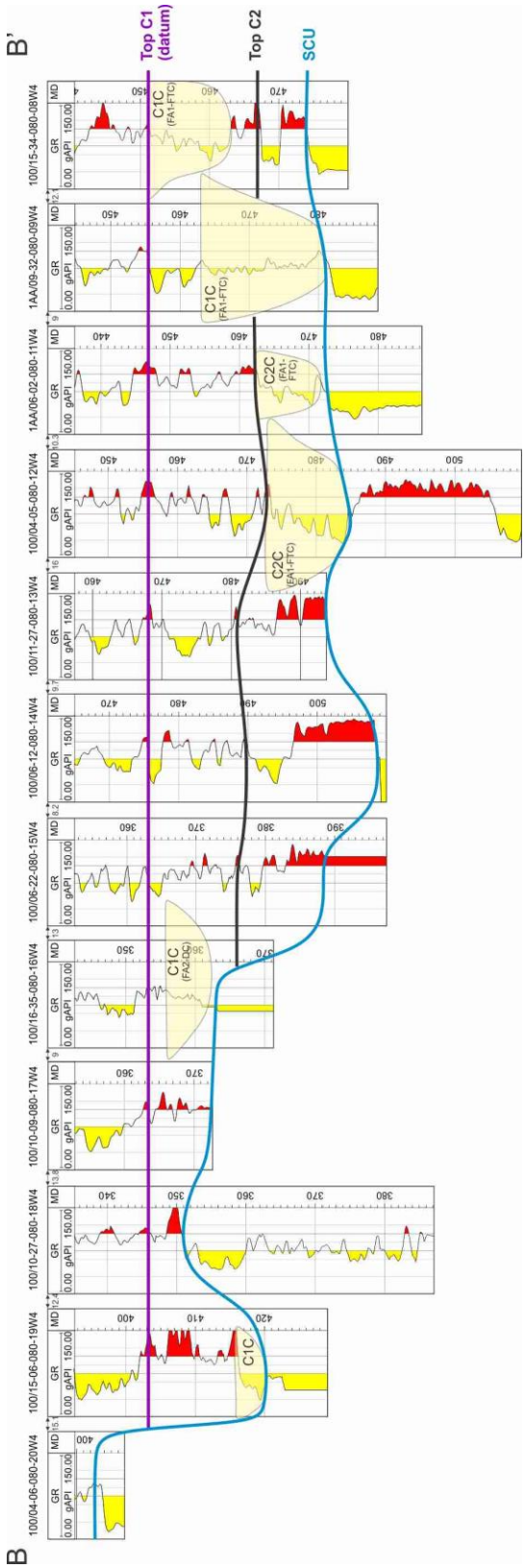
B'
B
Top C1 (datum)
Top C2
SCU
100/15-34-080-08W4
1AA/09-32-080-09W4
1AA/06-02-080-11W4
100/04-05-080-12W4
100/11-27-080-13W4
100/06-12-080-14W4
100/06-22-080-15W4
100/16-35-080-16W4
100/10-09-080-17W4
100/10-27-080-18W4
100/15-06-080-19W4
100/04-06-080-20W4
C1C (FA1-FTC)
C2C (FA1-FTC)
C1C (FA2-DC)
C1C
MD
GR
gAPI
0.00
150.00

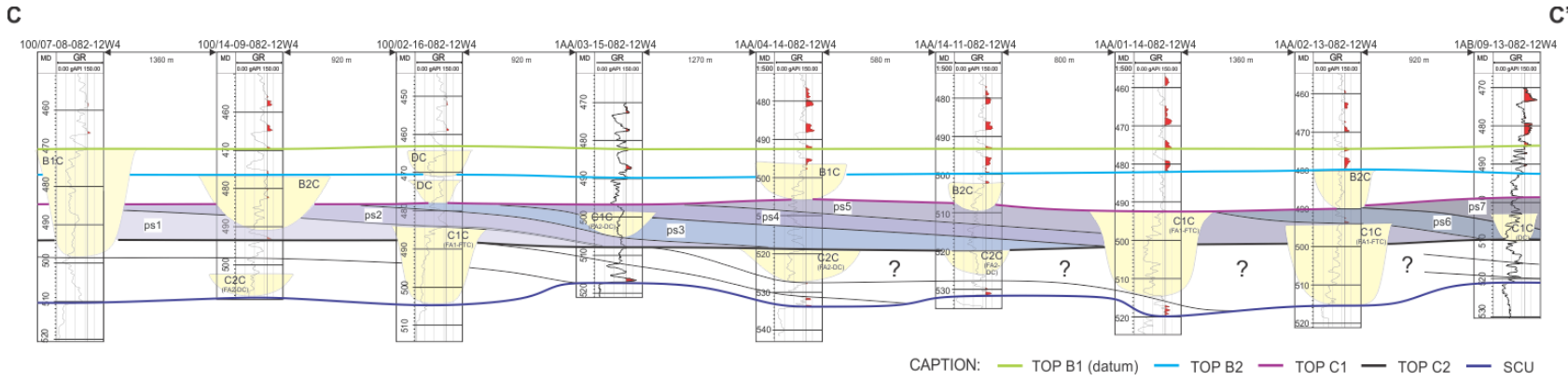
C
C'
100/07-08-082-12W4
100/14-09-082-12W4
100/02-16-082-12W4
1AA/03-15-082-12W4
1AA/04-14-082-12W4
1AA/14-11-082-12W4
1AA/01-14-082-12W4
1AA/02-13-082-12W4
1AB/09-13-082-12W4
1360 m
920 m
920 m
1270 m
580 m
800 m
1360 m
920 m
B1C
B2C
C1C
C2C
DC
ps1
ps2
ps3
ps4
ps5
ps6
ps7
?
CAPTION:
TOP B1 (datum)
TOP B2
TOP C1
TOP C2
SCU

Figure 3.12 Cross-section A−A', extending from south (100/06-11-069-11W4) to north (1AA/08-01-083-11W4) along Range 11W4

The datum is Top C1 (top of Regional C / C1 depositional unit). Throughout the cross-section, channels are represented by yellow polygons, labelled C1C or C2C based on their position relative to Top C2 and Top C1 flooding surfaces, and categorized as distributary channels (FA2-DC) and fluvio-tidal channels (FA1-FTC). Throughout the A to A' cross-section, a regionally mappable surface (Top C2) typically occurs 11 to 15 m below Top C1.

Figure 3.13 Cross-section B−B', extending from west (100/04-06-080-20W4) to east (100/15-34-080-08W4) along Township 80

The datum is Top C1 (top of Regional C / C1 depositional unit). Throughout the cross-section, channels are represented by yellow polygons, labelled C1C or C2C based on their position relative to Top C2 and Top C1 flooding surfaces, and categorized as distributary channels (FA2-DC) and fluvio-tidal channels (FA1-FTC). Throughout the B to B' cross-section, a regionally mappable surface (Top C2) typically occurs 11 to 15 m below Top C1.

Figure 3.14 Cross-section C−C', extending from west (100/07-08-082-12W4) to east (1AB/09-13-082-12W4) within Township 82, Range 12W4

The datum is Top B1 (top of B1 depositional unit). Throughout the cross-section, channels are represented by yellow polygons, labelled C1C or C2C based on their position relative to Top C2 and Top C1 flooding surfaces, and categorized as distributary channels (FA2-DC) and fluvio-tidal channels (FA1-FTC). The seven parasequences observed between the Top C2 and Top C1 surfaces prograded northeastward (gradient of colored purple polygons). Below Top C2 surface, the numerous channel belts make it challenging to correlate C2 parasequences (thin continuous black lines).

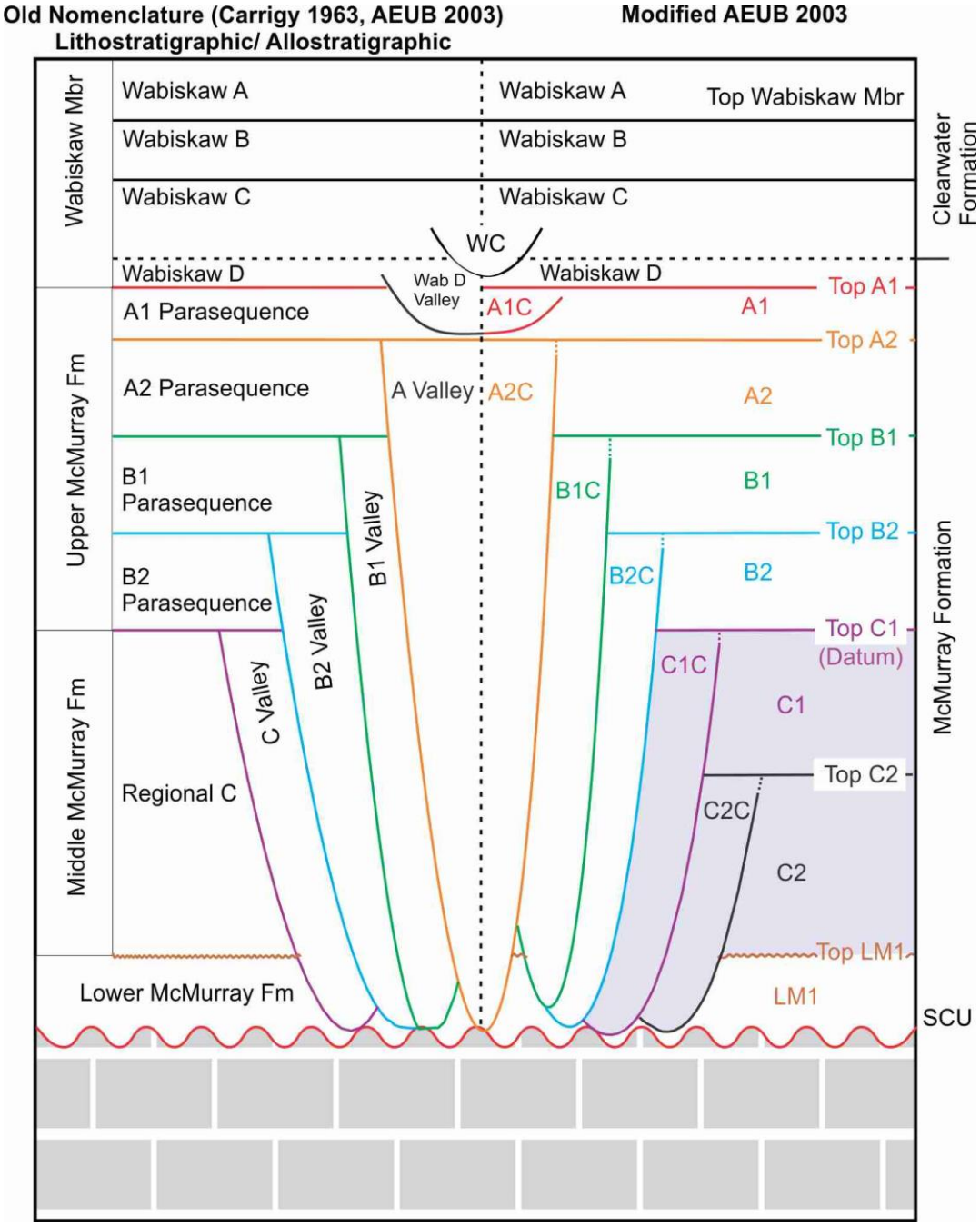

Figure 3.15 Revised stratigraphic model proposed for the McMurray Formation
On the far left (vertical text) is the lithostratigraphic nomenclature proposed by Carrigy (1963). In the middle left is the lithostratigraphic and allostratigraphic model developed by the Alberta Energy and Utilities Board (2003; now Alberta Energy Regulator). On the right is new model used by the McMurray Geology Consortium. In the revised stratigraphic model, the purple shaded area highlights the part of the succession of the McMurray Fm investigated in this study. The Top C2 flooding surface divides the Regional C interval into C2 and C1 depositional units. Based on their relative position to the Top C2 and Top C1 flooding surfaces, channel belts are labelled C2C or C1C.

3.4.3. Regional C Distribution

For depositional units C2 and C1, isopach maps were created for the parasequences, the fluvio-tidal channels, the distributary channels, and the full stratal package (Figs. 3.16, 3.17). Isopach maps of the Regional C interval are impacted by some limitations. First, the contour-extrapolation methodology used to generate each map (see methods and database section) produces some overlap of parasequences, fluvio-tidal channels, and distributary-channels. Thus, it is possible for three FAs to occupy the same spatial position on isopach maps. In other words, the contour-extrapolation methodology increases the spatial distribution of the elements and leads to an extension of the area of deposition when superimposing maps. Second, amalgamation of channel and/or parasequence thicknesses produces bulls-eye patterns on maps. Therefore, it is impossible to determine from the map whether the thickness is linked to the amalgamation of multiple geobodies (e.g., stacked parasequences) or corresponds to a single, thick geobody (e.g., fluvio-tidal channels).

Distribution of Depositional Unit C2

Depositional Unit C2 extends from T69 to 83 and R8 to 16W4, covering an area of 2,550 km^2 (Fig. 3.16B). The maximum thickness of C2 correlates to the central axes of the Grouse, Pelican, and Sparrow paleovalleys and decreases toward the margins of the paleovalleys and onto the paleotopographic highs. C2 parasequences are particularly well developed in the Pelican Paleovalley (Fig. 3.16C). Distributary channels occur primarily in the seaward part of the Pelican Paleovalley and in the Sparrow Paleovalley (Fig. 3.16C). Fluvio-tidal channels occupy the central axes of the paleovalleys (Fig. 3.16C). Where fluvio-tidal channels are more prevalent, preservation of distributary channels and parasequences is limited (Fig. 3.16C).

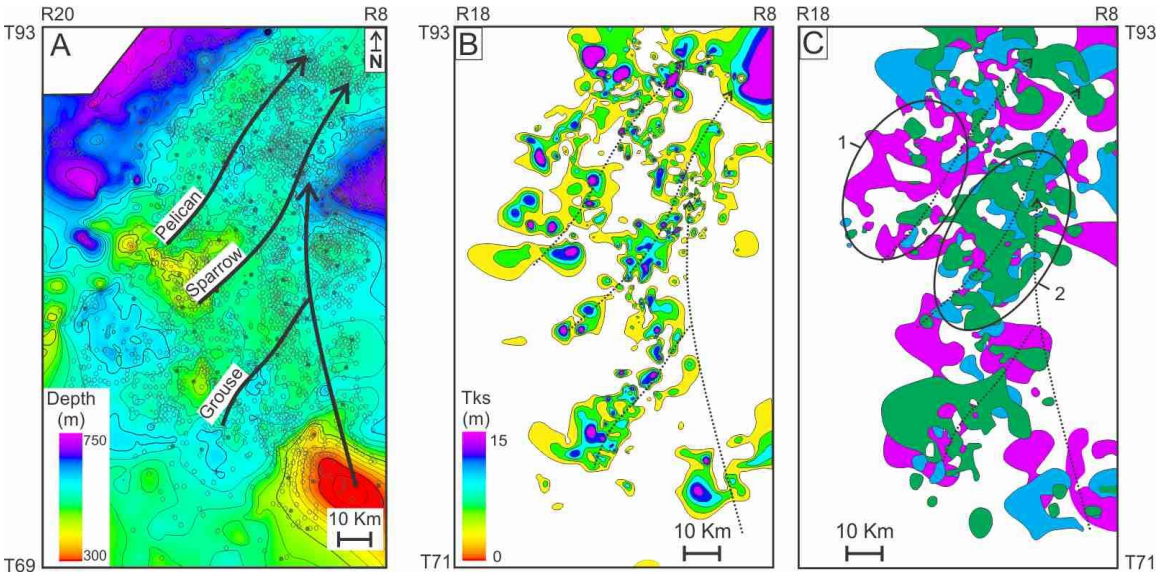

Figure 3.16 Isopach maps of C2 in the southwest quadrant of the McMurray Depocenter

A) Structure contour map of the Sub-Cretaceous Unconformity (SCU) in the study area, showing the distribution of well logs (gray dots) and cored wells (black dots). The thalwegs of the Pelican, Sparrow, and Grouse paleovalleys are highlighted by the thick black lines. B) Isopach map of C2 (i.e., stratal package between the SCU and Top C2 surfaces). The thalwegs of the Pelican, Sparrow, and Grouse paleovalleys are highlighted by thin black dashed lines. C) Map superimposing the contours of the parasequences (FA3; purple), distributary channels (FA2; blue), and fluvio-tidal channels (FA1; green) in C2. C2 parasequences are particularly well developed in the Pelican Paleovalley (circle 1), while fluvio-tidal channels and distributary channels are more prevalent in Grouse and Sparrow paleovalleys (circle 2). Thalwegs are depicted in a manner similar to those in part B.

Distribution of Depositional Unit C1

Depositional Unit C1 extends from T69 to 83 and R8 to 17W4, covers an area of 4,000 km^2, and extends farther west than C2 in the Grouse, Sparrow, and Pelican paleovalleys (Fig 3.17b). The maximum thickness of C1 occurs along the central axes of the three paleovalleys, with the deposits thinning towards the valley margins and onto the paleotopographic highs (Fig. 3.17B). C1 parasequences are well developed along the paleovalley margins, particularly in the Grouse Paleovalley. Channels (e.g., distributary channels and fluvio-tidal channels) are well developed in the central axes of all three paleovalleys. Where fluvio-tidal channels are more prevalent, preservation of distributary channels and parasequences is limited (Fig. 3.17C).

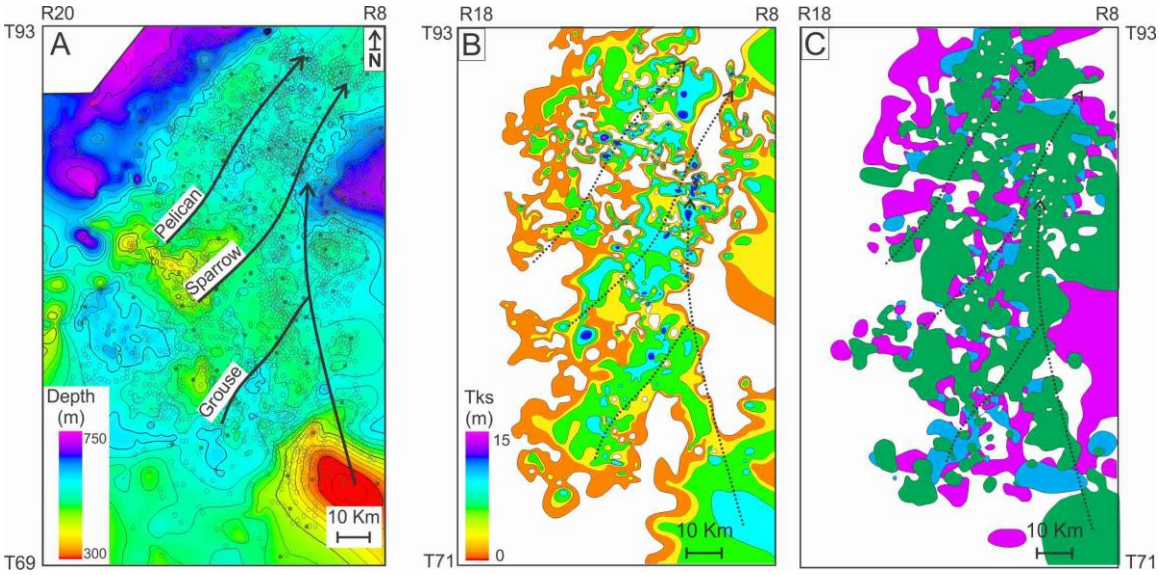

Figure 3.17 Isopach maps of C1 in the southwest quadrant of the McMurray Depocenter

A) Structure contour map of the Sub-Cretaceous Unconformity (SCU) in the study area showing the distribution of well logs (gray dots) and cored wells (black dots). The thalwegs of the Pelican, Sparrow, and Grouse paleovalleys are highlighted by the thick black lines. B) Isopach map of C1 (i.e., the stratal package constrained between the Top C2 and the Top C1 surfaces). The thalwegs of the Pelican, Sparrow, and Grouse paleovalleys are highlighted by thin black dashed lines. C) Map superimposing the contours of the parasequences (FA3; purple), distributary channels (FA2; blue), and fluvio-tidal channels (FA1; green) in C1. C1 parasequences are well developed along the paleovalley margins, whereas distributary channels and fluvio-tidal channels are well developed in the paleovalleys thalwegs. Thalwegs are depicted in a manner similar to those in part B. Revised Stratigraphy and Implications for Early Transgression of the Alberta Foreland Basin

3.4.4. The Relation of Channels to Parasequences and Their Stratigraphic Significance

Distributary-channel deposits represent the distal expressions of a distributive-channel system. These distributary channels are genetically linked to the adjacent parasequences, and their seaward shift is intrinsically associated with shoreline progradation (Fig. 3.18; Axelsson, 1967; Van Heerden and Roberts, 1988; Coleman et al., 1998; Olariu and Bhattacharya, 2006). Distributary channels and correlative parasequences are locally incised by fluvio-tidal channels. Numerous studies have interpreted the fluvio-tidal channels to record valley incision linked to major relative sea-level falls in the McMurray Sub-Basin (e.g., Ranger and Pemberton, 1997; Hein et al., 2000, 2013; Hein and Cotterill, 2006; Horner et al., 2018, 2019). However, the observation of uncoupled fluvio-tidal channels with overlying regional flooding surfaces indicates that at least some fluvio-tidal channels are autogenic in origin (Baniak and

Kingsmith, 2018; Château et al., 2019; Weleschuk and Dashtgard, 2019). In this case, channel-belt migration is interpreted to be part of the trunk channel system that shifted seaward during progradation and autogenically incised into older PSs. Moreover, the fluvio-tidal channel deposits relate to distributary channels and parasequences deposited farther basinward (Fig. 3.18B, D). A similar scenario was proposed for channel-belt complexes of the Blackhawk Formation to Lower Castlegate Sandstone stratigraphic interval in the Book Cliffs region of Utah, USA (Pattison, 2018a, 2018b, and 2019).

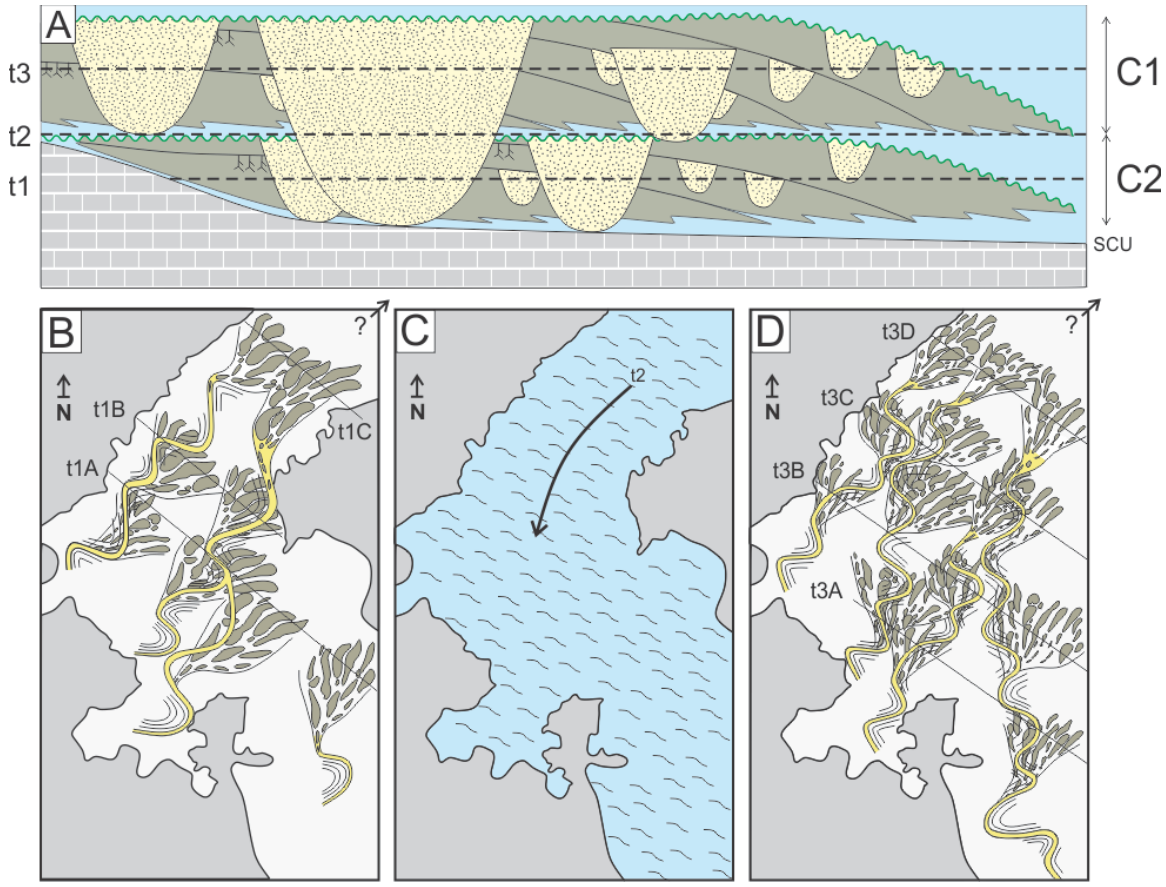

Figure 3.18 Diagrams showing a schematic cross-section and paleoenvironment reconstruction map of C2 and C1 across the southwest quadrant of the McMurray Sub-Basin

A) Schematic cross-section of C2 and C1 across the southwest quadrant of the McMurray Sub-Basin. The deposits are aggradational and retrogradational, with C1 deposition occurring landward relative to C2. In each unit, parasequences (FA3) genetically linked to distributary channels (FA2) record basinward progradation during normal regression, and are incised by fluvio-tidal channels (FA1). Thin black dashed lines highlight time of deposition (t1, t2, and t3). Paleoenvironment maps B, C, and D equate to t1, t2, and t3, respectively. B) Paleoenvironment reconstruction map of C2 at time 1, with meandering fluvio-tidal channels (yellow) feeding basinward parasequences of tide-dominated deltas through a network of distributary channels. Thin black dashed lines highlight time of deposition (t1A, t1B and t1C), and show the shoreline's

progradation. C) Paleoenvironment reconstruction map at time 2, with shoreline retreat and paleovalley inundation linked to transgression of the Boreal Sea. D) Paleoenvironment reconstruction map of C1 at time 3, where meandering fluvio-tidal channels (yellow) represent a distributary channel complex feeding parasequences lying farther basinward by the interplay of distributary channels. Thin black dashed lines highlight time of deposition (t3A, t3B, t3C, and t3D), and show the shoreline's progradation.

3.4.5. C2 and C1 Stratigraphy and Implications for Early Evolution of the Alberta Foreland Basin

The stratigraphy of marginal-marine environments requires the recognition and mapping of flooding surfaces (e.g., Van Wagoner et al. 1988; Galloway, 1989; Bhattacharya, 1993; Kamola and Van Wagoner, 1995; Van Wagoner, 1995; Posamentier and Allen, 1999). In the McMurray Sub-Basin, multiple successive channel-belt incisions have resulted in reduced certainty in the correlation of flooding surfaces in C2 and C1. However, the southwest corner of the MDC experienced limited fluvio-tidal channel-belt incision and, by extension, displays relatively good preservation of flooding surfaces bounding C2 and C1 DUs. These surfaces record base-level changes, and demonstrate that the maximum thickness of both C2 and C1 DUs is < 15 m. Consequently, C2 and C1 DUs are interpreted as having accumulated in a limited- to moderate-accommodation setting, which is consistent with the rest of the middle and upper McMurray Fm in the area (e.g., Hein et al., 2013).

The relatively thin PS thicknesses recorded in C2 and C1 indicate this limited creation of local accommodation space (see Fig. 3.14). Creation of accommodation space was easily surpassed by sediment supply, leading to a seaward migration of the depocenter and parasequences that rapidly migrated basinward. This led to the progradation of the system to the northeast during a period of stable or only slowly rising base level (equivalent of T1 and T3 of Fig. 3.18A, B, and D). However, successive DUs show a retrogradational stratal stacking pattern, with the shoreline of C1 lying landward of C2, indicating that the system backstepped during longer-term transgression of the Boreal Sea (Figs. 3.16 to 3.18). In the area, the onset of transgression of the Boreal Sea is manifested only in the preservation of the regional flooding surface (equivalent of T2 of Fig. 3.18A and C). The absence of distinctive estuarine deposits in the area is attributed to the limited accommodation space and/or to the lithological similarities between deltaic FTC and estuarine FTC. During transgression, even with only small amounts of relative sea-level rise, the low gradient of the shoreline associated with a

reduced sediment supply resulted in rapid backstepping of the shoreline and hence a rapid shift from marginal-marine to marine conditions. In addition, during the period of transgression, the water will preferentially inundate pre-existing channel conduits, then, FTC records estuarine settings during periods of transgression and deltaic settings during periods of normal regression. Similar multistory channel fills have been defined previously in the McMurray Fm for the B2, B1, and A2 FTCs of the Assiniboia Paleovalley (Horner et al., 2018). The architecture of C2 and C1 is similar to that of overlying DUs (B2 to A1), characterized by a series of prograding parasequences (PSs) organized into discrete and retrogradationally stacked depositional units (DUs), and pointing to overall base-level rise (Fig. 3.18; Château et al., 2019; Weleschuk and Dashtgard, 2019). When considered in combination with the fluvial strata of the lower McMurray Fm and the marine strata of the A2 and A1 DUs (e.g., Carrigy, 1967; Mossop and Flach, 1983; Flach and Mossop; 1985; Ranger and Pemberton, 1997; Hein and Cotterill, 2006; Ranger et al., 2008; Hein et al., 2013; Weleschuk and Dashtgard, 2019), the overall succession records the progressive drowning of the Alberta Foreland Basin during the Early Cretaceous. Additionally, the consistent thickness of DUs from C2 to A1 suggests that accommodation of the basin in its early stages was low, averaging 15 m or less. Given the time intervals represented by the C2 to A1 succession (approximatively 8.4 Myr; see Hein and Dolby, 2017; Rinke-Hardekopf et al., 2019), the early drowning of the Alberta Foreland Basin was slow, enabling periods of major shoreline progradation during progressive but incremental transgression.

3.5. Conclusions

The MDC study area includes multiple paleotopographic lows (paleovalleys), filled with regionally extensive DUs that are cut into by nested and deeply incised fluvio-estuarine channel belts. From a dataset comprising over 100 cores and 2750 well logs, the Regional C depositional unit, an understudied interval of the McMurray Formation, was investigated. The observations and interpretations from this study corroborates previously published work that asserts that brackish-water and tidal conditions existed in the basin during deposition of the Regional C interval (e.g., Pemberton et al., 1982; Ranger and Pemberton, 1992; Hein and Cotterill, 2006, Hein et al., 2013; Gingras et al., 2016).

Limited fluvio-tidal channel-belt incision and, by extension, relatively good preservation of allogenic as well as autogenic flooding surfaces occurs in the study area. In the thick Regional C depositional unit, a surface located 11 to 15 m below Top C1 surface is readily identified and mappable over 2,550 km^2 in the Grouse, Pelican, and Sparrow paleovalleys. This regional flooding surface has geophysical and core signatures characteristic of allogenic flooding surfaces and is herein named “Top C2”. The surface divides the Regional C interval into the C2 and C1 DUs. The maximum thickness of both C2 and C1 DUs is < 15 m, indicating that deposition occurred in a limited- to moderate-accommodation setting, which is consistent with other depositional units of the upper McMurray Fm (e.g., Ranger and Pemberton, 1997; Hein and Cotterill, 2006; Ranger et al., 2008; Hein et al., 2013; Château et al., 2019).

Owing to the limited accommodation available, sediments supplied by the trunk channel system had limited space in which to accumulate, and the shoreline (manifested by the distributary channels and the seaward limits of their associated parasequences) prograded rapidly basinward. These fluvio-tidal channel belts are interpreted to be of autogenic origin and genetically linked to terminal distributary channels and the parasequences they fed farther basinward.

DUs show a retrogradational stratal stacking pattern, with the shoreline of C1 lying landward of C2 and indicating that the shoreline backstepped during the early stages of transgression of the Boreal Sea. Finally, in the C2 and C1 DUs, individual cycles record short-lived periods of normal regression, showing that the early drowning of the Alberta Foreland Basin was slow and incremental, enabling periods of major shoreline progradation during the overall transgression.

Acknowledgements

The authors thank the sponsors of the McMurray Geology Consortium: BP plc, Cenovus Energy Inc., Husky Energy, Nexen CNOOC Ltd, and Woodside Energy Ltd, for funding this research. The authors also thank the reviewers, Bogdan Varban and Milovan Fustic, the associate editor, Cornel Olariu, and the editor Gray Hampson, whose comments served to improve this manuscript.

References

Alberta Energy and Utilities Board, 2003, Athabasca Wabiskaw−McMurray regional geological study: Alberta Energy and Utilities Board, Report 2003-A, 187p.

Alberta Geological Survey, 2015, Alberta Table of Formations: Alberta Energy Regulator: https://ags.aer.ca/activities/table-of-formation (accessed February 2020).

Ainsworth, R.B., Vakarelov, B.K., and Nanson, R.A., 2011, Dynamic spatial and temporal prediction of changes in depositional processes on clastic shorelines: Towards improved subsurface uncertainty reduction and management: American Association of Petroleum Geologists, Bulletin, v. 95, p. 267−297.

Ashworth, P.J., Best, J.L., and Parsons, D.R., 2015, Fluvial-Tidal Sedimentology: Amsterdam, Elsevier, Developments in Sedimentology, v. 68, 656 p.

Axelsson, V., 1967, The Laitaure Delta: A study of deltaic morphology and processes: Geografiska Annaler, Series A, Physical Geography, v. 49, p. 1−127.

Baniak, G.M., and Kingsmith, K.G., 2018, Sedimentological and stratigraphic characterization of Cretaceous upper McMurray deposits in the southern Athabasca oil sands, Alberta, Canada: American Association of Petroleum Geologists, Bulletin, v. 102, p. 309−332.

Barton, M.D., Porter, I., O'Byrne, C., and Mahood, R., 2017, Impact of the Prairie Evaporite dissolution collapse on McMurray stratigraphy and depositional patterns, Shell Albian Sands Lease 13, northeast Alberta: Bulletin of Canadian Petroleum Geology, v. 65, p. 175–199.

Bhattacharya, J.P., 1993, The expression and interpretation of marine flooding surfaces and erosional surfaces in core: Examples from the Upper Cretaceous Dunvegan Formation, Alberta Foreland Basin, Canada: *in* Summerhayes C.P., and Posamentier H.W. eds., Sequence Stratigraphy and Facies Associations, Internal association of Sedimentologists, Special Publication 18, p. 125–160.

Broughton, P.L., 2013, Devonian salt dissolution-collapse breccias flooring the Cretaceous Athabasca oil sands deposit and development of lower McMurray Formation sinkholes, northern Alberta Basin, Western Canada: Sedimentary Geology, v. 283, p. 57–82.

Broughton, P.L., 2014, Syndepositional architecture of the northern Athabasca Oil Sands Deposit, northeastern Alberta: Canadian Journal of Earth Sciences, v. 52, p. 21–50.

Broughton, P.L., 2015a, Collapse-induced fluidization structures in the Lower Cretaceous Athabasca Oil Sands Deposit, Western Canada: Basin Research, v. 28, p. 507–535.

Broughton, P.L., 2015b, Incipient vertical traction carpets within collapsed sinkhole fills: Sedimentology, v. 62, p. 845–866.

Carrigy, M.A., 1963, Paleocurrent directions from the McMurray Formation: Bulletin of Canadian Petroleum Geology, v. 11, p. 389–395.

Carrigy, M.A., 1967, Some sedimentary features of the Athabasca oil sands: Sedimentary Geology, v. 1, p. 327–352.

Carrigy, M.A., 1971, Deltaic sedimentation in Athabasca tar sands: American Association of Petroleum Geologists, Bulletin, v. 55, p. 1155−1169.

Château, C.C., Dashtgard, S.E., MacEachern, J.A., and Hauck, T.E., 2019, Parasequence architecture in a low-accommodation setting, impact of syndepositional carbonate epikarstification, McMurray Formation, Alberta, Canada: Marine and Petroleum Geology, v. 104, p. 168−179.

Christopher, J., 1997, Evolution of the Lower Cretaceous Mannville sedimentary basin in Saskatchewan: *in* Pemberton S.G., and James, D.P., eds., Petroleum Geology of the Cretaceous Mannville Group, Western Canada: Canadian Society of Petroleum Geologists, Memoir 18, p. 191−210.

Coleman, J.M., Roberts, H.H., and Stone, G.W., 1998, Mississippi River delta: An overview: Journal of Coastal Research, v. 14, p. 699−719.

Crerar, E.E., and Arnott, R.W.C., 2007, Facies distribution and stratigraphic architecture of the Lower Cretaceous McMurray Formation, Lewis property, northeastern Alberta: Bulletin of Canadian Petroleum Geology, v. 55, p. 99–124.

Dashtgard, S.E., and La Croix, A.D., 2015, Sedimentological trends across the tidal-fluvial transition, Fraser River, Canada: A review and some broader implications: *in* Ashworth, P.A., Best, J.J., and Parsons D.R., eds., Fluvial−Tidal Sedimentology, Amsterdam, Elsevier, Developments in Sedimentology 68, p. 111−126.

Dalrymple, R.W., and Choi, K., 2007, Morphologic and facies trends through the fluvial–marine transition in tide-dominated depositional systems: a schematic framework for environmental and sequence-stratigraphic interpretation: Earth-Science Reviews, v. 81, p. 135−174.

Davis R.A., Jr., and Dalrymple, R.W., 2011, Principles of Tidal Sedimentology: Springer Science & Business Media, New York, 621p.

Flach, P.D., and Mossop, G.D., 1985, Depositional environments of Lower Cretaceous McMurray Formation, Athabasca Oil Sands, Alberta: American Association of Petroleum Geologists, Bulletin , v. 69, p. 1195–1207.

Fustic, M., Bennett, B., Huang, H., and Larter, S., 2012, Differential entrapment of charged oil – new insights on McMurray Formation oil trapping mechanisms: Marine and Petroleum Geology, v. 36, p. 50−69.

Galloway, W.E., 1989, Genetic stratigraphic sequences in basin analysis II: Application to Northwest Gulf of Mexico Cenozoic Basin: American Association of Petroleum Geologists, Bulletin, v. 73, p. 143−154.

Gingras, M.K., Pemberton, S.G., Saunders, T., and Clifton, H.E., 1999, The ichnology of modern and Pleistocene brackish-water deposits at Willapa Bay, Washington: Variability in estuarine settings: Palaios, v. 14, p. 352−374.

Gingras, M.K., MacEachern, J.A., and Dashtgard, S.E., 2012, The potential of trace fossils as tidal indicators in bays and estuaries: Sedimentary Geology, v. 279, p. 97−106.

Gingras, M.K., MacEachern, J.A., Dashtgard, S.E., Ranger, M.J., and Pemberton, S.G., 2016, The significance of trace fossils in the McMurray Formation, Alberta, Canada: Bulletin of Canadian Petroleum Geology, v. 64, p. 233−250.

Hagstrom, C.A., Hubbard, S.M., Leckie, D.A., and Durkin, P.R., 2019, The effects of accretion package geometry on lithofacies distribution in point-bar deposits: Journal of Sedimentary Research, v. 89, p. 381−398.

Hauck, T.E., Peterson, J.T., Hathway, B., Grobe, M., and MacCormack, K., 2017, New insights from regional-scale mapping and modelling of the Paleozoic succession in northeast Alberta: Paleogeography, evaporite dissolution, and controls on Cretaceous depositional patterns on the Sub-Cretaceous Unconformity: Bulletin of Canadian Petroleum Geology, v. 65, p. 87–114.

Hein, F.J., Berhane, H., and Cotterill, D.K., 2000, An atlas of lithofacies of the McMurray Formation, Athabasca oil sands deposit, northeastern Alberta: Surface and subsurface: Alberta Energy Utilities Board/Alberta Geological Survey, Earth Sciences Report 2000-07, 217 p.

Hein, F.J., and Cotterill, D.K., 2006, The Athabasca oil sands – a regional geological perspective, Fort McMurray area, Alberta, Canada: Natural Resources Research, v. 15, p. 85–102.

Hein, F.J., Dolby, G., and Fairgrieve, B., 2013, A regional geologic framework for the Athabasca oil sands, northeastern Alberta, Canada: *in* Hein F.J., Leckie D., Larter S., and Suter J.R., eds., Heavy-Oil and Oil-Sand Petroleum Systems in Alberta and Beyond: American Association of Petroleum Geologists, Studies in Geology 64, p. 207–250.

Hein, F., and Dolby, G., 2017, Lithostratigraphy, palynology, and biostratigraphy of the Athabasca Oil Sands deposit, northeastern Alberta: Alberta Geological Survey, Open File Report 8, 105 p.

Horner, S.C., Hubbard, S.M., Martin, H.K., Hagstrom, C.A., and Leckie, D.A., 2018, The impact of Aptian glacio-eustasy on the stratigraphic architecture of the Athabasca Oil Sands, Alberta, Canada: Sedimentology, v. 66, p. 1600-1642.

Horner, S.C., Hubbard, S.M., Martin, H.K., and Hagstrom, C.A., 2019, Reconstructing basin-scale drainage dynamics with regional subsurface mapping and channel-bar scaling, Aptian, Western Canada Foreland Basin: Sedimentary Geology, v. 385, p. 26−44.

Hubbard, S.M., Smith, D.G., Nielsen, H., Leckie, D.A., Fustic, M., Spencer, R.J., and Bloom, L., 2011, Seismic geomorphology and sedimentology of a tidally influenced river deposit, Lower Cretaceous Athabasca Oil Sands, Alberta, Canada: American Association of Petroleum Geologists, Bulletin, v. 95, p. 1123−1145.

Jean, T.R., 2018, The Eastern Flank: Predicting the Architecture of the McMurray Formation Beyond its Subcrop Edge [unpublished MSc. Thesis], Simon Fraser University, 99 p.

Kamola, D.L., and Van Wagoner, J.C., 1995, Stratigraphy and facies architecture of parasequences with examples from the Spring Canyon Member, Blackhawk Formation, Utah: *in* Van Wagoner, J.C., and Bertram, G.T., eds., Sequence Stratigraphy of Foreland Basin Deposits: Outcrop and Subsurface Examples from the Cretaceous of North America: American Association of Petroleum Geologists, Memoir 64, p. 27–54.

La Croix, A.D., and Dashtgard, S.E., 2015, A synthesis of depositional trends in intertidal and upper subtidal sediments across the tidal–fluvial transition in the Fraser River, Canada: Journal of Sedimentary Research, v. 85, p. 683−698.

La Croix, A.D., Dashtgard, S.E., Gingras, M.K., Hauck, T.E., and MacEachern, J.A., 2015, Bioturbation trends across the freshwater to brackish-water transition: Refinement of the brackish-water ichnological model: Palaeogeography, Palaeoclimatology, Palaeoecology, v. 440, p. 66−77.

La Croix, A.D., Dashtgard, S.E., and MacEachern, J.A., 2019, Using a modern analogue to interpret depositional position in ancient fluvial-tidal channels: Example from the McMurray Formation, Canada: Geoscience Frontiers, v. 10, p. 2219−2238.

Martin, H.K., Hubbard, S.M., Hagstrom, C.A., Horner, S.C., and Durkin, P.R., 2019, Planform recognition and implications of a Cretaceous-age continental-scale river avulsion node in the Western Interior Basin, Alberta, Canada: Sedimentary Research, v. 89, p. 610−628.

Martinius, A.W., Fustic, M., Garner, D.L., Jablonski, B.V.J., Strobl, R.S., MacEachern, J.A., and Dashtgard, S.E., 2017, Reservoir characterization and multiscale heterogeneity modeling of inclined heterolithic strata for bitumen-production forecasting, McMurray Formation, Corner, Alberta, Canada: Journal of Marine and Petroleum Geology, v. 82, p. 336−361.

McPhee, D.A., and Wightman, D.M., 1991, Timing of the dissolution of Middle Devonian Elk Point Group Evaporites − Twps. 47 to 103 and Rges. 15 W3M to 20 W4M: Bulletin of Canadian Petroleum Geology, v. 39, 218 p.

Mossop, G.D., and Flach, P.D., 1983, Deep channel sedimentation in the Lower Cretaceous McMurray Formation, Athabasca Oil Sands, Alberta: Sedimentology, v. 30, p. 493-509.

Musial, G., Reynaud, J.-Y., Gingras, M.K., Féniès, H., Labourdette, R., and Parize, O., 2012, Subsurface and outcrop characterization of large tidally influenced point bars of the Cretaceous McMurray Formation (Alberta, Canada): Sedimentary Geology, v. 279, p. 156–172.

Olariu, C., and Bhattacharya, J.P., 2006, Terminal distributary channels and delta front architecture of river-dominated delta systems: Journal of Sedimentary Research, v. 76, p. 212−233.

Pattison, S.A.J., 2018a, Rethinking the incised-valley fill paradigm for Campanian Book Cliffs strata, Utah–Colorado, USA: Evidence for discrete parasequence-scale, shoreface-incised channel fills: Journal of Sedimentary Research, v. 88, p. 138−1412.

Pattison, S.A.J., 2018b, Using classic outcrops to revise sequence stratigraphic models: Reevaluating the Campanian Desert Member (Blackhawk Formation) to lower Castlegate Sandstone interval, Book Cliffs, Utah and Colorado, USA: Geology, v. 47, p. 11−14.

Pattison, S.A.J., 2019, High resolution linkage of channel-coastal plain and shallow marine facies belts, Desert Member to Lower Castlegate Sandstone stratigraphic interval, Book Cliffs, Utah−Colorado, USA: Geological Society of America, Bulletin, v. 131, p. 1643−1672.

Pemberton, S.G., Flach, P.D., and Mossop, G.D., 1982, Trace fossils from the Athabasca oil sands, Alberta, Canada: Science, v. 217, p. 825−827.

Pemberton, S.G., and Wightman, D.M., 1992, Ichnological characteristics of brackish water deposits: *in* Pemberton, S.G., ed., Applications of Ichnology to Petroleum Exploration, A Core Workshop: SEPM, Core Workshop 17, p. 141–167.

Posamentier, H., and Allen, G., 1999, Siliciclastic Sequence Stratigraphy: Concepts and applications,in SEPM, Concepts in Sedimentology and Paleontology, 7, 210 p.

Ranger, M.J., and Pemberton, S.G., 1992, The sedimentology and ichnology of estuarine point bars in the McMurray Formation of the Athabasca Oil Sands deposit, north-eastern Alberta, Canada: *in* Pemberton, S.G., ed., Application of Ichnology to Petroleum Exploration: A Core Workshop: SEPM, Core Workshop 17, p. 401−421.

Ranger, M.J., and Pemberton, S.G., 1997, Elements of a stratigraphic framework for the McMurray Formation in south Athabasca area, Alberta: *in* Pemberton S.G., and James D.P., eds., Petroleum Geology of the Cretaceous Mannville Group, Western Canada: Canadian Society of Petroleum Geologists, Memoir, 18, p. 263–291.

Ranger, M.J., Gingras, M.K., and Pemberton, S.G., 2008, The role of ichnology in the stratigraphic interpretation of the Athabasca oil sands: in 2007 Hedberg Conference, Heavy Oil and Bitumen on Foreland Basins− From Processes to Products, v.30 p. 1–8.

Rinke-Hardekopf, L., Dashtgard, S.E., and MacEachern, J.A., 2019, Earliest Cretaceous transgression of North America recorded in thick coals: McMurray Sub-Basin, Canada: International Journal of Coal Geology, v. 204, p. 18–33.

Sibson, R., 1981, A brief description of natural neighbour interpolation: Interpreting multivariate data: *in* Barnett V., ed., Interpreting Multivariate Data: John Wiley, New York, p. 21−36.

Smith, D., 1988, Tidal bundles and mud couplets in the McMurray Formation, northeastern Alberta, Canada: Bulletin of Canadian Petroleum Geology, v. 36, p. 216−219.

Smith, D.G., Hubbard, S.M., Leckie, D.A., and Fustic, M., 2009, Counter point bar deposits: Lithofacies and reservoir significance in the meandering modern Peace River and ancient McMurray Formation, Alberta, Canada: Sedimentology, v. 56, p. 1655−1669.

Smith, D.G., Hubbard, S.M., Lavigne, J.R., Leckie, D.A., and Fustic, M., 2011, Stratigraphy of counter point bars and eddy accretion deposits in low energy meander belts of the Peace-Athabasca Delta, Northeast Alberta, Canada: *in* Davidson, S.K., Leleu S., and North, C.P., eds., From River to Rock Record: The Preservation of Fluvial Sediments and Their Subsequent Interpretation: SEPM, Special Publication 97, p. 143−152.

Taylor, A.M., and Goldring, R., 1993, Description and analysis of bioturbation and ichnofabric: Geological Society, Journal of London, v. 150, p. 141−148.

Thomas, R.G., Smith, D.G., Wood, J.M., Visser, J., Calverley-Range, E.A., and Koster, E.H., 1987, Inclined heterolithic stratification − Terminology, description, interpretation and significance: Sedimentary Geology, v. 53, p. 123−179.

Van Heerden, I.L., and Roberts, H.H., 1988, Facies development of Atchafalaya Delta, Louisiana: A modern bayhead delta: American Association of Petroleum Geologists, Bulletin, v. 72, p. 439−453.

Van Wagoner, J.C., Posamentier H.W., Mitchum R.M., Vail P.R., Sarg J.F., Loutit T.S., and Hardenbol, J., 1988, An overview of sequence stratigraphy and key definitions: *in* Wilgus, C.K., Hastings, B.S., Kendall, C.G.S.C., Posamentier, H.W., Ross, C.A., and Van Wagoner, J.C., eds., Sea Level Changes: An Integrated Approach: SEPM, Special Publication 42, p. 39−45.

Van Wagoner, J.C., Mitchum, R., Campion, K.M., and Rahmanian, V.D., 1990, Siliciclastic Sequence Stratigraphy in Well Logs, Cores, and Outcrops: Concepts for High-Resolution Correlation of Time and Facies, Tulsa, American Association of Petroleum Geologists, Methods in Exploration Series 7, 55 p.

Van Wagoner, J.C., 1995, Sequence stratigraphy and marine to nonmarine facies architecture of foreland basin strata, Book Cliffs, Utah, USA: *in* Van Wagoner, J.C. and Bertram, G.T., eds., Sequence Stratigraphy of Foreland Basin Deposits: American Association of Petroleum Geologists, Memoir 64, p. 137−223.

Weleschuk, Z.P., and Dashtgard, S.E., 2019, Evolution of an ancient (Lower Cretaceous) marginal-marine system from tide-dominated to wave-dominated deposition, McMurray Formation: Sedimentology, v. 66, p. 2354−2391.

Wilson, J.L., 1975, Carbonate Facies in Geologic History: Springer-Verlag, New York, 471 p.

Chapter 4.

Changes in the rate of transgression in the Lower Cretaceous McMurray Depocenter, Canada and implications for the advance of the Boreal Sea

4.1. Introduction

Accommodation, as originally defined by Jervey (1988), refers to the amount of space available for potential sediment accumulation. Accommodation is controlled by the interplay of sediment supply, eustasy and tectonics (Jervey 1988; Posamentier and Allen, 1999; Catuneanu, 2002). Changes in accommodation play an important role in the distribution and geometry of sequences and parasequences and in the nature of their bounding surfaces (Jervey, 1988; Zaitlin et al., 2002). During transgression, an increase in accommodation is responsible for the landward shift of the shoreline (Mitchum, 1977). Based on the thickness of (compacted) sediment deposited over a specific time period, the paleo-depositional environment is characterised as low accommodation (meters−decameters per million years (Myr^{-1})) through to high accommodation (kilometers Myr^{-1}; Zaitlin et al., 2002; Davies and Gibling, 2003; Ratcliffe et al., 2004; Rygel and Gibling, 2006; Allen and Fielding, 2007).

In low accommodation settings, persistent top truncation of parasequences renders it challenging to accurately quantify changes in accommodation space creation across a basin, and to determine the processes responsible for creating this space. The McMurray Fm was deposited during the Early Cretaceous over a period of 8.4 Myr (121.4−113 Ma; Hein and Dolby, 2017; Rinke-Hardekopf et al., 2019). Six DUs accumulated in the McMurray Depocenter (MDC) during that time, and include (from oldest to youngest): C2, C1, B2, B1, A2 and A1 (Fig. 4.2). The maximum thickness of individual DUs within the C2−A1 interval is <15 m, and this led to the interpretation that the MDC was a low-accommodation setting during accumulation of the McMurray Fm (e.g., Ranger and Pemberton, 1997; Hein and Cotterill, 2006; Ranger et al., 2008; Hein et al., 2013; Château et al., 2019, in press). Accommodation space creation during the

Chapter 4 is in preparation as
Château, C.C., Dashtgard, S.E., MacEachern, J.A., in press, Changes in the rate of transgression in the Lower Cretaceous McMurray Depocenter, Canada and implications for the advance of the Boreal Sea

deposition of DUs C2 to A1 was primarily controlled by relative sea-level rise in the Boreal Sea. Additional creation of accommodation space during deposition of C2 to A1 is attributed to syndepositional carbonate epikarstification, and is manifested by localised stratal overthickening (e.g., McPhee and Wightman, 1991; Wightman and Pemberton, 1997; Broughton, 2014, 2015a,b; Barton et al., 2017; Château et al., 2019).

In the southwest quadrant of the MDC, cross-sections and isopach maps are employed to determine the areal extent of McMurray Fm depositional units (DUs), and statistics are used to quantitatively assess thickness variations between them. The relation between DU thickness and the character of the transgressive mudstone bounding the units is investigated. As well, the implications of upward changes in DU thicknesses as a record of the rate of transgression of the Boreal Sea are discussed. These data are used to propose a paleogeographic reconstruction for the McMurray Formation, a sequence stratigraphic model for the McMurray Fm and to comment on the southward transgression of the Lower Cretaceous Boreal Sea into the southwest quadrant of the MDC.

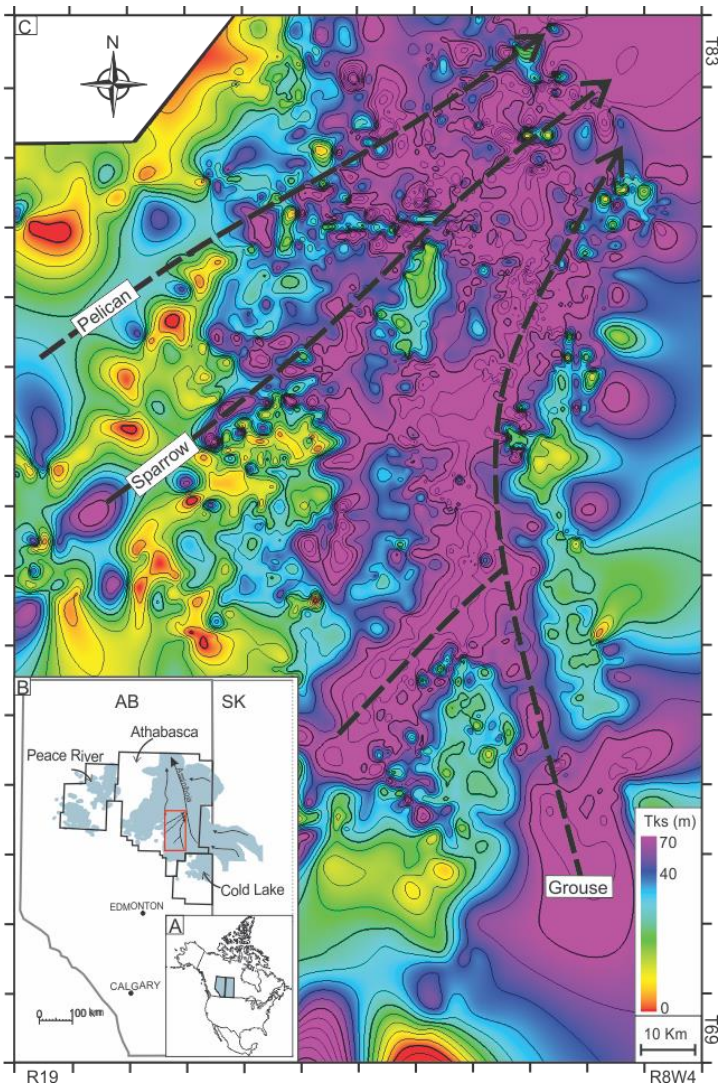

Figure 4.1 (A) Position of Alberta (AB) and Saskatchewan (SK) in North America.

B) The three main oil sands regions (Peace River, Athabasca, and Cold Lake) are demarcated by the black polygons. The blue shaded area in the Athabasca oil sands region marks the approximate limit of the McMurray Fm and time-equivalent strata, which is taken to represent the limits of the McMurray depocenter (MDC). The margins of the MDC in the south, west and north are derived from the AEUB (2003), whereas the eastern extent is theoretical and is based on surface projections and basin reconstruction presented in Jean (2018). The study area is outlined by the red rectangle. C) Isopach map of the McMurray Fm in the study area with maximum thicknesses (tks) observed along the axes of the Pelican, Sparrow and Grouse paleovalleys, and minimum thicknesses over the carbonate highlands.

4.1.1. Geological Setting

The MDC is situated in the northeast corner of the Western Canada Sedimentary Basin (WCSB) and is part of its foreland basin succession (Mossop and Shetsen, 1994). From the Late Jurassic to Early Eocene, the oblique collision of allochthonous terranes

against the western margin of the westward-moving North American craton led to tectonic loading and the formation of a foreland basin in the craton interior (Porter et al., 1982; Mossop and Shetsen, 1994; Price, 1994). Prior to, and during the onset of foreland basin development, uplift and eastward migration of the forebulge generated forced sea-level fall (Poulton, 1994). This led to the erosion of previously deposited Paleozoic carbonate-dominated, passive-margin strata and the formation of the Sub-Cretaceous Unconformity (SCU; Jardine, 1974; Plint et al., 1993). Paleotopography on the SCU significantly influenced the architecture of the McMurray Fm.

The McMurray Fm broadly consists of fluvial strata at the base, informally referred to as the “lower McMurray”. These strata are progressively overlain by estuarine and increasingly marine strata, informally named the “middle” and “upper” McMurray, respectively (Figs. 4.1 and 4.2; Carrigy, 1963, 1967). The initial stratigraphic framework subdivided the McMurray Fm into the informally defined lower, middle, and upper members, based on the interpreted degree of marine influence (Fig. 4.2; Carrigy, 1963, 1967). This initial stratigraphic model did not address the complexity of the McMurray Fm stratigraphic subdivision, and hence, a coupled lithostratigraphic and sequence stratigraphic model was proposed by the Alberta Energy and Utilities Board (2003; now Alberta Energy Regulator (AER), AEUB). The AER model subdivides the McMurray Fm based on the occurrence of mudstone intervals at the base of regionally extensive stratigraphic units, and this framework remains largely accepted. Regionally extensive stratigraphic units (e.g., stacked parasequences or parasequence sets) are interpreted as prograding coastal- and shallow-marine successions deposited during short-lived periods of relative stillstand during an overall transgression. These regionally extensive stratigraphic units are incised into by channels of variable thickness, which have been interpreted to subtend from the tops of the units (Alberta Energy and Utilities Board, 2003). Hence, channels are commonly interpreted as the products of valley incision that occurred during major relative sea-level falls and during subsequent relative sea-level rise (Hein et al., 2013). The implications of this model are that valley fills are genetically unrelated to the deposition of the regionally extensive stratigraphic units they cross-cut. Other workers (e.g., Ranger et al., 2008; Musial et al., 2012) do not consider all of the channels to be of incised valley fill origin, and instead regard them as channel belt complexes. Regardless of the origin of the channels themselves, some workers interpret

them as mainly fluvial, based on scaling relationships with modern fluvial systems (e.g., Durkin et al., 2017a, b; Horner et al., 2019)

Herein, we employ a revised version of the Alberta Energy and Utilities Board (2003) stratigraphic model, wherein the middle and upper McMurray Fm are divided into six parasequences or parasequence sets organized into discrete stratigraphic units referred to as depositional units, that comprise (from oldest to youngest): C2, C1, B2, B1, A2 and A1 (Fig. 4.2). The base of each DU is defined by a mudstone interval overlying a regionally significant flooding surface (Fig. 4.2). We consider DUs to represent regressive cycles deposited during minor relative sea-level fluctuations (equivalent to sequences in the AEUB (2003) stratigraphic model). Channel belts are contemporaneous with each DU (Fig. 4.2; Ranger and Pemberton, 1997; Musial et al., 2012; Weleschuk and Dashtgard, 2019; Château et al., 2019, in press). The limited accommodation space created through both the relative sea-level rise of the Boreal Sea and epikarstification was rapidly infilled by sediments supplied by the paleo-distributive channel system, and during periods of stable or only slowly rising base level, this led to progradation of the shoreline (e.g., Ranger and Pemberton, 1997; Ranger et al., 2008; Château et al., 2019, in press; Weleschuk and Dashtgard, 2019).

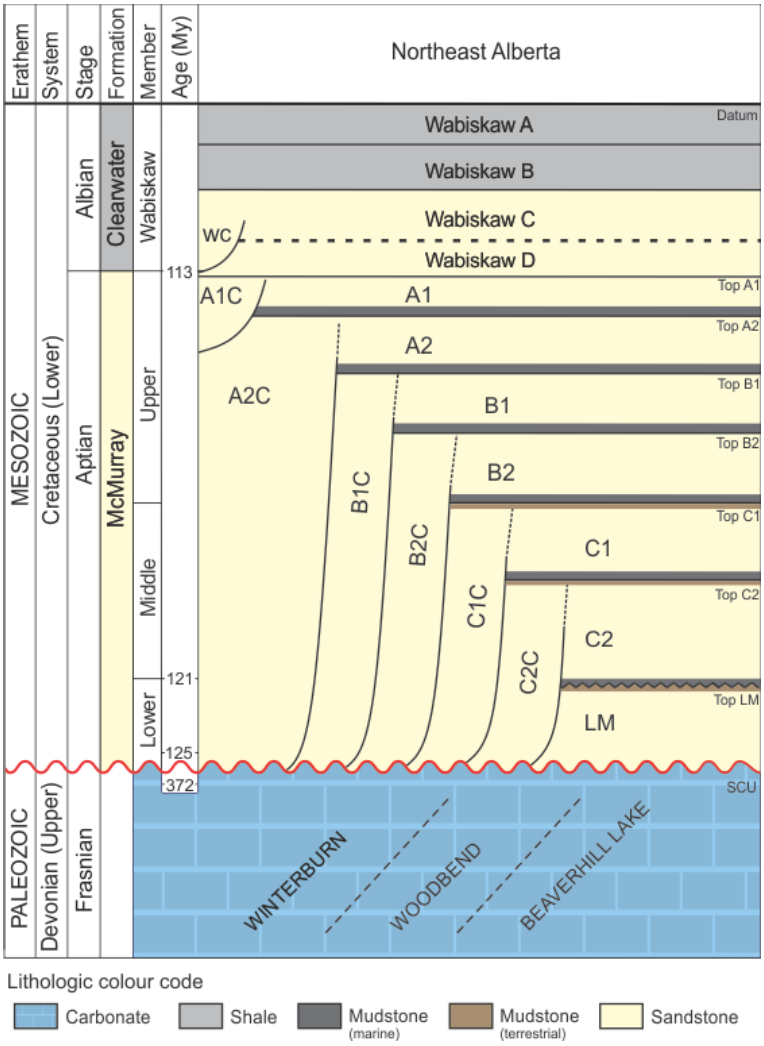

Figure 4.2 Composite of stratigraphic frameworks proposed for the McMurray Fm in the McMurray depocenter (MDC).

On the left (vertical text) is the chronostratigraphic framework for the MDC (Alberta Geological Survey, 2015). The McMurray Formation overlies the Sub-Cretaceous Unconformity (SCU, red wavy line) and is, in turn, overlain by the Wabiskaw Member of the Clearwater Formation. The age of the top of the lower McMurray Fm is derived from Rinke-Hardekopf et al. (2019). On the right is a modified version of the lithostratigraphic/allostratigraphic model proposed by the Alberta Energy and Utilities Board (2003; now Alberta Energy Regulator).

4.1.2. Study Area

The MDC extends over 44 000 km^2 from 55–58° N and 110–114° W (Fig. 4.1). It encompasses multiple paleovalleys cut into the SCU, and the main north-south topographic low is commonly referred to as the Assiniboia Valley (e.g., Christopher, 1984). Along the axis of the Assiniboia Valley, DUs were completely removed by subsequent channel-belt incision and migration. The southwestern quadrant of the MDC

(townships (T) 69–83, ranges (R) 9–20W4; Fig. 4.1C) is located west of the Assiniboia Valley and along the margins of the Grosmont Highlands. It extends over 15 850 km^2 and includes the Grouse, Sparrow, and Pelican paleovalleys. These paleovalleys preserve minimal strata from the lower member of the McMurray Fm (LM, Fig. 4.1), but a nearly continuous succession of DUs from C2 to A1, with only limited removal by channel belts (Ranger and Pemberton, 1997; Weleschuk and Dashtgard, 2019; Château et al. 2019, in press). The Grouse Paleovalley extends over 150 km from SW to NE and covers an area of 4 570 km^2, the Sparrow Paleovalley extends over 139 km from SW to NE and covers an area of 3 260 km^2, and the Pelican Paleovalley extends over 96 km from SW to NE and covers an area of 2 420 km^2 (Fig. 4.1). All three paleovalleys coalesce towards the NE.

4.2. Methods and Database

Data used in this study includes 100 cored intervals and 6 500 well logs with LAS files. Cores were logged at the Core Research Centre in Calgary, Alberta, Canada during the summers of 2015 and 2016. Well logs and core locations are given as unique well identifiers (UWI) that define a position based on the Dominion Land Survey. In each core, sedimentological and ichnological characteristics were recorded using AppleCORE logging software (donated by Mike Ranger). Sedimentological descriptions include lithology (grain-size, sorting, roundness, color, and accessories), sedimentary structures, and post-depositional features (diagenesis, fractures). Ichnological descriptions include bioturbation index (BI), trace fossil identification, and trace fossil diversity. Strata were then grouped into facies and facies associations (FAs; Table 4.1), and primary, secondary, and tertiary depositional processes are assigned to facies and FAs using the semi-quantitative classification proposed by Ainsworth et al. (2011).

In the SW quadrant of the MDC, over 11 000 wells have been drilled through the McMurray Fm and have publicly available geophysical well logs. Of the 11 000 wells, 6 500 include digital (LAS) well-log files with gamma-ray, spontaneous potential, caliper, resistivity, neutron porosity, and sandstone density porosity curves. LAS well log files were exported from geoSCOUT® (donated to SFU by geoLOGIC Systems Ltd.) and imported into Petrel® 2016 (donated to SFU by Schlumberger), wherein cross-sections were generated and stratigraphic intervals were correlated and mapped. Cross-sections were generated to resolve the architecture of the McMurray Fm. The Top Wabiskaw A

surface (top of the Wabiskaw Member of the Clearwater Fm) corresponds to a regionally extensive and easily correlated marine flooding surface that caps a largely healed paleotopography. It is interpreted to have been relatively horizontal at the time of formation; hence, the Top Wabiskaw A surface is employed as the stratigraphic datum for the McMurray Fm.

Isopach maps were constructed to delineate the distribution of each DU of the McMurray Fm in the study area, and were created using a convergent interpolation method in Petrel® 2016. The convergent interpolation algorithm reduces extrapolation by tuning values (i.e., decrease/increase values) using neighboring data points (Sibson, 1981), and is the most suitable algorithm to map the relatively flat DUs of the McMurray Fm. Outlier values remaining in the dataset are interpreted to represent complex geologic features (e.g., faulting, karsting). Depositional units are not laterally continuous through the study area, and for each DU (C2−A1) a zero thickness is assigned to wells in which the DU is not present (e.g., eroded by younger channels), to limit extrapolation and improve the accuracy of Petrel's interpolation algorithm (e.g., Rinke-Hardekopf et al., 2019; Château et al., in press).

4.2.1. Statistical Analysis

Statistical analysis was done using data derived from the 6 500 geophysical well logs with LAS files to quantitatively assess DU thicknesses and their variations. Thicknesses of C2–A1 in all wells were exported from Petrel into a spreadsheet. Exported data included unique well identifiers, longitude, latitude, kelly bushing (height relative to sea level), true vertical depth, and DU thicknesses. To limit the impact of minor local variations in DU thickness (e.g., faulting, karsting) for C2–A1, anomalous thickness outliers were excluded from the dataset. Anomalous thickness outliers include any values that are not between the 10^{th} and 90^{th} percentiles on a Gaussian distribution of thicknesses for the DU. Additional statistical work was completed using data derived from 57 cores widely distributed across the study area (Fig. 4.10D) to quantitatively assess the distribution of the transgressive mudstone facies (F6a, F6b and F6c) that bound the DUs. Core-derived data were entered into a spreadsheet. Data organised into spreadsheets were statistically analyzed using the RStudio environment of the open-source R Project software (Marx, 2013; Gandomi and Haider, 2015; Rstudio Team, 2015). Statistical analysis of the mean, median, variance, and standard deviation were

calculated to quantitatively estimate the DU thickness in the area and tests the hypotheses that DU thicknesses 1) decreases upward, and 2) correlate to changes in transgressive mudstone facies. The thickness distributions of DUs as well as the facies distributions of transgressive mudstone are plotted using the ggplot functionality of the tydiverse package in R (Wickham, 2016; Wickham and Grolemund, 2016).

4.3. Results

4.3.1. Facies and Facies Associations

Based on the sedimentological and ichnological characteristics of the cored intervals, strata are grouped into 10 discrete facies (Table 4.1; Fig. 4.3−4.5). Eight facies successions are defined from the vertical relationships of these 10 facies, and these are grouped into four recurring facies associations (FAs) that correspond to depositional environments. Abbreviated sedimentological descriptions of FA1, FA2 and FA3 are provided in the following section. Refer to Château et al. (in press) for detailed sedimentological descriptions of FAs 1–3. For FA4, a detailed sedimentological and ichnological description is provided in this paper, as it has not been described previously (Fig. 4.4).

Table 4.1 **Sedimentological and ichnological characteristics, geophysical character, and contacts of facies in the McMurray Fm, southwest quadrant of the MDC. Acronyms in the Facies Name, Grain Size, and Facies Description/Sedimentology columns include: inclined heterolithic stratification (IHS) very fine lower (vfL), very fine upper (vfU), fine lower (fL), fine upper (fU), medium lower (mL), medium upper (mU), millimetre (mm), centimetre (cm), decimetre (dc), metre (m), and decametre (dam). Ichnology is recorded in two ways: Bioturbation Index (BI; Taylor and Goldring, 1993) and trace fossil diversity. Trace fossils include *Arenicolites* (*Ar*), *Asterosoma* (*As*), *Chondrites* (*Ch*), *Cylindrichnus* (*Cy*), *Diplocraterion* (*Di*), fugichnia (fu), *Gyrolithes* (*Gy*), navichnia (na), *Palaeophycus* (*Pa*), *Phycosiphon* (*Ph*), *Planolites* (*Pl*), roots (rt), *Siphonichnus* (*Si*), *Skolithos* (*Sk*), *Taenidium* (*Ta*), *Teichichnus* (*Te*) and *Thalassinoides* (*Th*). All trace fossils in the facies are diminutive (i.e., smaller than traces deposited under optimal fully marine conditions). Gamma-ray log signature reports values in American Petroleum Institute (API) units.**

Facies		Facies Name	Grain-Size	Facies Description/Sedimentology	Ichnology		Depositional Process(es)	Contacts	Depositional Environment	Gamma-Ray Log Signature
					BI	Traces				
F1		Unbioturbated sand and/or conglomerate with mud clasts	Gravel: granule−pebble Sand: vfU to mU Mud clasts: pebble−cobble	cm−dm scale lag overlain by dune-scale cross-stratified sands, with uncommon pebble and granule stringers. Abundant mud clasts and mud clast-breccias; abundant carbonaceous debris and pyrite concretions.	0	None	Traction transport of sand as dunes *via* unidirectional currents.	Erosional basal contact. Gradational upper contact with F2a.	Channel thalweg/base of channel lag.	Blocky signature with values < 45 API.
F2	a	Weakly bioturbated cross-stratified to current rippled sand	Sand: vfU to mU Mud clasts: pebble−cobble	dm−dam scale intervals of cm-dm thick, dune-scale cross-stratified and/or current rippled sand with reactivation surfaces. Mud drapes, mud clasts, mud-clast breccia, thin mud flasers (mm-cm scale) and carbonaceous debris.	0−2	Cy, fu, Pl, Sk (diminutive)	Mainly traction transport of sand as dunes and ripples *via* unidirectional and/or bidirectional currents.	Gradational lower contact with F1. Gradational upper contact with F3a. Sharp/gradational upper contact F4a.	Base of channel/ lower (subtidal) point bar.	Blocky to upward increasing API values that range from > 45 to < 75 (*i.e.*, fining upward).
	b		Sand: vfU to mU Mud clasts: pebble	m scale interval of cm-dm thick, dune-scale cross-stratified sand beds, current ripples, and rare oscillation ripples. Mud drapes, mud clasts, thin (mm-cm thick) mud flasers and carbonaceous debris.	0−4	Ar, Ch, Cy, Di, Pa, Pl, Si, Sk (diminutive)	Mainly traction transport of sand as dunes and ripples *via* unidirectional, bidirectional and/or oscillatory currents.	Erosional basal contact. Gradational upper contact with F3b.	Distributary channels (bay head delta/ bay margin).	
F3	a	Weakly to thoroughly bioturbated sand- dominated IHS	Sand: vfU to mL Mud: undifferentiated	dm−dam scale interval of cm−dm thick beds of sand and mudstone with current ripples (locally aggradational), planar parallel lamination, reactivation surfaces, mud drapes, thin (mm-cm scale) mud flasers and abundant carbonaceous debris.	Sand: 0−5 Mud: 1−5	Sand: Cy, na, Pa, Pl, Sk, Th Mud: Ch, na, Pa, Pl, Te (diminutive)	Lateral and downstream accretion of sand and mud on bars *via* unidirectional and/or bidirectional currents.	Gradational lower contact with F2a. Gradational upper contact with F4a. Sharp internal contacts.	Subtidal point bar IHS (lateral accretion).	Serrated profile, generally upward increasing API values that range from < 75 to < 90 (*i.e.*, fining upward).
	b			dm−m scale interval of cm−dm thick beds of sand and mudstone with current ripples, planar parallel lamination, rare oscillation ripples, uncommon syneresis cracks, mud drapes, thin (mm-cm scale) mud flasers and abundant carbonaceous debris.	Sand: 1−4 Mud: 2−5	Sand: Cy, na, Pa, Pl, Si, Sk, Th Mud: Ch, na, Pa, Pl, Te, Th (diminutive)	Accretion of sand and mud along channel margins *via* unidirectional, bidirectional and/or oscillatory currents.	Gradational lower contact with F2b. Gradational upper contact with F4b. Sharp internal contacts.	Channel margin IHS.	
F4	a	Thoroughly bioturbated mudstone-dominated IHS	Sand: vfU to mL Mud: undifferentiated	dm−dam scale interval of mm−cm thick sand units in a mudstone matrix with planar parallel lamination, normal grading, soft-sediment deformation structures and abundant carbonaceous debris.	Sand: 1−5 Mud: 1−5	Sand: Cy, fu, Pl, roots, Sk, Te Mud: Ch, na, Pl, rt, Te, Th (diminutive)	Bar top deposition during high tide *via* ebb-oriented currents and possibly upstream *via* flow separation.	Gradational lower contact with F3a. Sharp/erosional upper contact with F1/F2a,b/F5/F6. Sharp internal contacts commonly overprinted by bioturbation.	Upper (intertidal) point bar IHS, counter point bar.	Oblong signature, with API values > 90.
	b			dm−m scale interval of mm−cm thick sand layers in a mudstone matrix with planar parallel lamination (normal grading), rare syneresis cracks, soft-sediment deformation structures and abundant carbonaceous debris.	Sand: 1−5 Mud: 1−5	Sand: Cy, fu, Pl, Sk, Te Mud: Ch, na, Pl, Ta, Te (diminutive)		Gradational lower contact with F3b. Sharp/erosional upper contact with F1/F2a,b/F5/F6. Sharp internal contacts commonly overprinted by bioturbation.	Channel margin IHS.	

Facies		Facies Name	Grain-Size	Facies Description/Sedimentology	Ichnology		Depositional Process(es)	Contacts	Depositional Environment	Gamma-Ray Log Signature
					BI	Traces				
F5		Weakly bioturbated preserved to pedogenetically altered silty mudstone	Sand: vfL to fU Mud: undifferentiated	dm−dam scale interval of mm−cm thick silty sand layers in a mudstone matrix, with planar parallel lamination, rare syneresis cracks, soft-sediment deformation structures, normal micro-faults, carbonaceous debris, abundant fractures, siderite concretion and rare pyrite concretion.	Sand: 0−2 Mud: 0−1	Sand: Ar, na, Pl, Sk, Te Mud: Ch, Pl, rt (diminutive)	Vertical aggradation of sediment during channel abandonment (unidirectional currents) *via* settling and/or accretion of sediment *via* bidirectional currents; subaerial exposure.	Sharp lower contact with F2a/F3a. Erosional upper contact, locally with omission suite of the *Glossifungites* Ichnofacies.	Abandoned channel.	Oblong signature, with API values > 100.
F6	a	Unburrowed dark grey mudstone to shale	Sand: vfL to fL Mud: undifferentiated	cm−dm scale interval of dark grey mudstone to shale, with mm−cm thick silty sand lamina/lenses/beds	0−1	Pl, (diminutive)	Vertical aggradation of sediment *via* unidirectional and/or oscillatory currents.	Sharp/erosional basal contact. Gradational upper contact with F7a.	Restricted embayment to offshore deposits	Oblong signature with values >100 API.
	b	Weakly to thoroughly bioturbated, dark grey mudstone		cm−dm scale interval of mm−cm thick silty sand lamina/lenses/beds in a dark grey mudstone matrix, with planar to wavy parallel lamination, normal micro-faults and syneresis cracks.	1−5	Ch, Pl, Ph, Sk, (diminutive)		Sharp/erosional basal contact. Gradational upper contact with F7a, b.		
	c	Weakly to thoroughly bioturbated, steel blue-grey mudstone		cm−dm scale interval of mm−cm thick silty sand lamina/lenses/beds in a steel blue-grey mudstone matrix, with planar to wavy parallel lamination, normal micro-faults and syneresis cracks.	1−5	Ar, As, Ch, Pl, Ph, Sk, Te (diminutive)		Sharp/erosional basal contact. Gradational upper contact with F7a, b.		
F7	a	Weakly to moderately bioturbated, convolute bedded silty mudstone	Sand: vfL to fL Mud: undifferentiated	cm−dm scale interval of rare mm−cm thick silty sand beds in a mudstone matrix, with carbonaceous debris and convolute bedding.	1−4	Ch, Cy, fu, Ph, Pl, Sk, Th (diminutive)	Vertical aggradation of sediment *via* unidirectional currents.	Sharp or gradational (F6) basal contact. Gradational upper contact with F8a. Sharp internal contacts.	Proximal prodelta. Protected embayment/ lagoon.	Oblong signature with API values ranging from 80−100.
	b	Weakly to moderately bioturbated, lenticular to wavy silty laminae in a mudstone matrix		cm−dm scale interval of rare mm−cm thick silty lenses/ laminae in a mudstone matrix, with irregular to wavy parallel lamination, normal micro-faults, convolute bedding, loading and flames structures, syneresis cracks and carbonaceous debris.	1−3	Ch, Cy, fu, Ph, Pl, Sk, Te, Th (diminutive)	Vertical aggradation of sediment *via* oscillatory currents.	Sharp or gradational (F6) basal contact. Gradational upper contact with F8b. Sharp internal contacts.	Wave/ storm-dominated proximal prodelta.	

Facies		Facies Name	Grain-Size	Facies Description/Sedimentology	Ichnology		Depositional Process(es)	Contacts	Depositional Environment	Gamma-Ray Log Signature
					BI	Traces				
F8	a	Weakly to thoroughly bioturbated heterolithics	Sand: vfL to mL Mud: undifferentiated	dm−m scale interval of interbedded cm−dm thick interbedded sand and mudstone beds, with planar to wavy parallel lamination, current ripples, combined flow ripples, convolute bedding, normal micro-faults, syneresis cracks, and carbonaceous detritus	1−5	Ar, Ch, Cy, fu, Gy, na, Pa, Ph, Pl, Sk, Te, Th (diminutive)	Vertical aggradation of sediment *via* unidirectional and/or oscillatory currents.	Gradational lower contact with F7a. Gradational upper contact with F9a. Sharp internal contacts typically overprinted by bioturbation.	Distal tidal sand bar.	Upward decreasing signature with API values that range from >75 to >100 (*i.e.,* coarsening upward).
	b	Weakly to thoroughly bioturbated wavy heterolithics		dm−m scale interval of interbedded cm−dm thick interbedded sand and mudstone beds, with irregular to wavy parallel lamination, combined flow ripples, oscillatory ripples, convolute bedding, normal micro-faults, loading and flames structures, syneresis cracks, and carbonaceous detritus.	1−5	Ar, As, Ch, Cy, fu, Gy, na, Pa, Ph, Pl, rt, Sk, Te, Th (diminutive)	Vertical aggradation of sediment *via* oscillatory currents.	Gradational lower contact with F7b. Gradational upper contact with F9b. Sharp internal contacts typically overprinted by bioturbation.	Wave/ storm-dominated distal delta-front. Distal mouth bar.	
F9	a	Unburrowed to thoroughly bioturbated, current rippled to low-angle cross-stratified sand	Sand: vfL to mL	m-scale interval of cm−dm thick dune-scale cross-stratified sand, with micro-hummocky cross-stratification, hummocky cross-stratification, current ripples with reactivation surfaces, rare oscillatory ripples, combined flow ripples, normal micro-faults, mud drapes and carbonaceous debris.	0−5	Ar, As, Ch, Cy, Di, Gy, fu, na, Pa, Ph, Pl, Sk, Te (diminutive)	Vertical aggradation of sediment *via* unidirectional, bidirectional and/or oscillatory currents.	Gradational lower contact with F8a. Sharp/erosional upper contact.	Tidal sand bar.	Upward decreasing to blocky signature with API values <75 (*i.e.,* coarsening upward).
	b	Unburrowed to thoroughly bioturbated, oscillation rippled to hummocky cross-stratified sand		m-scale interval of cm−dm thick dune-scale cross-stratified sand, with micro-hummocky cross-stratification, hummocky cross-stratification, abundant oscillatory ripples, combined flow ripples, normal micro-faults, flaser bedding, carbonaceous debris, pyrite and siderite concretions.	0−5	Ar, As, Ch, Cy, Di, Gy, fu, na, Pa, Ph, Pl, rt, Sk, Te, Th (diminutive)	Vertical aggradation of sediment *via* oscillatory currents.	Gradational lower contact with F8b. Sharp/erosional upper contact.	Wave/ storm-dominated delta-front. Mouth bar.	
F10		Moderately bioturbated, siltstone to root-bearing sand	Sand: vfL to fL Mud: silt	dm−m scale coarsening-upward interval of siltstone to sand, with rare convolute bedding. Most structures are overprinted by bioturbation and locally by rooting.	2−4	Ch, rt, Sk, Te, Th (diminutive)	Vertical aggradation of sediment, subaerial exposure at the top (rooting).	Gradational (F6/F7/F8) or sharp lower contact. Sharp upper contact.	Supratidal bar.	API values ranging from 60−90.

Facies Association 1 (FA1): Fluvio-Tidal Channels

Description: Five facies generate 3 facies successions that define FA1, interpreted as fluvio-tidal channels (Table 4.1; Fig. 4.3). Channel-belts range from 6−65 m thick and are typically 10−25 m thick. Within the 5 facies, physical sedimentary structures are exclusive of current origin and comprise dune-scale cross-stratified sand, with subordinate planar-parallel lamination, flaser bedding, and stacked current ripple cross-lamination. Ichnologically, the bioturbation index (BI; Taylor and Goldring, 1993) increases upwards from BI 0 in cross-bedded sand of F1 to BI 5 in some intervals of muddy IHS (F4a). The trace fossil suite in FA1 encompasses 8 ichnogenera: *Arenicolites, Chondrites, Cylindrichnus, Palaeophycus, Planolites, Skolithos, Teichichnus* and *Thalassinoides*, as well as fugichnia and navichnia. The trace fossils in FA1 are diminutive (i.e., smaller than counterparts deposited under optimal, fully marine conditions; see Pemberton and Wightman, 1992; Gingras et al., 2011). Root structures also occur rarely in mudstone-dominated intervals of F4a and F5. On gamma-ray geophysical well logs, FA1 shows a blocky to upward increasing API (fining-upward) signature.

Interpretation of FA1: Facies Association 1 is interpreted to represent fluvio-tidal channels, based on the combined sedimentological and ichnological characteristics of the facies. Similar deposits in the MDC were interpreted as purely fluvial channels (e.g., Flach and Mossop, 1985; Blum and Pecha, 2014; Durkin et al., 2017a, b; Horner et al., 2019; Martin et al., 2019). By contrast, the trace fossil suites within facies of this facies association are interpreted to record brackish-water conditions (e.g., Pemberton et al., 1982; Pemberton and Wightman, 1992; Hubbard et al., 2011; Barton, 2016; Gingras et al., 2016). When considered together, the sedimentological and ichnological observations support the interpretation that these channel-belts record deposition associated with fluvio-tidal channels (Ranger and Pemberton, 1997; Hein et al., 2000; Baniak and Kingsmith, 2018; La Croix et al., 2019a; Weleschuk and Dashtgard, 2019; Château et al., in press).

Three facies successions form the dominant expressions of FA1. Facies Succession 1 (F1, F2a, F3a, F4a) is interpreted to represent tidally influenced point bars. Facies Succession 2 (F1, F3a, F4a) is interpreted as either tidally influenced muddy point bar or counter point-bar deposits. Facies Succession 3 (F1, F2a, F3a or F4a, F5) is

interpreted as channel abandonment, with remnant cross-bedded channel-floor sandstone abruptly overlain by an abandonment mud plug.

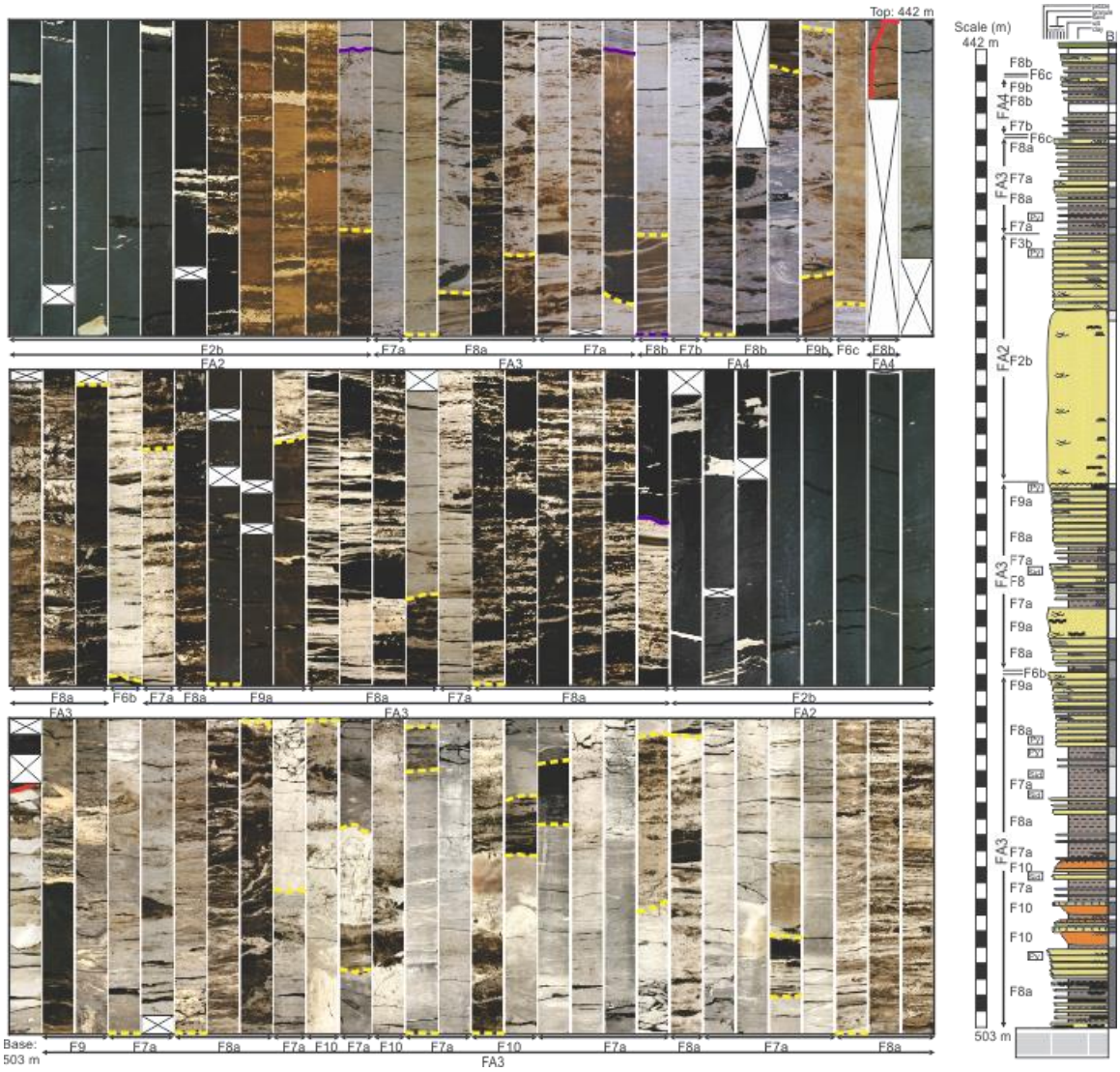

Figure 4.3 Near continuous core photos and log for 1AA-16-05-079-13W4 well from 442–503 m depth.

Note that the sand is either light brown (water- or gas-saturated) or dark (bitumen saturated) in color. Mudstone beds are either beige or light to dark grey. Core columns are 7.6 cm wide and 75 cm long. Facies and facies association distributions are labelled at the bottom of the core box photos and on the left side of the core log. Contacts between facies are demarcated by dashed yellow lines; contacts between facies associations are highlighted by purple lines in the core photo and by dashed black lines in the core log. Stacked successions of the same FA are not distinguished except as facies breaks. Devonian-aged carbonates are separated from the overlying Lower Cretaceous McMurray deposits by the Sub-Cretaceous Unconformity (SCU; red line near the bottom of the cored interval). A Glossifungites Ichnofacies-demarcated surface (red line near the top of the cored interval) separates the McMurray Fm from the glauconitic sandstone of the overlying Wabiskaw Member of the Clearwater Formation.

Facies Association 2 (FA2): Distributary Channels

Description: Three facies generate 2 fining-upward facies successions that define FA2, interpreted as distributary channels (Table 4.1; Fig. 4.3). FA2 channel-belts differ from the fluvio-tidal channel-belts of FA1 in that FA2 channel-belts are an order of magnitude smaller. FA2 channel-belts range from 2−15 m in thickness and are typically 3−8 m thick. Facies Succession 1 of FA2 typically exhibits a fining-upward trend that comprises an erosional basal surface overlain by a thick interval of weakly bioturbated, cross-stratified to current-rippled sand (F2b) fining upward into sand-dominated IHS of F3b; and then into mudstone-dominated IHS of F4b. Facies Succession 2 is also a fining-upward succession and only differs from Facies Succession 1 with respect to facies thicknesses; Facies Succession 2 comprising only a thin interval F2b overlain by well-developed intervals of F3b and F4b.

Within FA2, physical sedimentary structures are of both current and oscillatory origin, and include mainly dune-scale cross-stratification with subordinate planar-parallel lamination, current ripples, rare oscillatory ripples, mud drapes, and flaser bedding. Abundant carbonaceous detritus is intercalated and soft-sediment deformation and syneresis cracks occur locally. Ichnologically, FA2 deposits exhibit BI 0−5, and the trace-fossil suite comprises 11 ichnogenera: *Arenicolites, Chondrites, Cylindrichnus, Diplocraterion, Palaeophycus, Planolites, Siphonichnus*, *Skolithos, Taenidium, Teichichnus* and *Thalassinoides*, in addition to fugichnia and navichnia. The trace fossils in FA2 are diminutive. On gamma-ray geophysical well logs, FA2 shows a blocky to upward-increasing API (fining-upward) signature.

Interpretation of FA2: Physical sedimentary structures observed in FA2 successions are characteristic of fluvial settings subjected to tidal and wave influence (e.g., Olariu and Bhattacharya, 2006; Dashtgard and La Croix, 2015; La Croix and Dashtgard, 2015; Ghinassi et al., 2019). The ichnological suite is interpreted to reflect brackish-water conditions, but with lower levels of physico-chemical stress than is interpreted for the FA1 channels (e.g., Howard and Frey, 1975; Howard et al., 1975; Gingras et al., 1999; Johnson and Dashtgard, 2014; Weleschuk and Dashtgard, 2019). FA2 successions show a stronger degree of marine influence than in is expressed by facies of FA1 (e.g., Gugliotta et al., 2016, 2017; Collins et al., 2019). The combined sedimentological and ichnological observations of FA2 support the interpretation that

these channel-belt deposits represent distributary channels, with the two fining-upward facies successions recording lateral facies changes (Château et al., in press). Facies Succession 4 (thick F2b, absent or thin F3b, and absent or thin F4b) is interpreted to record deposition along the channel margin, whereas Facies Succession 5 (thin F2b, thick F3b, and thick F4b) is interpreted as in-channel bar deposits.

Facies Association 3 (FA3): Tide-Dominated Deltas

Description: Four facies arranged in two facies successions define Facies Association 3 (FA3), interpreted as tide-dominated deltas (Table 4.1; Figs. 4.3 and 4.5). Within those facies, physical sedimentary structures are of both current and oscillatory origin. Primary structures include current, oscillatory and combined-flow ripples, dune-scale cross-stratification, micro-hummocky and hummocky cross-stratification, and local zones of soft-sediment deformation. Bioturbation is typically variable (BI 0−5, but mainly BI 1−4). Trace fossils are diminutive, and the suite encompasses 12 ichnogenera: *Arenicolites, Asterosoma, Chondrites, Cylindrichnus, Diplocraterion, Gyrolithes, Palaeophycus, Phycosiphon, Planolites, Skolithos*, *Teichichnus* and *Thalassinoides*, in addition to fugichnia and navichnia. Root structures are common in F10. On gamma-ray geophysical well logs, FA3 deposits are typically expressed by decreasing-upward API (i.e., upward increase in sand content) profiles.

Interpretation of FA3: The sanding- and coarsening-upward facies successions of FA3 are interpreted as parasequences (PS). Physical sedimentary structures observed in FA3 record unidirectional currents, bidirectional currents, and/or oscillatory flow. Facies Succession 6 (F7a, F8a, F9a and F10) is dominated by unidirectional and/or bidirectional current-generated structures (>80%), with subordinate oscillatory-generated structures (<20%). Facies Succession 7 (F7a, F8a and F9a) shows that the proportion of oscillatory-generated structures reaches 40%, and the ichnological suites comprise diminutive trace fossils indicative of persistent brackish-water conditions (e.g., Ranger and Pemberton, 1997; Gingras and MacEachern, 2012; Gingras et al., 2011, 2016; Barton, 2016; Weleschuk and Dashtgard, 2019). Rare root-bearing intervals are attributed to autogenic subaerial exposure, associated with deposition on the delta plain. Based on the combination of sedimentological and ichnological observations, and following the process classification of Ainsworth et al. (2011), FA3 is interpreted as a series of tide-dominated (T) delta deposits. Facies Succession 1 is interpreted as tide-

dominated, fluvial-influenced, and storm-affected (Tfw) delta lobes, whereas Facies Succession 2 represents tide-dominated, storm-influenced, and fluvial-affected (Twf) delta lobes.

Facies Association 4 (FA4): Wave-Dominated, Tide-Influenced, Fluvial-Affected (Wtf) Deltas

Description: Four facies generate a facies succession that defines FA4, interpreted as wave-dominated, tide-influenced, fluvial-affected (Wtf) delta (Table 4.1; Figs. 4.3−4.5). Within these facies, physical sedimentary structures are of both oscillatory and current origin. Primary structures include micro-hummocky and hummocky cross-stratification, oscillatory and combined-flow ripples, dune-scale cross-stratification, and local zones of soft-sediment deformation. Facies also contain mudstone interbeds with irregular to wavy parallel laminae and/or sand lenses, carbonaceous debris, and syneresis cracks. Ichnologically, bioturbation is typically variable (BI 0−5, but mainly BI 1−3), and the trace fossil suite includes 12 ichnogenera: *Arenicolites, Asterosoma, Chondrites, Cylindrichnus, Diplocraterion, Gyrolithes, Palaeophycus, Phycosiphon, Planolites, Skolithos*, *Teichichnus* and *Thalassinoides*, in addition to fugichnia and navichnia. Trace fossils are diminutive and mainly record mobile deposit-feeding behaviours and the dwellings of deposit-feeders and carnivores (e.g., MacEachern and Gingras, 2007; MacEachern et al., 2012). Root structures are very rarely preserved, and occur only in F10 at the top of FA4 successions. On gamma-ray geophysical well logs, FA4 deposits are typically expressed by decreasing-upward API (i.e., upward increase in sand content) profiles and the gamma-ray response in FA4 is higher than 60 API.

In core, FA4 succession sand and coarsen upward. Facies succession 8 typically overlies a sharp and non-erosional basal surface. The lowermost strata consist of weakly to moderately bioturbated, lenticular to wavy silty laminae in a mudstone matrix (F7b). Facies 7b passes upwards into weakly to thoroughly bioturbated, wavy heterolithic bedsets (F8b), and then into unburrowed to thoroughly bioturbated, oscillation rippled to hummocky cross-stratified sand (F9b). In some locations, F9b deposits are capped by moderately bioturbated, siltstone to root-bearing sand (F10). There are numerous occurrences of the coarsening-upward Facies Successions 8 of FA4 that terminate prior to deposition of F9b, or where F9b has been erosionally removed.

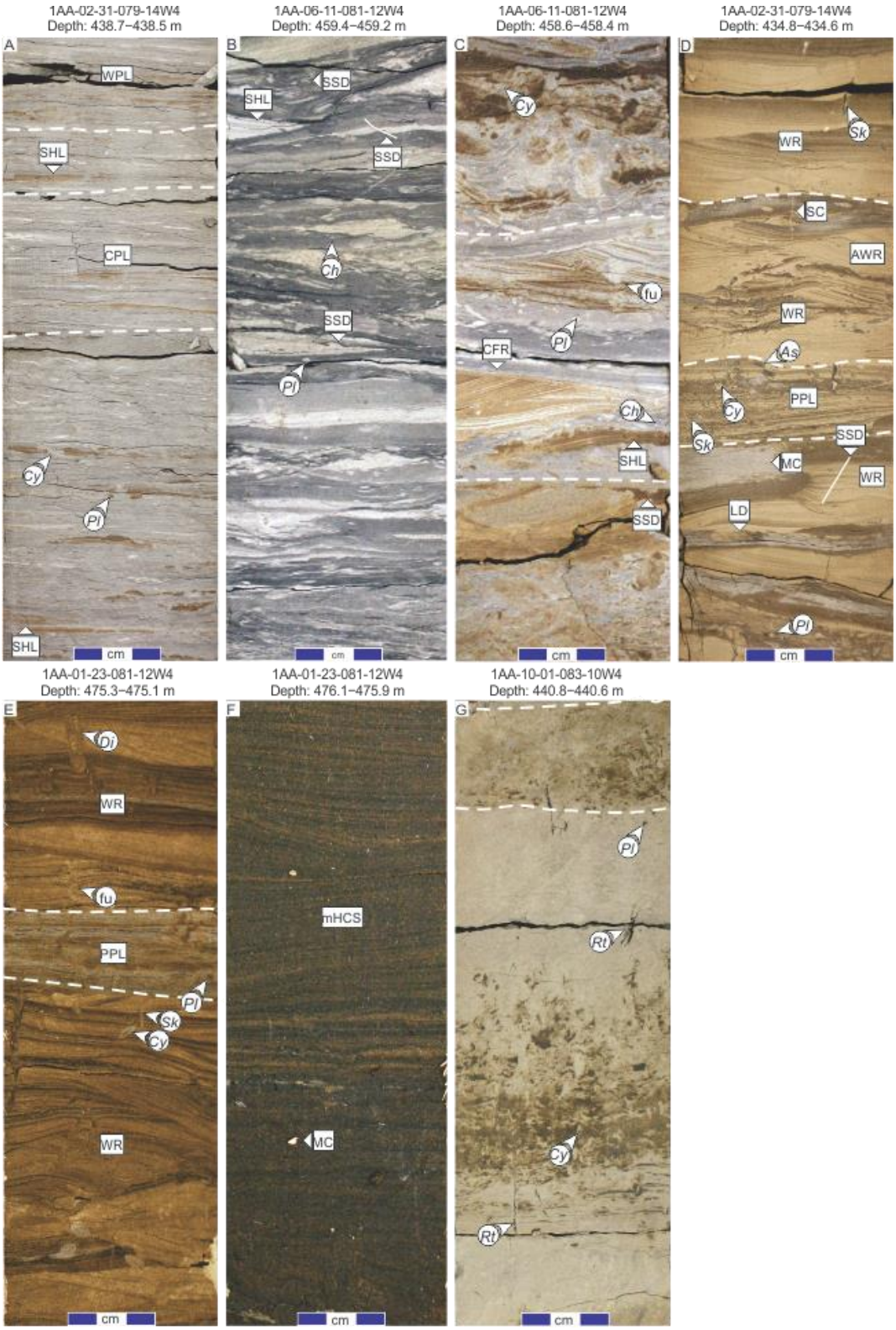

Figure 4.4 Core photos for Facies Association 4 (F7b, F8b, F9b and F10) – wave-dominated, tide-influenced, fluvial-affected delta.

Note that the sand is either light yellow/brown (bitumen stained but water- or gas-saturated) or dark brown (bitumen saturated). Mudstones are light to dark grey, and siltstones are white. A)

and B) Two expressions of weakly to moderately bioturbated (BI 1−3) lenticular to wavy silt-laminated mudstone (F7b), showing the range in siltstone and sand content within the facies. C) and D) Two expressions of weakly to thoroughly bioturbated (BI 1−5) wavy heterolithic bedsets of F8b, showing the range of mudstone and sand content within the facies. E) and F) Two expressions of unburrowed to thoroughly bioturbated (BI 0−5), oscillation rippled to hummocky cross-stratified sand (F9b). G) Facies 10 (F10) corresponds to weakly to moderately bioturbated (BI 2−4), siltstone to root-bearing sand. Acronyms: sedimentology – aggradational wave ripples (AWR), combined flow ripples (CFR), curvilinear parallel laminae (CPL), load structure (LD), micro-hummocky cross-stratification (m-HCS), planar-parallel lamination (PPL), sandy heterolithic lenses (SHL), soft-sediment deformation structures (SSD), syneresis cracks (SC), wave ripples (WR), wavy parallel laminae (WPL); ichnology – Asterosoma (As), Chondrites (Ch), Cylindrichnus (Cy), Diplocraterion (Di), fugichnia (fu), Planolites (Pl), roots (rt), and Skolithos (Sk); other – mudstone clasts (MC).

Interpretation of FA4: The coarsening-upward Facies Succession 8 of FA4 is interpreted as shoaling-upward cycles bounded by flooding surfaces, and is referred to as parasequences (PS). Physical sedimentary structures observed in FA4 PS are primarily formed by oscillatory flow (>50%) with subordinate unidirectional and/or bidirectional current-generated structures. The ichnology in FA4 comprises a moderately to a highly diverse suite of diminutive trace fossils, indicative of periodic brackish-water conditions in an embayment or restricted seaway (e.g., MacEachern et al., 2005; Hansen and MacEachern, 2007; Bhattacharya and MacEachern, 2009). Carbonaceous detritus and coal fragments are present and are interpreted to reflect sediment input from the terrestrial realm. The very rare root-bearing intervals capping F10 are attributed to subaerial exposure. Based on the combination of sedimentological and ichnological observations, and following the process classification of Ainsworth et al. (2011), FA4 is interpreted as a wave-dominated, tide-influenced, fluvial-affected (Wtf) delta, and parasequences record shallowing upward from the prodelta (F7b/F8b), through shore-parallel bars of the wave-/storm-dominated delta-front (F8b/F9b), and (rarely) into subaerially exposed (supratidal) bar tops (F10).

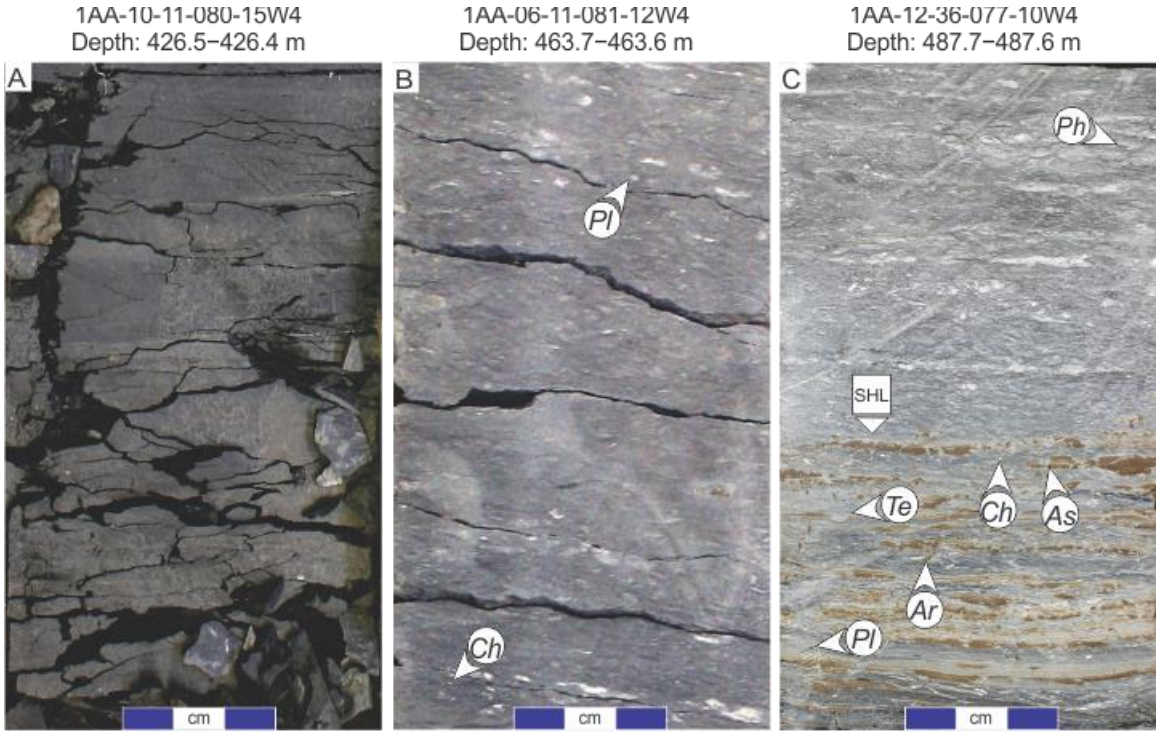

Figure 4.5 Three expressions (subfacies) of weakly to thoroughly bioturbated (BI 0−5), steel-blue grey to dark grey mudstone of Facies 6 (F6a, F6b and F6c) – restricted embayment to offshore.

Note that mudstone is light to dark grey, and siltstone is white or brown if bitumen stained. A) F6a consists of largely unburrowed (BI 0-1) dark grey mudstone to shale. B) F6b consists of moderately to thoroughly bioturbated (BI 3−5) dark grey mudstone. C) F6c consists of moderately to thoroughly bioturbated (BI 3−5), steel-blue grey mudstone, locally with discrete laminae of very fine-grained sand and silt. Acronyms: sedimentology – silty heterolithic lenses (SHL); ichnology – Arenicolites (Ar), Asterosoma (As), Chondrites (Ch), Phycosiphon (Ph), Planolites (Pl), Teichichnus (Te).

4.3.2. Stratigraphically Significant Surfaces in the McMurray Fm

Multiple stratigraphic surfaces are observed in the McMurray Fm in the SW quadrant of the MDC, and recognized based on their core and geophysical well log expression. Both autogenic and allogenic surfaces are present; however, refer to Château et al. (2019, in press; Chapter 3) for detailed descriptions and comparisons of allogenic and autogenic surfaces in the study area. Given the size of the dataset and for the purpose of resolving the architecture and sequence stratigraphy of DUs C2−A1, only allogenic surfaces are identified and described in the following section.

Surfaces bounding the tops of depositional units

From base to top, the McMurray Fm includes six regionally extensive (>1000 km^2) allogenic surfaces recording base-level rise, which are recognizable both in core and on geophysical well logs (Figs. 4.3 and 4.6; Table 4.2). In cores, they are identified by an increase in marine facies across the surface. The surfaces are sharp, scoured and/or are demarcated by firmground omission suites of the *Glossifungites* Ichnofacies. On well-logs, the surfaces show high gamma-ray responses (>100 API gamma-ray) and low density-porosity values (<18%; Table 4.2).

The six surfaces record an increase in water depth, and depending on whether the surfaces were subaerially exposed prior to deepening and/or exhibit erosion, are interpreted to represent one of three surface types: 1) composite transgressive surface of erosion/subaerial exposure surface (TSE/SE); 2) a transgressive surface of erosion (TSE); or 3) a flooding surface (FS). TSE/SE generally represents the development of the delta plain/coastal plain during normal regression (initial subaerial exposure), followed by transgressive erosion during ensuing base-level rise. As such, the SE does not correspond to a SU (subaerial unconformity) in the interval of study. The TSE records erosion during base-level rise without evidence of subaerial exposure (i.e., the area was either never subaerially exposed or the TSE removed the evidence of exposure). The FS represents base-level rise, showing no evidence of erosion. From the base to top of the McMurray Fm, the six regionally extensive surfaces include Top C2, Top C1, Top B2, Top B1, Top A2 and Top A1 (Fig. 4.6). Top McMurray is equivalent to either Top A2 or Top A1, depending on the presence or absence of DU A1. In the study area, the 4 regionally extensive surfaces from Top C2 to Top B1 include both TSE and FS surfaces. Only Top A2 and Top A1 surfaces have examples of all three surface types (TSE/SE, TSE and FS).

Table 4.2 **Recognition and distinction of surface types defined in this study. Surfaces presented in this table include composite transgressive surface of erosion/subaerial exposure surface (TSE/SE); transgressive surface of erosion (TSE), flooding surface (FS) and maximum flooding surface (MFS). The table includes the core signatures (contact and lithology), well-log signatures, and lateral extents of surfaces. The gamma-ray log signature reports values in American Petroleum Institute (API) units.**

Surface		TSE/SE; TSE	FS	MFS
Core signature	Contact	Sharp, scour, *Glossifungites*	Sharp	Gradational
	Facies Transition	Landward shift in facies	Landward shift in facies	Seaward shift in facies
Well-log signature		>100 API gamma-ray <18% density porosity	>100 API gamma-ray <18% density porosity	80-100 API gamma-ray <24% density porosity
Lateral extent		MDC >1000 km^2	MDC >1000 km^2	MDC >1000 km^2

Maximum Flooding Surfaces

Maximum flooding surfaces (MFS) are allogenic boundaries that mark the end of transgression and the onset of normal regression; hence, they record the maximum landward position of the shoreline within each DU. In cores, they are recognized by a gradational contact placed approximately at the top of a succession that shows a progressive increase in marine facies upwards. In most cases, this equates to approximately the middle of the mudstone intervals at the base of each DU. On geophysical well-logs, the MFS show lower gamma-ray responses (80−100 API gamma-ray) and higher density-porosity values (>24%; Table 4.2) than do the allogenic transgressive surfaces that bound the DUs (>100 API gamma-ray; <18% density-porosity). From the base to top of the McMurray Fm, six MFS associated with each DU can be distinguished: MFS C2, MFS C1, MFS B2, MFS B1, MFS A2 and MFS A1 (Figs. 4.6 and 4.11).

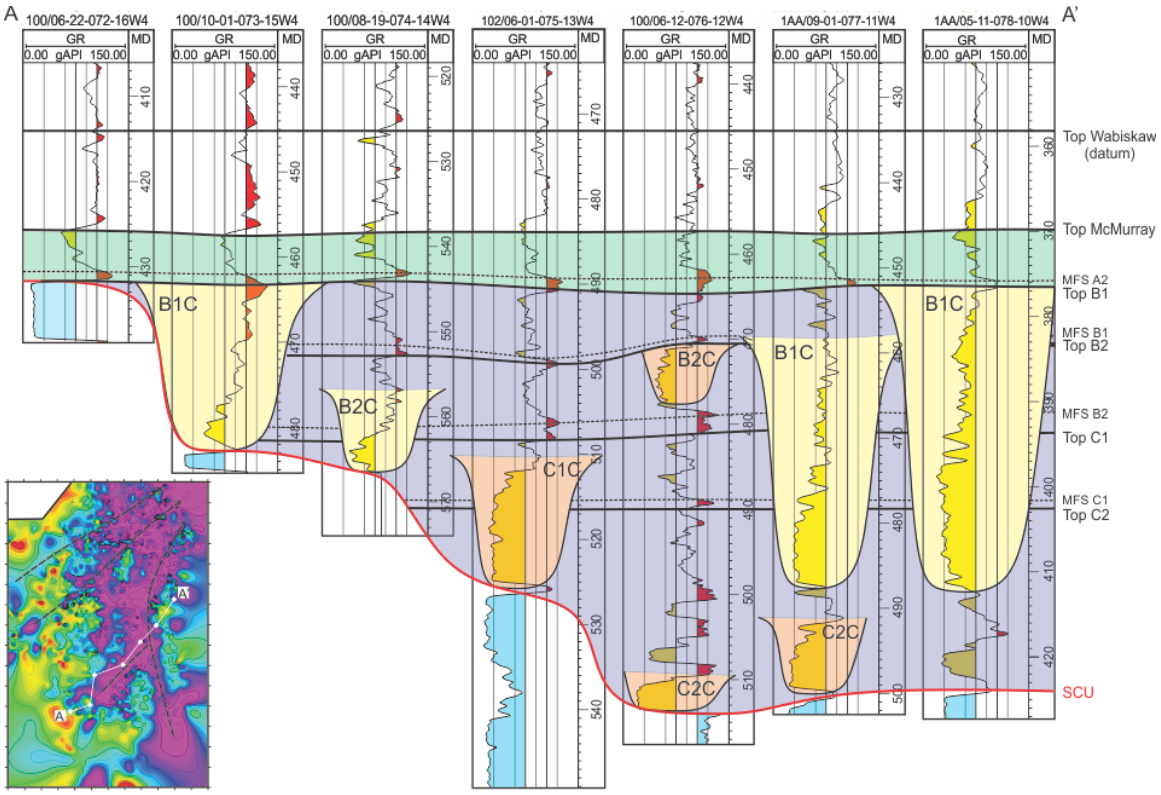

Figure 4.6 Cross-section A−A' is based solely on well logs, and extends from the southwest (100/06-22-072-16W4) to northeast (1AA/05-11-078-10W4) along Grouse Paleovalley.

The datum is Top Wabiskaw (top of Wabiskaw A), which is equivalent to the top of the Wabiskaw Member of the Clearwater Formation. Throughout the cross-section, channels of FA1 are represented by yellow polygons, channels of FA2 by orange polygons, FA3 by a purple polygon

and FA4 by a green polygon. Regionally mappable allogenic surfaces are shown either by thick black lines (Top Wabiskaw, Top McMurray, Top B1, Top B2, Top C1 and Top C2) or by dashed black lines (MFS). The Sub-Cretaceous Unconformity (SCU) is highlighted by a thick red line.

4.3.3. McMurray Fm Distribution

Based on stratigraphic correlations through the study area, the distribution of the six DUs, C2 to A1, is outlined (Fig. 4.6 and 4.7). Thicknesses of FTC, DC, T delta and Wtf delta deposits presented in this section are derived from visual observation of cross-sections and isopach maps and corroborated by statistical analysis (Fig. 4.6, 4.7 and 4.8).

In the southwest corner of the MDC, the maximum thickness of the McMurray Fm is 83 m. Each DU from C2 to A1 ranges from 1−65 m thick. DUs comprise stacked parasequences and their related channel belts. Stacked parasequences are relatively flat and are typically 1−15 m thick, whereas channel belts are more deeply incised and range from 3−65 m thick. Channel-belt deposits form a continuum from thin (= shallow) channel deposits usually interpreted as DCs to thick (= deep) channels typically interpreted as FTCs (Fig 4,8). Both DCs and FTCs cut down / hang from various elevations within DUs, and hence, many of the channels are unrelated to the regional flooding surfaces (Fig. 4.6). Based on channel positions relative to the allogenic flooding surfaces, channel-belts are labelled C2C through to A1C.

At the base of the McMurray Fm, DU C2 has a mean thickness of 12.6 m (Fig. 4.8), and the maximum thickness is 37 m. DU C2 comprises 1−4 PS, each ranging from 0.8–12 m (Fig. 4.6), and mainly consisting of FA3. DU C2 typically consists of 1−2 relatively thick (>5 m), mud-dominated parasequences that are overlain by 2−3 relatively thin (<5 m) stacked sand-dominated parasequences. These deposits are cross-cut by DC that range in thickness from 1–12 m and FTC that are 6–26 m thick. C2 extends from T69–83 and R9–16W4, covering an area of 2 550 km^2. Its distribution correlates exclusively to the central axes of the Grouse, Pelican and Sparrow paleovalleys (Fig. 4.7).

DU C1 has a mean thickness of 14.2 m thick (Fig. 4.8), with a maximum thickness of 43 m. DU C1 encompasses 1−7 PSs composed of FA3. Individual PSs range in thickness from 0.8−11 m (Fig. 4.6). In DU C1, 1−2 relatively thick (>5 m) mud-dominated parasequences are progressively overlain by 2−6 relatively thin (<5 m),

stacked, sand-dominated parasequences. PSs are cross-cut by DCs that range in thickness from 1–11 m and FTCs that range in thickness from 6–35 m. DU C1 extends from T69–83 and R9–17W4 and covers an area of 4 000 km^2. This DU also occurs in the Grouse, Sparrow and Pelican paleovalleys but, unlike DU C1, is not confined to the valley axes and extends further to the south and west (Fig. 4.7).

DU B2 has a mean thickness of 11 m (Fig. 4.8) with a maximum thickness of 49 m. DU B2 includes 1−5 PS of FA3, each ranging from 0.8–10 m thick (Fig. 4.6). DU B2 typically comprises one mud-dominated parasequence at the base that is overlain by 2−4 stacked, sand-dominated PSs. These deposits are cross-cut by DCs that range in thickness from 1–10 m and FTCs that are 8–49 m thick. DU B2 extends from T69–83 and R9–18W4, an area of over 6 900 km^2, but is sparsely distributed across R19−20W4. It occurs further west than DU C1 in the Grouse, Sparrow and Pelican paleovalleys (Fig. 4.7).

DU B1 has a mean thickness of 15.4 m (Fig. 4.8), with a maximum thickness of 65 m. It encompasses 1−6 PS of FA3, with each PS ranging from 1–8 m thick (Fig. 4.6). DU B1 comprises one mud-dominated parasequence overlain by 2−5 stacked, sand-dominated PSs. These deposits are cross-cut by DCs that range in thickness from 1–8 m, and FTCs that are 8–65 m thick. DU B1 extends from T69–83 and R9–19W4, an area of more than 9 697 km^2, although it is sparsely distributed across R20W4 (Fig. 4.7). DU B1 extends further west than DU B2 in the Grouse and Pelican paleovalleys, and pinches out westward along the margins of the paleotopographic highs (Fig. 4.7).

DU A2 has a mean thickness of 6.2 m (Fig. 4.8), and a maximum thickness of 59 m. DU A2 is composed of 1−3 PSs of FA4, with each ranging from 0.5−5 m (Fig. 4.6) thick. DU A2 comprises one mud-dominated parasequence overlain by 1−2 stacked sand-dominated PSs. DU A2 deposits are cross-cut by DCs that range from 1–5 m thick, and FTCs that range from 5–59 m thick. DU A2 extends from T69–83 and R9–20W4, covering an area of more than 11 841 km^2. It occurs further west than DU B1 in the Grouse, Sparrow and Pelican paleovalleys (Fig. 4.7), and its areal extend is not limited by the paleotopographic highs surrounding these paleovalleys.

DU A1 has a mean thickness of 3 m (Fig. 4.8) and comprises 1−2 PSs of FA4. Individual PSs range from 0.5−3 m thick. DU A1 is composed of one mud-dominated

parasequence overlain by 0−1 sand-dominated PS. These deposits are cross-cut by DCs up to 5 m thick (Fig. 4.6). DU A1 is sporadically distributed and covers an area of 1 212 km2. Its distribution is localised and principally occurs in Sparrow and Pelican paleovalleys, as well as towards the southern limit of Grouse Paleovalley (Fig. 4.7). The areal extent of DU A1 is not confined to the axes of the three paleovalleys nor by the paleotopographic highs surrounding the paleovalleys; however, Château et al. (2019) showed that in Sparrow Paleovalley, the distribution of DU A1 correlates to areas of potential syndepositional epikarstification of Devonian carbonate strata that subcrops below the MDC.

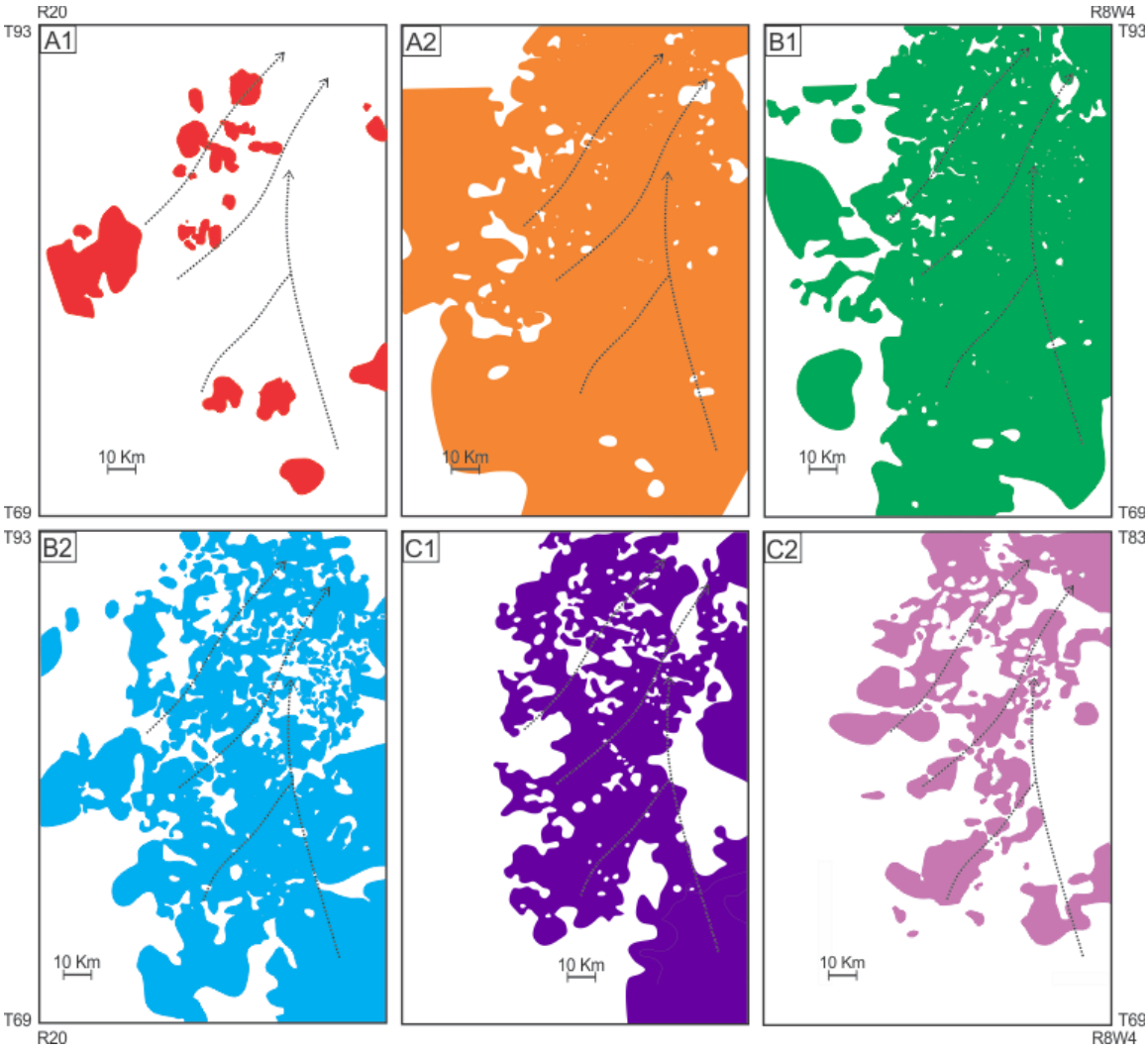

Figure 4.7 Distribution maps for DUs C2–A1.
Maps do not differentiate FAs (i.e., channels and parasequences), and hence, show the distribution of all deposits associated with each DU. The thalweg of the Pelican, Sparrow and Grouse paleovalleys are highlighted on all maps by thin, dashed black lines.

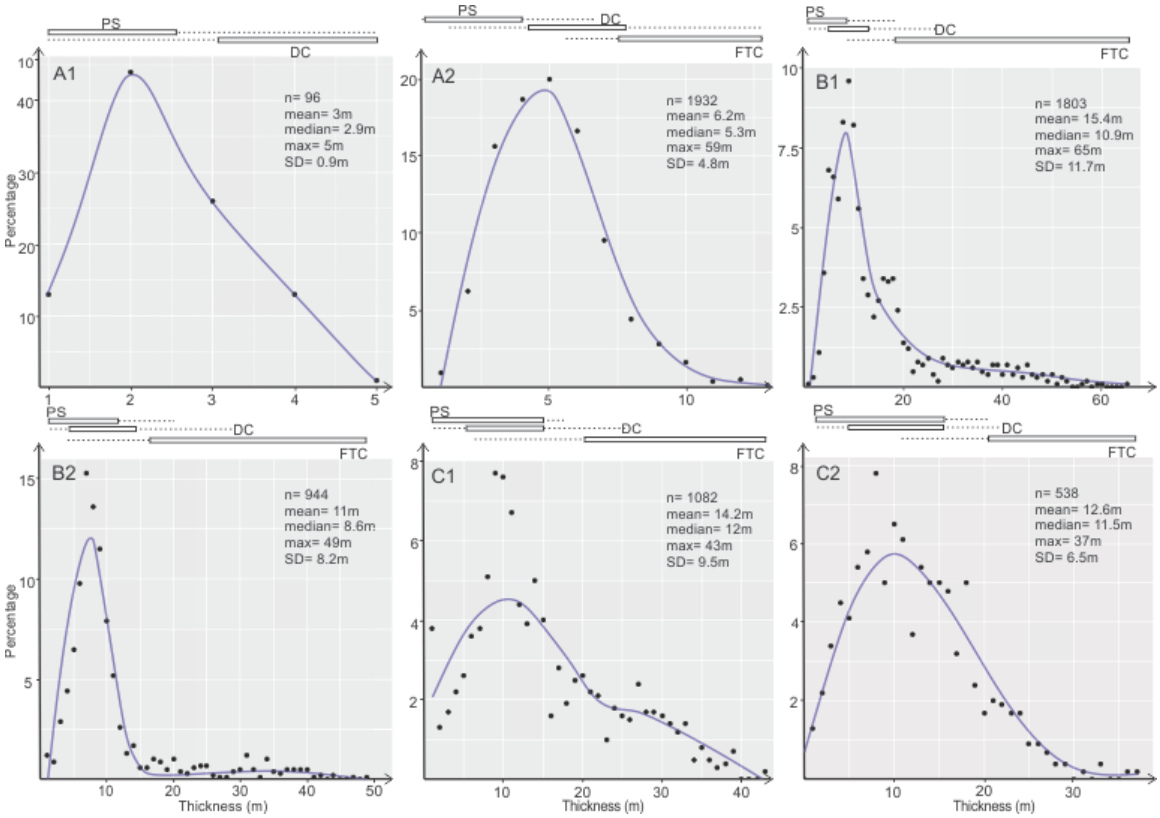

Figure 4.8 Graphical comparison of thickness distributions of DUs C2−A1. Each graph (C2−A1) plots thickness in 1 m increments *versus* percentage, and includes a smooth curve (blue line; conditional mean: mean thickness calculated for a defined percentage). The box and whisker plots at the top of each graph refer to the approximate thickness distributions PS, DC, and FTC in each DU. Boxes reflect the observed thickness distribution of parasequences, distributary channels and fluvio-tidal channels in cross-sections, while dashed lines highlight their potential limit of the maximum thickness distribution.

4.4. Discussion

4.4.1. Architecture of Depositional Units and their Stratigraphic Significance

Across the study area, DUs of the McMurray Fm consist of vertical successions of genetically related strata bounded by surfaces of allogenic origin (Château et al., in press). Figure 4.9 depicts an idealized DU and two potential interpretations of its depositional evolution. The base of the idealized DU is a relatively flat, regionally mappable surface. This surface records the onset of progradation following transgression and is interpreted as a maximum flooding surface (MFS).

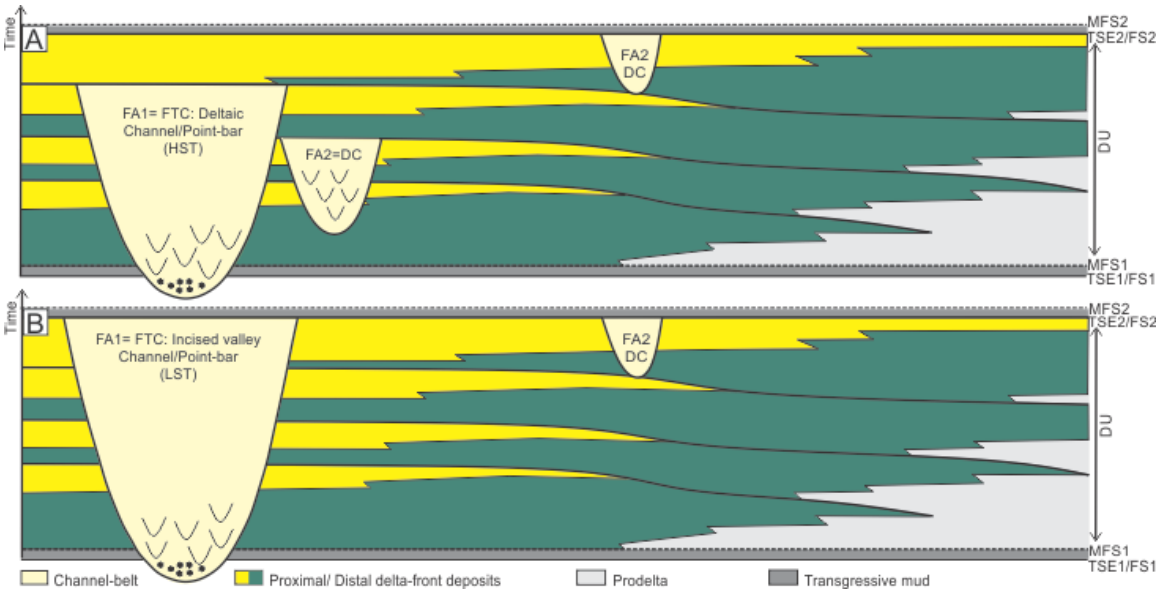

Figure 4.9 Schematic diagram depicting the possible architectures for depositional units and their associated channels.

The implications of these scenarios for the deposition and evolution of each DU are discussed in Section 4.4.1.

Overlying the MFS (MFS1) are series of vertically stacked, coarsening-upward cycles that represent incremental normal regression, bounded by autogenic flooding surfaces (FS). These cycles are the parasequences that comprise each DU. The stacked cycles are composed of FA3 or FA4 successions, and are interpreted as the composite deposits of delta lobes that built out the shoreline during slow to negligible base-level rise. The cycles are also interpreted to be genetically linked to the DCs (FA2; e.g., Baniak and Kingsmith, 2018; Weleschuk and Dashtgard, 2019; Château et al., in press).

Fluvio-tidal channels (FA1) are bounded at their bases by an autogenic erosive surface scoured during lateral and downstream accretion of the channels (e.g., Hubbard et al., 2011; Musial et al., 2012) and at their top by an autogenic FS, an allogenic FS, by a TSE or by a composite TSE/SE. Lateral- and downstream-migration/accretion of the FTC channel-belts are interpreted to be autogenically incised into older deposits, and record trunk channel systems that shifted seaward during shoreline progradation (Château et al., in press); a model similar to that proposed by Pattison (2018a) for some channel deposits of the Castlegate Fm.

The top of the idealized DU is capped by a relatively flat, regionally mappable surface marking the onset of transgression. Depending on its proximal/distal position in the MDC, the surface is expressed as an allogenic FS, a TSE or by a composite TSE/SE. Overlying the surface (labelled TSE2/FS2 in Fig. 9) is a thin (cm−dm) interval of mud (equivalent of F6a, b or c in section 4.3.1) deposited during transgression. The transgressive mud is capped by the MFS2, with overlying deposition recording the onset of normal regression.

There are two alternative interpretations for the relation of the FTCs to the regional cycles and the DCs (Fig. 4.9). In scenario A, FTCs are not necessarily linked to the upper TSE/FS (TSE2/FS2) surface, whereas in scenario B, FTCs only occur at the TSE2/FS2 surface. In scenario A, DCs and FTCs are interpreted to be linked to autogenic cycles within the DU (Weleschuk and Dashtgard, 2019). Channels exist during deposition of the entire depositional unit, and channel deposits associated with the upper TSE/FS surface are the most prevalent FTC deposits, as they were the last unit deposited prior to transgression and have the highest preservation potential. The implications of scenario A (Fig. 4.9) are twofold. First, both the FTCs and DCs were contemporaneous with deposition of the coarsening-upward cycles, and present during the deposition of the entire DU. Second, owing to the limited accommodation available in the MDC during deposition of the McMurray Fm (Hein et al., 2013; Château et al., in press), sediment supplied by the distributary channel system drove shoreline progradation, which is manifested by the seaward shift of cycles and associated channels.

In scenario B, FTCs are interpreted to be exclusively linked to the TSE2/FS2 surface. In this case, the channel network is interpreted as a valley that was incised into older cycles during base-level fall and filled during lowstand and early transgression. The implications of scenario B (Fig. 4.9) are that the FTCs are unrelated to deposition of the regional cycles (i.e., FTCs were not present during deposition of cycles). The fate of the channel systems during the deposition of the regional cycles is unknown. A similar scenario was proposed for channel-belt complexes of the McMurray Fm in the Assiniboia Paleovalley, albeit, those channels are interpreted as mainly fluvial deposits of continental-scale drainage (Hubbard et al., 2011; Hein et al., 2013; Horner et al., 2019).

In the southwest corner of the MDC, FTCs of variable thickness cut down / hang from various elevations within DUs, and hence, either subtend from regional flooding surfaces or are unrelated to them (Fig. 4.6). This observation contrasts with scenario B, in which FTCs solely subtend from allogenic surfaces. In addition, the absence of evidence of significant base-level fall in adjacent areas (e.g., no relief on the TSE/FS surfaces) better fits scenario A, in which cycles, DCs and FTCs are genetically linked. In this case, FTCs distribution is primarily controlled by trunk channel avulsions; this was previously documented west of the study area by Martin, 2018 for the A2C channel-belt system. Hence, in scenario A, deposits of FTCs relate to cycles and DCs deposited basinward (Château et al., in press). A similar scenario was proposed for channel-belt complexes of the Blackhawk Fm to Lower Castlegate Sandstone stratigraphic interval in the Book Cliffs region of Utah, USA (Pattison, 2018a, b; 2019).

4.4.2. Accommodation Space Creation during Early Transgression of the Boreal Sea

The mean thickness of each DUs (C2−A1) is 10.4 m, and this agrees with previous interpretations that the McMurray Fm was deposited in a low to moderate accommodation setting (e.g., Ranger and Pemberton, 1997; Hein and Cotterill, 2006; Ranger et al., 2008; Hein et al., 2013; Château et al., 2019, in press). However, the thickness of DUs is statistically the same for C2 to B1 and decreases substantially from B1 to A1 (Fig. 4.10a). For DUs C2 to B1, the median thickness is 11.2 m. This decreases to 8.9 m when thick FTCs (>15 m) are excluded from thickness calculations (Fig. 4.10b). The thickness of DUs rapidly decreases through DUs A2 and A1, with DUs reduced by 40% from B1 to A2 and by 45% from A2 to A1 (Fig. 4.10 a,b). Accommodation space creation was primarily controlled by the onset of transgression of the Boreal Sea in the area, however, multiple mechanisms presented below could generate a rapid decrease in DU thicknesses above B1.

First, in the study area and excluding DU A1, the lateral extent of the depocenter increased from 2 550 km^2 (C2) to 11 841 km^2 (A2) during the deposition of the McMurray Formation (Fig. 4.7). Hence, with presumed constant sediment supply during the deposition of the formation, the change in basin morphology is anticipated to generate a decrease in DUs thicknesses.

The thickness variation observed between the lower (C2–B1) and upper (A2–A1) DUs is partially attributed to changes in basin morphology, which is linked to the Boreal Sea transgression, and was driven, in part, by changes in depositional processes upwards. During deposition of the basal DUs (C2–B1), the MDC was protected from wave action by carbonate topographic highlands to the north and west (i.e., the Grosmont High and Beaverhill Lake Spur; e.g., Weleschuk and Dashtgard, 2019), and this enabled deposition of tide-dominated delta deposits (see Section 4.4.3). In contrast, the upper DUs (A2−A1) were deposited under strong wave action, following the drowning of the carbonate highlands. The change in process regime from DUs C2–B1 to A2–A1 is hypothesized to have increased erosional truncation of the upper DUs (A2−A1) via wave action during allogenic induced transgression, and the intensity of erosion increased as transgression accelerated.

Spatial variations in the preserved thickness of DU A1 cannot be explained by transgressive wave ravinement alone. Depositional unit A1 varies markedly in thickness and is sporadically distributed, and this is attributed to syndepositional carbonate epikarstification. Locally, carbonate strata upon which the McMurray Fm is deposited experienced erosion and epikarstification (McPhee and Wightman, 1991; Anderson and Knapp, 1993; Dembicki and Machel, 1996; Hauck et al., 2017; Walker et al., 2017). This, in turn, impacted pre-, syn-, and post-deposition of DUs C2−A1 and generated localized accommodation space (Broughton, 2013, 2014, 2015a, b, 2016; Barton et al., 2017; Château et al., 2019). In the southwest quadrant of the MDC, epikarstification is primarily manifested by the overthickening of DUs (Château et al., 2019), including DU A1. The sporadic distribution of DU A1 across the study area corresponds to areas of epikarstification wherein DU A1 experienced local accommodation space creation both syn- and post-depositionally. Post-depositional wave ravinement eroded most of DU A1 across the study area, with the exception of these sporadically distributed karsted lows.

The change in DU thicknesses also correlates to a change in the characteristics of the transgressive mudstone underlying each DU (Fig. 4.10C). In the southwest corner of the MDC, transgressive deposits consist of cm−dam thick mudstone (Fig. 4.5; Table 4.1; Hein and Cotterill, 2006). The thickness of these mudstones does not vary significantly between DUs; however, there are well-defined changes in the facies expression of the mudstones upwards (Fig 4.10C). The transgressive mudstones are grouped into Facies 6 – dark grey mudstone, and this facies is interpreted to represent

offshore to restricted embayment deposits. Facies 6 is subdivided into three distinct subfacies (Table 4.1): F6a – largely unburrowed (BI 0-1) dark grey mudstone to shale; F6b – moderately to thoroughly bioturbated (BI 3−5) dark grey mudstone; and F6c – moderately to thoroughly bioturbated (BI 3−5), steel-blue grey mudstone with discrete laminae of very fine-grained sand and silt (Fig. 4.5; Table 4.1). The distal versus proximal characterisation of the three expressions of F6 is based on ichnological observations. From F6a to F6c, the trace fossil abundance and diversity increases (Fig. 4.5; Table 4.1).

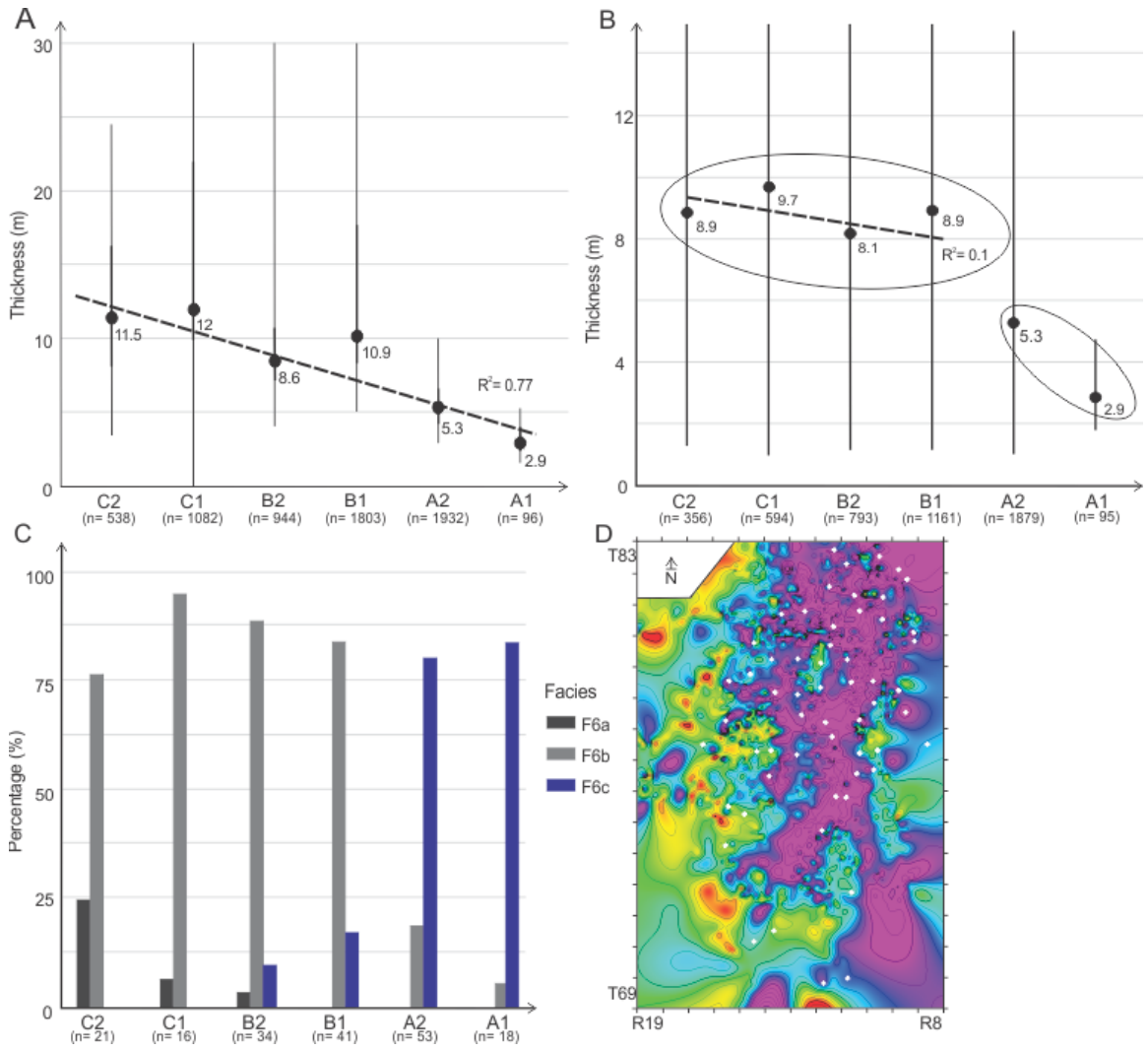

Figure 4.10 A) and B) graphical comparison of C2−A1 DU thicknesses; using thickness data shown in Figure 4.8.

A) includes all data between the 10th and 90th percentiles on graphs in Fig. 8 while B) only considers DU thicknesses below 15 m (mainly PS and DC). In both graphs, the median thickness of each DU is shown by the black dot and the thick black line represents 50% of the dataset surrounding the median. The thin dashed black line represents the lower and upper quartile. C) The histogram plots the percentage of each transgressive mud facies (F6a−F6c) for each DU

(C2−A1). D) Map of the study area, plotting the distribution of the 57 cores used to create graph C).

There is a well-defined break in subfacies between the transgressive mudstone underlying the lower DUs (C2−B1) versus those underlying the upper DUs (A2−A1; Fig. 4.10C). The transgressive mudstones bounding the lower DUs (C2−B1) are characterized by a prevalence of F6b (75% of cores); subfacies F6a and F6c comprise less than 25% of mudstone intervals. The inverse occurs in the mudstones bounding the upper DU A2 and A1, with F6c being the dominant subfacies (> 80%) and subfacies F6b comprising less than 20% of mudstone expressions (Fig. 4.10C). No core expressions of mudstones underlying DU A2 or A1 consist of F6a. Hence, the facies work reveals a facies change in the marine expression of the transgressive mudstone underlying the lower DUs (C2−B1; i.e. distal expression of F6) to those underlying the upper DUs (A2−A1;i.e. proximal expression of F6; Fig. 4.10C).

In summary, the McMurray Fm in the study area is interpreted to consist of interstratified high-frequency DUs deposited during still-stand or minor base-level rise (Fig. 4.11). The thicknesses of DUs remain relatively constant during the deposition of the lower DUs (C2–B1), and rapidly decreases during the deposition of the upper DUs (A2–A1; Fig. 4.10A–B). The change in thickness of DUs corresponds to a change in the facies character of the transgressive mudstone underlying each DU, with a pronounced change in the character of mudstone facies underlying the lower DUs compared to those underlying the upper DUs (Fig. 4.10C). Together, these data and interpretations suggest that transgression of the Boreal Sea in the MDC did not really occur until the deposition of DU A2, and rapidly accelerated after that. This increase in the rate of transgression also correlates to the final drowning of the carbonate highlands to the north and west of the MDC, and the concomitant change in basin morphology, increase in the generation and preservation of oscillatory sedimentary structures as well as the development of wave ravinment surfaces (Ranger and Pemberton, 1997; Ranger et al., 2008; Weleschuck and Dashtgard, 2019; Château et al., in press).

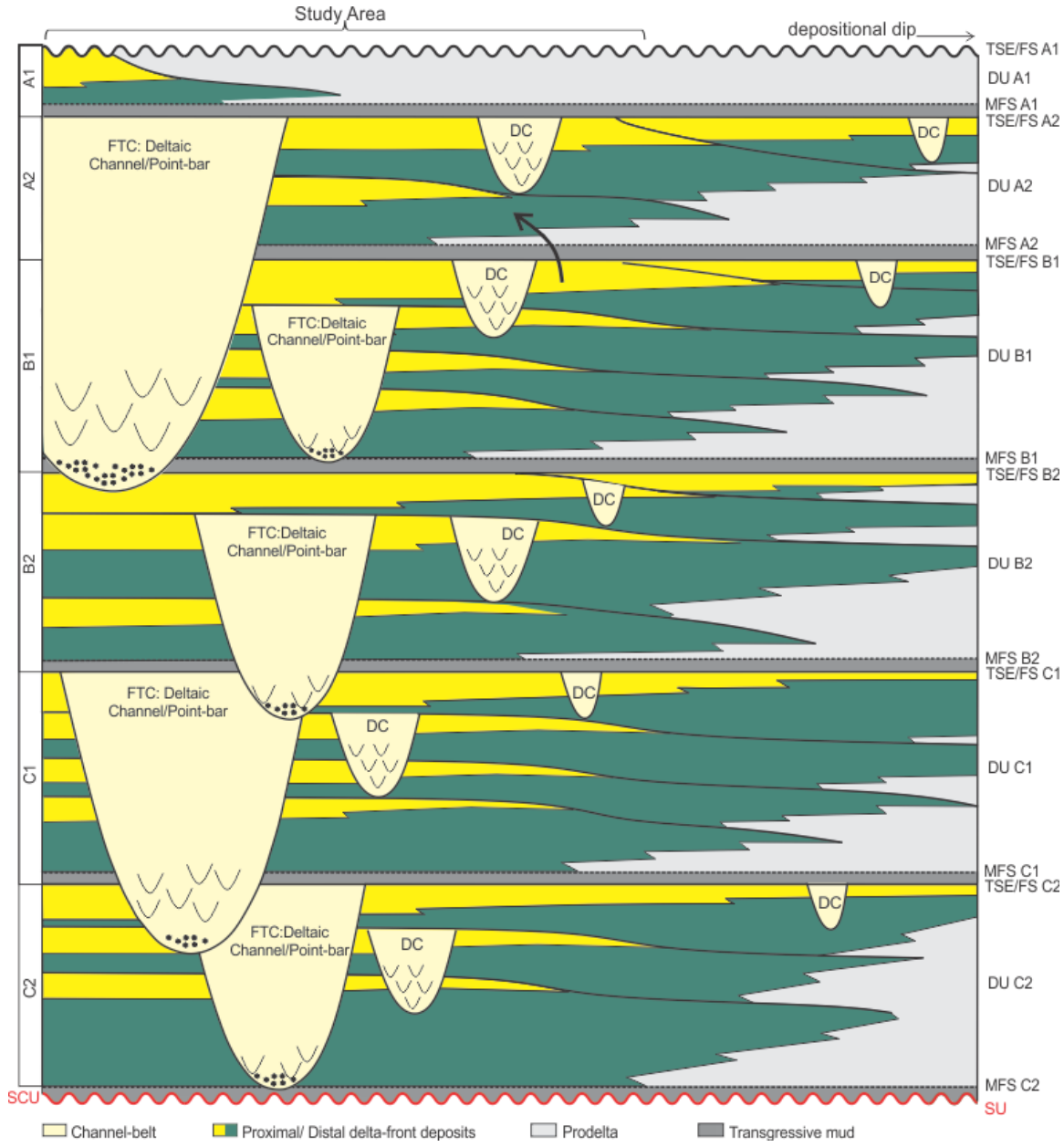

Figure 4.11 Schematic diagram showing the detailed architecture of the McMurray Formation in the southwest corner of the McMurray depocenter and its stratigraphic significance.

On the left is the lithostratigraphic/allostratigraphic nomenclature, in the center is the detailed architecture of the formation, and on the right is the sequence stratigraphic interpretation. The thick black arrow points out the change in mudstone subfacies marking the base of DU A2.

4.4.3. Paleogeographic reconstruction of the McMurray Depocenter during the Early Evolution of the Alberta Foreland Basin

Paleogeographic reconstructions of the McMurray Fm, based on the scaling relationship of deposits in the Assiniboia Valley commonly rely on the Mississippi River and delta as a potential modern analog (Smith et al., 2009; Musial et al., 2012; Durkin et al., 2017a). Hence, the McMurray/Wabiskaw interval is interpreted as the distal portion of continental-scale south- to- north paleo-drainage network that receives sediment from across the continent (Miall et al., 2008; Benyon et al., 2014; Blum and Pecha, 2014; Blum et al., 2017). The connection between the distributive channel network investigated in this thesis (Fig. 4.12) and the main channel system that occupied the Assiniboia Valley is not established. Multiple sediment transport patterns could explain sediment origin. First, the distributive channel network observed in the study area may represent a small bifurcation of the main channel system that occupied the Assiniboia Valley (Smith et al., 2009; Hubbard et al., 2011). Alternatively, tidal channels could be disconnected from the main channel system; in this case, the sediment source would probably be marine sediment remobilized during transgression stages. However, testing these hypotheses lies beyond the scope of this study, therefore, this section solely discusses the two paleogeographic reconstructions of the McMurray Fm in the southwest corner of the McMurray depocenter (MDC) presented in figure 4.12 as well as similarities with potential modern analogs.

During deposition of DUs C2−B1 (Fig. 4.12A), the southwest quadrant of the MDC consisted of paleotopographic lows (Grouse, Sparrow and Pelican) surrounded by paleotopographic highs (e.g., Grosmont High; Keith et al., 1988; Ranger and Pemberton, 1997; Weleschuk and Dashtgard, 2019), which generated a wide but laterally restricted embayment. The restricted embayment was protected from wave action, and tide-dominated deltas are interpreted to have developed within the valley system. The deltas forced incremental shoreline progradation (Fig. 4.12A). The paleoenvironment of DUs C2–B1 is interpreted to include tidal sand bars and muddy and sandy tidal flats that were fed by a network of brackish-water, fluvio-tidal channels and genetically related tributary and distributary fluvio-tidal and tidal channels. Similar paleogeography is observed in the modern Fly River Delta, Papua New Guinea. The Fly River Delta is also deposited in a foreland basin setting and includes a complex network of fluvio-tidal channels that split

into distributary channels separated by several-kilometer long, shore normal tidal sand bars (Baker et al., 1995; Dalrymple et al., 2003; Harris et al., 2004).

During deposition of DUs A2 and A1 (Fig. 4.12B), the southwest quadrant of the MDC is interpreted to have been a relatively continuous, E–W oriented shoreline on the margin of the Boreal Sea, punctuated by small, wave-dominated deltas (Fig. 4.12B; Weleschuk and Dashtgard, 2019). The strata of DUs A2 and A1 comprise shore-parallel mouth bars and beach ridges/strand plains fed by a network of brackish-water, fluvio-tidal channels and some distributary channels. This concurs with a previous paleogeographic reconstruction for the Grouse Paleovalley (Weleschuk and Dashtgard, 2019). Potential modern analogs showing a tide-dominated to wave-dominated transition were previously documented in Weleschuk and Dashtgard, (2019), and include the Mekong River and Red River deltas in Vietnam (Ta et al., 2002, 2005; Tanabe et al., 2003, 2006; Xue et al., 2010). Finally, the paleogeographic transition observed in the area is concomitant to changes in the stratigraphic organization of the deposits producing a complex vertical succession consisting of aggrading tide-dominated delta deposits, followed by prograding wave-dominated delta deposits.

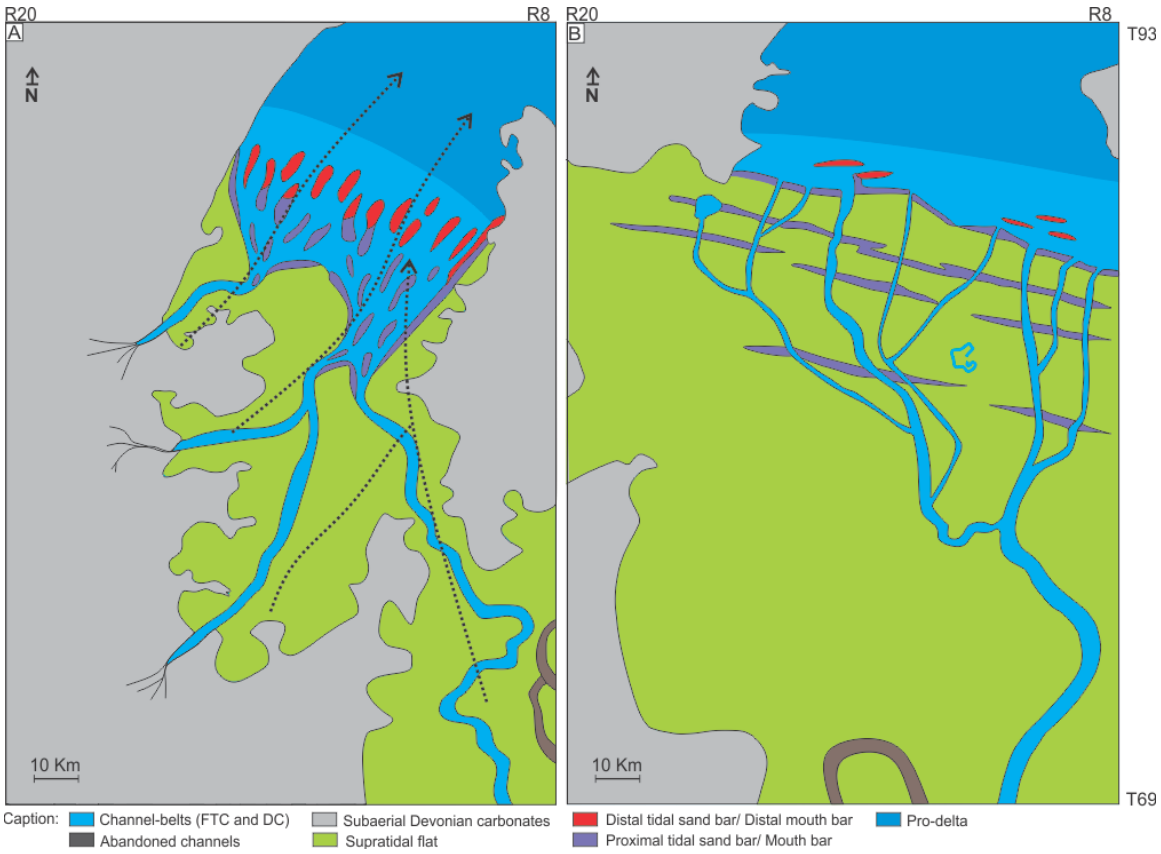

Figure 4.12 Schematic maps showing paleogeographic reconstruction of the McMurray Formation in the southwest corner of the McMurray depocenter.

Maps display a paleogeographic reconstruction A) during deposition of C2−B1 units and B) during deposition of A2−A1 units.

4.5. Conclusion

The southwest quadrant of the McMurray depocenter includes multiple paleotopographic lows (paleovalleys) filled with 6 regionally extensive depositional units. The DUs C2−A1 are interpreted to have evolved from tide-dominated deltas (T) into wave-dominated, tide-influenced, fluvial-affected deltas (Wtf). Each DU overlies a maximum flooding surface and consists of a series of autogenically stacked coarsening-upward cycles and genetically linked channel-belts (fluvio-tidal channels (FTC) and distributary channels (DC)), which record the progressive basinward shift of the shoreline during normal regression. DUs are capped by allogenic transgressive surface recording periodic transgression of the Boreal Sea. These surfaces are, in turn, overlain by mudstone that accumulated during transgression.

Accommodation space creation was rather limited during the deposition of the McMurray Fm. Mean thickness DUs is 10.4 m. DU thicknesses were primarily controlled by accommodation space creation linked to Boreal Sea transgression. A Secondary mechanism of accommodation space creation is attributed to syndepositional carbonate epikarstification, which led to localized deposition of DU A1

DU thicknesses are relatively consistent through C2 to B1, but decrease markedly from B1 through to A1. This decrease in thicknesses in the upper DUs of the McMurray Fm correlates to a pronounced change in the facies character of the transgressive mudstones underlying each DU, and is interpreted to represent pronounced landward shifts of the shoreline. The filling of the paleotopography led to a regionally extensive transgression. This change in topography allowed the transgression to be dominated by oscillatory processes and the truncation of DU tops by wave ravinement.

Acceleration in the rate of transgression of the Boreal Sea across the MDC is proposed to explain the relationship between DU thickness and the change in transgressive mudstone subfacies at their bases. We hypothesize that the duration of still-stands, during which DUs were deposited, diminished as transgression progressed. DUs A2 and A1 aggraded vertically during these shorter still-stands, in contrast to the longer duration and progradational character of DUs C2 to B1. Here, we demonstrate that sedimentological work tied to statistical analysis can be used to identify changes in the rate of transgression in limited accommodation space settings.

Acknowledgements

The authors thank the sponsors of the McMurray Geology Consortium: BP plc, Cenovus Energy Inc., Husky Energy, Nexen CNOOC Ltd, and Woodside Energy Ltd, for funding this research.

References

Ainsworth, R.B., Vakarelov, B.K., and Nanson, R.A., 2011, Dynamic spatial and temporal prediction of changes in depositional processes on clastic shorelines: Towards improved subsurface uncertainty reduction and management: American Association of Petroleum Geologists Bulletin, v. 95, p. 267−297.

Alberta Energy and Utilities Board, 2003, Athabasca Wabiskaw-McMurray regional geological study: Alberta Energy and Utilities Board, Report 2003-A, 187p.

Alberta Geological Survey, 2015, Alberta Table of Formations: Alberta Energy Regulator: https://ags.aer.ca/activities/table-of-formation.html (accessed July 2020).

Allen, J.P., and Fielding, C.R., 2007, Sequence architecture within a low-accommodation setting: an example from the Permian of the Galilee and Bowen basins, Queensland, Australia: American Association of Petroleum Geologists Bulletin, v. 91, p. 1503–1539.

Anderson, N.L., and Knapp, R., 1993, An overview of some of the large scale mechanisms of salt dissolution in western Canada: Geophysics, v. 58, p. 1375–1387.

Baker, E.K., Harris, P.T., Keene, J.B. and Short, S.A., 1995, Patterns of sedimentation in the macrotidal Fly River delta, Papua New Guinea: *in* Flemming, B.W., and Bartholomä, A, eds., Tidal Signatures in Modern and Ancient Sediments, International Association of Sedimentologists, Special Publication 24, p.193−211.

Baniak, G.M., and Kingsmith, K.G., 2018, Sedimentological and stratigraphic characterization of Cretaceous upper McMurray deposits in the southern Athabasca oil sands, Alberta, Canada: American Association of Petroleum Geologists Bulletin, v. 102, p. 309−332.

Barton, M.D., 2016, The architecture and variability of valley-fill deposits within the Cretaceous McMurray Formation, Shell Albian Sands Lease, northeast Alberta: Bulletin of Canadian Petroleum Geology, v. 64, p. 116−198.

Barton, M.D., Porter, I., O'Byrne, C., and Mahood, R., 2017, Impact of the Prairie Evaporite dissolution collapse on McMurray stratigraphy and depositional patterns, Shell Albian Sands Lease 13, northeast Alberta: Bulletin of Canadian Petroleum Geology, v. 65, p. 175–199.

Benyon, C., Leier, A., Leckie, D.A., Webb, A., Hubbard, S.M., and Gehrels, G., 2014, Provenance of the Cretaceous Athabasca Oil Sands, Canada: Implications for Continental-scale Sediment Transport: Journal of Sedimentary Research, v. 84, p. 136–143.

Bhattacharya, J.P., and MacEachern, J.A., 2009, Hyperpycnal rivers and prodeltaic shelves in the Cretaceous seaway of North America: Journal of Sedimentary Research, v. 79, p. 184−209.

Blum, M., and Pecha, M., 2014, Mid-Cretaceous to Paleocene North American drainage reorganization from detrital zircons: Geology, v. 42, p. 607−610.

Blum, M.D., Milliken, K.T., Pecha, M.A., Snedden, J.W., Frederick, B.C., Galloway, W.E., 2017, Detrital-zircon records of Cenomanian, Paleocene, and Oligocene Gulf of Mexico drainage integration and sediment routing: Implications for scales of basin-floor fans: Geosphere, v.13, p. 2169–2205.

Broughton, P.L., 2013, Devonian salt dissolution-collapse breccias flooring the Cretaceous Athabasca oil sands deposit and development of lower McMurray Formation sinkholes, northern Alberta Basin, Western Canada: Sedimentary Geology, v. 283, p. 57–82.

Broughton, P.L., 2014, Syndepositional architecture of the northern Athabasca Oil Sands Deposit, northeastern Alberta: Canadian Journal of Earth Sciences, v. 52, p. 21–50.

Broughton, P.L., 2015a, Collapse-induced fluidization structures in the Lower Cretaceous Athabasca Oil Sands Deposit, Western Canada: Basin Research, v. 28, p. 507–535.

Broughton, P.L., 2015b, Incipient vertical traction carpets within collapsed sinkhole fills: Sedimentology, v. 62, p. 845–866.

Broughton, P.L., 2016, Alignment of fluvio-tidal point bars in the middle McMurray Formation: implications for structural architecture of the Lower Cretaceous Athabasca Oil Sands Deposit, northern Alberta: Canadian Journal of Earth Sciences, v. 53, p. 896–930.

Catuneanu, O., 2002, Sequence stratigraphy of clastic systems: concepts, merits, and pitfalls: Journal of African Earth Sciences, v. 35, p. 1−43.

Carrigy, M.A., 1963, Paleocurrent directions from the McMurray Formation: Bulletin of Canadian Petroleum Geology, v. 11, p. 389–395.

Carrigy, M.A., 1967, Some sedimentary features of the Athabasca oil sands: Sedimentary Geology, v. 1, p. 327–352.

Château, C.C., Dashtgard, S.E., MacEachern, J.A., and Hauck, T.E., 2019, Parasequence architecture in a low-accommodation setting, impact of syndepositional carbonate epikarstification, McMurray Formation, Alberta, Canada: Journal of Marine and Petroleum Geology, v. 104, p. 168−179.

Château, C.C., Dashtgard, S.E., and MacEachern, J.A., in press, Refinement of the stratigraphic framework for the Regional C depositional unit of the McMurray Formation and implications for the early transgression of the Alberta Foreland Basin, Canada: Journal of Sedimentary Research.

Christopher, J.E., 1984, The Lower Cretaceous Mannville group, northern Williston basin region, Canada: *in* Stott, D.F., and Glass, D.J., eds., The Mesozoic of middle North America: Calgary, Alberta, Canada: Canadian Society of Petroleum Geologists Memoir 9, Calgary, p. 109−126.

Collins, D.S., Johnson, H.D., Baldwin, C.T., and Fielding, C., 2019, Architecture and preservation in the fluvial to marine transition zone of a mixed-process humid-tropical delta: Middle Miocene Lambir Formation, Baram Delta Province, north-west Borneo: Sedimentology, v. 67, p. 1−46.

Dalrymple, R.W., Baker, E.K., Harris, P.T., Hughes, M., 2003, Sedimentology and stratigraphy of a tide-dominated, foreland–basin delta (Fly River, Papua New Guinea): *in* Sidi, F.H., Nummedal,D., Imbert, P., Darman, H., Posamentier H.W., eds.,Tropical Deltas of Southeast Asia–Sedimentology, Stratigraphy, and Petroleum Geology, SEPM Special Publication, v. 76, p.147-173.Dashtgard, S.E., and La Croix, A.D., 2015, Sedimentological trends across the tidal-fluvial transition, Fraser River, Canada: A review and some broader implications: *in* Ashworth, P.A., Best, J.J., and Parsons D.R., eds., Fluvial-Tidal Sedimentology, Elsevier, Developments in Sedimentology 68, Amsterdam, p. 111−126.

Davies, S.J., and Gibling, M.R., 2003, Architecture of coastal and alluvial deposits in an extensional basin: the Carboniferous Joggins Formation of eastern Canada: Sedimentology, v. 50, p. 415– 439.

Dembicki, E.A., and Machel, H.G., 1996, Recognition and delineation of paleokarst zones by the use of wireline logs in the bitumen-saturated Upper Devonian Grosmont Formation of northeastern Alberta, Canada: American Association of Petroleum Geologists Bulletin, v. 80, p. 695–712.

Durkin, P.R., Boyd, R.L., Hubbard, S.M., Shultz, A.W., and Blum, M.D., 2017a, Three-dimensional reconstruction of meander-belt evolution, Cretaceous McMurray formation, Alberta Foreland Basin, Canada: Journal of Sedimentary Research, v. 87, p. 1075−1099.

Durkin, P.R., Hubbard, S.M., Holbrook, J.M., and Boyd, R., 2017b, Evolution of fluvial meander-belt deposits and implications for the completeness of the stratigraphic record: Geological Society of America Bulletin, v. 130, p. 721−739.

Flach, P.D., and Mossop, G.D., 1985, Depositional environments of Lower Cretaceous McMurray Formation, Athabasca Oil Sands, Alberta: American Association of Petroleum Geologists Bulletin, v. 69, p. 1195–1207.

Gandomi, A., and Haider, M., 2015, Beyond the hype: Big data concepts, methods, and analytics: International Journal of Information Management, v. 35, p. 137–144.

Ghinassi, M., D'Alpaos, A., Tommasini, L., Brivio, L., Finotello, A., Stefani, C., and Walsh, J.P., 2019, Tidal currents and wind waves controlling sediment distribution in a subtidal point bar of the Venice Lagoon (Italy): Sedimentology, v. 66, p. 2926−2949.

Gingras, M.K., Pemberton, S.G., Saunders, T., and Clifton, H.E., 1999, The ichnology of modern and Pleistocene brackish-water deposits at Willapa Bay, Washington: Variability in estuarine settings: Palaios, v. 14, p. 352−374.

Gingras, M.K., MacEachern, J.A., and Dashtgard, S.E., 2011, Process Ichnology and the elucidation of physico-chemical stress: Sedimentary Geology, v. 237, p. 115–134.

Gingras, M.K., and MacEachern, J.A., 2012, Tidal ichnology of shallow-water clastic settings: *in* Davis, R.A. and Dalrymple, R.W., eds., Principles of Tidal Sedimentology, Springer, Netherlands, p. 57−77.

Gingras, M.K., MacEachern, J.A., Dashtgard, S.E., Ranger, M.J., and Pemberton, S.G., 2016, The significance of trace fossils in the McMurray Formation, Alberta, Canada: Bulletin of Canadian Petroleum Geology, v. 64, p. 233−250.

Gugliotta, M., Flint, S.S., Hodgson, D.M., Veiga, G.D., and Fielding, C., 2016, Recognition criteria, characteristics and implications of the fluvial to marine transition zone in ancient deltaic deposits (Lajas Formation, Argentina): Sedimentology, v. 63, p. 1971−2001.

Gugliotta, M., Saito, Y., Nguyen, V.L., Ta, T.K.O., Nakashima, R., Tamura, T., Uehara, K., Katsuki, K., and Yamamoto, S., 2017, Process regime, salinity, morphological, and sedimentary trends along the fluvial to marine transition zone of the mixed-energy Mekong River delta, Vietnam: Continental Shelf Research, v. 147, p. 7−26.

Hansen, C.D., and MacEachern, J.A., 2007, Application of the asymmetric delta model to along-strike facies variations in a mixed wave- and river-influenced delta lobe, Upper Cretaceous Basal Belly River Formation, central Alberta: *in* MacEachern, J.A., Bann, K.L., Gingras, M.K., and Pemberton, S.G., eds., Applied Ichnology, SEPM Short Course 52, Tulsa, USA, p. 256−272.

Harris, P.T., Hughes, M.G., Baker, E.K., Dalrymple, R.W. and Keene, J.B., 2004, Sediment transport in distributary channels and its export to the pro-deltaic environment in a tidally dominated delta: Fly River, Papua New Guinea: Continental Shelf Research, v. 24, p.2431−2454.

Hauck, T.E., Peterson, J.T., Hathway, B., Grobe, M., and MacCormack, K., 2017, New insights from regional-scale mapping and modelling of the Paleozoic succession in northeast Alberta: paleogeography, evaporite dissolution, and controls on Cretaceous depositional patterns on the Sub-Cretaceous Unconformity: Bulletin of Canadian Petroleum Geology, v. 65, p. 87–114.

Hein, F.J., Berhane, H., and Cotterill, D.K., 2000, An atlas of lithofacies of the McMurray Formation, Athabasca oil sands deposit, northeastern Alberta: Surface and subsurface: Alberta Energy Utilities Board/Alberta Geological Survey, Earth Sciences Report 2000-07, 217p.

Hein, F.J., and Cotterill, D.K., 2006, The Athabasca oil sands – a regional geological perspective, Fort McMurray area, Alberta, Canada: Natural Resources Research, v. 15, p. 85–102.

Hein, F.J., Dolby, G., and Fairgrieve, B., 2013, A regional geologic framework for the Athabasca oil sands, northeastern Alberta, Canada: *in* Hein F.J., Leckie D., Larter S., and Suter J.R., eds., Heavy-oil and Oil-sand Petroleum Systems in Alberta and Beyond: American Association of Petroleum Geologists Studies in Geology 64, p. 207–250.

Hein, F., and Dolby, G., 2017, Lithostratigraphy, palynology, and biostratigraphy of the Athabasca Oil Sands deposit, northeastern Alberta: Alberta Geological Survey, Open File Report 8, 105 p.

Horner, S.C., Hubbard, S.M., Martin, H.K., and Hagstrom, C.A., 2019, Reconstructing basin-scale drainage dynamics with regional subsurface mapping and channel-bar scaling, Aptian, Western Canada Foreland Basin: Sedimentary Geology, v. 385, p. 26-44.

Howard, J.D., Elders, C.A., and Heinbokel, J.F., 1975, Animal-sediment relationships in estuarine point bar deposits, Ogeechee River-Ossabaw Sound, Georgia: Senckenbergiana Maritima, v. 7, p. 181−203.

Howard, J.D., and Frey, R.W., 1975, Regional animal-sediment characteristics of Georgia estuaries: Senckenbergiana Maritima, v. 7, p. 33−107.

Hubbard, S.M., Smith, D.G., Nielsen, H., Leckie, D.A., Fustic, M., Spencer, R.J., and Bloom, L., 2011, Seismic geomorphology and sedimentology of a tidally influenced river deposit, Lower Cretaceous Athabasca Oil Sands, Alberta, Canada: American Association of Petroleum Geologists Bulletin, v. 95, p. 1123−1145.

Jardine, D. 1974, Cretaceous oil sands of Western Canada: *in* Hills, L.V., ed., Oil Sands, Fuel of the Future: Canadian Society of Petroleum Geologists, Memoir 3, p. 50−67.

Jean, T.R., 2018, The Eastern Flank: Predicting the Architecture of the McMurray Formation Beyond its Subcrop Edge [unpublished MSc. Thesis], Simon Fraser University, 99p.

Jervey, M.T., 1988, Quantitative geological modeling of siliciclastic rock sequences and their seismic expression: *in* Wilgus, C.K., Hasting, B.S., Kendall, C.G.St.C, Posamentier, H.W., Ross, C.A., and Van Wagoner, J.C., eds., Sea-level changes: an integrated approach: Society of Economic Paleontologists and Mineralogists, Special Publication 42, p. 47−69.

Johnson, S.M. and Dashtgard, S.E., 2014, Inclined heterolithic stratification in a mixed tidal-fluvial channel: Differentiating tidal versus fluvial controls on sedimentation: Sedimentary Geology, v. 301, p. 41−53.

Keith, D.A.W., Wightman, D.M., Pemberton, S.G., MacGillivray, J.R., Berezniuk, T., and Berhane, H., 1988, Sedimentology of the McMurray Formation and Wabiskaw Member (Clearwater Formation), Lower Cretaceous, in the central region of the Athabasca oil sands area, northeastern Alberta: *in* James, D.P., and Leckie, D.A., eds., Sequences, Stratigraphy, Sedimentology: Surface and Subsurface, Canadian Society of Petroleum Geologists, Memoir 15, p. 309–324.

La Croix, A.D., and Dashtgard, S.E., 2015, A synthesis of depositional trends in intertidal and upper subtidal sediments across the tidal–fluvial transition in the Fraser River, Canada: Journal of Sedimentary Research, v. 85, p. 683−698.

La Croix, A.D., Dashtgard, S.E., and MacEachern, J.A., 2019a, Using a modern analogue to interpret depositional position in ancient fluvial-tidal channels: Example from the McMurray Formation, Canada: Geoscience Frontiers, v. 10, p. 2219−2238.

MacEachern, J.A., Bann, K.L., Bhattacharya, J.P., and Howell, C.D.J., 2005, Ichnology of deltas: Organism responses to the dynamic interplay of rivers, waves, storms, and tides: *in* Giosan, L. and Bhattacharya, J.P., eds., River Deltas - Concepts, Models, and Examples, SEPM Special Publication 83, Tulsa, USA, p. 49−85.

MacEachern, J.A., and Gingras, M.K., 2007, Recognition of brackish-water trace-fossil suites in the Cretaceous interior seaway of Alberta, Canada: *in* Bromley, R.G., Buatois, L.A., Mángano, G.M., Genise, J.F., and Melchor, R.N., eds., Sediment-Organism Interactions: A Multifaceted Ichnology, Volume Special Publication No. 88: Tulsa, Oklahoma, SEPM, p. 149−193.

MacEachern, J.A., Bann, K.L., Gingras, M.K., Zonneveld, J.-P., Dashtgard, S.E., and Pemberton, S.G., 2012, The ichnofacies paradigm: Trace fossils as indicators of sedimentary environments: Developments in Sedimentology, v. 64, p. 103−138.

Martin, H.K., 2018, Stratigraphic Characterization of an Early Cretaceous Channel-belt Avulsion: Implications for Paleoenvironmental Interpretations of the McMurray Formation, Alberta: Msc. thesis, University of Alberta, 178 p.

Martin, H.K., Hubbard, S.M., Hagstrom, C.A., Horner, S.C., and Durkin, P.R., 2019, Planform Recognition and Implications of a Cretaceous-age Continental-scale River Avulsion Node in the Western Interior Basin, Alberta, Canada: Journal of Sedimentary Research, v. 89, p. 610−628.

Marx, V., 2013, The big challenges of big data: Nature, v. 498, p. 255–260.

McPhee, D.A., and Wightman, D.M., 1991, Timing of the dissolution of Middle Devonian Elk Point Group Evaporites - Twps. 47 to 103 and Rges. 15 W3M to 20 W4M: Bulletin of Canadian Petroleum Geology, v. 39, 218p.

Miall, A.D., Catuneanu, O., Vakarelov, B.K., and Post, R., 2008, The Western Interior Basin, in Miall, A.D., ed., The Sedimentary Basins of the United States and Canada: The Sedimentary Basins of the World, Elsevier, Amsterdam , v. 5, p. 329–362.

Mitchum Jr., R.M., 1977, Seismic stratigraphy and Global Changes of Sea Level: Part 11. Glossary of Terms used in Seismic stratigraphy: Section 2: Application of Seismic Reflection Configuration to Stratigraphic Interpretation, Memoir 26, p. 205−212.

Mossop, G.D., and Shetsen, I., 1994, Introduction to the Geological Atlas of the Western Canada Sedimentary Basin: *in* Mossop G.D., and Shetsen, I., eds., Geological Atlas of the Western Canadian Sedimentary Basin: Canadian Society of Petroleum Geologists and Alberta Research Council, Calgary, Alberta, p. 1–12.

Musial, G., Reynaud, J.-Y., Gingras, M.K., Féniès, H., Labourdette, R., and Parize, O., 2012, Subsurface and outcrop characterization of large tidally influenced point bars of the Cretaceous McMurray Formation (Alberta, Canada): Sedimentary Geology, v. 279, p. 156–172.

Olariu, C., and Bhattacharya, J.P., 2006, Terminal distributary channels and delta front architecture of river-dominated delta systems: Journal of Sedimentary Research, v. 76, p. 212−233.

Pattison, S.A.J., 2018a, Rethinking the incised-valley fill paradigm for Campanian Book Cliffs strata, Utah–Colorado, USA: Evidence for discrete parasequence-scale, shoreface-incised channel fills: Journal of Sedimentary Research, v. 88, p. 138−1412.

Pattison, S.A.J., 2018b, Using classic outcrops to revise sequence stratigraphic models: Reevaluating the Campanian Desert Member (Blackhawk Formation) to lower Castlegate Sandstone interval, Book Cliffs, Utah and Colorado, USA: Geology, v. 47, p. 11−14.

Pattison, S.A.J., 2019, High resolution linkage of channel-coastal plain and shallow marine facies belts, Desert Member to Lower Castlegate Sandstone stratigraphic interval, Book Cliffs, Utah-Colorado, USA: Geological Society of America Bulletin, v. 131, p. 1643−1672.

Pemberton, S.G., Flach, P.D., and Mossop, G.D., 1982, Trace fossils from the Athabasca oil sands, Alberta, Canada: Science, v. 217, p. 825−827.

Pemberton, S.G., and Wightman, D.M., 1992, Ichnological characteristics of brackish water deposits, *in* Pemberton, S.G., ed., Applications of Ichnology to Petroleum Exploration, A Core Workshop: SEPM, Core Workshop 17, p. 141–167.

Plint, A.G., Hart, B.S. and Donaldson, W.S., 1993, Lithospheric flexure as a control on stratal geometry and fades distribution in Upper Cretaceous rocks of the Alberta foreland basin: Basin Research, v. *5*, p.69−77.

Porter, J.W., Price, R.A., and McCrossan, R.G., 1982, The Western Canada Sedimentary Basin: Philosophical Transactions of the Royal Society A: Mathematical, Physical and Engineering Sciences, v. 305, p. 169–192.

Posamentier, H.W., and Allen, G.P., 1999, Siliciclastic sequence stratigraphy: concepts and applications: SEPM, Concepts in Sedimentology and Paleontology, 210 p.

Poulton, T.P., Christopher, J.E., Hayes, B.J.R., Losert, J., Tittemore, J. and Gilchrist, R.D., 1994, Jurassic and Lowermost Cretaceous strata of the Western Canada Sedimentary Basin: *in* Mossop, G.D., Shetsen, and I., eds., Geological Atlas of the Western Canada Sedimentary Basin: Canadian Society of Petroleum Geologists and Alberta Research Council, Chapter 18, 20 p.

Price, R.A., 1994, Cordilleran tectonics and the evolution of the Western Canada Sedimentary Basin, *in* Mossop, G.D. and Shetsen, I., eds., Geological Atlas of the Western Canada Sedimentary Basin: Canadian Society of Petroleum Geologists and Alberta Research Council Edmonton, AB, Canada, p. 13–24.

Ranger, M.J., and Pemberton, S.G., 1997, Elements of a stratigraphic framework for the McMurray Formation in south Athabasca area, Alberta: *in* Pemberton S.G. and James D.P., eds., Petroleum Geology of the Cretaceous Mannville Group, Western Canada, Canadian Society of Petroleum Geologists Memoir18, p. 263–291.

Ranger, M.J., Gingras, M.K., and Pemberton, S.G., 2008, The role of ichnology in the stratigraphic interpretation of the Athabasca oil sands: Search and Discovery Article, v.30, p. 1–8.

Ratcliffe, K.T., Wright, A.M., Hallsworth, C., Morton, A., Zaitlin, B.A., Potocki, D. and Wray, D.S., 2004, An example of alternative correlation techniques in a low-accommodation setting, nonmarine hydrocarbon system: the (Lower Cretaceous) Mannville Basal Quartz succession of southern Alberta: American Association of Petroleum Geologists Bulletin, v. 88, p. 1419–1432.

Rinke-Hardekopf, L., Dashtgard, S.E., and MacEachern, J.A., 2019, Earliest Cretaceous transgression of North America recorded in thick coals: McMurray Sub-Basin, Canada: International Journal of Coal Geology, v. 204, p. 18–33.

Rstudio Team, 2015, RStudio: integrated development for R: RStudio, Inc., Boston, MA URL http://www. rstudio. com.

Rygel, M.C., and Gibling, M.R., 2006, Natural geomorphic variability recorded in a high-accommodation setting: fluvial architecture of the Pennsylvanian Joggins Formation of Atlantic Canada: Journal of Sedimentary Research, v. 76, p. 1230–1251.

Sibson, R., 1981, A brief description of natural neighbour interpolation: Interpreting multivariate data: *in* Barnett V., ed., Interpreting Multivariate Data, John Wiley, New York, p. 21−36.

Smith, D.G., Hubbard, S.M., Leckie, D.A., and Fustic, M., 2009, Counter point bar deposits: Lithofacies and reservoir significance in the meandering modern Peace River and ancient McMurray Formation, Alberta, Canada: Sedimentology, v. 56, p. 1655−1669.

Ta, T.K.O., Nguyen, V.L., Tateishi, M., Kobayashi, I., Saito, Y., and Nakamura, T., 2002, Sediment facies and Late Holocene progradation of the Mekong River Delta in Bentre Province, southern Vietnam: an example of evolution from a tide-dominated to a tide-and wave-dominated delta: Sedimentary Geology, v. 152, p. 313–325.

Ta, T.K.O., Nguyen, V.L., Tateishi, M., Kobayashi, I., and Saito, Y., 2005, Holocene delta evolution and depositional models of the Mekong River Delta, southern Vietnam: *in* Giosan, L., and Bhattacharya, J. P., eds., River Deltas—Concepts, Models, and Examples, SEPM Special Publication 83, p. 453–466.

Tanabe, S., Ta, T.K.O., Nguyen, V.L., Tateishi, M., Kobayashi, I., and Saito, Y., 2003, Delta evolution model inferred from the Holocene Mekong Delta, southern Vietnam: Quaternary Science Revue, v. 22, p. 22345–22361.

Tanabe, S., Saito, Y., Vu, Q.L., Hanebuth, T.J., Ngo, Q.L., and Kitamura, A., 2006, Holocene evolution of the Song Hong (Red River) delta system, northern Vietnam: Sedimentary Geology, v. 187, p. 29–61.

Taylor, A.M. and Goldring, R., 1993, Description and analysis of bioturbation and ichnofabric: Journal of the Geological Society, v. 150, p. 141−148.

Walker, J., Almási, I., Stoakes, F., Potma, K., and Jennifer, O.K., 2017, Hypogenic karst beneath the Athabasca Oil Sands: Implications for oil sands mining operations: Bulletin of Canadian Petroleum Geology, v. 65, p. 115–146.

Weleschuk, Z.P., and Dashtgard, S.E., 2019, Evolution of an ancient (Lower Cretaceous) marginal-marine system from tide-dominated to wave-dominated deposition, McMurray Formation: Sedimentology, v. 66, p. 2354−2391.

Wickham, H., 2016, ggplot2: elegant graphics for data analysis: Springer, New York, 224p.

Wickham, H., and Grolemund, G., 2016, R for data science: import, tidy, transform, visualize, and model data: O'Reilly Media, Inc., Sebastopol, 494 p.

Wightman, D.M., and Pemberton, S.G., 1997, The Lower Cretaceous (Aptian) McMurray Formation; an overview of the Fort McMurray area, northeastern Alberta: Petroleum Geology of the Cretaceous Mannville Group, Western Canada: Memoir - Canadian Society of Petroleum Geologists, Memoir 18, p. 312–344.

Xue, Z., Liu, J.P., DeMaster, D., Van Nguyen, L., and Ta, T.K.O., 2010, Late Holocene evolution of the Mekong subaqueous delta, southern Vietnam: Marine Geology, v. 269, p. 46–60.

Zaitlin, B.A., Warren, M.J., Potocki, D., Rosenthal, L., and Boyd, R., 2002, Depositional styles in a low accommodation foreland basin setting: an example from the Basal Quartz (Lower Cretaceous), southern Alberta: Bulletin of Canadian Petroleum Geology, v. 50, p. 31–72.

Chapter 5.

Conclusions

A sedimentological-statistical approach was applied to the Lower Cretaceous McMurray Formation (Fm) in the southwest quadrant of the McMurray depocenter (MDC; Fig. 5.1) to assess the controls of accommodation space creation on the facies characteristics, depositional architecture and stratigraphic record of coastal- to shallow-marine deposits in a low-accommodation space setting.

Figure 5.1 Position of the 3 main Oil Sands Regions, Peace River, Athabasca, and Cold Lake in Alberta (AB) and Saskatchewan (SK).
The blue-shaded area in the Athabasca oil sands region marks the approximate limit of the McMurray Fm and time-equivalent strata, which is taken to represent the limits of the MDC. The study area is outlined by the red rectangle (modified from Château et al., in press).

Based on a dataset comprising over 100 cores and 6500 geophysical well logs (Fig. 5.2), detailed facies observations linked to statistical analysis were used to: 1) recognize mechanisms that created accommodation space in the study area; 2) determine the amount of accommodation space created during deposition of the formation; and 3) analyse changes in the creation of accommodation space and outline how this relates to the rate of transgression in a low-accommodation space setting.

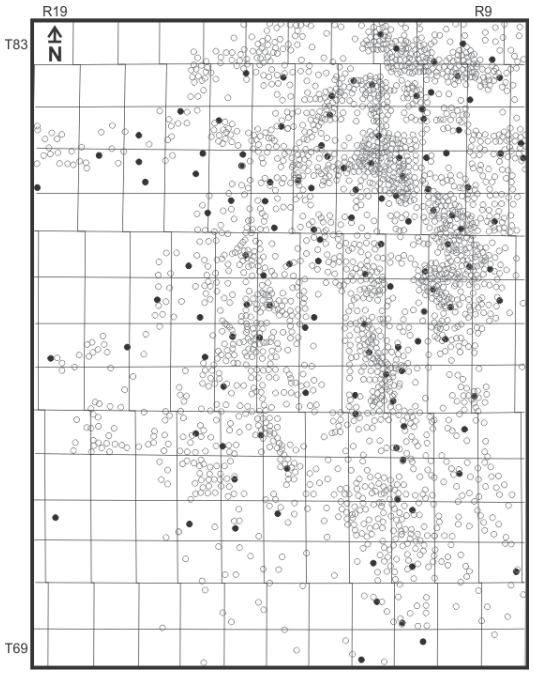

Figure 5.2 Map of the well-logs (grey dots) and core (black dots) used in this study.

The grid is based on the Dominion Land Survey (DLS) coordinate system, and each square comprises a 6-mile by 6-mile area. Columns are referred to as ranges (R) and rows are referred to as townships (T; modified from Château et al., in press).

The southwest quadrant of the MDC (townships (T) 69–83, ranges (R) 9–20W4) is located west of the Assiniboia Valley and along the margins of the Grosmont Highlands (Fig 5.1). It extends over 15 850 km^2 and includes the Grouse, Sparrow, and Pelican paleovalleys. These paleovalleys preserve minimal strata from the lower member of the McMurray Fm and a nearly continuous succession of DUs from the middle and upper McMurray Fm with only limited removal by channel belts. The sedimentological-statistical approach was undertaken on those depositional units, and the main conclusions derived from this thesis are presented below.

5.1. Mechanisms that Created Accommodation Space in the Low-Accommodation McMurray Depocenter

In Chapter 2, a sedimentological-statistical approach is employed in order to recognise the mechanisms that created accommodation space in a low-accommodation space setting. This work was undertaken on strata from the Sparrow Paleovalley (SPV) and a version of this chapter is published as Chateau et al. (2019).

Isopach maps of individual DUs show an overall consistent thickness, although stratal overthickening of DUs occurs in the landward part of the SPV and extend over an area of 400 km^2 (Fig. 5.3). Statistics were employed to first calculate an increase in Depositional Unit (DU) thicknesses in the overthickened area ranging from +21% (B1) to +45% (A1; Fig. 5.4). Then, statistics were used to determine that the difference in thickness between the 400 km^2 region of overthickened strata compared to the rest of the SPV is statistically significant (i.e., form two distinct populations) and hence, suggests an external control on DU thicknesses. Stratal overthickening is also accompanied by increases in both the abundance of soft-sediment deformation structures (SSD) and normal micro-faults in DUs, and an increase in the number and thickness of parasequences that comprise the DUs. The stratal thickening is interpreted to be the result of sediment failure and slumping due to syndepositional epikarst subsidence within underlying Devonian carbonates.

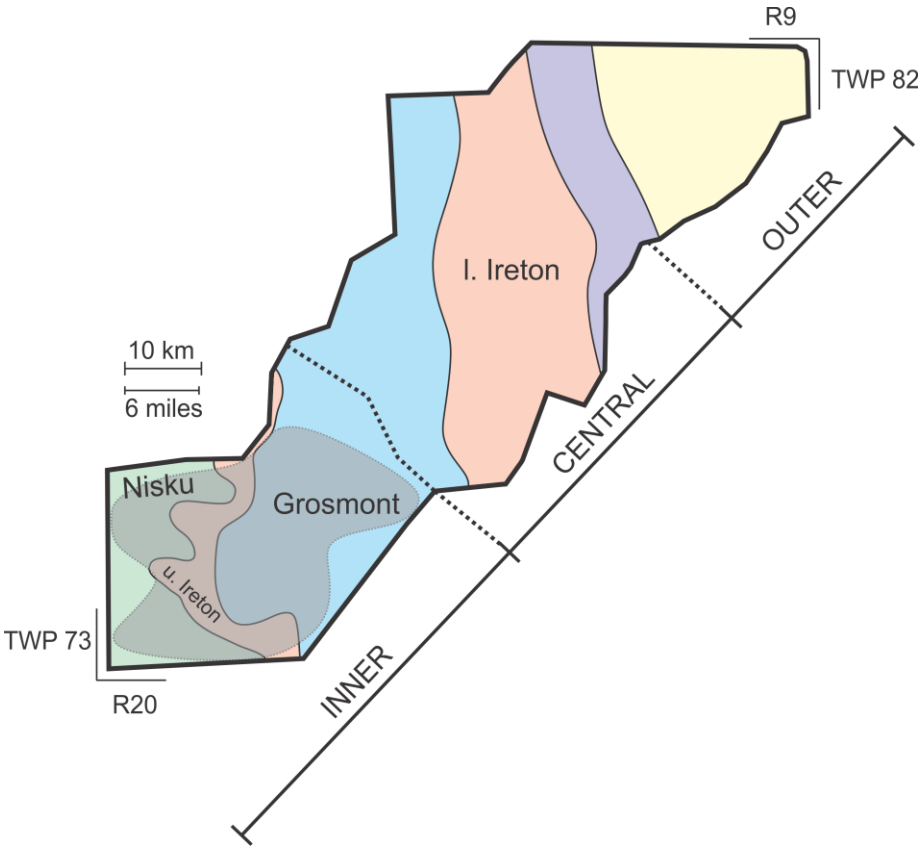

Figure 5.3 Map of Devonian carbonate stratal units that subcrop at the Sub-Cretaceous Unconformity below the McMurray depocenter in the Sparrow Paleovalley.

From west to east, these include the Nisku, upper Ireton, Grosmont, lower Ireton, Cooking Lake, and Waterways formations (Hauck et al., 2017). The inner, central and outer zone boundaries are

demarcated by black dashed lines. The 400 km^2 area of overthickening occurs in the inner part of the SPV and is highlighted in grey (reprinted from Château et al., 2019).

The McMurray Formation unconformably overlies a distribution of Devonian strata that subcrop below the SPV at the Sub-Cretaceous Unconformity. In the overthickened zone and throughout the southwestern extent of the SPV (inner zone; Fig. 5.3), McMurray Fm deposits overlie and are flanked by strata of the Woodbend and Winterburn groups, the latter of which experienced erosion and carbonate epikarstification when it was subaerially exposed. Subsidence through epikarstification of Devonian carbonates generated localized deepening in the Sparrow Paleovalley (i.e. inner zone), which was infilled during the deposition of DUs and resulted in overthickening of McMurray strata. This carbonate epikarst subsidence is also interpreted to have been responsible for generating accommodation space, which correspondingly impacted the distribution and thickness trends of parasequences within DUs B2−A1. In each DU (B2−A1), the lowermost PSs are overthickened and reflect epikarst subsidence or collapse before the onset of deposition. The increase in numbers of relatively small PSs on top of the lowermost thick PS is interpreted to reflect syndepositional collapse that prevented the seaward progradation of the shoreline.

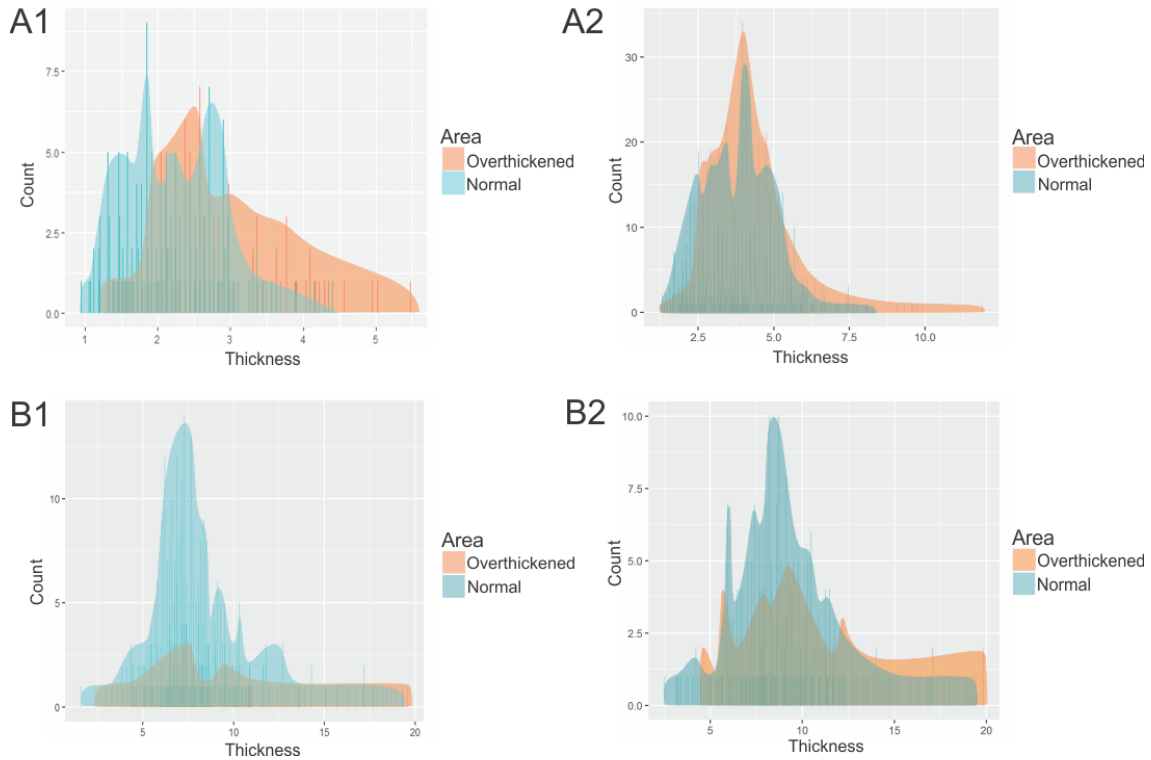

Figure 5.4 Graphical comparison of DU thickness for DUs B2 to A1, comparing the overthickened zone and the rest of the SPV (i.e. normal) using isopach thickness data derived from 1 000 wells.

The increase in Depositional Unit (DU) thicknesses in the overthickened area is 29% for B2, 21% for B1, 32% for A2, and 45% for A1. Regional C DU is not shown, as it displays substantial thinning into the overthickened zone and is attributed to paleotopography that restricted deposition during accumulation of the Regional C DU (reprinted from Château et al., 2019).

5.2. Amount of Accommodation Space Created During the Regional C Deposition

Chapter 3 presents a new allostratigraphic framework for the Regional C (equivalent to the middle McMurray), which is the most understudied depositional unit of the McMurray Fm in the study area. This work was undertaken in the southwest quadrant of the MDC (T69–83, R9–20W4) where the Regional C is well preserved and areally extensive, and a version of this paper is accepted for publication (Chateau et al., in press).

In this study, three environments were identified in the Regional C, recording fluvio-tidal channels, distributary channels and tide-dominated storm-affected deltas that accumulated in a brackish-water setting. This interpretation corroborates previously published work that asserts that brackish-water and tidal conditions existed in the basin

during deposition of the Regional C interval (e.g., Pemberton et al., 1982; Ranger and Pemberton, 1992; Hein and Cotterill, 2006, Hein et al., 2013; Gingras et al., 2016).

From core observation, a previously unrecognized flooding surface is identified, located 11−15 metres below the top of the Regional C depositional unit. The surface has a strong marine signature on cores and shows high gamma-ray responses (> 100 API gamma-ray) and low density-porosity values (< 18%) on geophysical well logs. The surface is identified in 796 well logs and is traceable over 2 550 km^2 within the Grouse, Pelican and Sparrow paleovalleys. This surface is interpreted as an allogenic flooding surface and is herein named ‘Top C2’ (Fig. 5.5).

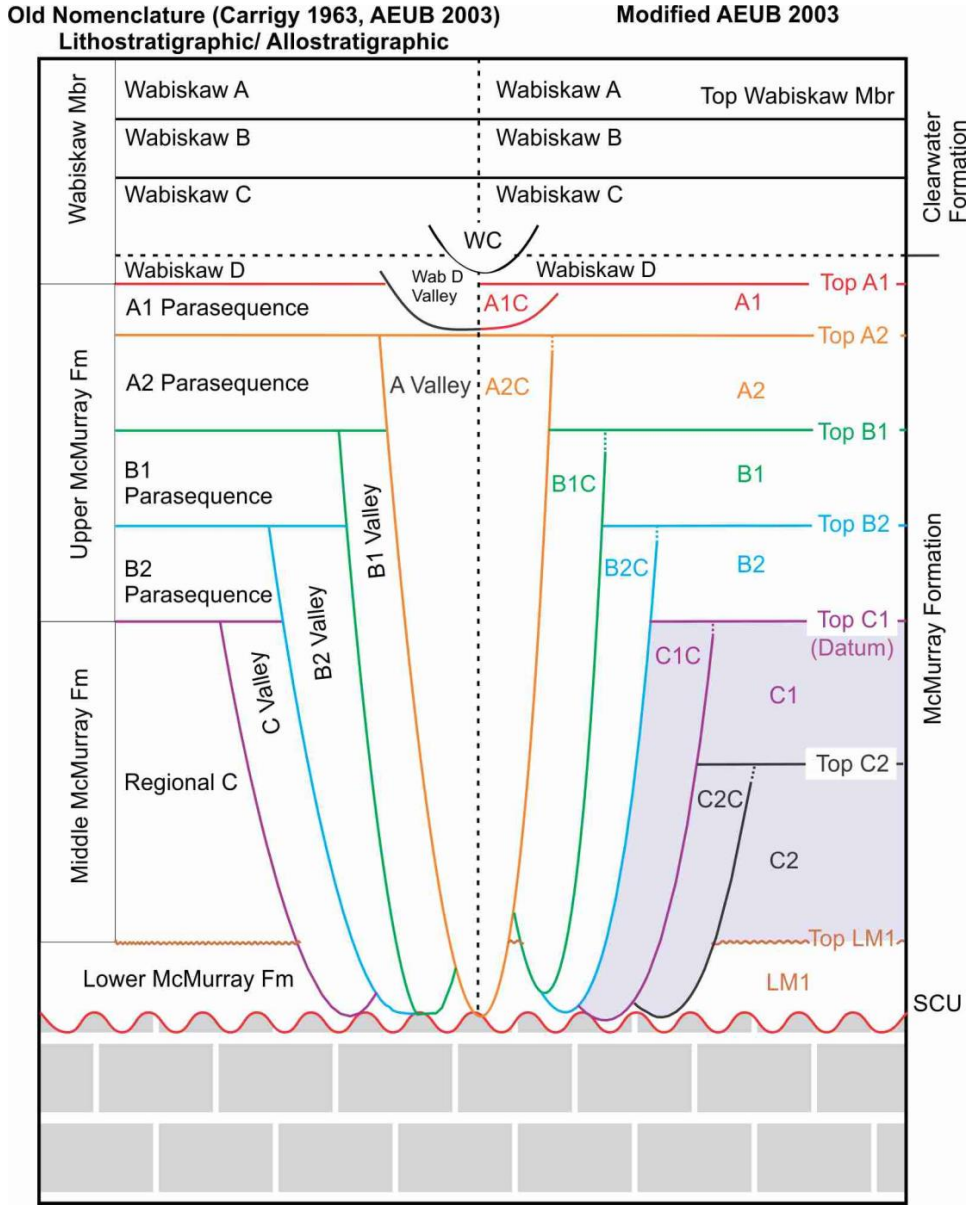

Figure 5.5 Revised stratigraphic model proposed for the McMurray Formation
On the far left (vertical text) is the lithostratigraphic nomenclature proposed by Carrigy (1963). In the middle, left of the black vertical dashed line is the lithostratigraphic/allostratigraphic model developed by the Alberta Energy and Utilities Board (2003; now Alberta Energy Regulator). To the right of the black vertical dashed line is a new model used by the McMurray Geology Consortium. In the revised stratigraphic model, the purple shaded area highlights the portion of the succession of the McMurray Fm investigated in this study. The Top C2 flooding surface divides the Regional C interval into C2 and C1 depositional units. Channel belts are labelled C2C or C1C, based on their position relative to the Top C2 and Top C1 flooding surfaces (reprinted from Château et al., in press).

Top C2 divides the Regional C (previously established as 20−45 m thick) into C2 and C1 depositional units. The maximum thickness of both C2 and C1 DUs is <15 m, which is similar to other DUs in the McMurray Formation. The limited available

accommodation space was easily surpassed by sediment supplied by the paleo-distributive channel system, leading to a basinward progradation of the shoreline during periods of stable or only slowly rising base level (i.e. during deposition of C2 and C1 DUs). The onset of transgression of the Boreal Sea is expressed only by the presence of the regional flooding surface (i.e., Top C2 and Top C1; Fig. 5.6).

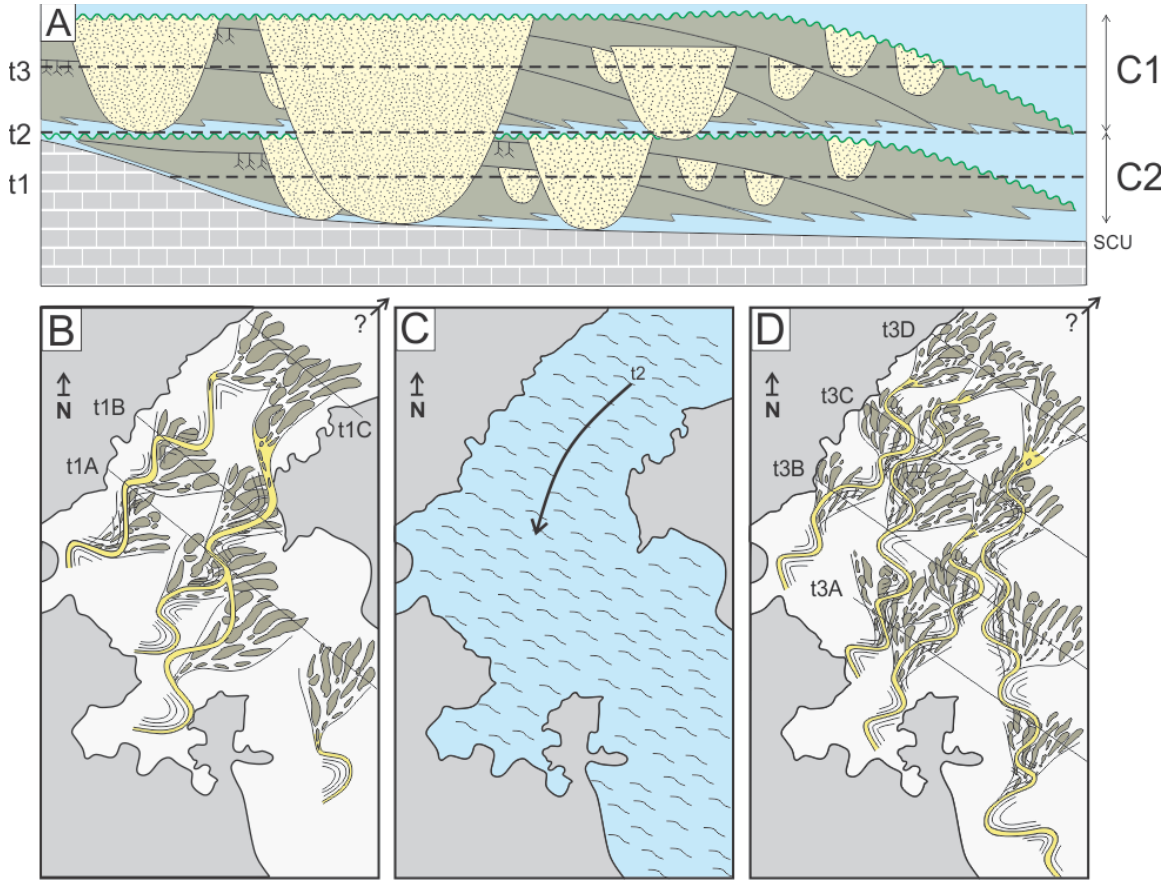

Figure 5.6 Diagrams showing a schematic cross-section and paleoenvironment reconstruction map of C2 and C1 across the southwest quadrant of the McMurray Sub-Basin.

A) Schematic cross-section of C2 and C1 across the southwest quadrant of the McMurray Depocenter. The deposits are aggradational and retrogradational, with C1 deposition occurring landward relative to C2. In each unit, parasequences genetically linked to distributary channels record basinward progradation during normal regression, and are incised by fluvio-tidal channels. Thin black dashed lines highlight times of deposition (t1, t2 and t3). Paleoenvironment maps B, C and D equate to t1, t2 and t3, respectively. B) Paleoenvironment reconstruction map of C2 at time 1, with meandering fluvio-tidal channels (yellow) feeding basinward parasequences of tide-dominated deltas through a network of distributary channels. Thin black dashed lines highlight times of deposition (t1A, t1B and t1C), and show the shoreline's progradation. C) Paleoenvironment reconstruction map at time 2, with shoreline retreat and paleovalley inundation linked to the transgression of the Boreal Sea and development of the regional allogenic flooding surface Top C2. D) Paleoenvironment reconstruction map of C1 at time 3, where meandering fluvio-tidal channels (yellow) represent a distributary channel complex feeding parasequences

lying further basinward through a network of distributary channels. Thin black dashed lines highlight times of deposition (t3A, t3B, t3C; reprinted from Château et al., in press).

Finally, when considered in combination with the fluvial strata of the lower McMurray Fm and the upward increase in the marine expression of the overlying DUs (B2−A1), the overall succession records the progressive drowning of the Alberta Foreland Basin during the Early Cretaceous. Additionally, the thickness of DUs from C2 to A1 suggests that accommodation in the basin in its early stages was low, averaging 15 m or less. Given the time intervals represented by the C2 to A1 succession (approximatively 8.4 My), the early drowning of the Alberta Foreland Basin was slow, enabling periods of major shoreline progradation during progressive but incremental transgression.

5.3. Changes in the Rate of Transgression

Chapter 4 focuses on constraining and quantifying changes in the rate of transgression in a low-accommodation space setting, using the McMurray Fm as an example. A version of this chapter has been submitted for publication (Chateau et al., in review).

From the sedimentological and ichnological work on the cored intervals, regional deposits of DUs C2−A1 are interpreted to have evolved from comprising dominantly tide-dominated deltas (T) during deposition of C2 to B1 to dominantly wave-dominated, tide-influenced, fluvial-affected deltas (Wtf; see Ainsworth et al., 2011) during deposition of A2 and A1 (Fig. 5.7).

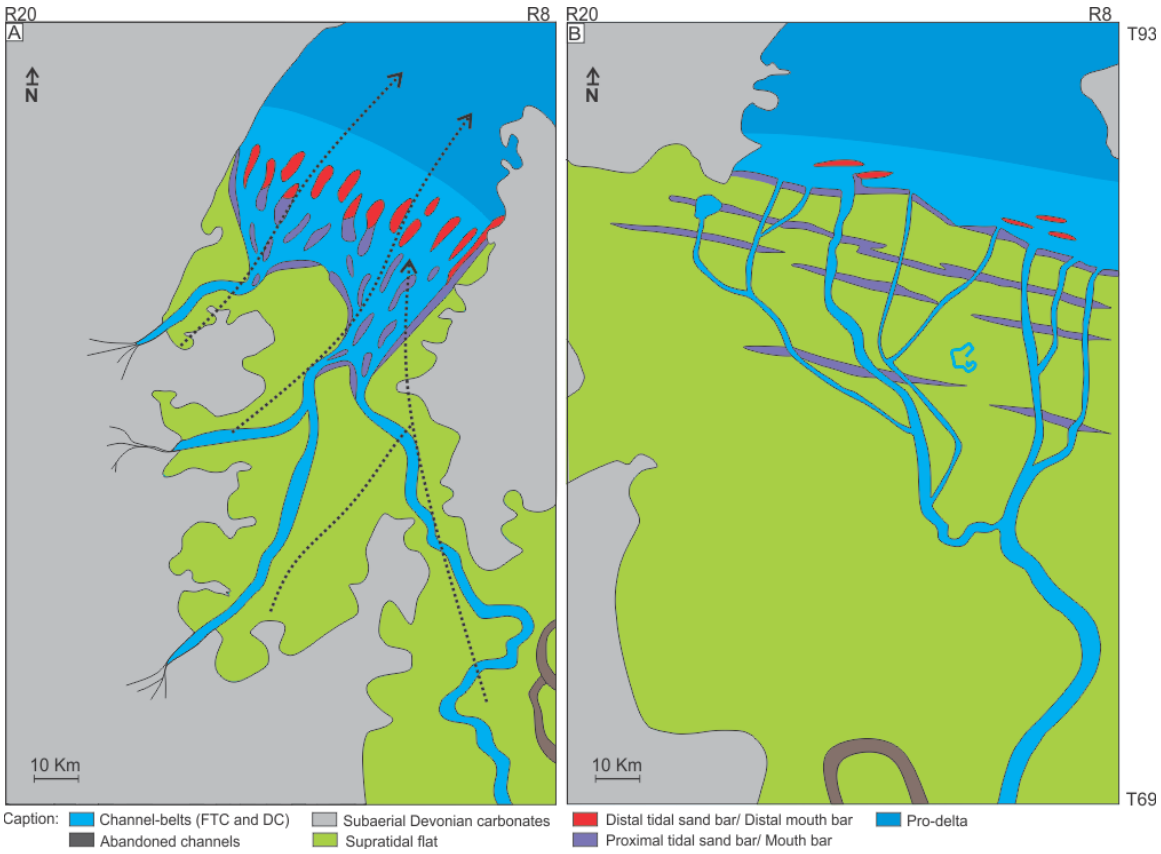

Figure 5.7 Schematic maps showing paleogeographic reconstructions of the McMurray Formation in the southwest corner of the McMurray depocenter.

A) Paleogeography during the deposition of the C2−B1 units and B) during the deposition of the A2−A1 units (reprinted from Château et al., in review).

Architecturally, each DU overlies a maximum flooding surface and consists of a series of autogenically stacked, coarsening-upward cycles and their genetically linked channel-belts (fluvio-tidal channels [FTC] and distributary channels [DC]) that records the progressive basinward shift of the shoreline during normal regression. DUs are capped by allogenic transgressive surfaces that record periodic transgression of the Boreal Sea. These surfaces are, in turn, overlain by mudstone that accumulated during transgression.

Creation of accommodation space was limited during the deposition of the McMurray Fm, with the mean thickness of each DU being 10.4 m (Fig. 5.8). DU thicknesses are relatively consistent from C2 to B1, but decrease markedly from B1 through to A1 (Fig. 5.8). Using statistical analysis, variations in DU thicknesses are tied to changes in the character of transgressive mudstone facies (Fig. 5.8). The decrease in

DU thickness correlates to a landward shift in the marine expression of the transgressive mudstone underlying each DU. Together, these data show that transgression of the Boreal Sea in the study area did not really occur until deposition of DU A2, and then rapidly accelerated after that. This increase in the rate of transgression also correlates to the final drowning of the carbonate highlands to the north and west of the MDC, the concomitant shift of the shoreline from tide-dominated to wave-dominated, and the development of wave ravinement surfaces. These data led to my hypothesis that the duration of still-stands, during which the DUs were deposited, diminished as transgression progressed.

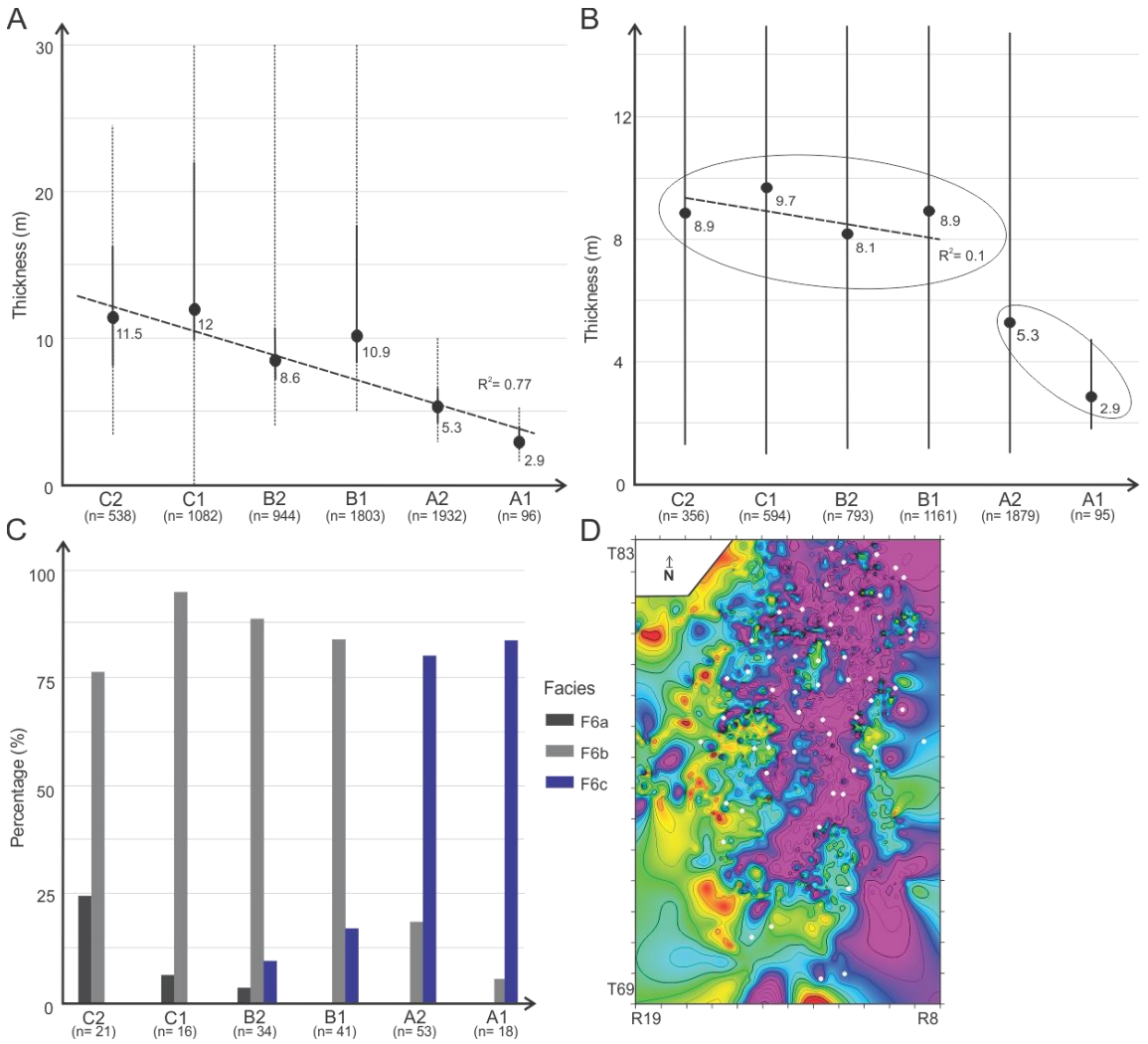

Figure 5.8 Graphical comparison of C2−A1 depositional units.
A) and B) graphical comparison of C2−A1 DU thicknesses. A) includes all data between the 10th and 90th percentiles, while B) only considers DU thicknesses below 15 m (mainly PS and DC). In both graphs, the median thickness of each DU is shown by the black dot and the thick black line represents 50% of the dataset surrounding the median. The thin dashed black line represents the lower and upper quartile. C) The histograms plot the percentage of each transgressive mud

facies (F6a−F6c) for each DU (C2−A1). D) Map of the study area, plotting the distribution of the 57 cores used to create graph C; reprinted from Château et al., in review).

The sedimentological-statistical approach used in this study has broader implications to the field of sedimentology, in that my approach can be used to quantify changes in the rate of transgression, even when regional parasequences are poorly preserved. This approach statistically analyses core and geophysical well-log observations to quantitatively answer depositional architecture and sequence stratigraphic problems.

5.4. Future work

Four distinct stratal stacking patterns linked to shoreline trajectories are historically recognized in shallow-marine stratigraphic successions: upstepping, downstepping, forestepping and backstepping (e.g. Van Wagoner et al., 1987, 1988, 1990). In low-accommodation space settings such as the McMurray Depocenter (MDC), persistent top truncation of parasequences coupled with pronounced channel incision renders it difficult to determine stratal stacking patterns using the interpreted maximum seaward position of the uppermost parasequence in each parasequence set. By contrast, the maximum flooding surface (MFS) at the base of each regressive unit can be reliably determined. In a new project, I will apply the sedimentological-statistical approach used in Chapter 4 to recognize and quantify shoreline trajectories in the southwest corner of the MDC by assessing the maximum landward limit of the MFS in each parasequence set. This work will be undertaken on the regressive units (C2−A1) of the McMurray Formation.

At least two future outcomes are anticipated from this project: 1) demonstrating the paleoshoreline backstepping from the base to the top of the McMurray Formation and mapping their locations; and 2) providing a new sequence stratigraphic method for demonstrating retrogradational stacking of parasequences in low-accommodation, top-truncated successions by demonstrating a clear, progressive landward shift in the position of the maximum flooding surface bounding successive parasequence sets.

5.5. References

Ainsworth, R.B., Vakarelov, B.K., and Nanson, R.A., 2011, Dynamic spatial and temporal prediction of changes in depositional processes on clastic shorelines: Towards improved subsurface uncertainty reduction and management: American Association of Petroleum Geologists Bulletin, v. 95, p. 267−297.

Alberta Energy and Utilities Board, 2003, Athabasca Wabiskaw−McMurray regional geological study: Alberta Energy and Utilities Board, Report 2003-A, 187p.

Carrigy, M.A., 1963, Paleocurrent directions from the McMurray Formation: Bulletin of Canadian Petroleum Geology, v. 11, p. 389–395.

Château, C.C., Dashtgard, S.E., MacEachern, J.A., and Hauck, T.E., 2019, Parasequence architecture in a low-accommodation setting, impact of syndepositional carbonate epikarstification, McMurray Formation, Alberta, Canada: Journal of Marine and Petroleum Geology, v. 104, p. 168−179.

Château, C.C., Dashtgard, S.E., and MacEachern, J.A., in press, Refinement of the stratigraphic framework for the Regional C depositional unit of the McMurray Formation and implications for the early transgression of the Alberta Foreland Basin, Canada: Journal of Sedimentary Research.

Château, C.C., Dashtgard, S.E., and MacEachern, J.A., in review, Changes in the rate of transgression in the Lower Cretaceous McMurray Depocenter, Canada and implications for the advance of the Boreal Sea: Geological Society of America Bulletin

Gingras, M.K., MacEachern, J.A., Dashtgard, S.E., Ranger, M.J., and Pemberton, S.G., 2016, The significance of trace fossils in the McMurray Formation, Alberta, Canada: Bulletin of Canadian Petroleum Geology, v. 64, p. 233−250.

Hauck, T.E., Peterson, J.T., Hathway, B., Grobe, M., and MacCormack, K., 2017, New insights from regional-scale mapping and modelling of the Paleozoic succession in northeast Alberta: Paleogeography, evaporite dissolution, and controls on Cretaceous depositional patterns on the Sub-Cretaceous Unconformity: Bulletin of Canadian Petroleum Geology, v. 65, p. 87–114.

Hein, F.J., and Cotterill, D.K., 2006, The Athabasca oil sands – a regional geological perspective, Fort McMurray area, Alberta, Canada: Natural Resources Research, v. 15, p. 85–102.

Hein, F.J., Dolby, G., and Fairgrieve, B., 2013, A regional geologic framework for the Athabasca oil sands, northeastern Alberta, Canada: *in* Hein F.J., Leckie D., Larter S., and Suter J.R., eds., Heavy-Oil and Oil-Sand Petroleum Systems in Alberta and Beyond: American Association of Petroleum Geologists, Studies in Geology 64, p. 207–250.

Pemberton, S.G., Flach, P.D., and Mossop, G.D., 1982, Trace fossils from the Athabasca oil sands, Alberta, Canada: Science, v. 217, p. 825−827.

Ranger, M.J., and Pemberton, S.G., 1992, The sedimentology and ichnology of estuarine point bars in the McMurray Formation of the Athabasca Oil Sands deposit, north-eastern Alberta, Canada: *in* Pemberton, S.G., ed., Application of Ichnology to Petroleum Exploration: A Core Workshop: SEPM, Core Workshop 17, p. 401−421.

Van Wagoner, J.C., Mitchum Jr, R.M., Posamentier, H.W., and Vail, P.R., 1987, Seismic stratigraphy interpretation using sequence stratigraphy: Part 2: Key definitions of sequence stratigraphy: *in* Bally, A.W., ed., Atlas of seismic stratigraphy: AAPG Studies in Geology 27, p. 11−14.

Van Wagoner, J.C., Posamentier H.W., Mitchum R.M., Vail P.R., Sarg J.F., Loutit T.S., and Hardenbol, J., 1988, An overview of sequence stratigraphy and key definitions: *in* Wilgus, C.K., Hastings, B.S., Kendall, C.G.S.C., Posamentier, H.W., Ross, C.A., and Van Wagoner, J.C., eds., Sea Level Changes: An Integrated Approach: SEPM, Special Publication 42, p. 39−45.

Van Wagoner, J.C., Mitchum, R., Campion, K.M., and Rahmanian, V.D., 1990, Siliciclastic Sequence Stratigraphy in Well Logs, Cores, and Outcrops: Concepts for High-Resolution Correlation of Time and Facies, Tulsa, American Association of Petroleum Geologists, Methods in Exploration Series 7, 55 p.